ARMY RESEARCH LABORATORY

ARL

Biobased Carbon Fibers and High-Performance Thermosetting Resins for Use in U.S. Department of Defense Applications

by John J. La Scala, Joshua Sadler, Anh-Phuong Lam, Amod Ogale, Meng Zhang, Annel Greene, Steven Chambers, Joseph Stanzione III, Richard Wool, Donghun Koo, and Giuseppe Palmese

NOTICES

Disclaimers

The findings in this report are not to be construed as an official Department of the Army position unless so designated by other authorized documents.

Citation of manufacturer's or trade names does not constitute an official endorsement or approval of the use thereof.

Destroy this report when it is no longer needed. Do not return it to the originator.

Army Research Laboratory
Aberdeen Proving Ground, MD 21005-5069

ARL-SR-245 **June 2012**

Biobased Carbon Fibers and High-Performance Thermosetting Resins for Use in U.S. Department of Defense Applications

John J. La Scala, Joshua Sadler, and Anh-Phuong Lam
Weapons and Materials Research Directorate, ARL

Amod Ogale, Meng Zhang, Annel Greene, and Steven Chambers
Clemson University

Joseph Stanzione III and Richard Wool
University of Delaware

Donghun Koo and Giuseppe Palmese
Drexel University

1. REPORT DATE *(DD-MM-YYYY)*	2. REPORT TYPE	3. DATES COVERED *(From - To)*
June 2012	Final	1 January 2010–31 December 2011

4. TITLE AND SUBTITLE	5a. CONTRACT NUMBER
Biobased Carbon Fibers and High-Performance Thermosetting Resins for Use in U.S. Department of Defense Applications	
	5b. GRANT NUMBER
	5c. PROGRAM ELEMENT NUMBER

6. AUTHOR(S)	5d. PROJECT NUMBER
John J. La Scala, Joshua Sadler, Anh Phuong Lam, Amod Ogale,* Meng Zhang,* Annel Greene,* Steven Chambers,* Joseph Stanzione III,† Richard Wool,† Donghun Koo,‡ and Giuseppe Palmese‡	WP-1758
	5e. TASK NUMBER
	5f. WORK UNIT NUMBER

7. PERFORMING ORGANIZATION NAME(S) AND ADDRESS(ES)	8. PERFORMING ORGANIZATION REPORT NUMBER
U.S. Army Research Laboratory ATTN: RDRL-WMM-C Aberdeen Proving Ground, MD 21005-5069	ARL-SR-245

9. SPONSORING/MONITORING AGENCY NAME(S) AND ADDRESS(ES)	10. SPONSOR/MONITOR'S ACRONYM(S)
	11. SPONSOR/MONITOR'S REPORT NUMBER(S)

12. DISTRIBUTION/AVAILABILITY STATEMENT
Approved for public release; distribution is unlimited.

14. ABSTRACT
Current constituent materials used to produce composites for the military are often made from both fibers and resins that are derived from petrochemical feedstocks. The use of biological resources to make advanced fibers and high-performance thermosetting resins will help reduce the dependence of military composites on the volatile cost of petroleum, thereby helping to reduce the cost of composite materials for the Department of Defense. In addition, the processes used to make these fibers and resins from biological sources should have reduced environmental effects. To this end, we have developed carbon fibers based on lignin and carbohydrate and lignin-derived thermosetting resins. We have used both bacterial and chemical decomposition of lignin to make tractable structures that are capable of fiber spinning. Current efforts have been successful in stabilizing and carbonizing the fibers, but the resulting properties need to be improved using some newly developed chemical routes and by improving processing. Unsaturated polyester, vinyl ester, and epoxy resin thermosets have been developed. So far, the unsaturated polyesters and epoxies have fairly poor properties, but we have developed materials with the highest-ever recorded glass transition temperature for a vinyl ester.

15. SUBJECT TERMS
thermoset, environmentally friendly, renewable resources, carbon fiber, lignin

16. SECURITY CLASSIFICATION OF:			17. LIMITATION OF ABSTRACT	18. NUMBER OF PAGES	19a. NAME OF RESPONSIBLE PERSON John J. La Scala
a. REPORT	b. ABSTRACT	c. THIS PAGE			19b. TELEPHONE NUMBER *(Include area code)*
Unclassified	Unclassified	Unclassified	UU	266	410-306-0687

Contents

List of Figures

xiii

xiv

List of Tables

Acknowledgments

Executive Summary

Current constituent materials used to produce composites for the military are often made from both fibers and resins that are derived from petrochemical feedstocks. Because advanced fibers and thermosetting resins are derived from petroleum, their costs are tied strongly to the price of oil. Furthermore, some of these processes produce environmental toxins. The use of biological resources to make advanced fibers and high-performance thermosetting resins will help reduce the dependence of military composites on the volatile cost of petroleum, thereby helping to reduce the cost of composite materials for the Department of Defense (DOD). In addition, the processes used to make these fibers and resins from biological sources should have reduced environmental effects. This work will benefit the DOD by providing critical, high-performance composite materials for DOD systems that are based on sustainable resources and processes. Such composite materials will not be dependent upon fossil fuel feedstocks and will have reduced environmental effects. This work will further enable us to reach the goals articulated in EO 13423 ("Strengthening Federal Environmental, Energy, and Transportation Management"), the Department of Defense Green Procurement Program, and the 2007 Army Environmental Requirements and Technology Assessments by developing biobased, environmentally friendly composite materials.

The goal of this work is to use renewable resources derived from plants and other sources to prepare high-performance carbon fiber and thermosetting matrix resins with high-strength and high-thermal resistance. The scientific objectives of this work are to (1) develop methods for breaking down, modifying, and processing renewable resources to make epoxy resins, vinyl resins, and carbon fibers and (2) determine structure-property relationships for these novel materials.

We have developed numerous scientific and engineering advancements in this project. Bacteria can successfully decompose lignin into useable structures for the formation of small filamanets that might be able to be converted into carbon fibers. Approximately 300 strains of bacteria that decompose lignin were identified, including *Pseudomonas.* We have chemically fractionated lignin to alter its molecular weight distribution and usefulness for separating chemically modifying lignin. Various chemical modifications of lignin have been used successfully in carbon fiber development. These methods include acetylation and methacrylation and have developed separation strategies to produce carbon fiber precursors. Both melt- and solution-spinnable lignin-based fibers were produced. Thermo-oxidation and UV curing were successful stabilization methods for these fibers. Carbon fibers were produced from a few types of lignin and chemically modified lignin. The resulting mechanical properties were relatively poor, but there are obvious steps that need to be taken to improve these properties. Electrical conductivity of these fibers ranged from moderately conductive, similar to that of polyacrylonitrile (PAN)-

based fibers, to highly conductive, indicating a significant graphitic content. Numerous biobased resins were developed, many with excellent properties. Lignin-based model compounds are an excellent reactive diluent to replace styrene in vinyl ester resins. The resulting vinyl ester polymers have thermal and mechanical properties similar to or better than that of styrenated vinyl esters, and they produce much less emissions. Sugar /cellulose-based unsaturated polyesters have been prepared. To solubilize these polyesters in common reactive diluents, the molecules must be end-capped or copolymerized during polyester synthesis with aliphatic components. These components reduce the glass transition temperature to no higher than 50 °C, and the mechanical properties are modest. Sugar-based epoxies have demonstrated good properties, but much more work is needed in this area. Sugar-based vinyl esters have been prepared with glass transition temperature and modulus higher than that of any known commercial vinyl ester. In addition, we have begun developing structure-property relationships for these biobased resins. Life-cycle analysis shows that lignin-based carbon fibers have at least a $2.5/lb benefit relative to current carbon fiber technology. Furthermore, various biobased resins cost less than commercial resins by as much as $4/lb.

Microbial decomposition of lignin has been successful. Approximately 300 different bacterial strains have been identified, but quantification of the characteristics of the more successful lignolytic bacteria has not been completed. In order to produce carbon fibers, larger-scale production of the bacteria-decomposed lignin must be prepared. In addition, we must perform a feasibility study to assess whether such a process is commercially and economically feasible. A chemical engineering design problem will be proposed at Clemson and Drexel to obtain this information. Chemical modification of lignin will continue. In particular, combinations of hydroxyl, acetate, and methacrylate functionality will be used to easily stabilize the polymeric fibers. The ash content in these modified lignin samples must be assessed to determine whether this is playing a role. In addition, we need to orient the fibers during spinning and improve the processing during carbonization in order to produce higher-performing carbon fibers.

We have been unsuccessful in developing high-performance polyesters using isosorbide-based unsaturated polyesters. Measurements to assess structure-property relationships will be completed in the near future to wrap up this work. In addition, publications will be completed, but no other work will be performed. Epoxy-based furans and carbohydrates are in development. We have not yet achieved optimum functionalization but intend to try additional chemical methodologies and variants. No diamines have been produced as of yet. However, some will be produced in 2012 from furans as well as depolymerization of chitosan. During 2012, we will take measurements to assess the structure-property relationships of lignin model compounds. One journal article has already been submitted, one will be submitted soon, and several other publications will be completed during 2012 and 2013 on this topic. Furan-based reactive diluents have had inferior properties relative to baseline diluents. Structure-property relationships have been developed. The assessed use of these diluents has been documented in one journal article, and an additional one to two articles will be completed in 2012.

Carbohydrate-based vinyl esters have demonstrated excellent success. These resins are being patented and will soon be published in a number of journal articles to show their properties and structure-property relationships. Life-cycle analysis of processes, carbon fibers, and resins will be continually assessed during the course of this project.

Intentionally left blank.

1. Introduction

1.1 Strategic Environmental Research Development Program (SERDP) Relevance

SERDP is the U.S. Department of Defense's environmental science and technology program, planned and executed in partnership with the U.S. Department of Energy (DOE) and the Environmental Protection Agency (EPA), with participation by numerous other federal and nonfederal organizations. SERDP invests across a broad spectrum of basic and applied research, as well as advanced development.

SERDP focuses on cross-service requirements and pursues solutions to the Department's environmental challenges. The development and application of innovative environmental technologies will reduce the costs, environmental risks, and time required to resolve environmental problems while, at the same time, enhancing and sustaining military readiness.

Current constituent materials used to produce composites for the military (figure 1) are often made from both fibers and resins that are derived from petrochemical feedstocks. Because advanced fibers and thermosetting resins are derived from petroleum, their costs are tied strongly to the price of oil. This was evidenced over the past few years where the cost of oil rose to unprecedented levels, causing a similar cost increase in advanced fibers and thermosetting resins. Furthermore, some of these processes produce environmental toxins. The use of biological resources to make advanced fibers and high-performance thermosetting resins will help reduce the dependence of military composites on the volatile cost of petroleum, thereby helping to reduce the cost of composite materials for the DOD. In addition, the processes used to make these fibers and resins from biological sources should have reduced environmental effects. There have been previous developments in biobased composite resins, including fatty acid vinyl esters (VEs) (*1*) and acrylated or maleinized soybean oil (*2*), but these have a reduced glass transition temperature (T_g) relative to commercial epoxy and VE resins typically used in DOD composites, limiting their use. High-performance macro-scale fibers have not yet been developed successfullyfrom biological sources. Thus, newly developed biobased fibers and resins must have the high performance necessary for DOD applications. This work will benefit the DOD by providing critical, high-performance composite materials for DOD systems that are based on sustainable resources and processes, are not dependent upon fossil fuel feedstocks, and have reduced environmental effects. This work will further enable us to reach the goals articulated in EO 13423 ("Strengthening Federal Environmental, Energy, and Transportation Management"), the Department of Defense Green Procurement Program, and the 2007 Army Environmental Requirements and Technology Assessments by developing biobased, environmentally friendly composite materials.

Figure 1. Various weapons platforms that use composite materials including the Apache
helicopter, the high-mobility multipurpose wheeled vehicle, Stiletto,
F-22, and USS *Radford*.

1.2 Background

Current constituent materials used to produce composites for the military are often made from
both fibers and resins that are derived from petrochemical feedstocks. In the Army, rotor blades
for rotorcraft helicopters and turbo propeller-driven aircraft are composite designs based on
high-strength carbon fiber technology (*3*). The lower mass of the blades increases both the
revolutions per minute (rpm) and the thrust and payload capacity for these platforms (*3*).
Composite sabots are the largest use of composite materials in the U.S. military at over 800,000
lb annually because the transition from aluminum to carbon fiber–reinforced composites allows
extended range and velocity to be achieved (*3*).

The U.S. Air Force uses composite materials in many of its fighter jets, including the B-2, F-16,
F-18, and F-22 (figure 1) (*4*). In fact, the use of composites has grown considerably in the Air
Force, as the F-14 was only composed of ~2 weight-percent (wt%) composite materials, while
the newer F-22 contains ~24 wt% composites (*4*). Specifically, carbon-epoxy composites are
used in the center and aft fuselage, wing and tail skins, and other areas for the F-18 and F-22 (*4*).

The Navy is also increasing its use of composite materials on ships. The Advanced Enclosed
Mast/Sensor, a composite structure that was installed on the USS *Radford*, has a reduced weight,
reduced structure and sensor maintenance, and higher performance relative to steel masts (*5*).
The M80 Stiletto is a new ship made using mostly carbon fiber-epoxy composites to reduce
weight and meet other performance criteria (*6*). In addition, a composite rudder is used on the
MCM-9 and is being evaluated for use on DDG ships to reduce cavitation damage and minimize
rudder maintenance (*7*). Unsaturated polyester (UPE) radomes are used in the Navy and Air

Force to protect sensitive electronics from environmental hazards while allowing the transmission of radio waves.

Overall, composites outperform traditional materials for these applications because of their light weight, high strength, high toughness, resistance to plastic deformation, and inherent corrosion resistance. Therefore, future classes of vehicles and equipment will use significantly higher amounts of composite materials, making these vehicles lighter, faster, more efficient, and more maneuverable.

1.2.1 Fibers Background

Commonly used fibers in the DOD for reinforcement of composite structures are glass fibers, Kevlar, and carbon fibers. Important properties of these fibers are listed in table 1. Glass fibers come in a variety of types, including E-glass, R-glass, and S-glass, that have slightly different chemical compositions. S-glass is generally superior to that of E-glass, while R-glass has properties intermediate of E- and S-glass. Glass fibers have relatively low moduli, especially when considering specific properties, because of their relatively high densities (~2.5 g/cm^3). Kevlar, or aramid fibers, is slightly stiffer than glass but with a lower strength. Kevlar comes in a few varieties, but Kevlar 49 is the most commonly used. Kevlar is most often used in body armor (*3*), and because it has approximately half the density of glass fibers, it is also used to substitute for glass when lighter-weight parts are needed. Carbon fibers are the stiffest fibers used for typical composite applications and also have lower densities relative to glass. Thus, carbon fibers are typically used when high stiffness and low weight are needed. Carbon fibers come in a variety of types, but AS4 and IM7 are among the most commonly used in DOD composites. IM7 generally performs higher than AS4. Higher-performing carbon fibers do exist, such as Dialead K13D2U fibers, which have a modulus of ~700 GPa and strength of ~4000 MPa. High-strength fibers such as Hexcel's IM9 have a strength of ~6500 MPa with about the same modulus of IM7.

Table 1. Properties of important composite fibers (*8–10*).

Property	E Glass	S2 Glass	K-49 Kevlar	AS4 Carbon	IM7 Carbon
Density (g/cm^3)	2.55	2.47	1.44	1.8	1.8
Tensile Modulus (GPa)	70	88	130	230	280
Tensile Strength (MPa)	5300	8300	4000	4300	5200
Ultimate Elongation (%)	5.5	4.7	2.7	1.8	1.9
Toughness (MPa)	65	85	50	37	40

High-strength carbon fibers used in structural composite applications, such as IM7 and AS4, are almost exclusively derived from solution-spinning of polyacrylonitrile (PAN) precursor fibers (*11*, *12*). In actuality, PAN-based carbon fibers are produced from copolymers of acrylonitrile and other monomers, such as acetic acid, vinyl acetate, and methacrylic acid, rather than pure PAN (figure 2) (*11*). Acrylonitrile is produced from propene generated during the refining of fossil fuels (*11*), and the other comonomers are produced from petroleum refining. The precursor fibers have to be produced by solution-spinning (figure 3) because ordinary grades of PAN degrade before melting. This strategy has been successfully used in the past to thermo-oxidatively stabilize precursor fibers into an intractable form by intra-chain cyclization of the CN moieties. This intractable form of precursor fiber is critical to the subsequent carbonization step (*11*). The fibers are carbonized at moderate temperature (~1000–1500 °C) to favor turbostratic carbon formation rather than graphite formation (*11*).
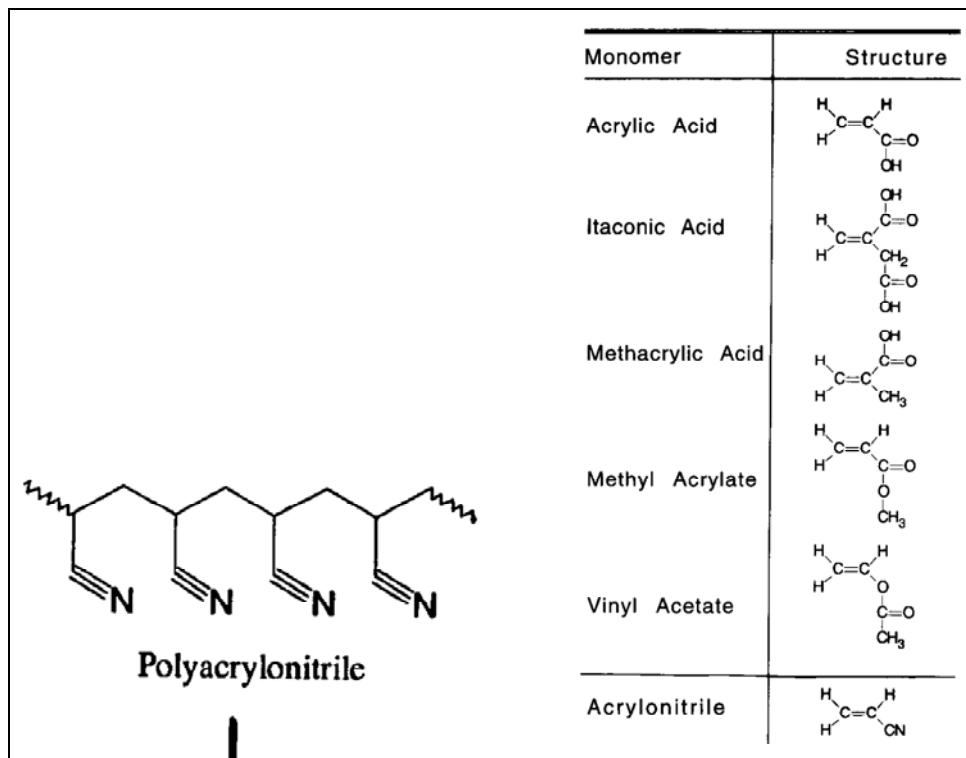
Figure 2. Schematic of polyacrylonitrile copolymers used in production of carbon fibers.
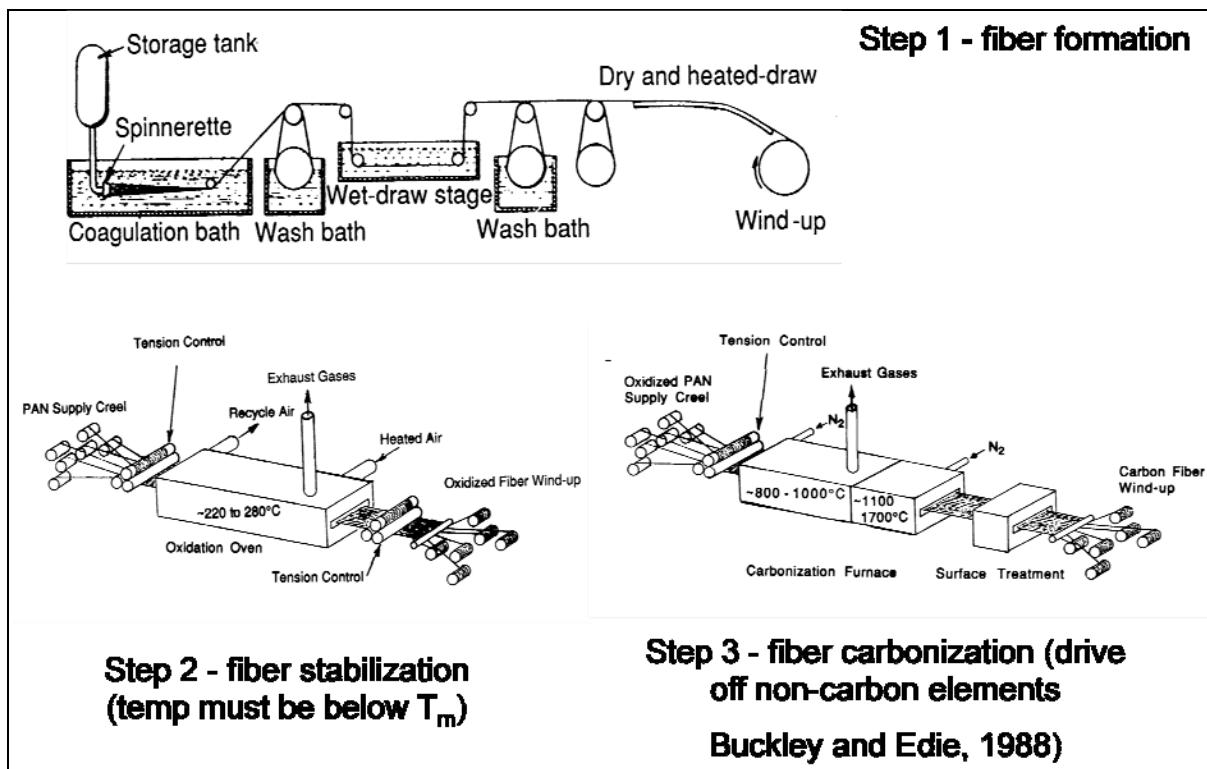
Figure 3. Commercial carbon fiber production process.

The solution-based process (figure 3) to produce carbon fiber suffers from three inherent limitations: (1) use of hazardous solvents, (2) creation of voids within the precursor fibers due to the removal of solvent, and (3) production of HCN during the thermal stabilization and carbonization steps. To avoid the use of solvents, prior research has focused on the development of carbon fibers from melt-spinnable PAN precursor fibers (*13*). However, most organic fibers, including PAN and biobased precursors, melt below the oxidative stabilization temperature range of 250–270 °C. Our prior research has led to the development of UV radiation curing of a photosensitive termonomer to stabilize the precursor fibers (*14, 15*). A high-power UV irradiation chamber was designed and constructed. Subsequently, the fibers were thermo-oxidatively cyclized. High-temperature graphitization furnaces were then used to successfully produce carbon fibers. UV-assisted cross-linking and cyclization of terpolymer composition was successfully demonstrated. These carbon fibers displayed good tensile modulus (~130 GPa) but low strength (~700 MPa) (*14, 15*). Although progress has been made in the elimination of solvents during precursor fiber-spinning, the precursor still remains PAN, which produces HCN and other toxic gases during the thermal stabilization and carbonization steps. Therefore, additional studies need to investigate the replacement of PAN by an environmentally friendly/sustainable precursor.

Although numerous hydrocarbons can be converted to carbon, very few have been actually converted to structural carbon fibers. Besides PAN, mesophase pitch (MP) and rayon are the

only other precursors that have produced carbon fibers. MP produces highly graphitic carbon fibers with high modulus and high thermal conductivity, but low strength. The highly polynuclear aromatic structure of MP, in conjunction with limited alkyl side groups, has been successfully exploited in melt spinning of the MP precursor followed by thermo-oxidative cross-linking at the alkyl groups at fairly high temperatures (such as 250 °C) because the softening point of MP is quite high at 300 °C followed by very high graphitization temperatures (figure 4) (*12*). The highly aromatic molecular architecture facilitates three-dimensional (3-D) graphitic crystal formation, which leads to ultrahigh thermal conductivity of over 1100 W/m·K and high tensile modulus of ~700 GPa, but only moderate tensile strength of 2 GPa and poor compressive strength of ~0.7 GPa (due to flaw sensitivity of the highly crystalline structure and microbuckling of graphene layers). As a result, MP carbon fibers are not often used in structural applications but are used in electronic applications because of their high conductivities.
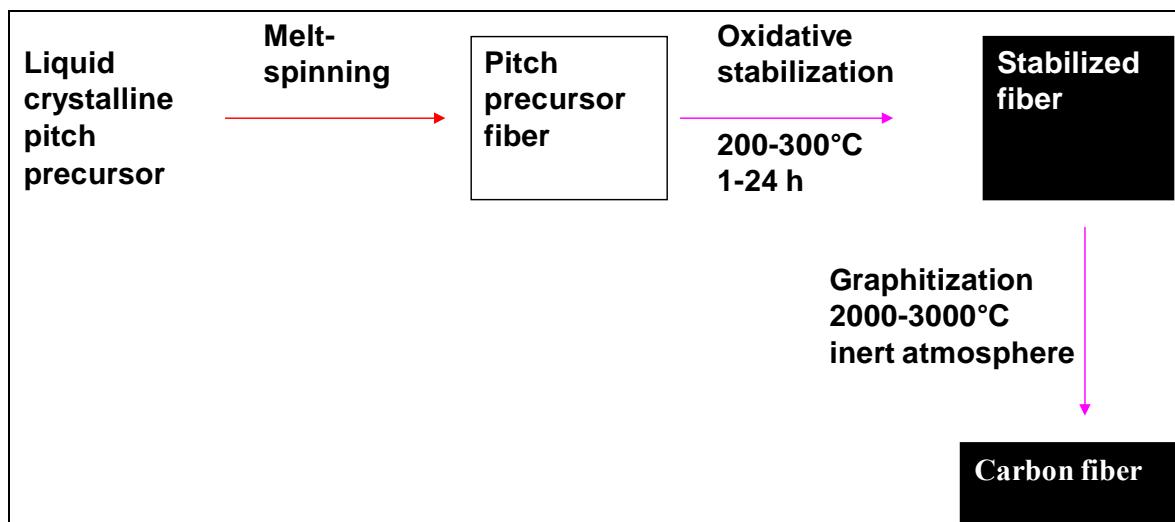
Figure 4. Commercial pitch-based carbon fiber production (*11*, *12*).

Current materials technology and processing techniques do not allow for carbon fibers that achieve both high modulus and high strength. Figure 5 clearly shows the function is larger for PAN-based fibers, but also PAN-based fibers are able to achieve much higher strengths than pitch-based fibers, while pitch-based fibers can achieve higher moduli. It is generally accepted that stresses created by high-temperature heat treatment cause splitting, reducing the mechanical and thermal properties of the fibers. Figure 6 shows these defects that limit the strength and modulus of these materials. In general, the properties of various types of carbon fibers are shown in table 2. The results show that PAN-based carbon fibers are typically much cheaper than pitch-based fibers. In addition, high-modulus fibers generally cost more than lower-modulus fibers. There are two reasons for this: (1) higher-modulus fibers are made with reduced fiber diameter, improving both modulus and strength, but requiring increased processing of the starting fibers (PAN or pitch) and (2) high-modulus materials require higher carbonization temperatures, increasing processing costs.
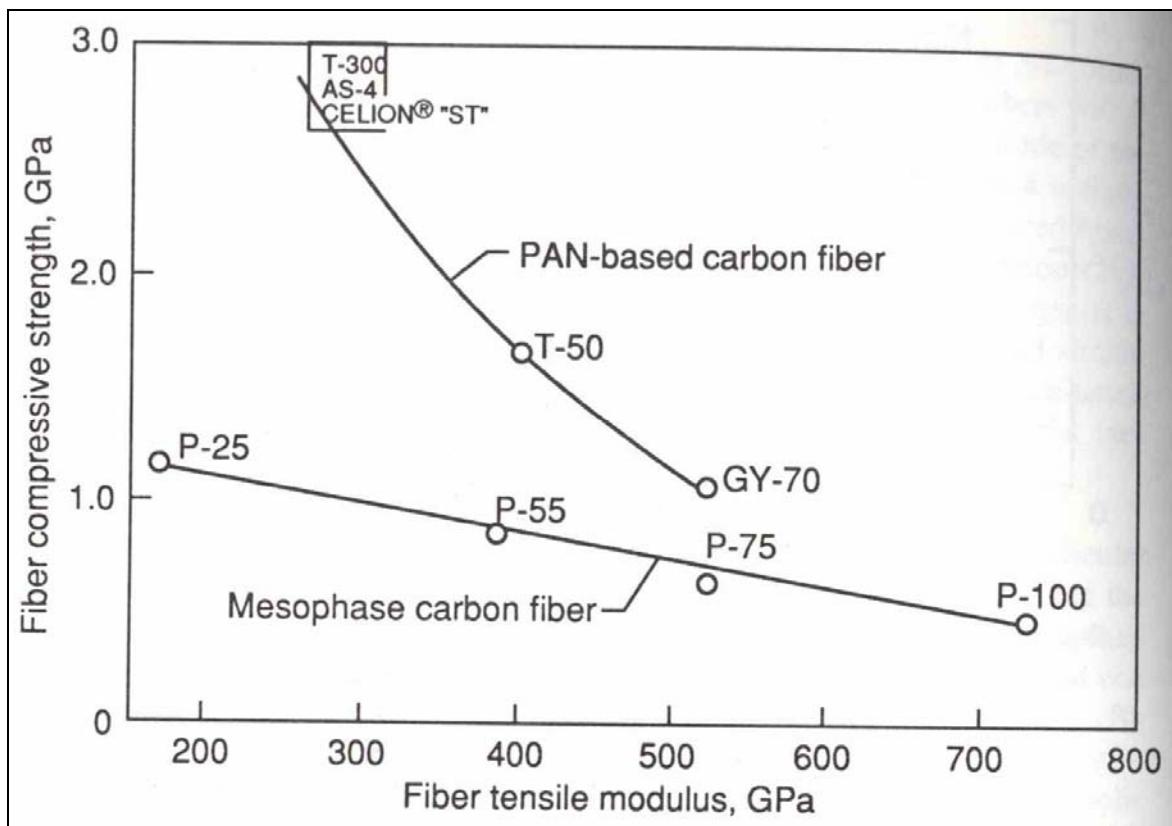
Figure 5. Carbon fiber properties trade-off between compressive strength and tensile modulus for pitch and PAN-based fibers.
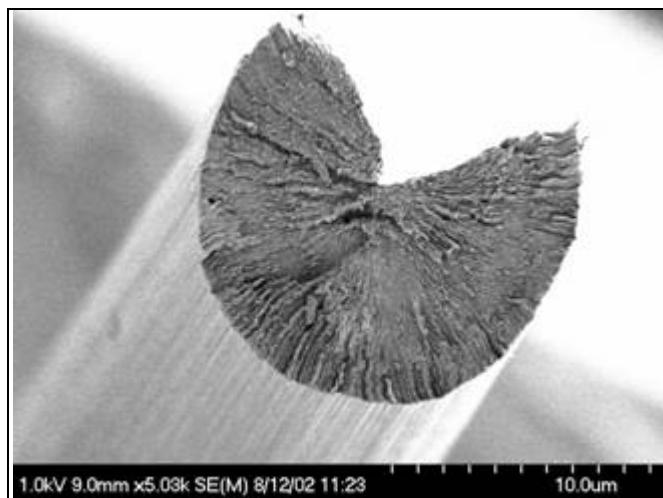
Figure 6. Defects seen in carbon fibers that limit strength and modulus of these materials as shown for mesophase pitch–based fibers produced at Clemson University by co-PI Ogale's group.

Table 2. Properties of carbon fibers.

Fiber	Tensile Modulus (Msi)	Thermal Conductivity (W/mK)	Cost ($/lb)
PAN-based carbon fiber[a]			
Heavy tow (48–320K)	33–35		8–11
Aerospace grade			
Standard modulus (12K)	33–35		18–20
Intermediate modulus (12K)	40–50		31–33
High modulus (12K0	50–70		60–65
Ultrahigh modulus (3K, 6K, 12K)	70–140		120–900
Pitch-based carbon fiber[b]			
P–55	55	120	55–80
P–120	120	640	800
K–1100		1100	1,750
[a] Source: High Performance Composites 1999 Sourcebook.			
[b] Source: Amoco (1998).			

Note: the price of petroleum has increased since 1999, so current carbon fiber costs are slightly higher than the listed prices.

Rayon, on the hand, uses naturally occurring cellulose, but its conversion to carbon is limited to carbon fibers with poor strength and low thermal conductivity. Removal of noncarbon elements from the main chain severely limits its ability to form a 3-D graphitic crystalline structure (*11*). Therefore, rayon-based carbon fibers cannot be used in primary reinforcement applications; instead, they find niche applications in ablative composites in rocket nozzles due to their low thermal conductivity (*12*).

Carbon fibers are used in a number of defense applications (table 3) (*16*). PAN-based carbon fibers have the widest use and are found in rotary and fixed-wing aircraft, missiles, and space platforms. Pitch-based carbon fibers are not used in rotary aircraft, launch vehicles, and tactical missiles, but are used in jets, strategic missiles, and satellites when increased stiffness is necessary. Rayon-based fibers are primarily used in missiles. Their overall demand for commercial and defense applications is estimated at 100 million lb/yr in 2011 (*17*).

Table 3. Uses of carbon fiber in defense applications.

Weapon System	Carbon Fiber Type		
	PAN	Pitch	Rayon
Missiles			
Strategic	X	X	X
Tactical	X		X
Space			
Launch vehicles	X		X
Satellites	X	X	
Aircraft			
Fixed-wing	X	X	
Rotary-wing	X		

There are numerous biobased fibers used in composites. These include jute, hemp, flax, sisal, and others. These fibers are based on cellulose and have specific moduli higher than that of glass fiber (*18*). However, these fibers tend to have defects due to processing that cause them to have low strengths. Cellulosic nanofibers have been developed recently (*19*). These nanofibers have dimensions of 20- to 100-nm-thick rods with lengths on the order of 1 µm. On the individual nanofiber scale, these nanofibers have excellent properties, including very high specific stiffness and strengths. However, the short length of these fibers does not allow for load transfer across the part, severely limiting the properties of the resulting composite.

1.2.2 Resins Background

The DOD uses various resin systems for composite materials, including epoxies, VEs, UPEs, bismaleimides, cyanate esters, and phenolics. Bismaleimides and cyanate esters are used typically for aircraft composites requiring very high-temperature performance (>250 °C). Phenolics are mainly used as spall liners in Army vehicles (*3*).

Epoxy resins are among the most highly used matrix materials (*20*). Epoxy resins are typically bisphenol-based monomers that are cross-linked using diamine curing agents (figure 7). Aliphatic epoxies also exist but produce low-temperature, flexible, and tough epoxies. Bisphenol epoxies and novolac epoxies, also based on phenol rings, are used to produce rigid, high-temperature epoxies. Similarly, aliphatic curing agents are used to produce tough low-
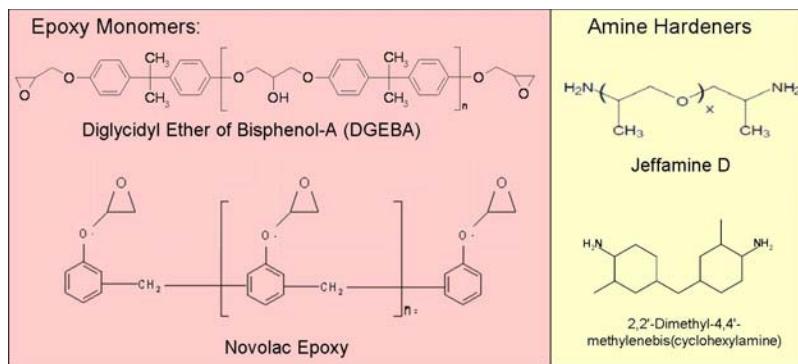
Figure 7. Epoxy monomers and amine hardeners used in typical
commercial epoxy formulations.

temperature epoxies, while cyclic curing agents, such as Amicure PACM, are used to produce higher-temperature epoxies. Thus, epoxy resins can have viscosities of 100–10,000 cP at room temperature, T_g's ranging from below freezing to as high as 250 °C, with moduli ranging from ~1 MPa to 3 GPa, strengths of <1 MPa to >100 MPa, and elongation to failure ranging from 1% to >50% (*20*). Rigid epoxy resins for typical DOD applications have viscosities of 100–1000 cP, T_g's > 100 °C, moduli > 2 GPa, strengths > 100 MPa, and elongation to failure of ~5% (*20*). Novolac epoxies have T_g's > 200 °C, elongation to failure of ~3%, and strengths slightly <100 MPa (*20*). Epoxy resins are produced from the reaction of a diol, such as bisphenol, or polyol and epichlorohydrin (*20*). Both bisphenol and epichlorohydrin produce known health problems and are currently entirely derived from chemicals produced during petroleum refining (*20*).

UPE resins and VE resins are also commonly used matrix resins (figure 8). VE monomers are simply methacrylated epoxies. UPEs are short chain polymers of diols, such as ethylene glycol, and diacids/anhydrides, such as maleic acid and terephthalic acid (*21*). The rigidity of UPEs increases as the length of the diol is reduced, the amount of aromatic acids is increased, and the amount of polymerizable unsaturation character from the maleic acid is increased (*21*). UPEs and VE resins cross-link upon addition of small amounts of peroxide initiators (1–2 wt%) that generate free radicals and cause the free-radical polymerization of the UPE unsaturation sites or vinyl sites on VE. Unfortunately, both resin types use styrene, a hazardous air pollutant (HAP), as a reactive diluent in the amount of 30–60 wt%. Commercial VEs typically have viscosities of 100–1000 cP, T_g's of ~100 °C (toughened VEs), 120–150 °C (standard diglycidyl ether of bisphenol A [DGEBA] VE) and ~180 °C (Novolac VE). VEs are currently derived from 100% petroleum-based products (*22*, *23*). Commercial UPE resins have a large variety of properties because of their low cost and general purpose nature. However, UPE resins for DOD applications typically have viscosities of 500–5000 cP, T_g's of ~100 °C, strengths of 50–100 MPa, moduli of 2–3 GPa, and elongation to failure of 2%–4% (*20*). UPEs currently can be derived partially from biobased sources, as maleic anhydride (MA) and diethylene glycol are currently manufactured in biological processes.
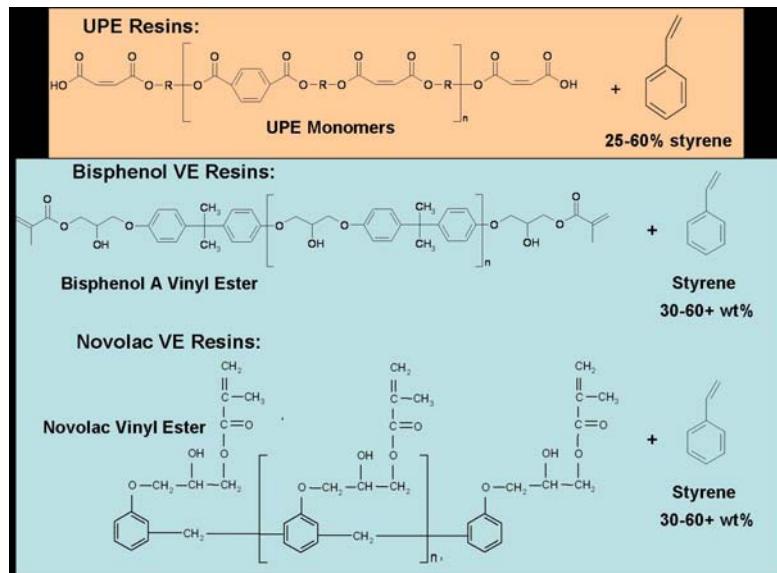
Figure 8. Chemical structure of the major components of UPE and VE
resins.

Fatty acid VE resins have viscosities <1000 cP, T_g's >100 ºC, and strength over 100 MPa, but
they only use 10–25 wt% renewable component. Higher renewable components result in
viscosities over 1000 cP and T_g's below 100 °C (*1*). Maleinized triglycerides have achieved T_g's
of 140 °C (*2*), but the moduli and heat distortion temperatures of these resins were very low.
This occurred because high cross-linking prevented complete thermal softening at temperatures
below 140 °C, but the aliphatic character of these resins enabled various motions of these
polymeric chains causing significant softening at temperatures as low as 50 °C.

1.3   Project Structure

Figure 9 shows the general concept of this project. Several natural resources are currently used
to produce biobased chemicals, including lignin, carbohydrates, cellulose, hemicellulose, chitin,
and plant oils. This work will focus on developing high-T_g biobased resins by selecting or
preparing cyclic and aromatic derivatives of lignin, carbohydrates, cellulose, hemicellulose,
chitin, and hybrid monomers based on multiple renewable sources. Biobased fibers will be
prepared from lignin-based oligomers. The biobased resins and fibers will be combined to make
high-performance biobased composites for DOD applications.

11
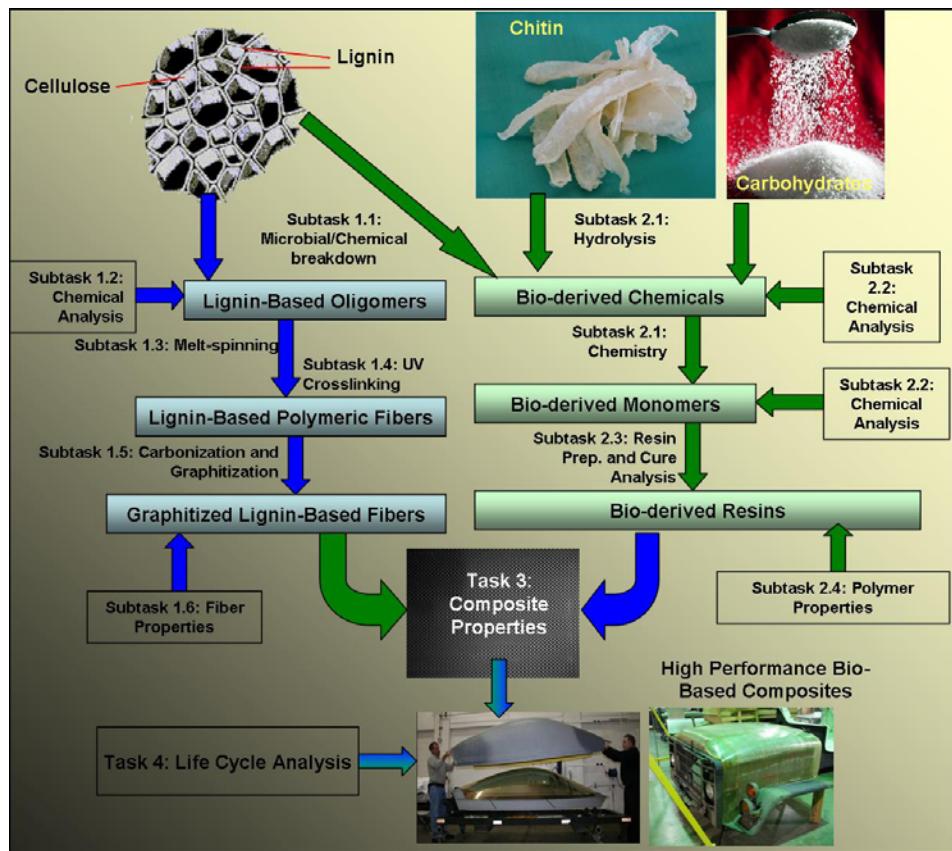
Figure 9. Overall structure of this project whereby natural resources will be used to make high-performance fibers, resins, and composites. (The tasks and subtasks are labeled according to the accepted WP-1758 proposal, not the sections of this report.)

1.4   Task 1: Lignin-Based Carbon Fibers

Task 1 entails using lignin to make high-performance carbon fibers. Among biobased alternatives, lignin is an aromatic encrusting material found in vascular plants, which confers rigidity and strength to wood. Lignin is abundantly available; over 3×10^{11} tons of lignin exist in the biosphere with $\sim 2 \times 10^{10}$ tons generated annually (*24*). Because of the aromatic nature of the compound, lignin may be used to generate a valuable source of aromatic precursors for melt processing into fibers. However, because of its 3-D aromatic structure, lignin is intractable in its unmodified state and must be broken down into lower-molecular-weight aromatic fragments largely involving the basic repeat units trans-coniperyl, trans-sinapyl, and trans-coumaryl. Thus, this project focuses on ways to degrade lignin into a tractable form so that carbon fibers can be produced as outlined in figure 10.
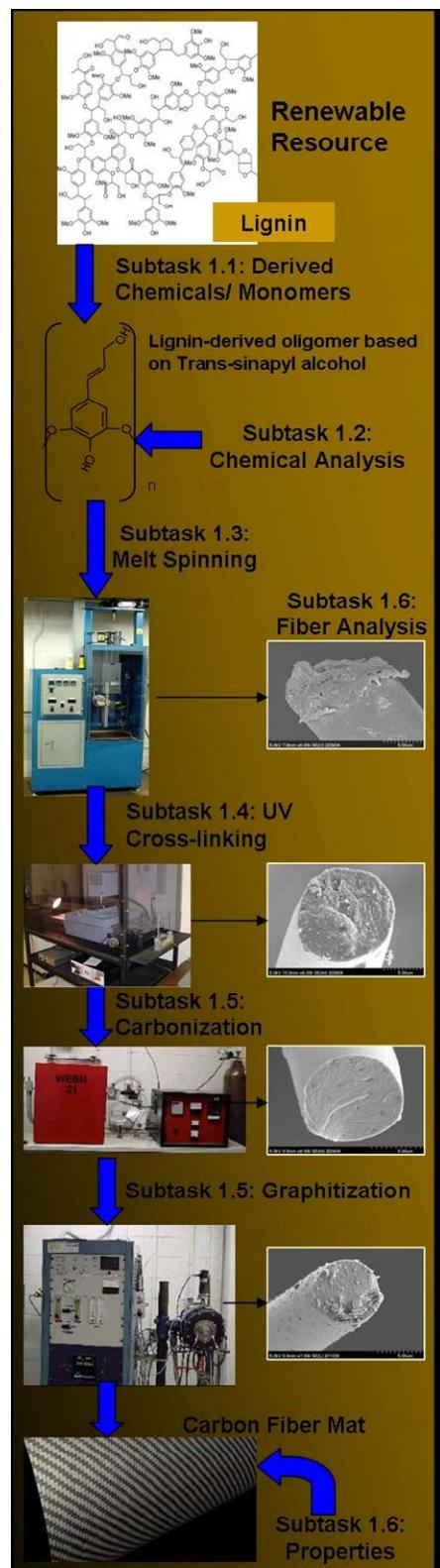
Figure 10. Process for making biobased
carbon fibers from lignin.

Since the 1960s, lignin has been studied as a precursor for carbon fibers. Overall, the properties of lignin-based fibers using these methods are low relative to commercial carbon fibers. Generally, the lignin-based fibers had significant amounts of defects causing low properties (*13*, *17*). In addition, the DOE at Oak Ridge National Laboratory (ORNL) is working to make low-cost, moderate-performance carbon fibers from lignin. These fibers are being developed for automotive applications to enable high automobile fuel economy. Although developments by ORNL are important, the low-performance goals are not sufficient for DOD applications. Thus, it is important that the DOD also work on developing lignin-based carbon fiber. This team will perform work that others have not done in order to make high-performance lignin-based fibers. This includes novel fractionation and decomposition techniques, surface stabilization of fibers, and other controls of the processing to limit defect growth as detailed in the following subsections.

1.4.1 Subtask 1.1: Preparation of Lignin-Based Oligomers for Fiber Production

The processes involved in the breakdown of lignin can be broadly identified as chemical or microbial. Chemical processes include high-rate but low-selectivity catalytic cracking and acidification. In contrast, microbial mechanisms produce better selectivity but often lack speed and do not require the use of elevated temperature processes. Therefore, both routes will be pursued in this work.

Other researchers have investigated the chemical breakdown of lignin mostly for fuel applications (*25*). Fluidizied lignin will be thermally cracked in a reactor by exposure to elevated temperatures for short durations. Simple thermal cracking using basic or acidic aqueous environments will be performed at elevated temperatures (250–450 °C) and pressures (1–20 atm) for durations ranging from 10 s to a few hours (*25*). Hydrogen peroxide has been effective in reducing the required temperatures down to 80–160 °C for cracking (*26*).

Microbial lignin degradation using eukaryotic organisms has previously failed because of long incubation times (*27*). Fungi in general produce more complex digestive enzymes but do so at a much slower rate than bacteria. Therefore, research into bacterial degradation of lignin, investigated by coinvestigator Greene, yielded wild-type bacteria capable of degrading lignin (*27*). Using an isolation chemostat method with methanol as the sole carbon source, we can rapidly screen potential isolates for potential lignolytic activity.

Lignin chemistry varies according to the plant it comes from and the process used to recover the cellulosic fibers from that plant. Some have suggested that birch lignin may be better than pine lignin for fiber production (*28*). Therefore, we are investigating different lignin and different lignin recovery processes.

1.4.2 Subtask 1.2: Chemical Analysis of Lignin Decomposition Products

A number of analytical techniques are being used to assess the chemistry and molecular weight of modified lignin. Fourier transform infrared (FTIR) spectroscopy is used to determine the general chemical makeup of the lignin-derived oligomers using known standards (figure 11) (*29*). A Bruker 600-MHz spectrometer with a spectral window of ±2000 Hz, 16 scans at 293 K, and 90° pulse width is used to run nuclear magnetic resonance (NMR) spectroscopy (figure 12). This allows us to determine the functionality and the approximate chemical makeup of the oligomers using known standards (*30*). We are using size exclusion chromatography (SEC) to measure the molecular weight of the lignin-derived oligomers (figure 13). Because high molecular weight species cannot diffuse into the packing, they elute first from the column, while lower molecular weight species elute later (*31*). Knowing the molecular weight of the lignin allows us to determine whether addition or decomposition reactions take place and the extent of these reactions.
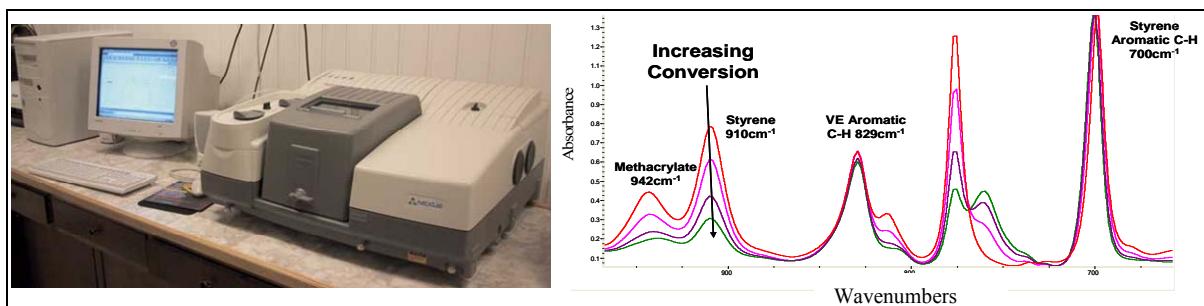
Figure 11. Thermo Nicolet Nexus 670 FTIR and FTIR spectra of VE as a function of conversion allowing us to measure individual component conversion.
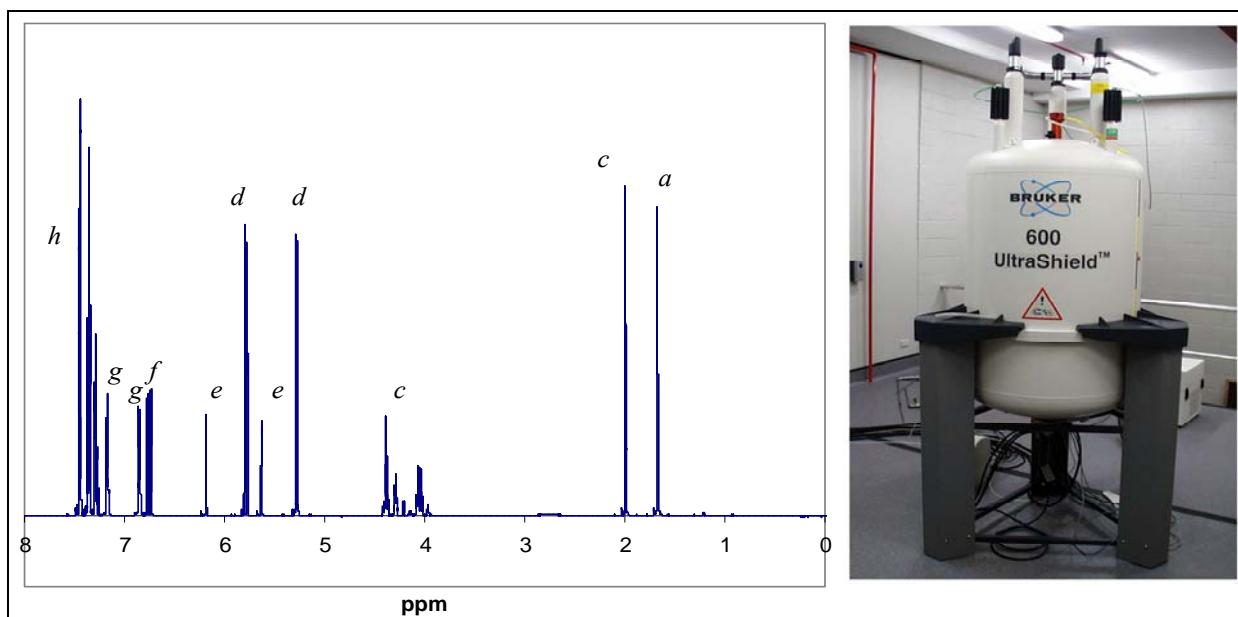
Figure 12. Bruker 600-MHz NMR and a representative spectrum for VE resins.

15
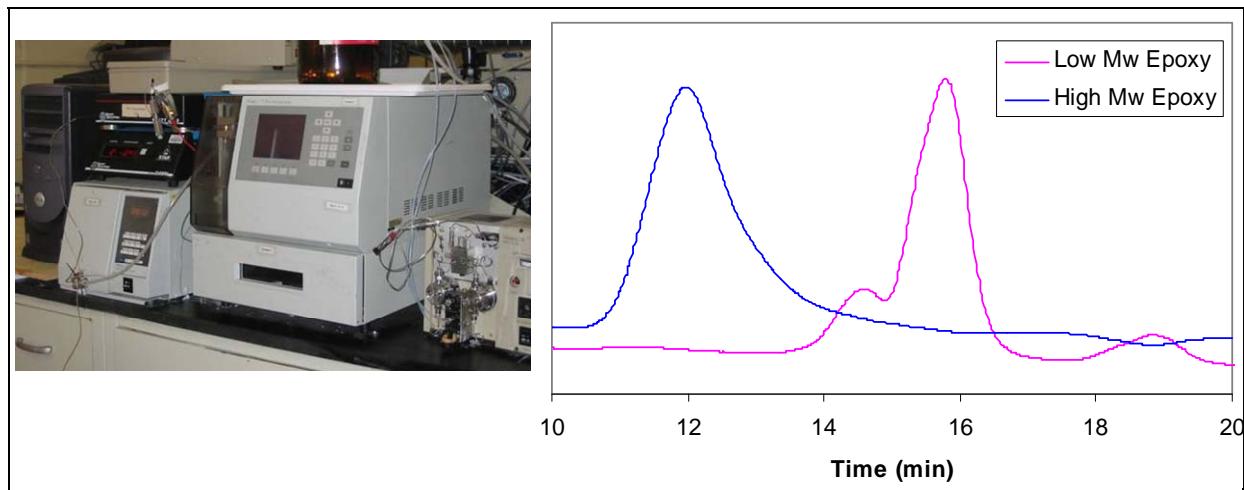
Figure 13. Waters SEC and SEC chromatographs of low- and high-molecular weight epoxies.

In order for lignin to be converted into carbon fibers, it must be spun into precursor polymeric fibers. It is first important to assess whether the fibers melt to determine if melt spinning is even possible. The softening point apparatus works by placing a metal weight on top of a charge of sample (figure 14). While the sample is solid, the weight is held up by the sample. As the temperature is raised and the sample softens, the weight will push the sample into the light path to enable the softening point (SP) of the material to be measured. The lignin samples are also being characterized for their viscosity using a host of rheometers available through the Center for Advanced Engineering Fibers and Films (CAEFF) at Clemson University. Typically, 100 Pa.s of viscosity is needed for fiber spinning, in conjunction with adequate melt strength, i.e., extensional hardening. Prior studies of MP derived from synthetic routes displayed the evolution stress in terms of the texture characterized by the size and orientation of the discotic phase (figure 15).
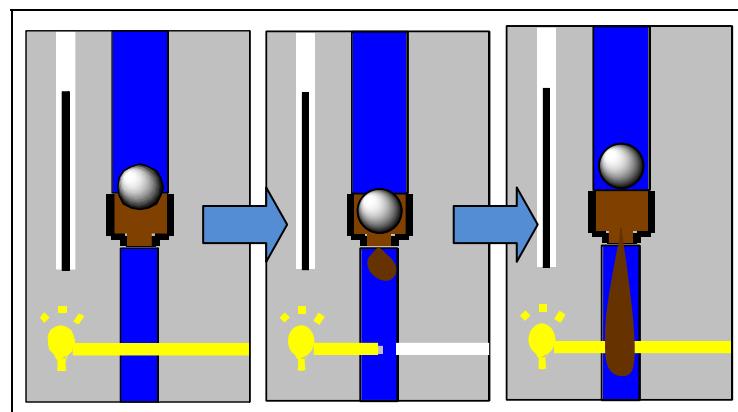
Figure 14. Depiction of softening point apparatus.
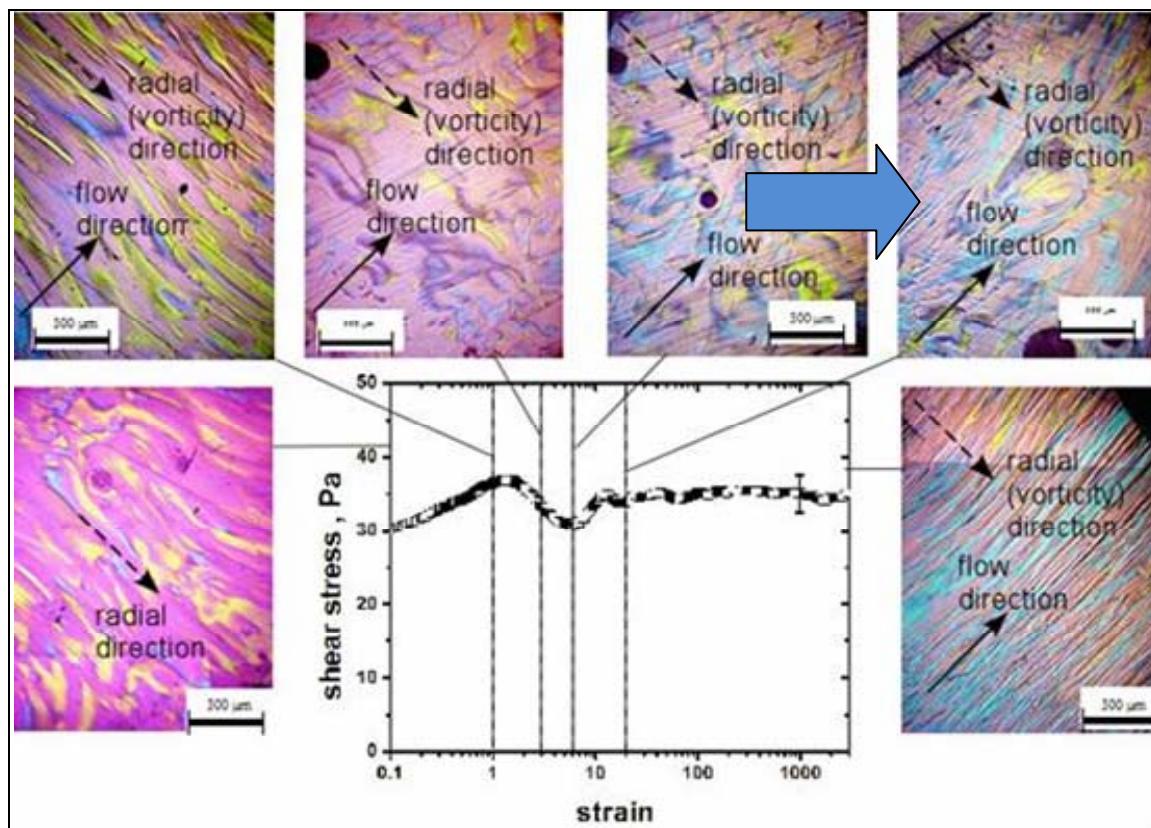
Figure 15. Rheostructural evolution of MP at a shear rate of 1 s^{-1} and a processing temperature of 297 °C (*32*).

1.4.3 Subtask 1.3: Rheostructural Investigation to Determine Melt Processability

An important component of rheological studies is the assessment of melt stability of the lignin samples. This step is important for biomass-derived precursors that contain alkoxy side groups that can cross-link or degrade during melting. Typically, precursors must possess thermal stability for ~30 min, which is measured by transient experiments. After melt processability and fiber-forming characteristics are determined, suitable fractions are processed in batch and continuous fiber spinning units (figure 16).

Figure 16. (a) Batch spinning unit for samples up to 100 g and (b) continuous fiber spinning unit for large-scale laboratory production of fibers at rates up to 5 kg/day.

1.4.4 Subtask 1.4: UV-Thermal Dual Mechanism Cross-Linking/Stabilization and Carbonization

Precursor fibers have to be made intractable to avoid meltdown of the fibers during the high-temperature carbonization process. This is the most critical step in the precursor conversion process because molecular structure necessary for turbostratic or graphitic carbon is locked in this step. We also emphasize that typical thermo-oxidative stabilization conditions established for solution-spun PAN fibers cannot be used with melt-spun precursor fibers because such fibers melt while being heated through the "melting region" into the oxidative temperature regime. Thus, irradiation and thermo-oxidative methods are being used to stabilize the fibers.

Irradiation studies are being conducted in a high-power UV reactor (figure 17) to explore UV sensitivity of the fractions. The presence of conjugated bonds in lignin fractions can help in resonance stabilization, but the kinetics can be very slow. Therefore, extrinsic UV-sensitive initiators are being added during the fiber-spinning step. Prior studies with acryloyl benzophenone (ABP) as a termonomer in PAN have established its thermal stability during melt spinning and retention of subsequent UV-sensitivity (*13*, *15*). We note, however, that the reactivity ratio for ABP is not established for lignin fractions and is being studied here. After or in place of UV cross-linking, thermo-oxidative reactions are conducted to obtain an intractable, polyaromatic structure. To assist in thermal cross-linking, we have demonstrated in an earlier study that lauroyl peroxide can survive UV-exposure and then be activated by thermal mechanism (*33*). A residence time of 50 s at 250–270 °C has led to almost 50% gel content in PAN precursors, but the duration and number of cycles must be determined experimentally for lignin-based fibers.

18
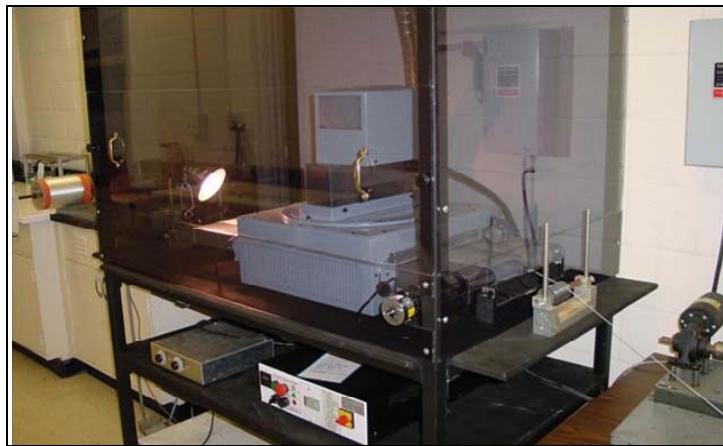
Figure 17. Custom-built, 5-kW UV irradiation chamber for batch
or continuous irradiation of carbon precursor fibers.

1.4.5 Subtask 1.5: Carbonization and Graphitization of Lignin-Based Fibers

Carbonization and graphitization of stabilized fibers are conducted using the extensive, ultrahigh
temperature capabilities at CAEFF (figure 18). These furnaces are capable of treating samples
ranging from a few grams to continuous treatment. Residence time and processing temperatures
up to 2400 °C for carbonization will have to be experimentally determined. Graphitization
residence time and temperature up to 2700 °C are being experimentally determined. Initially,
processing conditions mimicked PAN-based carbon fibers and are being adjusted during
processing by fiber visual appearance and from batch-to-batch based on fiber properties.
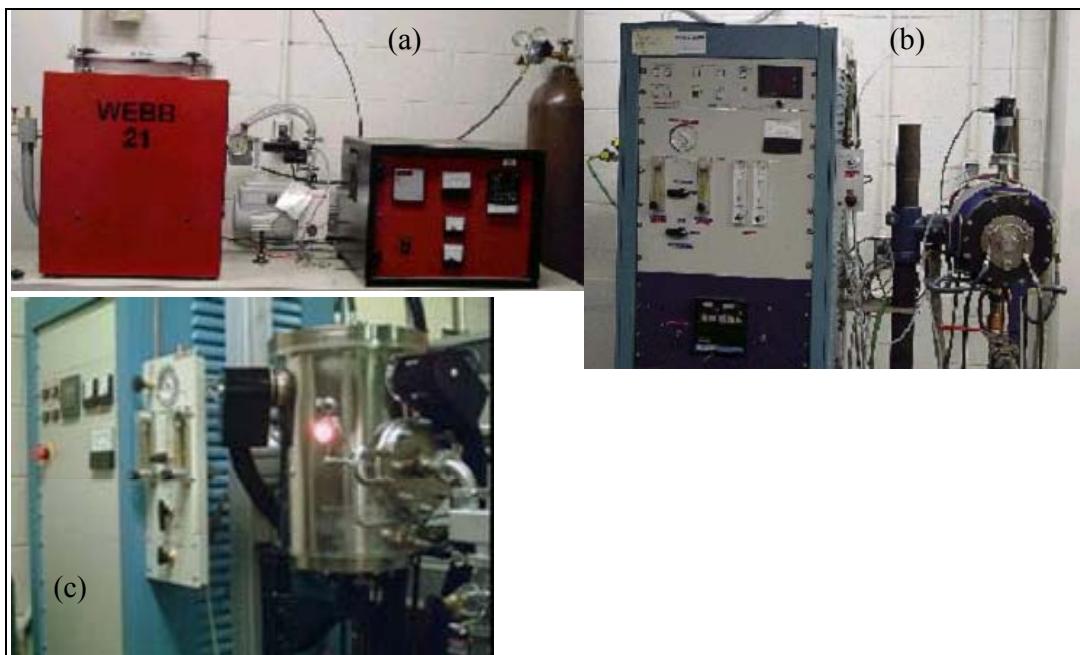
Figure 18. (a) Webb batch carbonization unit for treatment to 2100 °C; (b) ASTRO 1000 batch
/continuous unit for carbonization to 2400 °C; (c) ASTRO 1100 ultrahigh temperature
furnace for graphitization to 2700 °C.

1.4.6 Subtask 1.6: Testing and Analysis of Biobased Carbon Fibers

To measure 3-D graphitic crystallinity, wide-angle x-ray diffraction studies are being conducted. The average unit lattice spacing (d-spacing) for graphite is calculated from a maximum 2θ value in the integrated 2θ profile, which corresponds to (002) lattice plane, using the Bragg equation, $n\lambda = 2d\sin\theta$, where λ = wavelength of the x-ray, n = 1 for first-order scattering, and θ = Bragg angle (half of scattering angle [2θ]). Coherent length along the lattice plane (L_a) and coherent height of stack (L_c) are estimated from the amount of broadening, β, using the Scherrer equation, $L = \dfrac{K\lambda}{\beta\cos\theta}$, where L is the coherent length, β is the width at half peak height, and K is the Scherrer parameter. β for 002 and 110 plane is used to measure L_c and L_a, respectively. In this case, K is usually taken to be 0.9.

Misorientation of the graphene layers can be calculated from an azimuthal plot of the 002 reflection—either full width at half maxima (Z) in the azimuthal profile for 002 plane or Harman's orientation factor, measured as average squared cosine of the crystal plane orientation $<\cos^2\phi_{hkl}>$ to represent misalignment of the planes. As measured by d_{002} spacing of 0.337 nm, the graphitic content can range up to 85%, assuming d-spacing of 0.3354 and 0.3440 nm for perfect graphitic and turbostratic structures, respectively. The density of the fibers, another measure of nanotexture and graphitic content, is being measured using standard methods (ASTM C 693).

Scanning electron microscopy (SEM) is being used to characterize the fibers before and after testing to examine defect content and the effects on fiber failure (figure 19). SEM is being used to see defects in the fiber structure, including fractures, cracks, and roughness. The nanoscale graphene layer orientation in the fiber direction leads to fibers with an ultrahigh tensile modulus and thermal conductivity but results in low tensile strength and poor compressive strength. This combination of carbon fiber properties, typically obtained from disc-shaped MP molecules, is not optimum. In contrast, the linear molecular architecture of PAN precursors results in only a turbostratic crystal structure (not truly graphitic) of the carbon, which leads to a high tensile strength and good compressive strength, but moderate modulus and low thermal conductivity. A combination of aromatic and aliphatic molecular structures, possible with lignin fractions, presents a unique opportunity to develop an optimum level of nanotexture and graphene orientation in carbon fibers. The spinning process is being modified, as needed, to produce this nanotexture resulting in carbon fibers with the optimal combination of thermomechanical properties.
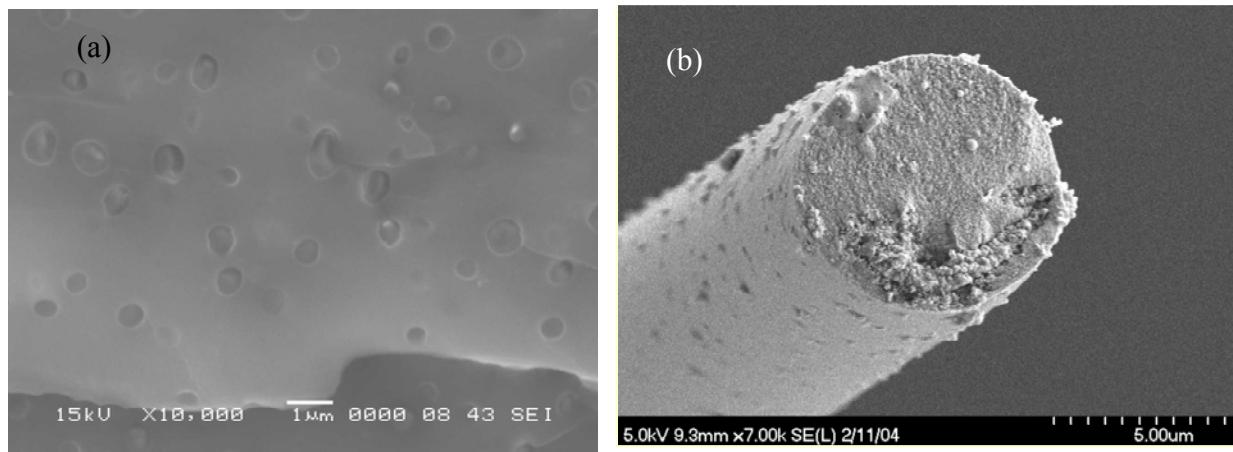
Figure 19. SEM photographs showing images of (a) microphase toughened epoxy and (b) graphitized carbon fiber.

Tensile testing using an MTI Phoenix instrument is being conducted using ASTM D 2101 standards for single-filament testing. The properties of these fibers are being compared to that of commercial carbon fibers, such as AS4, IM7, and pitch-based fibers. The effects of reaction conditions on these properties are being correlated with the fiber production method to determine optimum processing conditions. Thus, the role of precursor chemical structure on the properties of the resulting carbon fibers is being systematically assessed.

1.5   Task 2: Biobased Thermosetting Resins

1.5.1 Subtask 2.1: Preparation of Biobased Monomers

Biobased monomers are being prepared from multiple renewable resources, including starch, cellulose, and lignin. Figure 20 shows selected chemical routes to produce monomers from lignin. The cyclic and aromatic structures that can be derived from these renewable resources are ideal for the manufacture of high-performance resins. Model lignin components, such as trans-conipheryl, trans-sinapyl, and trans-p-coumaryl alcohols (*34*), are being used to make aromatic diluents and cross-linkers (figure 20). The lignin components have one phenyl alcohol and one primary alcohol. As a result, the reactivities of these hydroxyl groups are quite different (*35*), allowing the primary alcohol to be functionalized with one chemical group, while the phenyl hydroxyl can be functionalized with another chemical group. In particular, the primary hydroxyl can be converted to an aliphatic ester while leaving the phenyl hydroxyl essentially unreacted using the following methods:

1. Reaction of the hydroxyl group with acetic anhydride at 98 °C for ~2 h (*35*).

Cross-linking monomers based on lignin are more easily prepared in that they simply use the diol lignin-precursor.

21
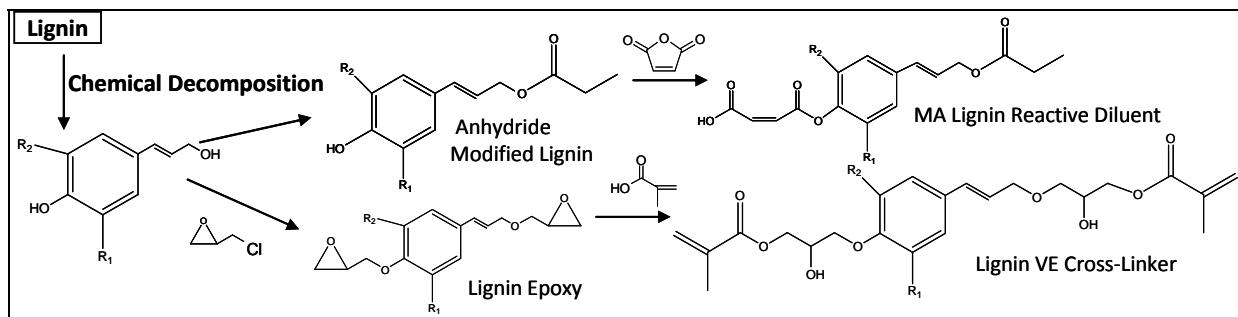
Figure 20. Selected schemes for preparing lignin-based monomers.

The hydroxyl functionality of mono- and di-hydroxyl lignin derivatives is being used to produce di-epoxies, VEs, UPE cross-linkers, and monofunctional reactive diluents (figure 7). This is being accomplished by four methods:

2. Reaction of the hydroxyl groups with a stoichiometric amount of epichlorohydrin at 70 °C, using acid catalysts to yield epoxy functional monomers (*21*).

3. Reaction of the epoxy functional monomers with a 3% stoichiometric excess of methacrylic acid at 90 °C for 3–6 h to yield a VE monomer (*21*, *23*). A secondary hydroxyl group will be added to the structure for each vinyl group added.

4. Reaction of the hydroxyl groups with a stoichiometric amount of methacryloyl chloride at 40 °C for 1 h to yield a vinyl functional monomer with no added hydroxyl groups (*35*).

5. Reaction of the hydroxyl groups with MA at ~80 °C for 3–4 h to yield maleate half-esters/UPEs (*36*).

Method 2 will be used to prepare di-epoxides, which will be the basis of biobased epoxy resins. Monofunctional epoxies will be prepared only to be methacrylated and used as a reactive diluent (method 3). Di-vinyl cross-linkers species will be produced from di-epoxides using method 3. The use of methacryloyl chloride to produce vinyl monomers (method 4) has advantages and drawbacks relative to the methacrylation of epoxy method (method 3). Method 4 allows for a higher renewable content and is accomplished in one reaction step instead of two. However, methacryloyl chloride is more expensive than epichlorohydrin and methacrylic acid.

UPEs generally do not perform as well as VE resins because they contain a distribution of unsaturation, with many molecules containing only one or even zero unsaturation sites, resulting in lower thermal and mechanical properties (*21*). These lignin-based UPE monomers, on the other hand, have either one unsaturation site per molecule and are potential reactive diluents or have two unsaturation sites per monomer and are cross-linkers. This could result in excellent properties relative to commercial UPE resins. The renewable content of the UPE monomers are extremely high, as MA is commercially produced from biological sources.

22

Lignin-derived chemicals from the chemical/thermal cracking process are being used to make aromatic monomers. This process is similar to the chemical/thermal process described in subtask 1.1, but the target molecules are much smaller in size. Therefore, longer residence times and higher temperatures are likely to be necessary.

Monomers are also being prepared from carbohydrates, cellulose, and hemicellulose. One requirement is that the monomer must possess a cyclic structure in order to provide stiffness to the resulting polymer backbone. For hexoses, we are using two major base molecules. The first is isosorbide, which is derived from sorbitol that is in turn derived from glucose (*37*). The second is 5-hydroxymethylfurfural (HMF) obtained from a variety of hexoses from starch and cellulose (*37*). Isosorbide has a bicyclic five-member ring structure with two hydroxyl groups, and HMF has a single five-member ring structure with a primary alcohol and an aldehyde group. For pentoses, the major platform molecule that is being used is furfural, which contains an aldehyde group and is produced from cellulose and starch. Furfuryl alcohol, furfuryl amine, and furoic acid are derived from furfural and are commercially available.

Figure 21 shows selected schemes for producing biobased monomers from hexoses and pentoses. Reaction methods 2–5 are being used to produce monomers from these starting biobased chemicals. Isosorbide is being used to produce di-epoxides, vinyl cross-linkers, and di-unsaturated polyesters. An additional means of producing di-epoxides and methacrylates can be realized with isosorbide and are described in the following methods:

6. Elimination of water from isosorbide with sulfuric acid at elevated temperatures above 120 °C to yield secondary unsaturations (*35*).

7. Epoxidation of the unsaturation sites in scheme 6 using peracetic acid or performic acid at 50 °C for 12 h to yield difunctional secondary epoxides (*38*).
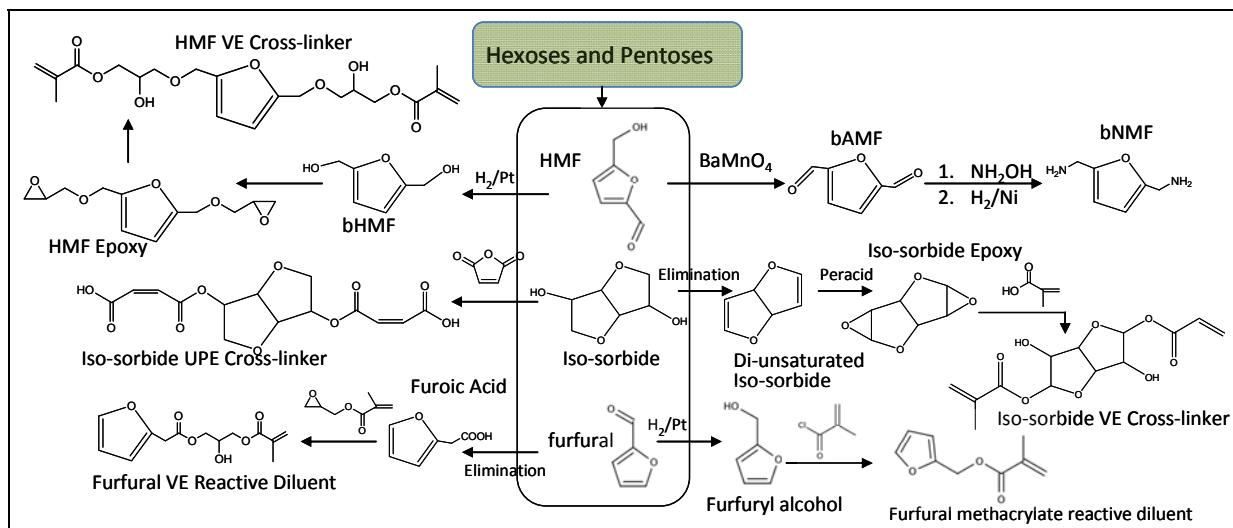
Figure 21. Schemes for preparing biobased monomers from hexoses and pentoses.

The unsaturation sites resulting from water elimination from isosorbide may readily polymerize as a result of the destabilizing effect of the oxygen atoms within the ring structure, and thus this molecule could potentially be used as a cross-linker. The secondary epoxides produced by reaction with a per-acid have low reactivity and thus may not produce good epoxy resins. However, the epoxy groups can be converted to VE groups using method 3.

The use of HMF and furfural are also being examined to produce monomers. To do this, these chemicals are first converted to other precursors using the following reaction methods:

8. Hydrogenation of the aldehyde over platinum catalyst to yield a hydroxyl group (*35*) converts HMF to 2,5-bis(hydroxymethyl) furan (bHMF) and furfural to furfuryl alcohol.

9. Conversion of the hydroxyl group to an aldehyde using barium manganate converts HMF to 2,5-bis(aldehydemethyl)furan (bAMF) (*35*).

10. Conversion of the aldehyde group to an amine by reaction with ammonium hydroxide followed by hydrogenation over nickel catalyst (*35*) converts bAMF to 2,5-bis(aminomethyl)furan (bNMF) and furfural to furfuryl amine.

11. Conversion of the aldehyde group to a carboxylic acid by oxidation of bAMF using silver oxide, and sodium hydroxide (*35*) converts bAMF to 2,5-furandicarboxylic acid and furfural to furoic acid.

bHMF is being converted to di-epoxides (method 2), difunctional VEs (method 3), dimethacrylates (method 4), and UPEs (method 5). bNMF should act as a stiff hardener for epoxy resins because it contains two primary amines and a rigid cyclic core. Carboxylic acid functionality is being converted to monomers using the following method:

12. Addition of a carboxylic acid to the epoxide of glycidyl methacrylate at 50 °C for 16 h using AMC-2 catalyst will produce a VE functional monomer (*1*).

Using method 12 should convert 2,5-furandicarboxylic acid to a divinyl cross-linker.

Reactive diluents are being produced using the same reaction schemes as listed here, but with judicious choice of the biologically derived starting chemical. Furfuryl alcohol is being converted to the reactive diluents furfuryl VE (methods 2 and 3), furfuryl methacrylate (FM) (method 4), and furfuryl maleate (method 5). Furfuryl amine would act as chain extender in epoxy resins. Furoic acid can be converted to a vinyl reactive diluent using method 12. HMF can also be used to prepare reactive diluents, as the aldehyde functionality will remain intact during the formation of a monofunctional VE (methods 2 and 3), methacrylate (method 4), and maleate (method 5). In addition, methods 11 and 12 can be used to prepare a distinct monofunctional VE reactive diluent.

Chitin (figure 22) is a linear biopolymer whose commercial source is primarily crustacean shells and insect exoskeletons. In nature, chitin is second only to cellulose in abundance but trails
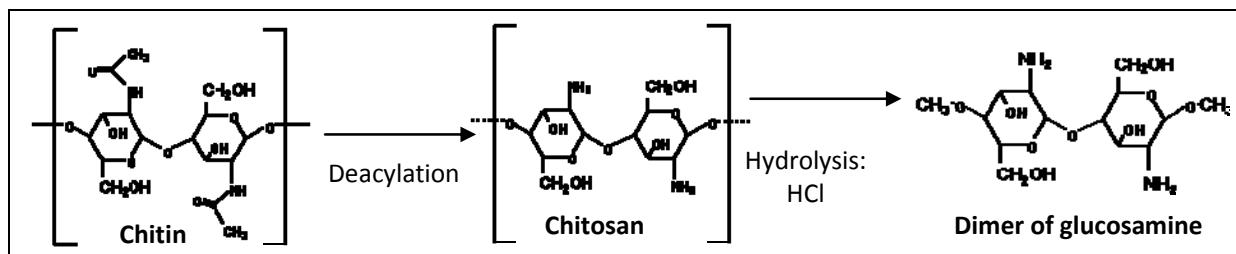
Figure 22. Preparation of dimers from chitin-based hardeners for epoxy resins.

cellulose in commercial products by a wide margin (*39*). The amine groups on chitosan, the deacetylated form of chitin (figure 22), make it a candidate to be used as a biobased amine hardener. Since chitin's and chitosan's molecular weights can reach 10^6 g/mol (*39*), selective hydrolysis will be required to reduce the molecular weight of the chitosan while retaining the desirable amine functionality. Hydrolysis of chitosan can occur in concentrated acids, often hydrochloric (*40*). The exact conditions and duration necessary will depend on the initial and targeted molecular weight. Remaining hydroxyl groups will likely need to be end-capped by reaction with short-chain anhydrides to reduce water uptake using figure 19. To simplify things initially, a single repeat unit of chitosan, a dimer of glucosamine, will be used as a model compound for preparation of biobased hardeners for epoxies. The glucosamine dimer is very similar in structure and chemical functionality to commercial amine hardeners, such as Amicure PACM or 2,2'-Dimethyl-4,4'-methylenebis(cyclohexylamine) (figure 7).

Hybrid molecules containing multiple renewable resources could also be used. For example, alcoholysis of triglycerides with the hydroxyl groups on sucrose, isosorbide, or the lignin-derived structures (e.g., trans-conipheryl) will yield carbohydrate/lipid or lignin/lipid hybrids. The unsaturation sites on the fatty acid can then be methacrylated to yield vinyl functional monomers (*1*).

1.5.2 Subtask 2.2: Chemical Analysis of Biobased Chemicals

FTIR (figure 11) is being used to determine the structure of the resulting biobased chemicals that are prepared synthetically. During the reaction of epichlorohydrin with hydroxyl functional molecules, the disappearance of hydroxyl groups and appearance of epoxy groups can be tracked by monitoring the peaks at ~3500 and 910 cm^{-1}, respectively (*29*). Methacrylation of epoxy functionality can be measured by tracking the disappearance of epoxy functionality and monitoring the appearance of methacrylate functionality at 942 cm^{-1}. Reaction of glycidyl methacrylate with carboxylic acid functionality can be monitored through disappearance of the epoxy group, and the reaction of MA with hydroxyl functional groups by the disappearance of the anhydride ring structure at 1850 cm^{-1} (*29*). NMR (figure 12) is being used to determine the molar content of functionality and the chemical content of any side-products. Epoxy groups typically appear at 2.8–3.5 ppm (*30*). Vinyl groups typically appear at 5.0–6.5 ppm, maleate groups at 6.3 and 6.8 ppm, while unreacted MA appears at 7.1 ppm (*30*). SEC (figure 13) is

being used to measure the molecular weight of the biobased monomers. Knowledge of the molecular weight of the monomers will allow us to determine whether addition or decomposition reactions took place. Addition reactions, such as the reaction of epichlorohydrin and furfuryl alcohol, result in higher molecular weight species, while decomposition of lignin and chitin can be observed by measuring the molecular weights and distribution of molecular weights.

1.5.3 Subtask 2.3: Resin Preparation and Cure Analysis

Biobased monomers are being mixed to form biobased resins. Epoxy resins contain di-epoxides and di-amine curing agents. Biobased epoxy monomers are being mixed with one-half the stoichiometric amount of a commercial diamine (Amicure PACM) and the biobased diamines. Biobased diamines will also be blended with twice the stoichiometric amount of commercial epoxy monomers, such as Epon 828, diglycidyl ether of bisphenol A. Vinyl resins contain a cross-linker and reactive diluent. Vinyl resins are being prepared by blending biobased cross-linkers with styrene and biobased reactive diluents. Biobased reactive diluents are also being blended with methacrylated Epon 828 VE monomers. Commercial petroleum-derived components are being used to determine benefits and problems associated with individual monomer components. However, the ultimate goal of this work is to develop completely biobased resins, where all components are derived from biobased chemicals.

In-situ FTIR is being used to determine the extent of cure (figure 11). Our setup allows us to heat samples while taking FTIR spectra as a function of time (*41*). This is important because resins with low extents of cure tend to be weak and have low ultimate properties. Our previous work has shown that we are able to track the extent of cure of individual components at various cure temperatures (*23*, *41*). Furthermore, FTIR can be used to determine reactivity ratios to determine the composition of the curing polymer and aspects of the microstructure, such as the presence and size of microgels (*22*).

Monomer viscosity and rheology are being measured using a rheometer to determine whether flow is Newtonian (shear thinning) and to determine the Newtonian viscosity (figure 23). Low-viscosity Newtonian resins are desired for most composite applications. Simple steady-state shear flow experiments at room temperature (with temperature stabilization) are used to measure component and resin rheology (*1*). Biobased component rheology does not need to match the monomer component it is targeted to replace. However, the biobased resin viscosity should be within 10% of the targeted replacement resin. In addition, the effect of chemical functionality and chemical structure as measured in subtask 2.2 on the rheology of biobased monomers is being determined.
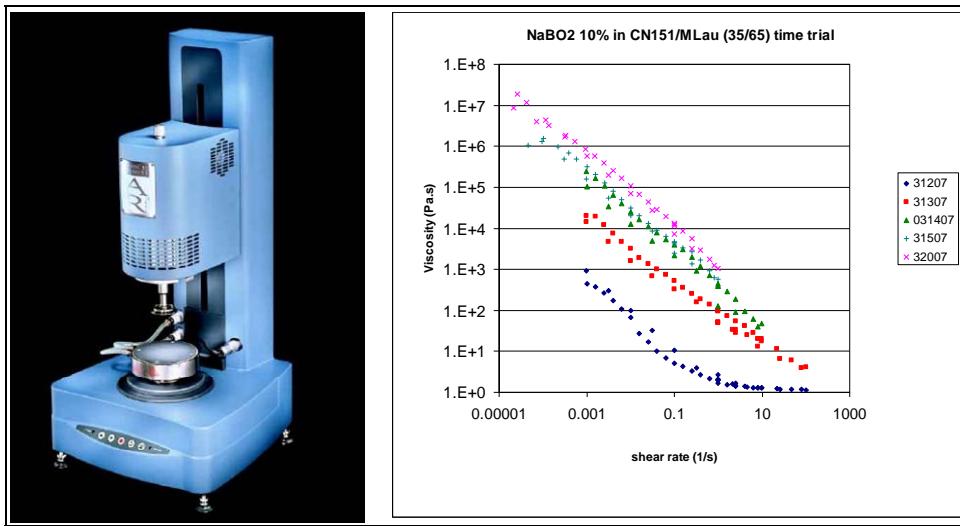
Figure 23. AR2000 rheometer and viscosity data as a function of shear rate for resins and shear thinning fluids.

1.5.4 Subtask 2.4: Polymer Properties

Dynamic mechanical analysis (DMA) using a TA Instruments Q800 is being used to determine thermomechanical properties of the resulting polymers (figure 24). Polymer samples will be prepared with nominal dimensions of $3 \times 10 \times 60$ mm. T_g, modulus, and cross-link density as a function of temperature will be measured from the viscoelastic response of the material at a strain of 7.5 µm, at 1 Hz, from room temperature to 200 °C at 2 °C/min. This will be a screening tool allowing us to determine whether the biobased resins produce T_g over 120 °C and moduli over 2 GPa. Cross-link density will be measured from the rubbery modulus and Rubber Elasticity Theory (*42*, *43*). Knowledge of the cross-link density will allow us to determine whether an efficient cure has occurred, or if highly cyclized structures have been produced.
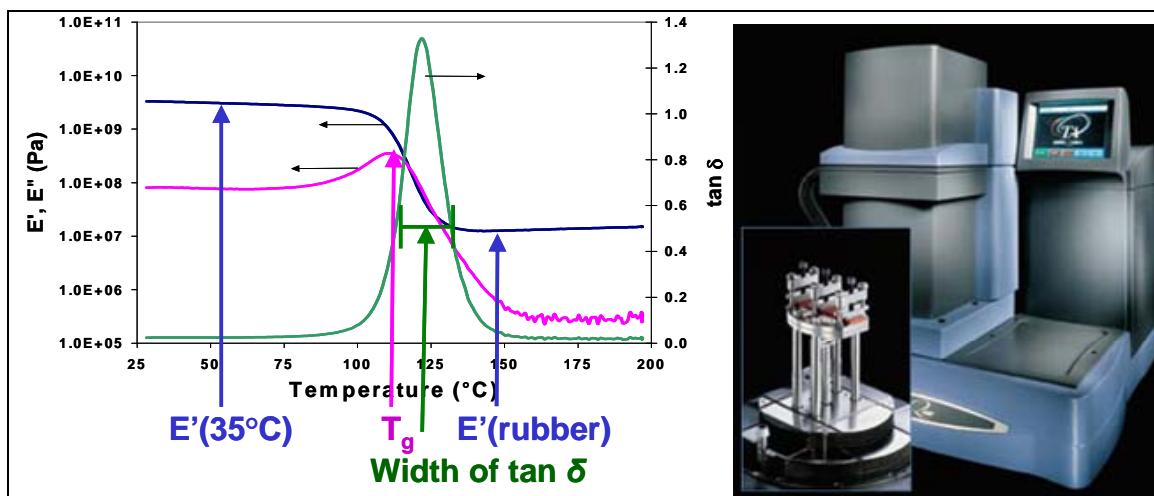
Figure 24. Q800 DMA and representative results showing storage modulus, loss modulus, and tan delta as a function of temperature and how T_g, glass transition width, glassy modulus, and rubber modulus are determined.

27

Instron mechanical testing is being used to assess the ultimate polymer properties. Mechanical testing will be performed according to ASTM standards. Flexural strength, modulus, and strain are being measured according to ASTM D 790 by testing samples with approximate dimensions of $3 \times 25 \times 80$ mm. Fracture toughness is being measured according to ASTM D 5045 using single-edge notch bend specimens. Good polymer samples have strength, modulus, and toughness of >100 MPa, >2 GPa, and >100 J/m^2, respectively.

SEM is being used to examine the morphology of fracture surfaces to correlate this with fracture behavior. It is entirely possible that some biobased monomers will form microphases during cure because of a thermodynamic tendency to segregate. Microphases typically result in toughening by disrupting crack growth. Larger macroscale segregation, which would also be visible with SEM, could cause a reduction in fracture properties because of poor component compatibility and connectivity.

1.6 Task 3: Testing and Analysis of Biobased Composites

Composites will be prepared using the biobased monomers and biobased carbon fibers. Vacuum-assisted resin transfer molding (VARTM) will be used to prepare composites. Initially, unidirectional AS4 or IM7 carbon fibers will be infused with biobased resins. These composites will be compared to composites prepared using the same fibers with commercially available resins. Biobased carbon fibers will be prepared into unidirectional mats. These mats will be infused with commercially available epoxy resin. Again, these will be compared to composites prepared using commercial AS4 and IM7 fibers. Composites containing both bioderived carbon fiber reinforcement and bioderived resins will be prepared. Mechanical properties of these composites, including strength, modulus, and short beam shear strength, will be tested according to ASTM standards. Lastly, SEM will be used to examine failure and to compare the biobased composites to the standard composites. The quality of fiber-matrix adhesion can be simply viewed using SEM, and the observed energy fracture mechanisms, like fiber-pullout rather than simple fiber cleavage, will be used to understand the composite fracture strength and toughness.

As a major aspect of the transition plan, optimum biobased composites will be transitioned to the user community. The Advanced Composites Office at Hill Air Force Base will make replacement parts for a jet fuselage as demonstration pieces using biobased VE/carbon fiber and to assess processability and qualitatively assess composite properties. Naval Surface Warfare Center Carderock Division will prepare small biobased epoxy/carbon panels to assess their use on ships, such as the M80 Stiletto. We will leverage the University of Delaware Center for Composite Materials (CCM) Composite Parts Replacement Program for Tactical Vehicles and subcontract Sioux Manufacturing Corporation to manufacture an M939 composite hood using the optimum biobased epoxy and standard E-glass reinforcement. Lastly, ARL will leverage the Future Combat Systems program and assess the optimum biobased resins and carbon fibers for use in composite armor.

1.7 Task 4: Environmental and Life Cycle Analysis

The environmental impact from this program is being determined by the reduction in HAP emissions and in the carbon footprint. Reactive diluents to replace styrene in VE and UPE resins could eliminate the production of HAPs in DOD composite manufacture. Volatile organic compound (VOC)/HAP reductions should reduce costs by eliminating the need for add-on devices to capture fugitive emissions from the fabrication process. The percentage of biobased components used in each resin formulation will eliminate pound for pound of carbon footprint.

An estimate of the costs of the biobased fibers relative to the current process is being determined. In addition, per-pound cost of the biobased resins will be compared to that of analogous commercial resins. Cost savings associated with environmental benefits are being factored into the life cycle analysis. Along with leveraged resources, we are calculating the environmental and cost savings of switching to candidate environmentally friendly systems. The cost of materials and waste stream management is being examined to determine cost savings.

1.8 Technical Objectives and Project Goals

The goal of this work is to use renewable resources derived from plants and other sources to prepare high-performance carbon fiber and thermosetting matrix resins with high strength and high thermal resistance. The scientific objectives of this work are to (1) develop methods for breaking down, modifying, and processing renewable resources to make epoxy resins, vinyl resins, and carbon fibers and (2) determine structure-property relationships for these novel materials.

There are a number of specific project areas and goals for each of these areas:

- Microbial degradation of lignin

    ○ Demonstrate that microbial degradation of lignin is feasible for producing carbon fiber precursors.

    ○ Identify optimum bacteria for decomposition of lignin.

    ○ Produce microbially degraded lignin at a small to moderate scale.

    ○ Perform life cycle cost analysis for production of microbially degraded lignin as carbon fiber precursors relative to PAN.

- Chemical modification/degradation/fractionation of lignin

    ○ Identify optimum chemical methods to obtain lignin-based carbon fiber precursors.

    ○ Produce chemically modified lignin at small to moderate scale.

- Lignin-based carbon fiber development

- ○ Identify modified lignin samples with optimum rheological properties for fiber spinning.

- ○ Identify modified lignin samples that can be stabilized to prevent fusion of fibers during carbonization.

- ○ Identify modified lignin samples that can be used to produce carbon fibers with high modulus and high strength.

- ○ Produce high-performance carbon fiber at small to moderate scale.

- ○ Perform life cycle cost analysis for production of chemically modified lignin as carbon fiber precursors relative to PAN.

- • High-performance biobased resins

  - ○ Identify biobased epoxy, polyamine, UPE, and VE cross-linkers that produce $T_g >$ 150 °C when used in conjunction with standard resin components or other biobased components.

  - ○ Identify biobased reactive diluents for UPE and VE resins that produce T_g no less than 10 °C lower than that of styrene-based resins.

  - ○ Produce optimum biobased resins at 250-g scale for composite production. Perform life cycle cost analysis for biobased resins relative to comparable epoxies, UPEs, and VE resins.

- • High-performance biobased composites

  - ○ Demonstrate composite production using biobased carbon fiber and biobased resins.

  - ○ Develop biobased composites with properties similar to that of comparable nonbiobased composites.

Each of these goals is expected to be met during the course of this project. The timelines for these accomplishments are discussed in the summary and conclusions.

1.9 Project Team

We have assembled a cooperative team, as shown in table 4, with extensive experience in resin formulation, fiber preparation, mechanical testing, and composite manufacture. The U.S. Army Research Laboratory (ARL) team has exceptional experience with composite materials and reducing environmental hazards associated with military coatings (SERDP PP-1056 and Environmental Security Technology Certification Program [ESTCP] 200024) and resins (SERDP PP-1109, PP-1271, and ESTCP WP-0617 along with Drexel University). John J. La Scala, Chief, Coatings, Corrosion, and Engineered Polymers Branch at ARL, is the PI for this project. He received a Ph.D. in chemical engineering from the University of Delaware and has

Table 4. Biobased resins and fibers team.

Organization	Team Members	Activities
ARL	Dr. J. J. La Scala Dr. J. Sadler Ms. P. Lam (M.S. student) Ms. F. Toulan	Biobased monomer preparation and chemical analysis, monomer and resin viscosity, polymer properties, composite properties, environmental and cost assessment
Clemson University	Dr. A. Ogale (co-PI) Ms. M. Zhang (Ph.D. student) Dr. A. Greene Dr. A. Bodine Mr. Steven Chambers	Lignin microbial breakdown, oligomer chemical and rheological analysis, melt spinning, UV stabilization, carbonization, graphitization, fiber mechanical properties, fiber characterization, composite properties
Drexel University	Dr. G. R. Palmese (Co-PI) Dr. D. Koo	Hexoses and pentoses biobased monomer preparation and chemical analysis, monomer and resin viscosity, polymer properties, composite properties
University of Delaware	Dr. R. P. Wool (Co-PI) Mr. J. Stanzione (Ph.D. student)	Lignin chemical/thermal decomposition, lignin-based monomers preparation and chemical analysis, monomer and resin viscosity, polymer properties, composite properties.

over 10 years experience in composite materials and materials from renewable sources. He was the PI for ESTCP WP-0617, which was awarded the ESTCP WP 2010 Project of the Year. He was lead scientist for SERDP WP-1271, which was also awarded SERDP WP Project of the Year. Dr. Joshua Sadler is a postdoctoral researcher at ARL with a Ph.D. in synthetic organic chemistry. Using that expertise, he is the lead synthetic chemist in this project. Ms. Phuong Lam is a contractor at ARL and an M.S. student in Chemical and Biological Engineering at Drexel University. Her role is to formulate and test VE resins. Ms. F. Toulan has an associate's degree in chemistry and years of experience in formulating adhesives. Her current role in this project is to formulate and test UPE resins.

The Drexel team also has extensive experience with polymeric resins and composite materials and was corecipient for the ESTCP and SERDP Project of the Year awards. Giuseppe Palmese is the department head of the Chemical and Biological Engineering Department at Drexel University and has 20 years experience in composite materials and over 10 years experience in materials from renewable sources. Dr. Donghun Koo is a postdoctoral researcher in chemical and biological engineering and is responsible for preparing isosorbide-based UPEs and furan-based epoxies.

Richard Wool is a professor of chemical engineering and a member of the CCM. He runs the Affordable Composites from REnewable Sources (ACRES) group, which has been at the forefront of developing biobased composite materials over the past 14 years. Mr. Joseph Stanzione is a Ph.D. student in chemical engineering and is responsible for chemical modification of lignin and lignin-based thermosetting resins.

At Clemson University, Amod Ogale (professor, chemical engineering) serves as the deputy director for the CAEFF, the only National Science Foundation Engineering Research Center on fibers. He has over 20 years of research experience with advanced composites and leads

CAEFF's effort on high-performance carbon fibers derived from alternative precursors. Ms. M. Zhang, a Ph.D. student in chemical engineering, is responsible for developing lignin-based carbon fibers. Annel Greene (professor, animal and veterinary sciences) serves as the director of Animal Coproducts Research Center, dedicated to the ecofriendly use of biobased coproducts. She is responsible for the microbial degradation of lignin.

References

1. La Scala, J. J.; Sands, J. M.; Orlicki, J. A.; Robinette, E. J.; Palmese, G. R. *Polymer* **2004**, *45*, 7729–7737.

2. Khot, S. N.; La Scala, J. J.; Can, E.; Morye, S. S. Williams, G. I.; Palmese, G. R. Kusefoglu, S. H.; Wool, R. P. *J. Applied Polym. Sci.* **2001**, *82*, 703–723.

3. Pilato, L.; Michno, M. *Advanced Composite Materials*; Springer: New York, 1994.

4. Quilter, A. Composites in Aerospace Applications, IHS White Paper, 2004.

5. Ackerman, R. Stiletto Cuts a Swatch to New Navy Technologies. *Signal* March 2006.

6. Potter, P. *Amptiac* **2003**, *7*, 37–40.

7. Griffiths, B. *Composites Tech.* **August 2006**, *12* (4), 60–62.

8. AGY. Product Specification Sheet for S-2 Glass Fiber; Aiken, SC, 2004.

9. Hexcel Corporation. Product Specification Sheet for Magnamite AS4C Carbon Fiber; Stamford, CT, 2002.

10. Hexcel Corporation. Product Specification Sheet for Magnamite IM7 (5000) Carbon Fiber; Stamford, CT, 2002.

11. Fitzer, E.; Manocha, L. M. *Carbon Reinforcements and Carbon/Carbon Composites*; Springer-Verlag Publishers: Berlin, 1998.

12. Buckley, J. D.; Edie, D. D. *Carbon-Carbon Materials and Composites*; Noyes Publications: Park Ridge, NJ, 1993.

13. Mukundan, T.; Bhanu, V. A.; Wiles, K. B.; Johnson, H.; Bortner, M.; Baird, D. G.; Naskar, A. K.; Ogale, A. A.; Edie, D. D.; McGrath, J. E. *Polymer* **2006**, *47*, 4163–4171.

14. Paiva, M. C.; Kotasthane, P.; Edie, D. D.; Ogale, A. A. *Carbon* **2003**, *41*, 1399–1409.

15. Naskar, A. K.; Walker, R. A.; Proulx, S.; Edie, D. D.; Ogale, A. A. *Carbon* **2005**, *43*, 1065–1072.

16. Traceski, F. T. Assessing Industrial Capabilities for Carbon Fiber Production. *Acquisition Review Quarterly* Spring 1999, 179–194.

17. Warren, C. D. *Future Low Cost Carbon Fiber for Autos: International Scale-Up and What is Needed*; Oak Ridge National Laboratory: Oak Ridge, TN, September 2008.

18. Fowler, P.; Hughes, J. M.; Elias, R. *J. Science Food Agriculture* **2006**, *86*, 1781–1789.

19. Kvien, I.; Oksman, K. *Applied Physics A* **2007**, *87*, 641–643.

20. Pascault, J. P.; Sautereau, H.; Verdu, J.; Williams, R. J. J. *Thermosetting Polymers*; Marcel Dekker: New York, 2002.

21. Malik, M.; Choudhary, V.; Varma, I. K. *Rev. Macromol. Chem. Phys.* **2000**, *C40***,** 139–165.

22. Ziaee, S.; Palmese, G. R. *J. Polym. Sci. B: Polym. Phys.* **1999**, *37***,** 725–744.

23. La Scala, J. J.; Orlicki, J. A.; Winston, C.; Robinette, E. J.; Sands, J. M.; Palmese, G. R. *Polymer* **2005**, *46*, 2908–2921.

24. Sanderman, H., Jr.; Scheel, D.; Trenck, T. V. D. Metabolism of Environmental Chemicals by Plants – Copolymerization Into Lignin. In *Proceedings of the Ninth Cellulose Conference*, *Part I*; Sarko, A., Ed.; John Wiley & Sons, Inc.: New York, 1983.

25. Lee, Y. Y.; Lee, B. H. Solvent-Phase Termal Cracking of Lignin for Production of Potential Liquid Fuels. *J. Industrial Eng Chemistry* **1998**, *4*, 334–339.

26. Xiang, Q.; Lee, Y. Y. *Applied Biochemistry and Biotechnology* **2000**, *84–86*, 153–162.

27. Greene, A. K. Biodegradation of Lignin by Mutants of *Erwinia* spp. Master of Science Thesis, Louisiana State University, Baton Rouge, LA, 1985.

28. Axegard, P. STFI-Packforsk AB. *Forest Based Sector Technology Platform Conference*, Lahti, Finland, 22–23 November 2006.

29. Pouchert, C. J., Ed. *The Aldrich Library of Infrared Spectra*, 3rd ed.; Aldrich Chemical Co.: Milwaukee, WI, 1981.

30. Pouchert, C. J., Ed. *Aldrich Library of NMR Spectra*, Vols. 1 and 2; Aldrich Chemical Co.: Milwaukee, WI, 1983.

31. Garcia, A. A.; Bonen, M. R.; Ramirez-Vick, J.; Sadaka, M.; Vuppu, A. *Bioseparation Process Science*; Blackwell Science: Malden, MA, 1999; pp 181–183.

32. Kundu, S.; Grecov, D.; Ogale, A. A.; Rey, A. D. Shear Flow Induced Microstructure of a Synthetic Mesophase Pitch. *J. Rheology* **2009**, *53* (10), 85–113.

33. Gupta, A.; Ogale, A. A. *Polymer Composites* **2002**, *23* (6), 1162–1170.

34. Thielemans, W.; Wool, R. P. *Biomacromolecules* **2005**, *6***,** 1895–1905.

35. Carey, F. A. *Organic Chemistry*, 2nd ed.; McGraw-Hill: New York, 1992.

36. Lu, J.; Khot, S.; Wool, R. *Polymer* **2005**, *46*, 71–80.

37. Kamm, B. *Biorefineries – Industrial Processes and Products: Status Quo and Future Directions*; Gruber, P. R., Kamm, M., Eds.; Wiley-VCH: Weinheim, Germany, 2006.

38. La Scala, J. J.; Wool, R. P. *J. Am. Oil. Chem. Soc.* **2002**, *79*, 59–63.

39. Dumitriu, S. *Polysaccharides: Structural Diversity and Functional Versatility*, 2nd ed.; CRC Press: Boca Raton, FL, 2004.

40. Rupley, J. A. *Biochimica et Biophysica Acta* **1964**, *83*, 245–255.

41. Brill, R. P.; Palmese, G. R. *J. Appl. Polym. Sci.* **2000**, *76*, 1572–1582.

42. Palmese, G. R.; McCullough, R. L. *J. Appl. Polym. Sci.* **1992**, *46* (10), 1863–1873.

43. Flory, P. J. *Principles of Polymer Chemistry*; Cornell University Press: Ithica, NY, 1953, pp 432–493.

2. Microbial Degradation of Lignin: Seeking New Bacterial Species to Selectively Break Lignin Bonds for Making Advanced Carbon Fibers

2.1 Introduction

Lignin, the polyaromatic encrusting material in plants, is the second most abundant organic compound on Earth after cellulose. This complex aromatic biopolymer has properties that make it attractive for use in manufacture of carbon fibers. However, it is important to break the large molecule into smaller subunits for carbon fiber formation. Chemical methods of breaking lignin lack specificity, which can lead to a wide variety of breakdown products. Use of a more specified method of lignin breakdown, such as is available by the microbial world, could yield improved carbon fiber manufacture. However, isolating and culturing microorganisms capable of degrading lignin are difficult challenges.

2.2 Background

Lignin consists of three primary building blocks: *p*-coumaryl alcohol (*p*-hydroxyphenyl propanol), coniferyl alcohol (guaiacyl propanol), and sinapyl alcohol (syringyl propanol) (figure 25).
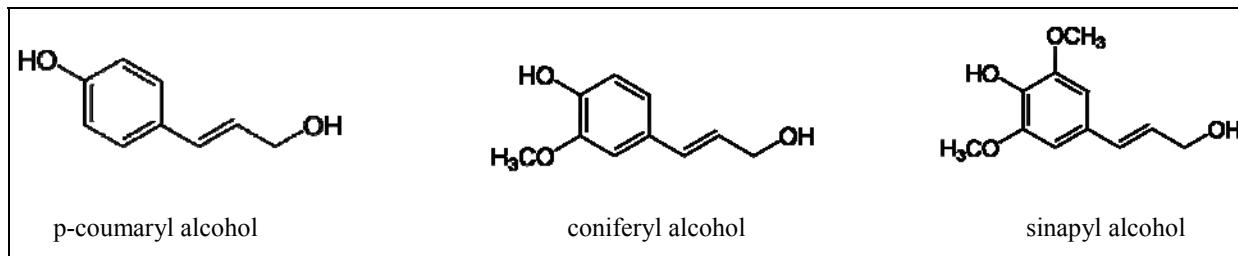
Figure 25. The primary building blocks of lignin: *p*-coumaryl alcohol, coniferyl alcohol, and sinapyl alcohol.

The compositions of lignins vary according to plant species with coniferyl alcohol being the primary subunit in softwood lignin. Similar chemical linkages are found in all species of lignin. In softwood, β-aryl ether linkages account for approximately 40% of the linkages within the lignin. Other linkages such as esterification of terminal hydroxyl groups of propyl side chains with p-coumaric acid constitute ~5% to 10% of lignin bonds (figure 26) (*1*, *2*).
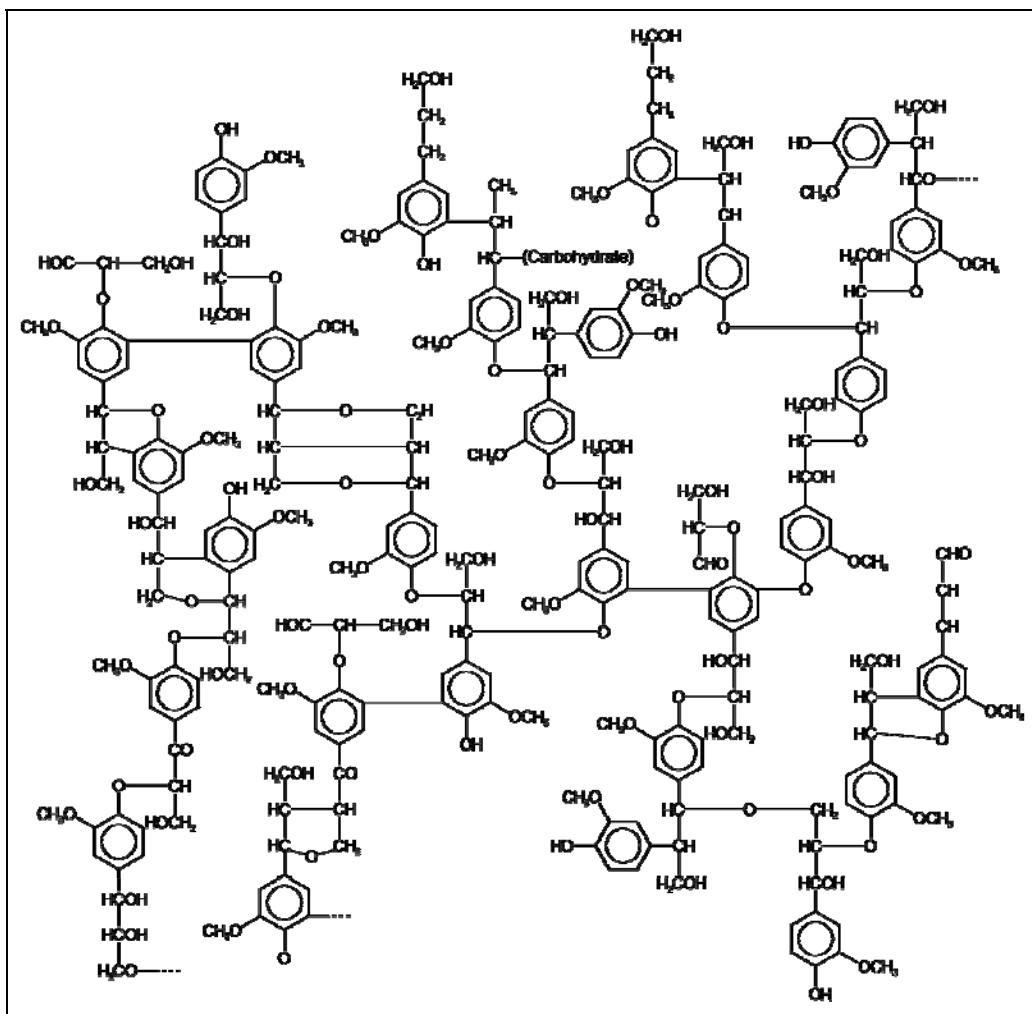
Figure 26. Typical softwood lignin molecule (*3*).

Because of the unique structural configuration of lignin, which is impossible to chemically synthesize, material scientists seek to study lignin as a starting material for developing green technology carbon fibers. However, because of the numerous linkages found within lignin, many of which would be susceptible during applied chemical attack, chemical degradation of the complex polymer could lead to a wide variety of breakdown products and/or could break the lignin into such small subunits that it would lose the chemical qualities which make it good for carbon fiber formation. Ideally, we desire a method of breaking the complex lignin matrix using a more targeted approach. Microbial degradation offers advantages of specificity. However, although microbial degradation of lignin has been long-studied, only a few species of bacteria that can degrade lignin have been identified.

Ligninolytic organisms use the chemicals in lignin for nutrition by breaking the large complex into smaller subunits. For many years, it was thought this task was relegated to only the fungi, but in the past few decades a limited number of lignolytic bacteria have been isolated. Since fungal degradation rates for lignin were slow, microbiologists hypothesized that more rapidly

growing bacteria probably account for a significant to major amount of the lignin breakdown that occurs in nature. However, microbiology is a relatively young science, with modern microbiology beginning in earnest with Louis Pasteur's 1862 experiments to disprove spontaneous generation. Although a few bacterial species that are capable of breaking lignin have been identified, it is believed that microbiologists have only just begun to understand the variety of species and capabilities of lignolytic bacteria. It has been estimated that there may be more than 4×10^{30} bacterial cells on Earth, and those prokaryotic organisms are believed to represent $>10^5$ to 10^7 unique species (*4*). In 1990, Torsvik et al. (*5*) determined that there were more than 4000 distinct species of bacteria in a single gram of soil. In 2002, Bach et al. (*6*) revised this to 10,000 distinct species of bacteria per gram of soil.

A saying often heard in the microbiological research community goes, "There is a bacterial species in the environment capable of breaking any compound." Each year thousands of new bacterial species are identified, but, as Sharma et al. (*7*) reported, more than 99% of all environmental samples contain bacteria that are "unculturable" simply because the proper conditions for their growth in the laboratory have not yet been deduced. Sharma et al. (*7*) also reported that these potentially valuable bacterial species remain "unexploited for biotechnical applications." The annual production of lignin from commercial separation (pulping) is estimated to be more than 50 million metric tons, and at least 500,000 metric tons (dry basis) of lignin products are generated annually (*8*, *9*). However, in nature there are many billions of metric tons of wood and wood products that are naturally degraded by the microbial world. With this huge volume of lignin deposited into bacteria-laden soils and similar environments, with the vast bacterial diversity on Earth and with the extensive ability of those bacteria to mutate to opportunistically take advantage of unique food sources, it is believed that there are potentially hundreds to thousands of unidentified bacterial species which can degrade lignin. Each unique species could have their own unique set of enzymes that could break the complex lignin molecule at specific linkages.

The purpose of this study is to investigate known bacterial species and to isolate new species of bacteria from the environment capable of degrading lignin. Researchers have spent the past many decades using traditional methods to isolate a few lignolytic bacterial species and then study each organism in detail. As such, only 10 lignolytic bacterial species have been reported (table 5).

There are a number of problems with these reported lignolytic bacteria. The first three in table 5 have slow growths and require low incubation temperatures. *Pseudomonas* fluorescens has potential and is used in this work to decompose lignin for carbon fiber formation. The next three and the last two require seawater for growth, which is rarely used in commercial industry because of the corrosivity and other issues. The one shown in green is not well characterized but does represent a possibility if a sample of the bacterial culture can be obtained.

Table 5. Reported lignolytic bacteria.

ATCC® Number	Description	Designation	
39115	*Streptomyces viridosporus* Pridham et al.	T7A	Low incubation temps/slow growth
39116	*Amycolatopsis* sp. deposited as *Streptomyces setonii* (Millard and Burr) Waksman	75iv2	
39117	*Streptomyces badius* (Kudrina) Pridham et al.	252	
49036	*Pseudomonas fluorescens* Migula	A1 [IFO 15839]	
700072	*Microbulbifer hydrolyticus* Gonzalez et al.	IRE-31	Requires seawater for growth
700073	*Sagittula stellata* Gonzalez et al.	E-37 [CIP 105237]	
700074	*Marinobacterium georgiense* Gonzalez et al. emend. Satomi et al.	KW-40	
BAA-396	*Sinorhizobium* sp. deposited as *Sinorhizobium termitidis*	M3A [DSM 10169]	Not much info on this organism
BAA-1142	*Sulfitobacter* sp.	EE-36	Requires seawater for growth
BAA-1142D-5	*Sulfitobacter* sp.	genomic DNA from strain EE-36 (ATCC BAA-1142)	

This study will be directed toward a broader approach of screening as many samples as possible for lignolytic organisms and then learning if these organisms can break lignin in different ways to assist in carbon fiber formation. This study will use a little-known and unique rapid screening method known as the chemostat isolation method. A lignolytic chemostat isolation method was developed by Dr. V. R. Srinivasan at Louisiana State University in the mid-1980s. The method allows rapid selection of organisms possessing certain attributes (such as lignin degradation) out of trillions of bacteria in an environmental sample. The chemostat isolation method is unique, and only a few of those students who studied in Dr. Srinivasan's laboratory are familiar with this unpublished technique. Currently, chemostat methodologies are most often used for generating large volumes of biomass, but only rarely are chemostat isolation methods used. As most microbiologists are now involved in molecular manipulation, there is little work being done in chemostat screening microorganisms for new isolates. Microbial continuous culture methods and kinetics, which provide the basis for understanding the chemostat isolation method, are now rarely taught, yet this information is of great value for rapidly screening populations of bacteria for specific traits.

This study is concentrated on isolating a library of new lignolytic organisms using the chemostat isolation method to separate potential strains from the trillions of bacterial species in environmental samples. After isolating potential bacterial species, we screen and characterize these organisms for lignolytic ability using thin layer chromatography to reveal the number of lignin subunits generated upon culturing under specific conditions. After characterization, we further screen lignolytic bacterial candidates to determine potential for carbon fiber formation from degraded lignin in the quest to find bacterial species that break lignin at the optimum site for best carbon fiber production. Once screening is completed, the best bacterial candidates will be used in scale-up studies for manufacturing carbon fibers.

2.3   Materials and Methods

2.3.1 Samples

Soil and humus samples were collected aseptically at various locations in Louisiana, Florida, Georgia, South Carolina, North Carolina, Tennessee, Maryland, and Delaware. Samples were transported to the laboratory under refrigeration.

2.3.2 Lignolytic Culture Isolation

Since the world population of bacteria is so immense (>10^{30} bacteria and more than 10^5 to 10^7 unique species), searching for a specific organism capable of breaking a specific molecule is a challenge. The traditional method for isolating such an organism involves plating billions and billions of cultures on solid microbial media in Petri dishes. However, this method is time consuming, costly, and often leads to failed results. A method of continuous culture chemostat isolation is a much more efficient preliminary screening method of searching through subsamples of the more than 10^{31} bacteria in the Earth's environment. In a chemostat isolation system, a liquid microbial media is prepared that contains only one carbon source. In seeking a lignolytic organism, the choice for sole carbon source is dependent on the many different linkages found within lignin, factoring in stereochemistry, unique bond strengths, and potential lethality to bacteria. In this study, the goal is to find organisms that can break one or more of the different linkages in lignin.

A bacterium will not produce a particular by-product if it is lethal to the bacterium because any organism that does so will kill itself. Therefore, noting the structure of lignin and surmising potential breakdown products, we find that the simplest sole carbon source for a chemostat used in the search for a lignolytic organism is methanol. Methanol is toxic to many organisms, but if a culture survives in the presence of methanol, then it is possible the organism may produce methanol as a by-product of lignin degradation. Other potential carbon sources are those compounds that contain similar linkages or that would be likely breakdown products of lignin degradation. All organisms require carbon for life. When a sole source of carbon is used in the only medium provided to bacteria, those organisms that survive and grow must either be able to use that carbonaceous compound for life-sustaining carbon or derive carbon from atmospheric

carbon (carbon dioxide). For this study, the search is for organisms that can use the sole carbon source provided.

In the chemostat (figures 27 and 28), a mixed culture of billions to trillions of bacteria is added to the vessel, and liquid media containing the sole carbon source is pumped into the vessel. Temperature and pH are controlled in the vessel. The flow rate of the liquid media is steadily increased. Those organisms capable of growing under the conditions and using the sole carbon source will multiply and increase in population size within the vessel. However, those organisms that are incapable of growing on the sole carbon source medium will not grow, their population will not increase, and they will be gradually washed out with continual dilution by the influx of new media.
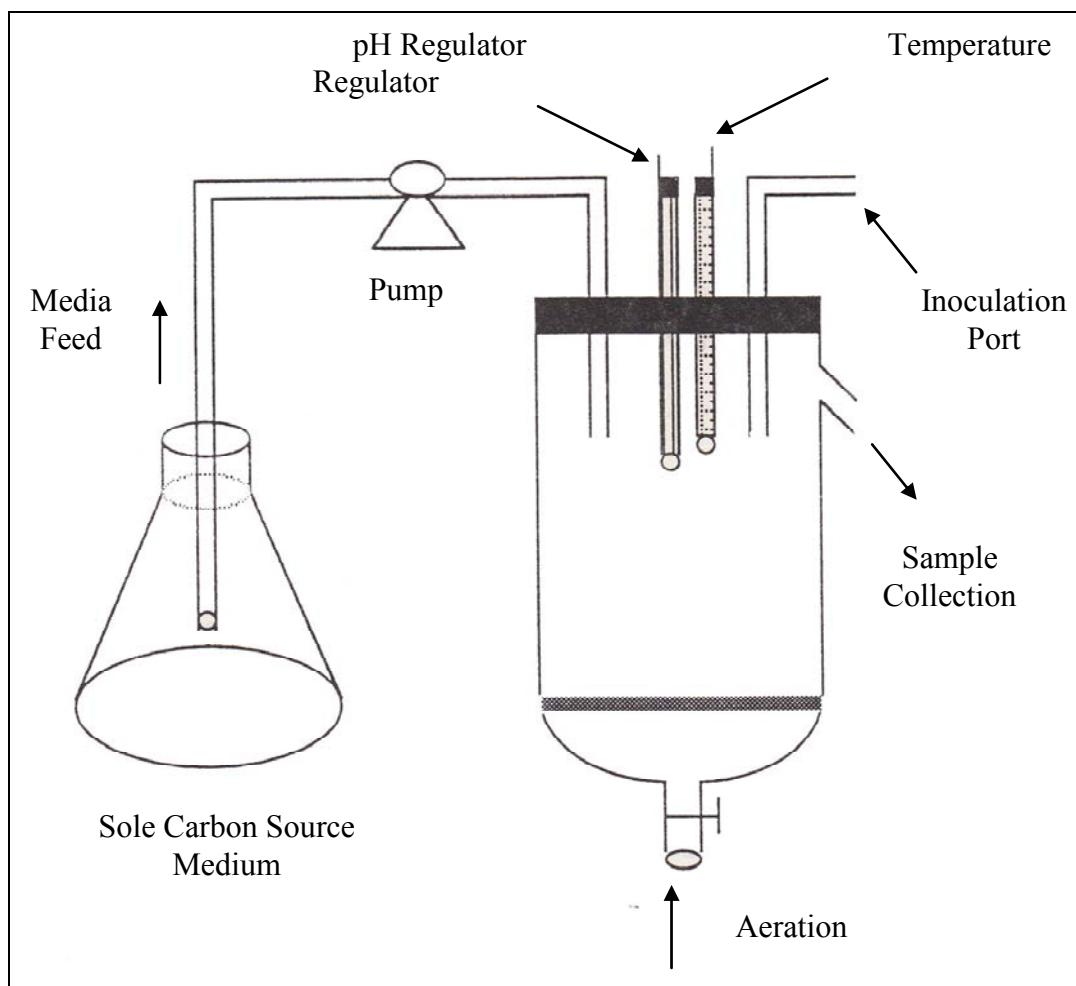
Figure 27. Schematic of chemostat used for isolation of lignolytic bacteria.

Figure 28. Chemostat assembled for lignolytic microorganism isolation.

The best choice of a bacterial population source to seed a chemostat would be from an environment where lignolytic organisms likely live in nature. Bacteria do not expend energy to generate degradative enzymes unless those enzymes are used in survival. Survival to a bacterium is the ability to access food and water. Natural bacterial selection leads to die-off of the species, which cannot survive within a particular environment. Therefore, to have such a specialized ability to degrade lignin, the organisms would most likely need to live in an environment where lignin is being degraded or where similar compounds exist, such as in rotting wood and wood products, decomposing bagasse, ruminant/cecal feces, lignin-attacking plant pathogens, oil-soaked soil, cresote posts, swamp soils, crude oil, soils, and decomposing hay.

For this study, a continuous culture isolation chemostat was aseptically assembled with temperature, pH, media infusion rate, and aeration controls (figures 27 and 28). Sole carbon source liquid media were formulated using a 0.5%–3.0% carbon source, a carbon-free vitamin

mixture, and stock solutions of mineral salts. For microbial growth, there is a limit to the concentration of solutes that can be presented within an aqueous microenvironment. At too high a concentration, osmotic pressure restrictions overwhelm microbial capability, prevent growth, and can even be lethal to sensitive organisms. In this experiment, an upper limit of 3% carbon source was chosen, since this typically is a safe concentration for most bacterial species. As the purpose of this phase of the experiment was to isolate as many potential lignolytic organisms from the environment as possible, it was important to maintain practical concentration conditions that would promote microbial growth. At some future date, isolated lignolytic organisms should be tested to determine the optimum lignin concentrations that allow maximum growth and lignin degradation.

Analogs were chosen as carbon source molecules based on similar chemical structure and bonding as in the complex lignin molecule. Analogs used in the chemostat media feed included methanol, vanillin, vanillic acid, guaiacol, veratraldehyde, and 4-hydroxy, 3-methoxy cinnamic acid. Indulin AT lignin also was used. A sterilized solution of 0.1-M NaOH was used for pH adjustment. Incubation temperature ranges included 21 to 35 °C and pH ranges included 7.0 to 9.5. With alterations to pH, temperature, analog, and formulation concentration, over 200 combinations of parameters were conducted using the chemostat. Temperature and pH ranges were selected based on typical growth parameters for bacteria and typical growth conditions that would be expected in the environment. Since it is highly unlikely that an organism would grow in conditions outside those typically encountered in its native conditions, conditions mimicking environmental conditions were selected.

Over 50 soils, rotting wood, creosote, and crude oil samples were collected from the environment in Louisiana, Florida, Georgia, South Carolina, North Carolina, Tennessee, Maryland, and Delaware. The environmental samples were inoculated into the chemostat, one sample at a time, and in mixtures of five samples at a time. Each sample was allowed to equilibrate and was then tested through the entire range of temperature, pH, and flow rate conditions through each sole source medium type while maintaining constant atmospheric conditions (aerobic).   Since aerobic metabolism generates 19 times more Adenosine triphosphate than anaerobic metabolism, it is understood that an aerobic organism would be preferred for rapidly degrading lignin. Therefore, the lignolytic screening study was designed to seek only aerobic organisms. At peak turbidity for each condition and each hour as flow rates were increased incrementally until washout, subsamples were collected for further isolation and study. These subcultures were transferred to fresh broth culture and then subsequently streaked for isolation on a variety of solid agar media containing lignin and lignin analogs as described previously. After more than 100 trials, we determined that a modified version of Dye's medium (*10*) (table 6) was the best agar medium for final culture isolation. The development of this modified Dye's medium using Indulin AT lignin as the sole carbon source proved beneficial for use in the chemostat, and a broth version was used in all subsequent chemostat runs. Samples collected from the chemostat were pre-enriched in 10 mL of modified Dye's broth overnight and

then streaked for isolation on modified Dye's agar through at least two subculture passages to ensure culture purity (figure 29). Isolates were scored for robust growth on the modified Dye's medium (table 6).

Table 6. Modified Dye's medium.

Broth
1 g ammonium phosphate
2 g potassium phosphate
2 g potassium chloride
0.2 g magnesium sulfate
1 g yeast extract
0.5 g Indulin AT in 2 mL of 1 M NaOH
1 L distilled, deionized water
pH adjusted to 7.8 and sterilized by autoclaving.
Agar
1 g ammonium phosphate
2 g potassium phosphate
2 g potassium chloride
0.2 g magnesium sulfate
1 g yeast extract
0.5 g Indulin AT in 2 mL of 1 M NaOH
1 L distilled, deionized water
15 g agar
pH adjusted to 7.8 and sterilized by autoclaving.

Figure 29. Bacterial cultures streaked for isolation on modified Dye's agar.

2.3.3 Isolate Characterization

The following procedure was used to identify the isolated bacterial cultures:

1. Ensure the culture is pure. Streak for isolation on agar, incubate 24–72 h and examine for pure cultures. If not, repeat.

2. Transfer pure culture to slants (figure 30); incubate 24–72 h. Also grow each pure culture in sterile broth (incubate 24–72 h) and freeze using sterile glycerol. Label and record library documentation.

3. Examine colony morphology and color. Gram stain each culture on microscope slide and examine under the microscope. Note gram reaction and cell morphology. Do wet mount to examine for movement, which would indicate the presence of flagella. Conduct biochemical assays to help narrow to genera.

4. On selected cultures: conducted colony polymerase chain reaction (PCR) on the isolates from the slants to amplify the 16S rRNA gene from the bacterial isolates using the forward oligonucleotide primer (8F, 5' AGAGTTTGATCMTGGCTCAG 3') and the reverse oligonucleotide primer (1492R, 5' GGYTACCTTGTTACGACTT 3'). Amplified 16S rRNA samples will be sequenced and then analyzed using the BLASTn program on the National Center for Bioinformatics Web site. Bacterial identity was selected from the top 25 BLAST nucleotide database results with max identity >90%.

This work allowed a level of confidence that the isolates were indeed different cultures and not multiple copies of the same organism(s).

Figure 30. Photograph
of agar slant.

By using the chemostat prescreening, researchers were able to rapidly screen trillions of bacteria through the continuous flow system. The selective nature of the chemostat system eliminated from consideration >99.999% of the organisms in each sample and allowed only those with greatest potential for lignolytic activity to be selected for further testing. Through this method, more than 300 potential lignolytic cultures were selected out of the trillions of organisms presented in the original environmental samples.

2.3.4 Lignolytic Activity Characterization

To examine each of the more than 300 isolated cultures for lignolytic activity, 1 L of modified Dye's broth was prepared and sterilized for each isolate. Each pure culture was inoculated, and the culture was incubated at 25–35 °C with shaking for 24–48 h depending on previous cultural

information derived during isolation. The broth was centrifuged (8000 × g) for 30 min at 4 °C to remove most of the cells. The supernatant was collected and lyophilized for 48 to 72 h. Uninoculated lignin controls were similarly incubated, centrifuged, and freeze-dried. Culture controls were grown without lignin (using glucose or another carbon source) to ensure bands observed on thin layer chromatography (TLC) plates were not generated as part of the cell. In cases where a secondary (non-lignin) broth could not be readily identified that would allow growth, cells were grown in modified Dye's broth containing Indulin AT lignin. The cultures were centrifuged to isolate the cells and washed three times in a sterile 4 °C phosphate buffer to remove broth components, and the pelleted cells were extracted as the cell control. This work is ongoing.

2.3.5 Extraction and Thin Layer Chromatography

Each lyophilized and extracted sample was examined by TLC for lignin degradation. TLC is a method of visualizing if lignin was broken into subunits. Dye's medium contains lignin but also a number of inorganic compounds and water. Freeze drying and subsequent extraction allow separation of lignin breakdown products. However, the choice of extraction solvent can greatly affect if all breakdown products are removed. Therefore, this portion of the study is a trial and error to seek the best extraction solvent for each cultured sample. A few extraction solvents were used including methanol, methylene chloride, acetone, and 50/50 binary mixtures thereof. After extraction, the samples in the solvent are spotted onto TLC plates. These plates are then resolved using a different solvent system that draws up the plate by capillary action. As the resolving solvent moves, it will move components in the mobile phase (figure 31). Choice of the resolving solvent can also affect subunit separation. Again, this portion of the study is a trial and error to seek the best resolving solvent for each cultured lignin broth.
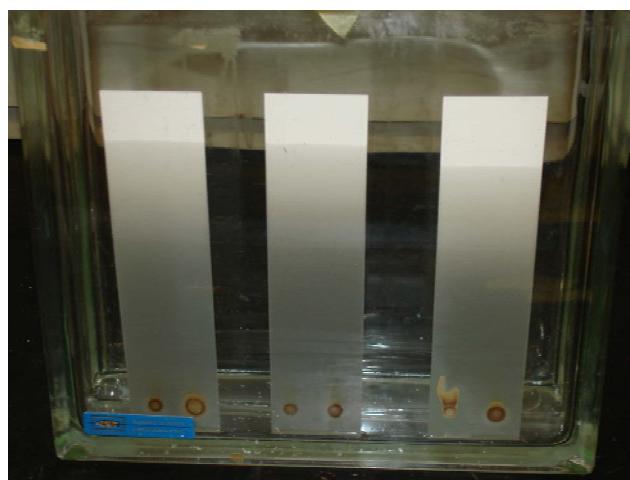
Figure 31. During TLC, samples are spotted onto a plate
and resolved by solvent drawing up the plate
by capillary action.

Lignin contains numerous aromatic rings. Aromatic rings fluoresce under ultraviolet light. If bands are noted on a TLC plate, then it is important to observe the two controls. The first control is a lignin (uninoculated control). This control should be extracted using the same extraction solvent as the cultured sample. The uninoculated lignin control will show if there are similar bands in the unmodified lignin. If there are, then the bacteria did not break down the lignin and generate that band. The second control is a culture control. In this case, it is important to ensure the culture does not produce an aromatic compound such as a pigment, which can be mistaken for a lignin breakdown product. Therefore, if a band appears or disappears on a cultured lignin in comparison with the control lignin and culture control, then it is surmised that the culture modified the lignin.

To achieve optimum separation on TLC, various mixtures of solvents (more than 20) were tested for extraction and resolving solvents. On average, six different combinations were tried per sample to identify the most effective resolution for that particular sample. These solvents generally included ethyl acetate, acetone, methanol, ethanol, water, and combinations thereof. Different combinations were tested until good band resolution was noted on TLC. Both reverse phase and silica gel (TLC) were used to visualize lignin breakdown. This work is ongoing.

2.3.6 Potential for Melt Fiber Formation

Extracted samples that displayed lignin breakdown, as per TLC, were further characterized for potential for melt fiber formation. A sample of the extracted material was placed on a glass microscope slide. A second slide was placed on top of the first, and the slides were heated on a hot plate. Upon obvious melting, the slides were quickly pulled apart, and any resultant strand formation was examined under a light microscope. Potential for fiber formation was scored for each culture. This work is ongoing for screening the more than 300 potential lignolytic isolates.

2.3.7 Lignin Degradation – Coculturing

Since biological systems act on large molecules by use of enzymes, there are cases where coculturing microorganisms can result in enhanced enzymatic degradation. Based on that principle, selected isolated cultures were cocultured, and subsequently, the same extraction, chromatography, and melt fiber assessments were conducted as mentioned previously. Unfortunately, only limited coculturing can be done, as coculturing the 300 isolates as combinations of two cultures would yield 45,000 different combinations to be tested. This is obviously beyond the scope of time and cost parameters for this project. However, some of the cocultured samples tested have yielded good results as scored by TLC and melt fiber formation. This work is ongoing.

2.4 Results and Discussion

2.4.1 Lignolytic Culture Isolation

The chemostat method using lignin analog compounds as sole carbon sources in microbial media was not as successful as anticipated. However, by using modified Dye's medium, which contained Indulin AT lignin as the sole carbon source, more than 300 cultures were isolated. It is hypothesized that although the chemostat media using lignin analogs contained linkages indicative of the bonding within lignin or which should have occurred during degradation of lignin, apparently one or more crucial growth factors were missing. More than 40 sole carbon source media formulations were tested using the various lignin analogs. However, during these trials with the chemostat, very few potential lignolytic organisms were collected. Researchers devised a modification of Dye's medium using Indulin AT lignin as the sole carbon source. This medium was highly successful and suggests that it contained an adequate combination of nutrients and/or trace cofactor(s) that were missing in the other sole carbon source media used previously. Upon using this modified Dye's medium in the chemostat, we were able to collect large numbers of potential lignolytic organisms (figure 32). Therefore, the chemostat procedure was repeated with Dye's medium for screening all collected environmental samples. Interestingly, the majority of the potentially lignolytic isolates selected were derived from samples collected from Louisiana, and very few isolates were derived from samples from Florida, Georgia, South Carolina, North Carolina, Tennessee, Maryland, and Delaware.

2.4.2 Characterization of Isolated Bacteria

The bacterial colonies were characterized using a number of techniques. First, a visual observation of the cultures was performed to characterize the various differences (and similarities) among the isolates, as illustrated in figure 32. Gram staining of the bacteria was performed, as shown in figure 33. These identification methods were cataloged for over 100 cultures. Approximately 25 bacterial cultures were submitted for 16S rRNA analysis to more specifically identify the bacteria cultures. Currently, the results are being compiled to determine trends and the range of properties. However, we have putatively identified a number of bacterial cultures that decompose lignin as *Pseudomonas, Klebsiella, Erwinia, Streptomyces, Bacillus badius, Petrobacter, Tepidophilus*, as well as unknown and potentially new bacterial species. The characterization of two representative lignolytic bacterial cultures is shown in figures 34 and 35.
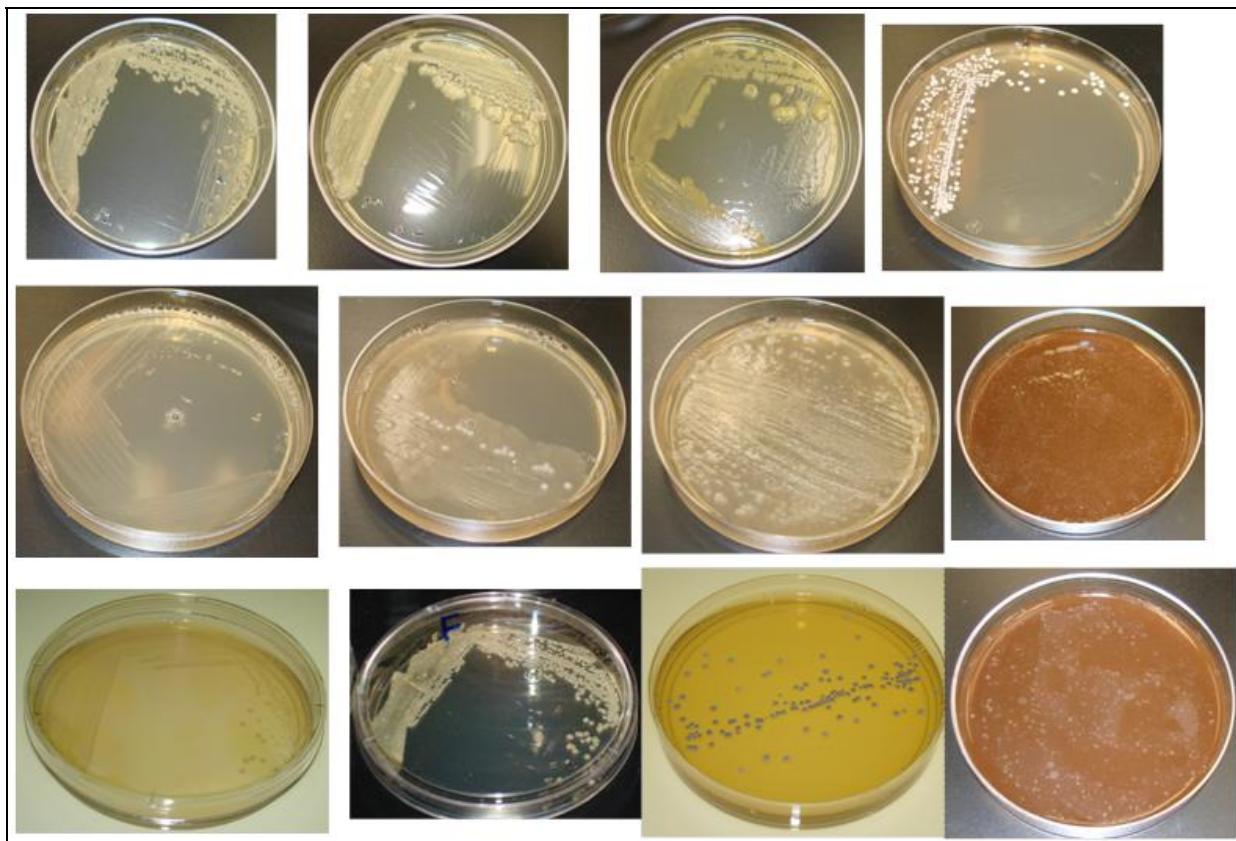
Figure 32. Selection of isolated bacterial cultures that successfully decompose lignin.
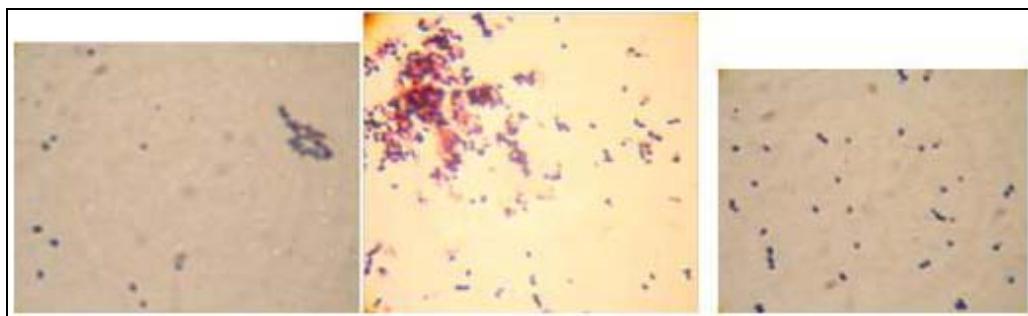
Figure 33. Micrographs of three selected gram-stained bacteria showing positive (purple) and negative gram (red) staining.

2.4.3 Verification of Lignolytic Activity

The cultures isolated from the chemostat broth were streaked isolated on modified Dye's agar through at least two subcultures (figure 34c). Isolated cultures were stored on agar slants for further testing, and broth cultures were frozen (–40 °C) in modified Dye's broth with 30% sterile glycerol for long-term storage. The individual cultures in this library are now being examined to score each culture for degree of robust growth, for lignolytic activity, and for potential of breakdown products for melt fiber formation. A data sheet is kept on each organism, and additional information is added as derived. Samples of data sheets shown in figures 34 and 35 indicate scoring of two of the 300+ lignolytic cultures.

So long as the growth of the organism occurs within a few days, the speed with which the bacteria cause the modification to lignin is not as important at this stage as the actual modification. High-volume fermentation methods are commonplace for microbial modifications and could be utilized in commercial modification if the organism(s) prove capable of modifying lignin for carbon fiber manufacture.

Samples are first evaluated for growth ability in the presence of lignin as a sole carbon source. Cultural characteristics including colony morphology, cell morphology, and Gram reaction were examined. After lyophilization, extraction, and TLC on cultured broth, those cultures that exhibit good separation and distinctive bands were noted on data sheets (figures 34d and 35b). The TLC results do indicate significant differences between the control and bacteria-modified lignin, with bands missing and new bands present. However, the TLC results show that much of the lignin solute is being carried across the entire TLC plate, and thus a better eluent would be preferred to better detail the results. A characterization of the differences, especially after improved solvent choice, will be compiled and reported later.

SERDP Project Data Sheet

Sample ID: LA-SiCr-49
Sample Source: Mount Hermon, Louisiana (Washington Parish)
Sample Characteristics: Rotted Cresote Fence Post
Date/Time Collected: 12/29/10   2:23 pm
Prelim. Isolation Method: Chemostat with Modified Dye's broth
                                pH 7-7.2
                                30°C
                                3 hours prior to washout
Sub-culture: Streaked for isolation – modified Dye's agar – 48 hr
                              incubation at 30°C - appears to be mixed culture
                              Re-streaked for isolation – modified Dye's agar – 48+ hr
                              incubation at 30°C - pure culture achieved
Colony Color: Grey/Lavender
Colony Morphology: Round, raised, stone-like, fibrous on agar
                              Stone-like adhesions in broth – adheres to flask walls
Growth Characteristics: Requires at least 48 hours for any observable growth;
                              afterward exhibits robust growth
Gram Reaction: Gram variable
Cell Morphology: Filamentous
Comments: Potentially a *Streptomyces*?
                              Better growth at lower temps
Lignin Breakdown?   Yes - as noted by TLC – one distinctive extra band
in cultured
Best Extracting Solvent: 1:1 v/v ethyl acetate/methanol
Best Resolving Solvent: 10:1:1:0.5 Ethyl Acetate:Methanol:Acetone: H_2O
Melt Fiber Formation? Yes – as noted microscopically
Melt Fiber Score?   9 out of 10 due to long fiber formation/uniform fibers
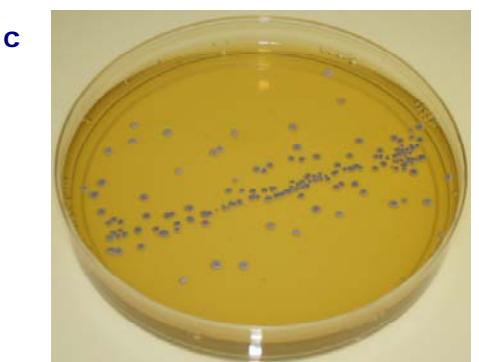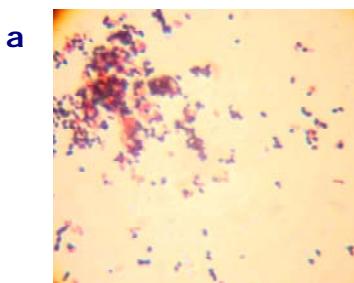
a) LA-SiCr-49 – Gram variable
b) LA-SiCr-49 culture in Modified Dye's broth; 49 hr
incubation at 30°C (adhesions)
c) LA-SiCr-49 culture in Modified Dye's agar; 49 hr
incubation at 30°C

Figure 34. Sample data sheet example for LA-SiCr-49.

SERDP Project Data Sheet

Sample ID: LA-SiCr-49
Sample Source: Mount Hermon, Louisiana (Washington Parish)

TLC:
Extracting Solvent: 1:1 v/v ethyl acetate/methanol
Resolving Solvent: 10:1:1:0.5 Ethyl Acetate:Methanol:Acetone: H_2O
Visualization: 280 nm ultraviolet – (banding more distinct on greyscale photo) –
        additional band noted on cultured lignin
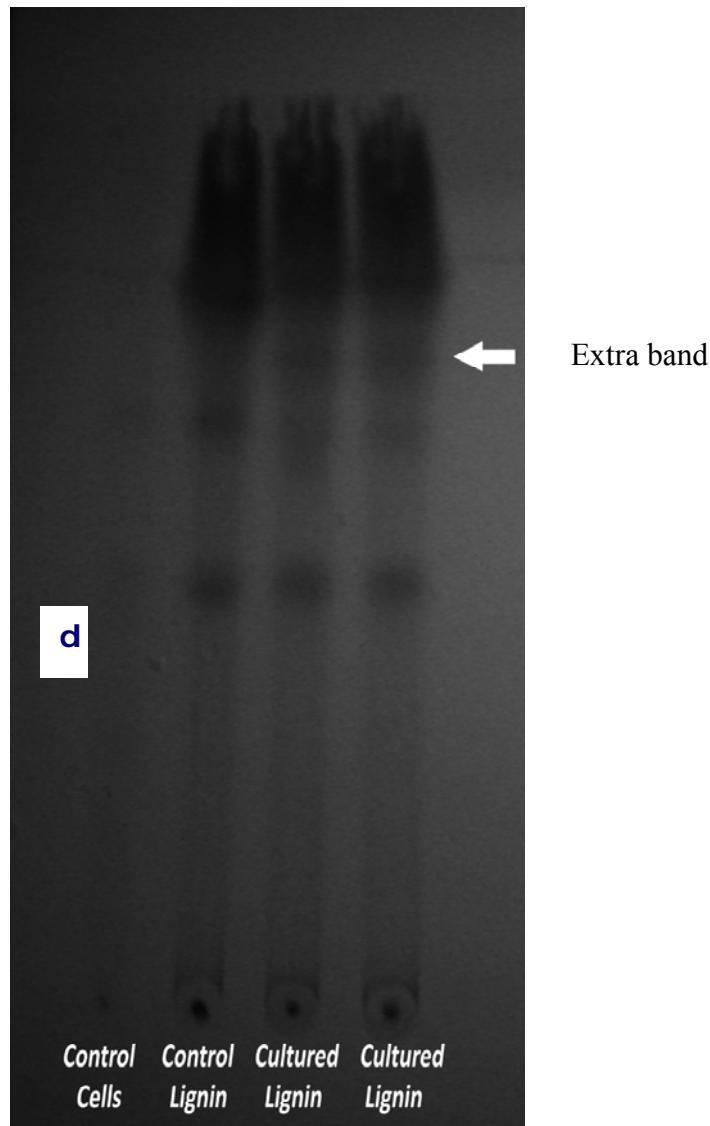
Figure 34. Sample data sheet example for LA-SiCr-49 (continued).

SERDP Project Data Sheet

Sample ID: LA-SiCr-49
Sample Source: Mount Hermon, Louisiana (Washington Parish)

Melt Fiber Formation Comments:

1:1 v/v ethyl acetate/methanol extracted
100X magnification – microscope slide
Long fiber formation – fibers fairly uniform in thickness along entire length

Figure 34. Sample data sheet example for LA-SiCr-49 (continued).

SERDP Project Data Sheet

Sample ID: LA-SiCr-14
Sample Source: Mount Hermon, Louisiana (Washington Parish)
Sample Characteristics: Upland swamp soil sample
Date/Time Collected: 12/29/10   3:15 pm
Prelim. Isolation Method: Chemostat with Modified Dye's broth
                                pH 7.3
                                30°C
                                5 hours prior to washout
Sub-culture: Streaked for isolation – modified Dye's agar – 48 hr
                                   incubation at 30°C - appears to be mixed culture
                                Re-streaked for isolation – modified Dye's agar – 48+ hr
                                   incubation at 30°C - appears to be mixed culture
                                Re-streaked for isolation – modified Dye's agar – 48+ hr
                                   incubation at 30°C - pure culture achieved
Colony Color: Cream
Colony Morphology: Moist, flat colonies
Growth Characteristics: Requires at least 24 hours for any observable growth;
                                   afterward exhibits robust growth

Gram Reaction: Gram negative
Cell Morphology: Short rod – possibly peritrichous flagella
Comments: Better growth at lower temps
Lignin Breakdown?   Yes - as noted by TLC – one distinctive extra band
                                and lost one band in cultured
Best Extracting Solvent: H_2O-saturated n-butanol
Best Resolving Solvent: 8:1:1 toluene/ethanol/1 M ammonium hydroxide
Melt Fiber Formation?   Yes – as noted microscopically
Melt Fiber Score?   7 out of 10 – MANY fibers – but all are short –
                                therefore
                                may be easy to form but can they provide length?

a
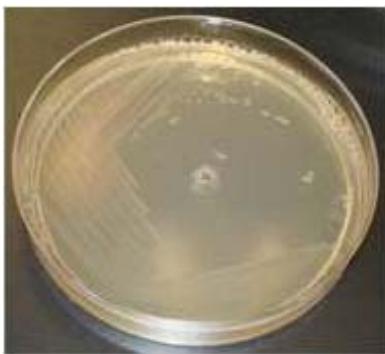
a) LA-SiCr-14 culture in Modified Dye's agar; 24 hr incubation at 32°C

Figure 35. Sample data sheet example for LA-SiCr-14.

SERDP Project Data Sheet

Sample ID: LA-SiCr-14
Sample Source: Mount Hermon, Louisiana (Washington Parish)

TLC: Silica gel
Extracting Solvent: H_2O-saturated n-butanol
Resolving Solvent: 8:1:1 toluene/ethanol/1 M ammonium hydroxide
Visualization: 280 nm ultraviolet
Notes: Control and sample broth were incubated at 30°C for 48 hr - one distinctive extra band and lost one band in cultured
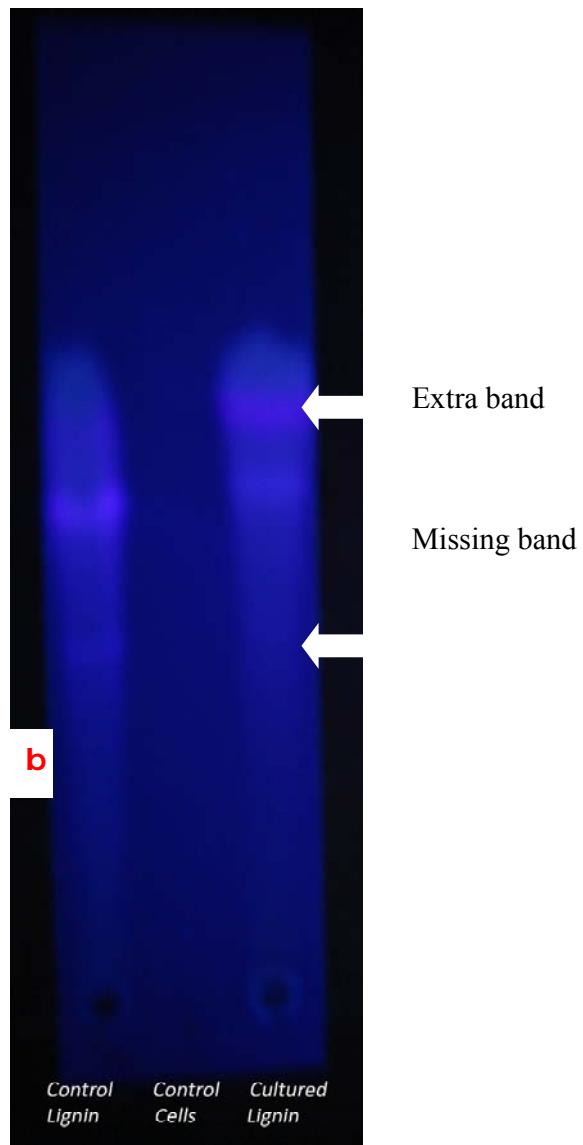
Figure 35. Sample data sheet example for LA-SiCr-14 (continued).

SERDP Project Data Sheet

Sample ID: LA-SiCr-14
Sample Source: Mount Hermon, Louisiana (Washington Parish)

Melt Fiber Formation Comments:

1:1 v/v ethyl acetate/methanol extracted
100X magnification – microscope slide
Short fiber formation – but high number of fibers formed per unit area
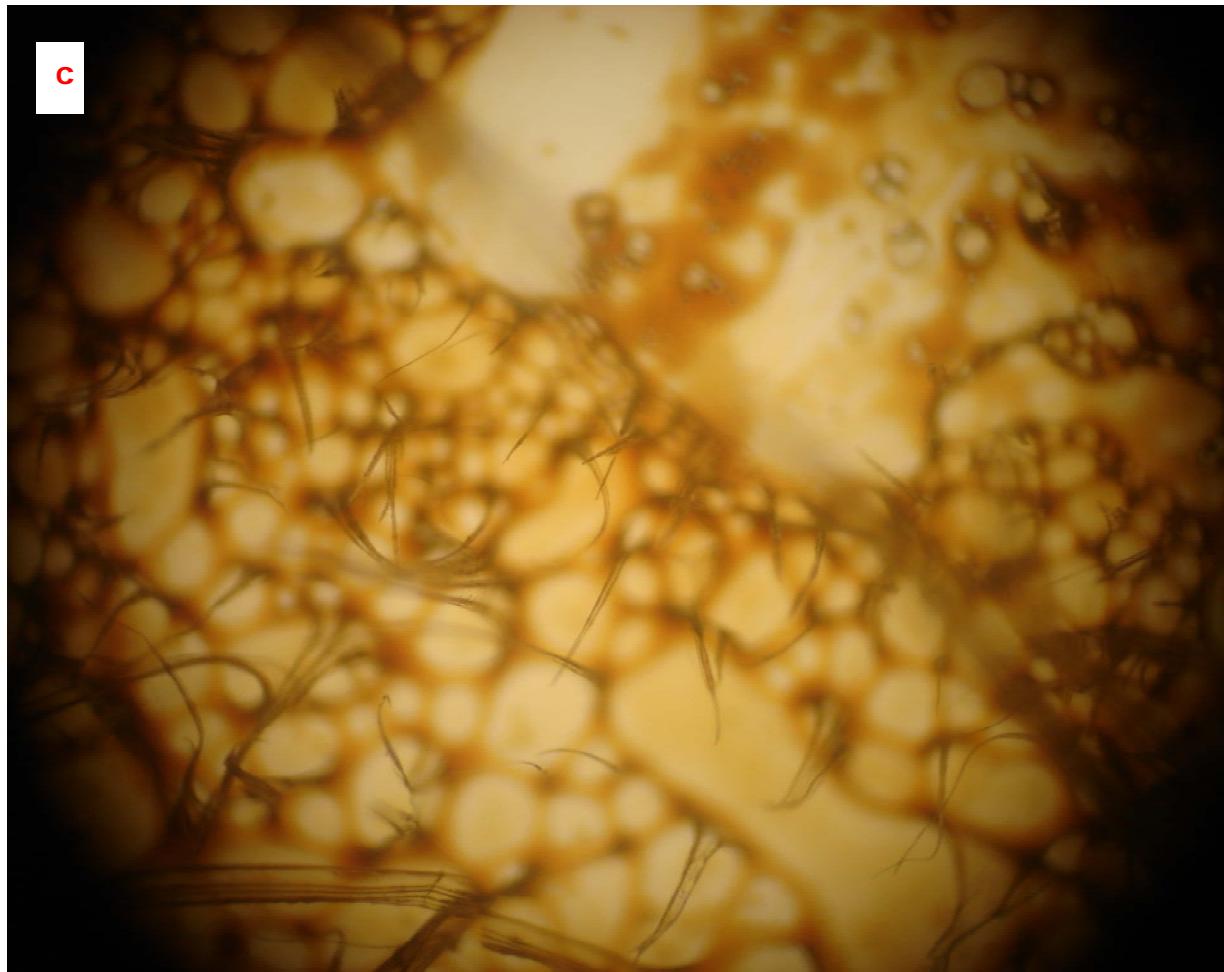
Figure 35. Sample data sheet example for LA-SiCr-14 (continued).

2.4.4 Fiber Formation From Microbially Decomposed Lignin

We created a scoring system using the test system of heating extracted samples between two microscope slides and analyzing them under the microscope (figures 34e and 35e). Criteria for scoring include whether any fibers are formed, relative ease of fiber formation, length of formed fibers, evenness of fiber thickness, whether any breakage or variation in uniformity of fibers is apparent, and relative number of fibers formed. This data is being obtained and recorded for each of the 300+ putative lignolytic cultures in the library. Nearly 200 out of the 300+ isolated cultures have been screened and data recorded as per the examples shown in figures 34 and 35. The distribution of scores and top 10 performers will be compiled shortly. This work is ongoing.

2.4.5 Lignolytic Bacteria Scale-Up

Lignin degradation using two bacteria strains was scaled up using the following process:

- Grow ~10 to 15 L of each culture 24 h in broth using Indulin lignin as the sole carbon source.

- Centrifuge to remove cells; collect supernatant. Freeze dry supernatant (5–10 days). Extract supernatant using solvent determined in previous stage.

- Concentrate via rotary evaporation.

Fractions will be provided to Dr. Amod Ogale for use in polymer manufacture.

The first bacterial strain used for scale-up was the *Pseudomonas* strand identified by Clemson researchers. The second was the literature identified *Pseudomonas fluoroscens*.

2.4.6 Fiber Formation From Scaled-Up Microbially Decomposed Lignin

Fiber formation was tested using the scaled-up modified lignin derived from the lignolytic *Pseudomonas* strand identified by Clemson researchers. The samples were picked up using tweezers, and the tweezers were opened and closed to place a stretching force on the material. As show in figure 36, fibril formation was induced in some cultures, indicating an ability of these decomposed lignin samples to form melt-spun fibers.
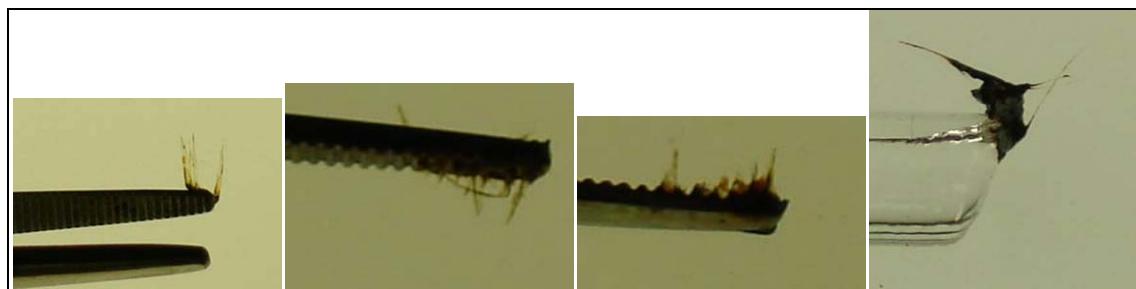
Figure 36. Tweezer stretching experiment of scaled-up *Pseudomonas* decomposed lignin sample.

2.5   Summary and Conclusions

The ultimate goal of this work is to determine the best lignolytic organisms to use for scale-up to produce sufficient material for carbon fiber spinning. In order to scale-up, 50 to 100 L of broth will be cultured, extracted, and submitted to Dr. Amod Ogale's laboratory for carbon fiber spinning. Since scale-up will be labor intensive and costly, it is important to know which organisms are the best candidates. Hence, it is imperative to screen each culture for lignolytic characteristics. Out of the nearly 200 screened cultures, there are several species which are displaying great potential for carbon fiber formation. Work is now being initiated to scale-up for carbon fiber preparation studies on several of these cultures. Screening will simultaneously continue on the remaining organisms in the library, and the cultures deemed of greatest potential for modifying lignin for carbon fiber formation will be added to the scale-up studies.

Recorded lignin research reveals that very few lignolytic bacteria have been previously isolated and characterized. A search of the American Type Culture Collection bacterial database for the keywords "lignin" and "lignolytic" reveal only 10 bacterial species. In fact, this laboratory has purchased the three aerobic species that, the literature reports, have significant lignolytic activity against lignin. These cultures have been included in the study. One of these purchased cultures is showing good promise for carbon fiber formation.

The results of this study are profound. This study has yielded more than 300 putative lignolytic organisms. Using 16s RNA identification methods, we have tentatively identified the first of these isolated cultures as species of *Pseudomonas, Klebsiella, Erwinia, Streptomyces, Bacillus badius, Petrobacter,* and *Tepidophilus.* Most of the species were unidentifiable by 16s RNA sequencing, indicating they may be new, previously unknown species. Many of the isolates may be duplicates, but colony morphology and Gram stain results indicate that there are many different species in this collection. Results of this study will provide considerable new knowledge for not only carbon fiber formation from lignin but also new lignolytic species of bacteria.

2.6   Continuing and Future Work

Based on the successful ability of many decomposed samples to form fibers, microbial decomposition of lignin was considered a "go" for the remainder of the project. Therefore, the following work will be conducted on this study:

1. Screen cultures for lignolytic activity and potential for carbon fiber formation.

2. Tabulate a description of the optimum fiber-forming bacteria, including their gram-staining identification, and other identifying features, along with how well they form fibers to see if there are any trends.

3. Assess chemically modified or fractionated lignin as the sole carbon source for microbial decomposition of lignin.

4. Scale-up of best cultures to generate sufficient modified lignin for carbon fiber spinning.

References

1. Jeffries, T. W. Biodegradation of Lignin and Hemicelluloses. In *Biochemistry of Microbial Degradation*; Ratledge, C., Ed.; Kluwer Academic Publishers: London, 1993.

2. Campbell, M. M.; Sederoff, R. R. Variation in Lignin Content and Composition Mechanisms of Control and Implications for the Genetic Improvement of Plants. *Plant Physiol.* **1996**, *110*, 3–13.

3. Lignin structure. http://en.wikipedia.org/wiki/File:Lignin_structure.svg (accessed 2 April 2012).

4. Whitman, W. B.; Coleman, D. C.; Wiebe, W. J. Perspective Prokaryotes: The Unseen Majority. *Proc. Natl. Acad. Sci.* **1998**, *95*, 6578–6583.

5. Torsvik, V.; Goksoyr, J.; Daae, F. L. High Diversity in DNA of Soil Bacteria. *Appl. Environ. Micro.* **1990**, *56* (3), 782–787.

6. Bach, H. J.; Tomanova, J.; Schloter, M.; Munch, J. C. Enumeration of Total Bacteria and Bacteria With Genes for Proteolytic Activity in Pure Cultures and in Environmental Samples by Quantitative PCR Mediated Amplification. *J. Microbiol. Methods* **2002**, *49*, 235–245.

7. Sharma, R.; Ranjan, R.; Kapardar, R. K.; Grover, A. "Unculturable" Bacterial Diversity: An Untapped Resource. *Current Science* **2005**, *89* (1), 72–77.

8. Belgacem, M. N., Gandini A., Eds. *Monomers*, *Polymers and Composites From Renewable Resources*; Elsevier: Oxford, 2008.

9. Higson, A. NNFCC Renewable Chemicals Factsheet: Lignin. http://www.nnfcc.co.uk /publications/nnfcc-renewable-chemicals-factsheet-lignin (accessed November 2011).

10. Dye, D. W. The Inadequacy of the Usual Determinative Tests for the Identification of Xanthomonas spp. *N. Z. J. Sci.* **1962**, *5*, 393–416.

3. Chemical Decomposition and Fractionation of Lignin

3.1 Introduction

Nondegraded and chemically modified lignins have been successfully incorporated into various materials, including polymeric materials (*1–6*). Additionally, much research has been conducted in selectively breaking down all types of lignin and multiphenolic lignin model compounds (LMCs) to develop new chemicals and renewable sources of predominantly petroleum-derived chemicals (figure 37) (*5–15*). Recently, a modest yield of vanillin from Kraft lignin has been obtained using aqueous polyoxometalates in the presence of alcohols to oxidatively degrade lignin (*7*). Additionally, vanillin production via Kraft lignin oxidation using a NaOH alkaline medium has been reported (*12*). Moreover, a 70% yield of guaiacol has been achieved from common β-O-4 LMCs, guaiacylglycerol-β-guaiacyl, and veratrylglycerol-β-guaiacyl ether under catalytic hydrolysis using an acidic ionic liquid (*10*). In 2011, Zakzeski and Weckhuysen (*8*) reported 22.2% and 12% yields of guaiacol from aqueous phase reforming of a β-O-4 linked and a 5-5′ carbon-carbon linked biphenyl model compounds, respectively, using a Pt/Al_2O_3 catalyst. Lastly, Sergeev and Hartwig (*15*) have reported yields as high as 99% of guaiacol from hydrogenolysis reactions of representative biphenyl LMCs.

The ultimate goal of this research is the employment of Kraft pine lignin (KPL) and LMCs— compounds that could come from the strategic breakdown of lignin—in the development of high T_g biobased resins by preparing derivatives thereof. KPL has been chosen as the primary lignin source in this study because of its supply dominance and cost-efficiency in industry compared to other forms of lignin, such as steam exploded, organosolv, soda, and sulfonated lignins. If the goal of this research comes to fruition, the utilization of modified KPL and functionalized LMCs in biobased composites could be both economical and environmentally friendly.
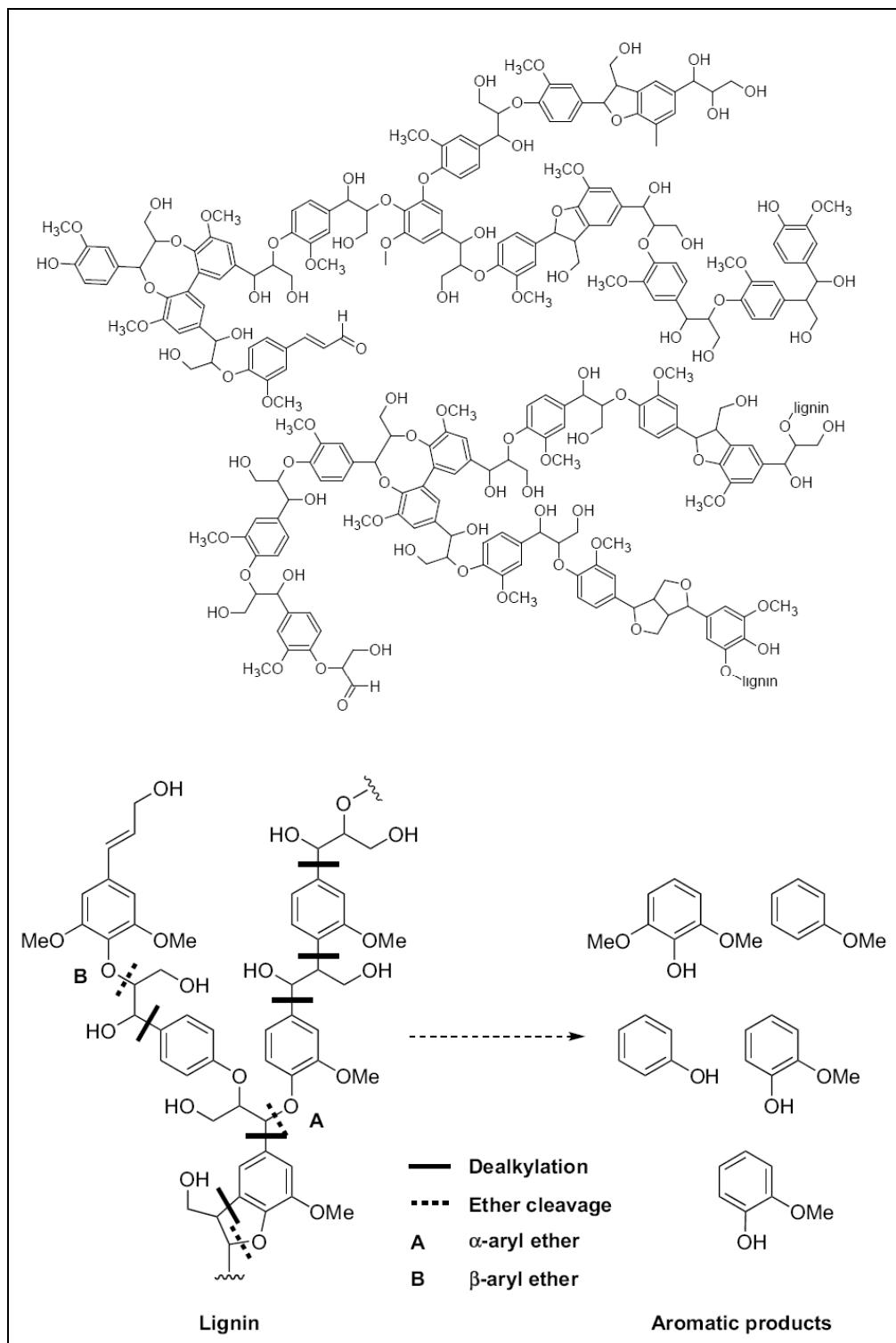
Figure 37. General chemical structure of lignin (top) with a schematic for its conversion into single aromatic chemicals (bottom) (*9*, *10*). (Reprinted with permission from John Wiley and Sons [top] and Elsevier [bottom].)

60

In order to test our hypothesis and achieve our ultimate goal, we are currently following the strategy illustrated in figure 38. Specifically, lignin (KPL) is being directly functionalized with free radically polymerizable groups. Lignin is also being fractionated into different fractions based on molecular weight and solubility in different organic solvents. Simultaneously, we are currently investigating the degradation of KPL via an olefin metathesis technique. A proposed model structure of KPL, shown in figure 39, includes aliphatic carbon-carbon double bonds (*1*, *16*). It is hypothesized that KPL can be chemically broken down via an olefin metathesis reaction of the aliphatic carbon-carbon double bonds using ethylene as the co-reactant and a ruthenium-based catalyst (figure 39) for highlighted, representative aliphatic carbon-carbon double bonds that may be present in KPL. Schrodi et al. (*17*) demonstrated that ethenolyses of methyl oleate, a natural seed oil derivative, to produce useful terminal olefins could be achieved in dichloromethane under low-pressure (150 psi) conditions using various ruthenium-based catalysts. In addition, Ferré-Filmon et al. (*18*) have shown that phenolics do not interfere or hinder the olefin metathesis reactions that utilized first- or second-generation Grubbs catalysts, or modified versions thereof. Moreover, the high activity and chemically tolerant nature of the ruthenium-based catalysts, particularly the first- and second-generation Grubbs catalysts, is well known, even in aqueous solutions (*17*, *19*, *20*). Therefore, it is proposed that KPL dissolved in either water or a polar solvent, such as ethylene glycol, can be chemically degraded via an ethenolysis reaction using a catalytic amount of ruthenium-based catalyst under moderate pressures at elevated temperatures in <6 h. Even though this degradation technique may not produce a high yield of very low molecular weight, single or multiphenolic compounds, it has the potential to lower the statistical molecular weight of the KPL, drastically reduce its polydispersity index (PDI), and chemically incorporate free radical polymerizable groups onto lignin structure. This is all contingent upon the presence, number, and availability of aliphatic carbon-carbon double bonds of KPL.
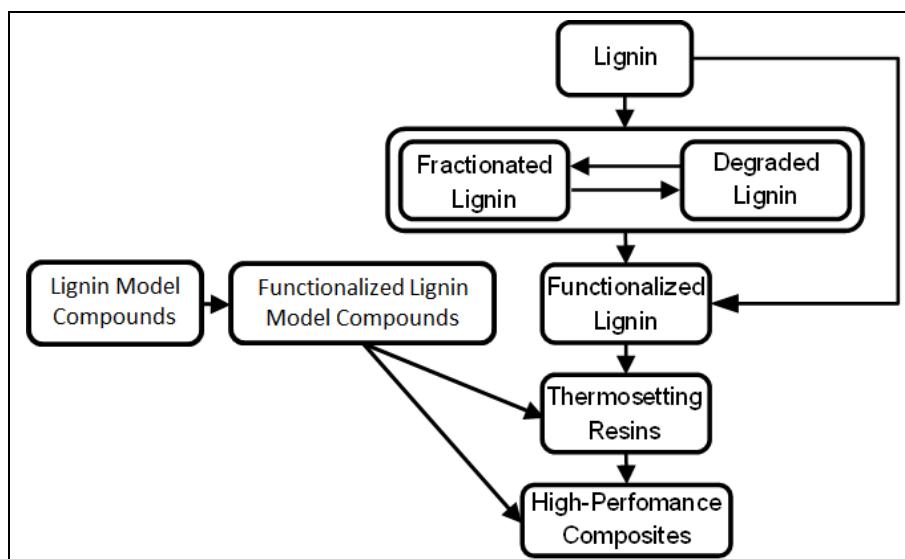
Figure 38. Lignin project block flow diagram.

61
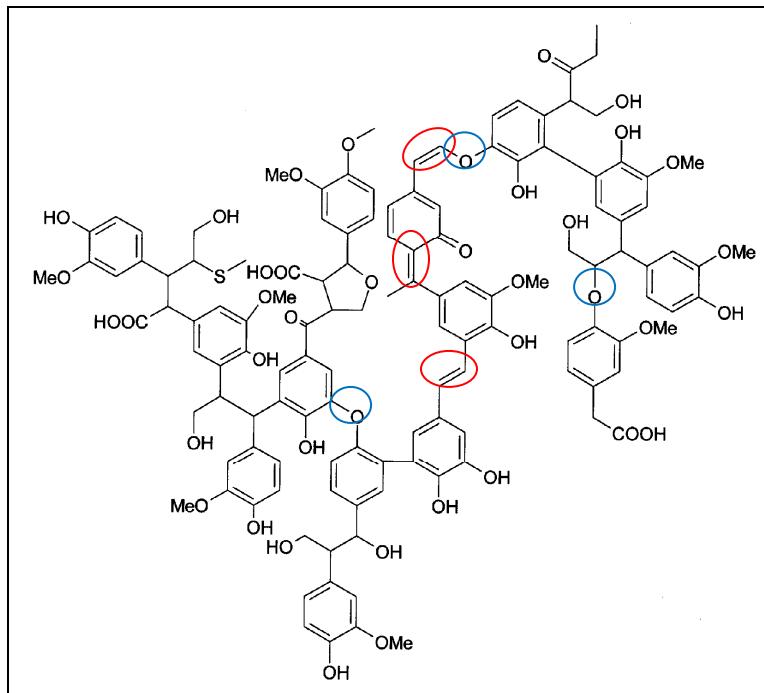
Figure 39. Proposed model structure of KPL (*1*, *16*). Aliphatic carbon-carbon double bonds present in the proposed model structure of KPL are highlighted by red circles, while ether linkages are highlighted by blue circles.

Additionally, we are investigating the degradation of KPL via a singlet oxygen mediated degradation technique. The proposed model structure of KPL by Marton, shown in figure 39, includes alkyl-aryl and alkyl-alkyl ether linkages (*1*, *16*). It is hypothesized that KPL can be chemically broken down via a singlet oxygen (sensitized by Rose Bengal) reaction of the ether linkages; see figure 39 for highlighted representative ether linkages that may be present in KPL. In the presence of both oxygen and Rose Bengal, Bonini et al. (*21*, *22*) demonstrated that singlet oxygen mediated degradation of steam-exploded pine lignin and steam-exploded beech lignin has the potential to yield single aromatic products. Additionally, as reviewed by Lanzalunga and Bietti (*23*), much research has been conducted on the photochemical-induced degradation of LMCs. Similar to the olefin metathesis degradation of KPL, this degradation technique may not produce a high yield of very low molecular weight, single or multiphenolic compounds. However, it has the potential to lower the statistical molecular weight of the KPL and reduce its PDI. This is all contingent upon the presence, number, and availability of residual ether linkages in the KPL.

Moreover, and as can be seen in figure 38, fractionated KPL, specifically a fraction that was soluble in methanol, is being directly functionalized with free radically polymerizable groups. Additionally, LMCs—namely, vanillin, guaiacol, and eugenol—are being methacrylated, with

methacrylated versions of guaiacol and eugenol being investigated as biobased reactive diluents as potential styrene replacements. Methacrylated vanillin, a solid at room temperature, is currently being studied in a thermosetting "green" resin. As a side note, the first synthesis of vanillin used eugenol from clove oil. Vanillin was commercially produced from eugenol until the 1920s when it was later discovered that vanillin could be obtained from the by-product of the sulfite process for making wood. Vanillin production from lignosulfonates started in 1937, and by 1981, a single pulp and paper mill in Ontario, Canada, supplied 60% of the world market for synthetic vanillin (*5*). However, because of growing public awareness on environmental issues—namely, the hazards associated with waste effluents—as well as cheaper synthesis routes—namely, petroleum-derived synthetic vanillin—mills began to close. Currently, synthetic vanillin is synthesized in a two-step process from petroleum-derived guaiacol (derived from phenol) and glyoxylic acid (*5*). Today and since 1993, the only vanillin producer from lignosulfonate that exists is the Norwegian company Borreegaard (*5, 24*). It is with great hope that vanillin, and similar chemicals, will be produced from lignin at a much higher volume with the development of sustainable biorefineries that are capable of completely mitigating waste streams or have the ability to drastically reduce the hazards and toxicities of such streams.

3.2   Experimental

3.2.1 Materials

All solvents, anhydrous phosphorus pentoxide (P_2O_5), acetic anhydride, pyridine, sodium chloride (NaCl), and Whatman no. 1 filter paper were purchased from Fisher Scientific and used as received. KPL (Indulin AT; lot no. MA27) was graciously provided by MeadWestvaco (Charleston, SC) and used as received.

3.2.2 Solvent Fractionation

The solvent fractionation method (figure 40) developed by Mörck et al. (*25*) was utilized. We added 100 g of KPL to methylene chloride (500 mL) and stirred vigorously for a half an hour at room temperature using a mechanical stirrer. Using a separation funnel and Whatman no. 1 filter paper, we filtered the mixture with the supernatant collected. The precipitate was added to methylene chloride (500 mL) and stirred for an additional half an hour. The mixture was again separated in the same manner with the precipitate subsequently washed with methylene chloride (1 L). The supernatants were collected as one, dried under reduced pressure, and further dried in vaccuo in the presence of P_2O_5. The precipitate was dried and then subjected to 1-propanol. This procedure was repeated for the next solvents, 1-propanol, methanol, and 7:3 methanol-methylene chloride (figure 40).
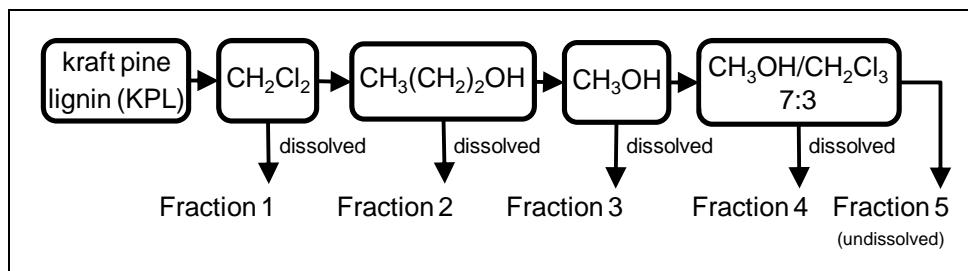
Figure 40. KPL solvent fractionation technique adapted from Mörck et al. (*25*).

3.2.3 Gel Permeation Chromatography

SEC was run on the acetylated KPL fractions. A Waters 2695 XE Separations Module was used, operated with Optima-grade tetrahydrofuran (THF) (1 mL/min) as the mobile phase, and calibrated with polystyrene standards. Samples were prepared by dissolving 2 mg of lignin in 1 mL of THF. The column eluent was monitored by a Waters 490E multiple wavelength detector operating at 214 and 254 nm (absorbed by phenyl rings) and a Waters 410 refractive index detector.

3.2.4 Acetylation of Kraft Pine Lignin

Various acetylation procedures were used to make acacetylated softwood Kraft lignin (Ace_SKL) (figure 41).
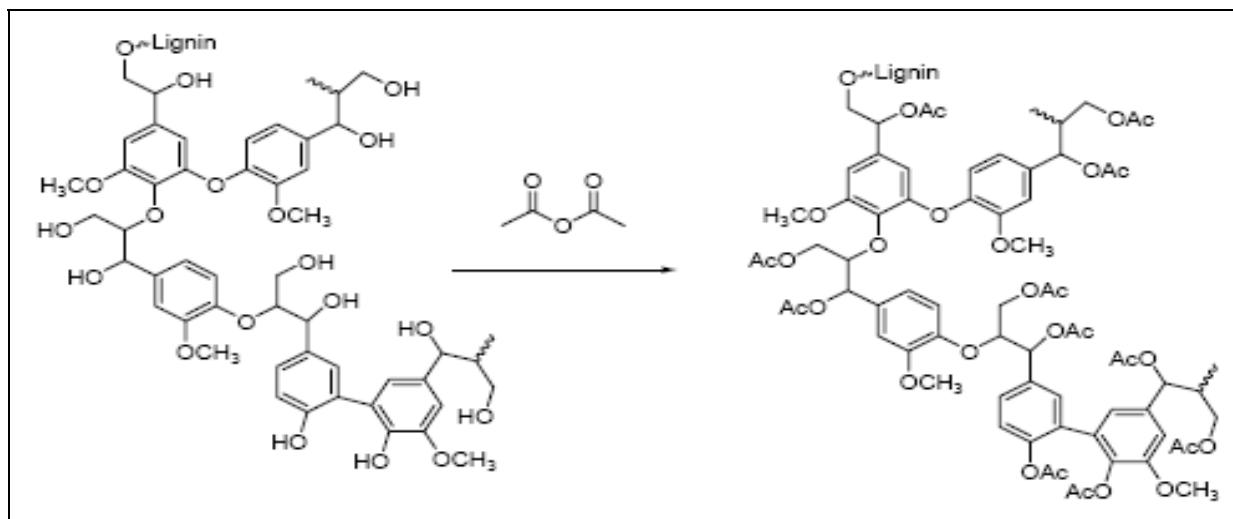
 Figure 41. Acetylation of lignin.

The general procedure was the same for all reactions: SKL or soda lignin powder was poured into a 500-mL round-bottomed flask. Acetic anhydride was added to the flask. The flask was connected with a reflux condenser and dipped into a water bath set at around 85–90 °C with continuous stirring. Prior to adding the catalyst pyridine (or alternative catalyst) to the flask, we sealed and subsequently purged the flask with argon gas for a half an hour to remove moisture

and oxygen from the reaction vessel, and then placed it in an ice bath. The reaction was allowed to progress as the reaction temperature increased to room temperature for a minimum of 24 h.

After reaction, the solvent present in the SKL reaction mixture was removed directly under reduced pressure to obtain the acetylated lignin (Ace_SKL). The following was the procedure used to prepare the Ace_SKL:

1. 10 g of Indulin AT + 150 mL of acetic anhydride, 80 °C, 4-h reaction

2. Extraction of Ace_SKL:

   • Ace_SKL in procedure 1 was extracted with acetic acid and washed with water until fractionated with 70% aqueous acetic acid, and the dissolved fraction was obtained by evaporating the aqueous acetic acid under reduced pressure. The undissolved fraction was discarded because its unmodified and higher molecular weight makes it intractable.

   • Ace_SKL in procedure 1 was extracted with acetic acid and washed with water until fractionated with 75% aqueous acetic acid, and the dissolved fraction was obtained by evaporating the aqueous acetic acid under reduced pressure. The undissolved fraction was discarded because its unmodified and higher molecular weight makes it intractable.

   • Ace_SKL in procedure 2a was washed with deionized water four times and dried over night at 80 °C. The fraction that dissolved in the water was discarded.

   • Ace_SKL in procedure 2b was washed with deionized water four times and dried over night at 80 °C. The fraction that dissolved in the water was discarded.

3. Perform reaction as described in procedure 1 with the following exceptions:

   • Reduce the amount of acetic anhydride to 2 mL/g SKL to 2, 1.5, 1, and 0.66 mL, with a 15-min reaction.

   • Reduce the amount of acetic anhydride to 1.5 mL/g SKL to 2, 1.5, 1, and 0.66 mL, with a 15-min reaction.

   • Reduce the amount of acetic anhydride to 1 mL/g SKL to 2, 1.5, 1, and 0.66 mL, with a 15-min reaction.

   • Reduce the amount of acetic anhydride to 0.66 mL/g SKL to 2, 1.5, 1, and 0.66 mL, with a 15-min reaction.

Note the stoichiometric amount of acetic anhydride was calculated using equation 1:

Acetic anhydride required per gram of SKL =

$$\frac{7.99\,\text{mmol}\,\text{OH}}{\text{g}} \times 1\,\text{g} \times \frac{102\,\text{g}}{\text{mol}} \times \frac{\text{mL}}{1.082\,\text{g}} = 0.7532\,\text{mL}\,, \tag{1}$$

where 7.99 mmol OH/g is the hydroxyl number of the lignin as provided by the manufacturer, 102 g/mol is the molecular weight of acetic anhydride, and 1.082 g/mL is the acetic anhydride density.

For soda lignin, the reaction mixture was cooled for about 12 h to allow the precipitation of any insoluble fraction. The insoluble fraction was filtered out, and solvent present in the dissolved fraction was evaporated under reduced pressure to obtain the favored product, acetylated soda lignin (Ace_Soda).

3.2.5 Acetylation of Soda Lignin

Acetylation of soda lignin was very similar to that of KPL—10 g of soda lignin was dissolved in 150 mL of acetic anhydride. The reaction was run at 80 °C for 4 h. The flask was cooled down to room temperature and left to stand to precipitate an undissolved fraction. The undissolved fraction was removed by filtration. Resulting Ace_Soda had a softening point between 130 to 143 °C.

3.2.6 Methacrylation of the Methanol KPL Fraction and Unmodified KPL

3.2.6.1 Meth_KPL_UD. Methacrylation of lignin involved reacting the hydroxyl groups of lignin with methacrylic anhydride as described in figure 42.
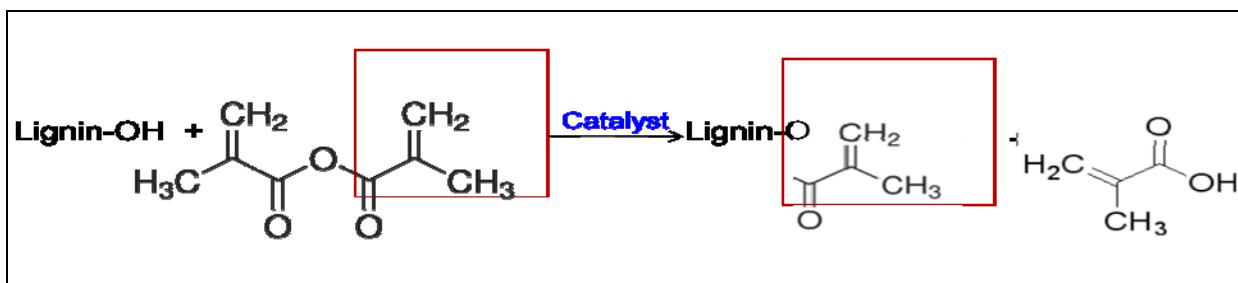
Figure 42. General reaction scheme to produce methacrylated lignin.

Meth_KPL_UD is the University of Delaware–prepared methacrylated KPL. Five methacrylations are currently being investigated to potentially enhance the solubility of KPL and methanol fraction of KPL in traditional and biobased monomers and to functionalize the KPL with polymerizable, terminal, carbon-carbon double bonds. The five methacrylation techniques are briefly described as follows:

1. Coreactant = methacrylic anhydride; catalyst = 1-methylimidazole; solvent = 1,4-dioxane or none; reaction temperature = ~50 °C; reaction time = minimum of 24 h; by-product = methacrylic acid.

2. Coreactant = methacrylic anhydride; catalyst = pyridine in equal mole ratio with methacrylic anhydride; solvent = none; reaction temperature = ice bath to room temperature or greater; reaction time = minimum of 24 h; by-product = methacrylic acid.

3. Part a: coreactant = acetic anhydride; catalyst = pyridine in equal mole ratio with acetic anhydride; solvent = none; reaction temperature = ice bath to room temperature or greater; reaction time = minimum of 24 h; by-product = acetic acid. Part b: primary reactant = acetylated KPL; coreactant = methyl methacrylate; catalyst = p-toluenesulfonic acid; inhibitor = hydroquinone; solvent = none; reaction temperature = 75 °C; reaction time = minimum of 24 h.

4. Coreactant = methacrylic anhydride; catalyst = 4-(N,N-dimethylamino)pyridine as little as 0.2 wt% of methacrylic anhydride; solvent = none; reaction temperauture = room temperature to 60 °C; reaction time = minimum of 8 h; by-product = methacrylic acid.

5. Coreactant = methyl methacrylate; catalyst = p-toluenesulfonic acid; solvent = none; reaction temperature = 70 °C or greater; reaction time = to be determined; by-product = methanol, which is distilled off during the reaction.

Currently, methacryation techniques 4 and 5 are being investigated and will be discussed in length at a later time.

3.2.6.2 Meth_SKL_Clemson. Meth_KPL_Clemson is the Clemson University–prepared methacrylated KPL.

The procedure followed was similar to that of the University of Delaware procedure but more closely matched the procedure outlined by Thielemans and Wool (3)—10 g of indulin AT was dissolved in 40 mL of 1,4-Dioxane, and 60 mL of methacrylic anhydride and 1 mL of 1-Methylimidazole (1MIM) were added to the reactor. The reaction was run at 50 °C for 24 h under a closed nitrogen atmosphere while stirring.

The product was purified by filling the flask with DI water while stirring for hours to allow the decomposition of methacrylic anhydride and the precipitation of solid. The solid was sediment overnight and filtered. The reaction product was washed three times with DI water.

3.2.7 Methacrylated and Acetylated SKL

Methacrylated and acetylated SKL samples were prepared using three procedures.

In procedure 1, 10 g of Ace_SKL (1.5 g/mL [1 g/0.66 mL]) was reacted with 60 mL of Methacrylic anhydride and 1 mL of 1MIM catalyst. No dioxane was used. The reaction was run for 24 h at 50 °C. The flask was filled with DI water to precipitate MA_Ace_SKL, then the product was washed three times with DI water. The solid was dried in a vacuum oven at ~55 °C for more than 48 h but was still "soft" at 55 °C (low T_g).

Procedure 2 was the same as procedure 1 except only 25 mL of methacrylic anhydride and 0.5 mL of 1MIM with 10 g of Ace_SKL was used.

In procedure 3, 10 g of Ace_SKL (1.5 g/mL [1 g/0.66mL]) was reacted with 10 mL of methacrylic anhydride and 0.2 mL of 1MIM catalyst. No dioxane was used. The reaction was

run for 16 h at 50 °C. The material was not soft when taken out from the 55 °C vacuum oven. MA_Ace_SKL was dissolved in acetone and coated on aluminum foil.

3.2.8 Olefin Metathesis Decomposition of KPL

So far, olefin metathesis degradation of KPL (Indulin AT; lot no. MA27) has been attempted three times. Each time, a first-generation Grubbs catalyst was employed (table 7). Prior to each experiment, unmodified KPL was dried under reduced pressure at ~40 °C for a minimum of 12 h.

Table 7. Experimental conditions of the attempted olefin metathesis degradation reactions of unmodified, dried KPL (Indulin AT).

Experiment No.	1	2	3
Unmodified, Dried KPL (g)	10	10	10
Ethylene Glycol (mL)	50	50	100
Catalyst (mg)	100	100	100
Ethylene Gas	Desired 200 psi	Desired 200 psi	300
Max Reaction Temp. (°C)	60	60	85
Reaction Time (h)	6	6	5

In experiment 1, and after adding the KPL, ethylene glycol, catalyst, and magnetic stir bar, the Parr bomb was cooled down to roughly −110 °C using an ethanol-liquid N_2 cooling bath. Ethylene gas was added to the Parr bomb via the relief valve opening and a long needle at a constant pressure of ~15 psi for 10 min. The reactor was then sealed and heated up to the desired reaction temperature while continuously stirring.

In experiment 2, and after adding the KPL, ethylene glycol, catalyst, and magnetic stir bar, the Parr bomb was chilled down to roughly liquid N_2 temperature (−196 °C) using a liquid N_2 cooling bath. Ethylene gas was added to the Parr bomb via the relief valve opening and a long needle at a constant pressure of ~15 psi for 10 min. The reactor was then sealed and heated up to the desired reaction temperature while continuously stirring.

In experiment 3, and after adding the KPL, ethylene glycol, and catalyst, the reactor was sealed. After connecting the Parr bomb (equipped with a pressure gauge and an internal mechanical stirrer) to an electrical motor and an ethylene gas cylinder, the reactor was pressurized with roughly 300 psi of ethylene gas.

To determine whether or not the olefin metathesis degradation reactions of KPL were successful, state-of-the-art chromatography instrumentation with online mass spectroscopy is desired. To limit error, the ideal situation would be to perform chromatography on aliquots of the reaction mixtures as is; separation of the lignin from the polar solvent is not required. It has been reported in the literature that alkaline solutions (0.1–0.5 M NaOH) with the addition of low concentration salt solutions (0.05 M LiCl or 0.1 M $NaNO_3$) were deemed necessary to perform aqueous size exclusion chromatography on KPL (*26*). Unfortunately, these conditions cannot be achieved at the University of Delaware, at least to the authors' knowledge, and may not be needed based on the expertise and instrumentation capabilities at Clemson University via Dr. Bodine.

The University of Delaware is currently utilizing the chromatography resources at Clemson University under the direction of Dr. A. B. Bodine. In particular, we are utilizing the Varian Prostar gradient system with quadrapole MS system, the Rainin isocratic system, and the Waters gradient system in order to characterize the ethenolysis products. The reaction mixture concentrations to date are the following: (1) two reaction mixtures that contain 0.2 g/mL of KPL in ethylene glycol and (2) one reaction mixture that contains 0.1 g/mL of KPL in ethylene glycol. All reaction mixtures contain catalytic amounts of the first-generation Grubbs catalyst.

3.2.9 Singlet Oxidation Decomposition of Kraft Pine Lignin

Unmodified KPL (Indulin AT; lot no.: MA27) (1.0 g) was added to a three-neck round bottom flask equipped with a mechanical stirred 1:1 acetonitrile-ethanol solution (100 mL) with Rose Bengal (a photoinitiator [PI], 5.4×10^{-4} M) and dried. The flask was placed in a 13 ± 0.1 °C water bath that contained a 1% (w/v) solution of $NaNO_{2(aq)}$; $NaNO_{2(aq)}$ solution was used to cut off the irradiation at 400 nm, as described by Bonini et al. (*22*). Irradiation was performed by using a 100-W tungsten-halogen lamp. Air or high-purity O_2 was continuously bubbled through the reaction mixture. Reactions were conducted for 4, 8, 12, and 24 h. Upon evaporation of the solvent, the KPL was acetylated using the procedure described in section 2.3.3.

3.3   Results and Discussion

3.3.1 Kraft Pine Lignin Solvent Fractionation

The yields of KPL in each fraction can be seen in figure 43. The average KPL recovery was 93.5% ± 1.2%. As can be seen in figure 43, roughly 40% of the KPL dissolved in methanol while over 50% was insoluble in any of the utilized solvents. Methanol has a solubility parameter of 14.5 $(cal/cm^3)^{1/2}$. KPL has been reported in the literature to have a solubility parameter >12.03 $(cal/cm^3)^{1/2}$ (*3*). Thus, 40% of the KPL has a solubility parameter close to 14.5. Upon fractionation, the KPL fractions were acetylated in order to enhance their solubility in THF for gel permeation chromatography (GPC) analysis. The GPC results can be seen in figure 44 where the average molecular weight and polydispersity index are plotted as a function of fraction number. Figure 44 shows a clear trend of increasing number average molecular weight and polydispersity with increasing fraction number, with the undissolved KPL (fraction 5) possessing a relatively high M_N and PDI. Fractions 1–3 possess molecular weights and PDIs that are sought for the utilization of lignin in biobased composite materials, most especially, fractions 1 and 2. Unfortunately, these fractions totaled <1 g of the starting material. However, fraction 3, the methanol fraction, is of considerable yield and possesses a molecular weight and PDI that are potentially workable. Currently, we are investigating the methacrylation of fraction 3 using the methacrylation techniques described previously. Additionally, we hope to be able to apply the olefin metathesis degradation technique to fraction 3 to reduce its molecular weight and PDI and send samples of the fractionated samples to Dr. Bodine for a more in-depth chromatography analysis.
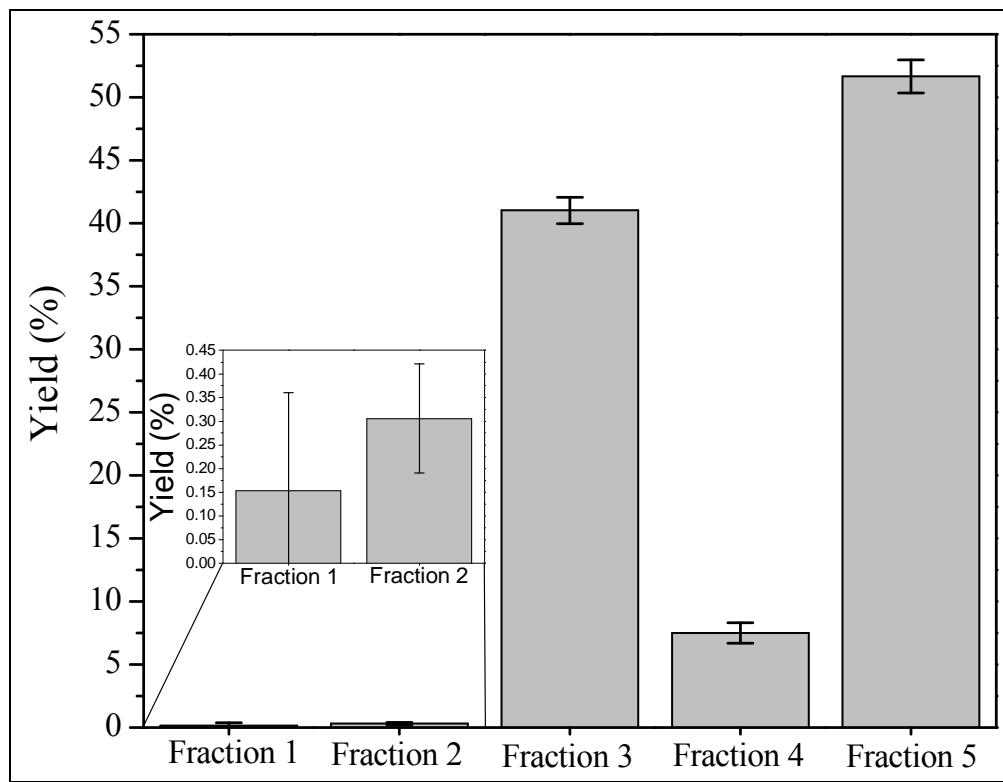
Figure 43. KPL yields as a function of solvent fraction.
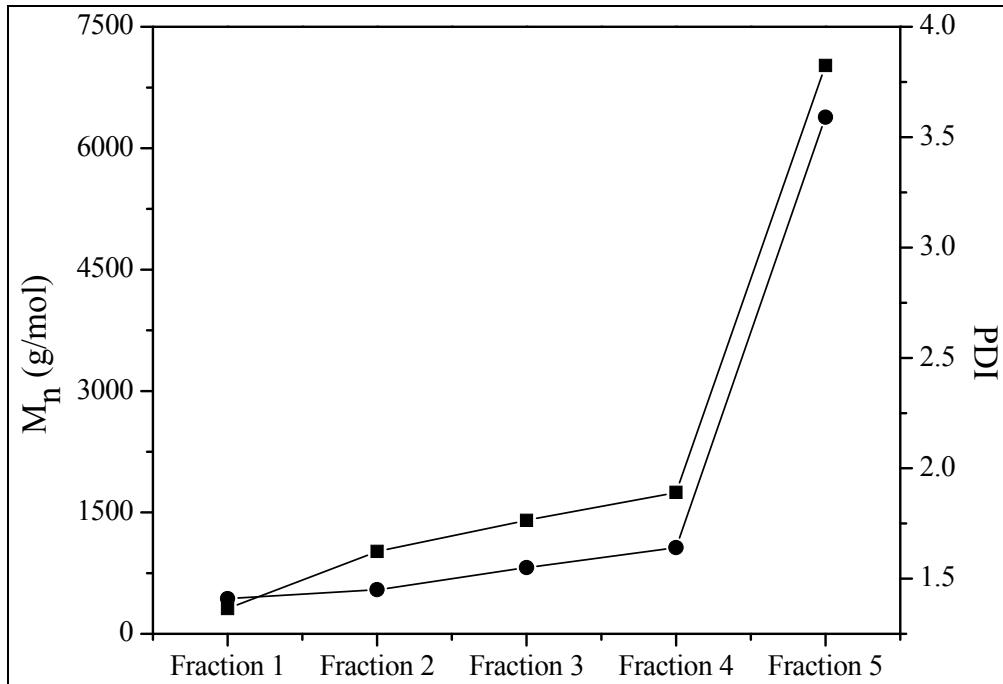
Figure 44. Number of average molecular weights (M_n) and PDI of acetylated KPL that was fractionated into five fractions.

3.3.2 Singlet Oxygen Mediated Decomposition of KPL

After each singlet oxygen mediated degradation reaction, the collected, potentially degraded, solid KPL contained a maroon color indicative of the presence of Rose Bengal. Upon acetylation and subsequent work-up, maroon color vanished with collected acetylated KPL part exhibiting brown hues. Based primarily on quantitative yields of aceylated degraded products (shown in figure 45), the KPL was not significantly degraded into smaller molecular weight products. This degradation technique was successful when a considerable amount of β-aryl ether bonds exist in the lignin. The results from this study suggest that KPL is not appreciatively degraded via singlet oxygen. The results are also a testimony to the Kraft delignification process success administered by MeadWestVaco since the Kraft pulping process primarily attacks α-aryl and β-aryl ether bonds in order to aid in separating lignin from cellulose and hemicelluloses. This study is currently on hold.
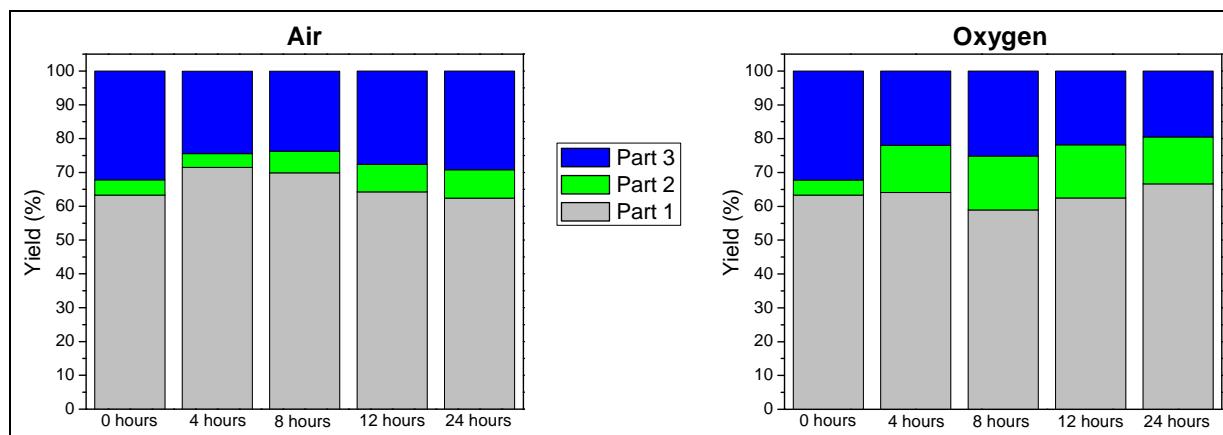
Figure 45. Yields (*y*-axis) of high molecular weight solid (Part 1), medium molecular weight solid (Part 2), and low molecular weight liquid (Part 3) of acetylated KPL that was potentially degraded via a singlet oxygen mediated degradation in air (left) or O_2 (right) for desired reaction times (*x*-axis).

3.3.3 Acetylation of SKL and Soda Lignin

To modify SKL into a fusible material, acetylation was performed by reacting SKL with acetic anhydride to convert the highly reactive hydroxyl group into acetyl group. FTIR spectra in figure 46a showed a broad band between 3300 cm^{-1} and 3500 cm^{-1} attributed to the hydroxyl groups in phenolic and aliphatic structures before acetylation. After acetylation, the OH group absorption band decreased significantly, as shown in figure 46b for procedure 1. Also, a strong peak around 1750 cm^{-1} appeared due to C=O stretching of acetyl group. Note, similar results were found for acetylation of soda lignin and methacrylation of lignin.
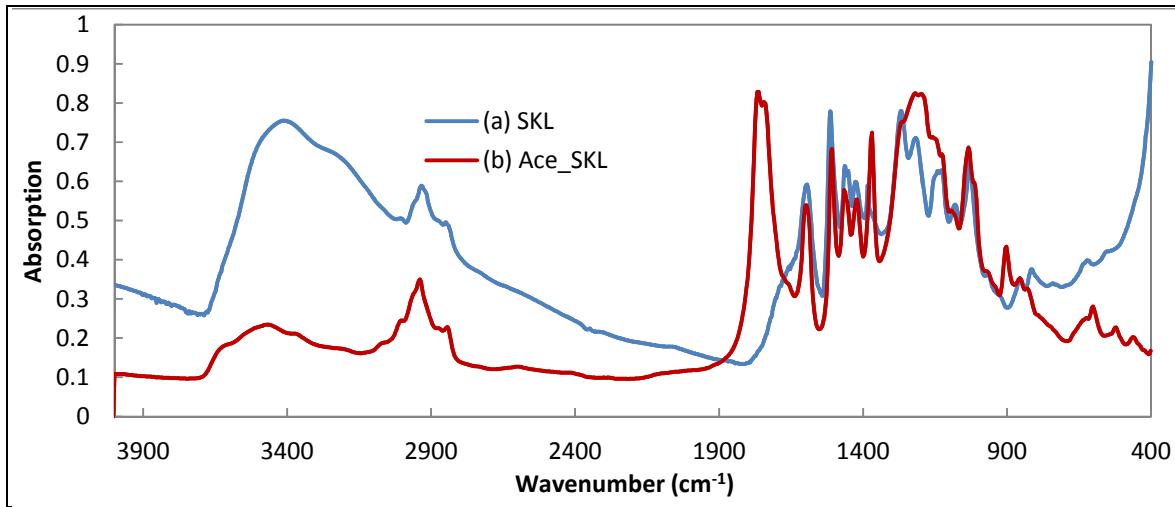
Figure 46. FTIR spectra of (a) as-received softwood Kraft lignin (SKL) and (b) acetylated softwood lignin (Ace_SKL).

Figure 47 shows the effect of reduced concentrations of acetic anhydride used to produce Ace_SKL. All of the FTIR spectra were normalized with peaks at 856 cm^{-1} (C-H bending on benzene rings). The absorption of the hydroxyl group increased as the amount of acetic anhydride per gram of SKL decreased. A higher content of the hydroxyl group is favorable for thermostabilization but not amenable to melt spinning.
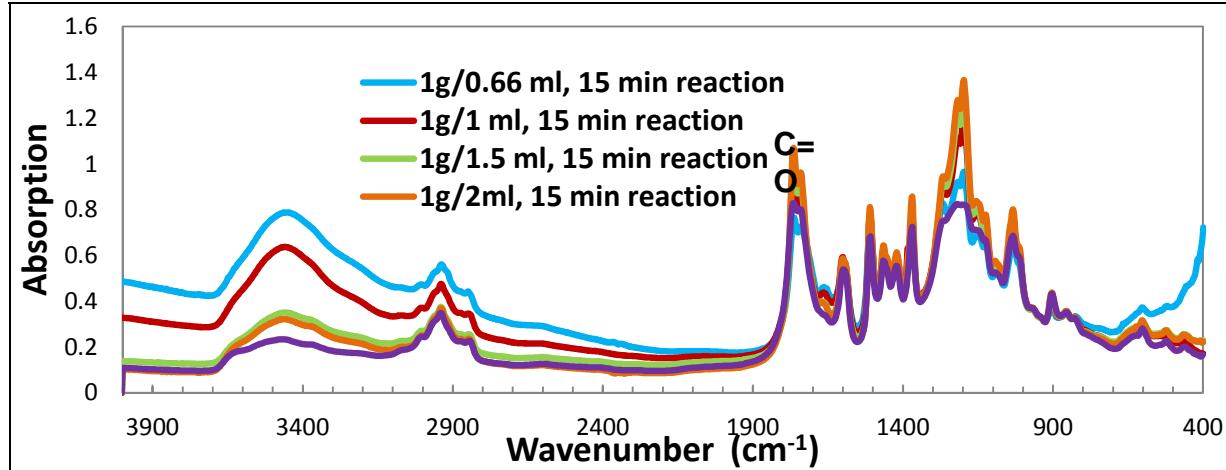
Figure 47. FTIR spectra of Ace_SKL as a function of the amount of acetic anhydride used.

3.4 Conclusions and Future Work

This work shows that there are chemical methods to both effectively fractionate and modify lignin. These modifications can reduce the molecular weight of the lignin, enabling the production of resins or melt-spinnable lignin polymer for fiber production. In particular, metathesis, methacrylation of lignin, and solvent fractionation have effectively improved the

processability of lignin for these applications. On the other hand, singlet oxygen decomposition of lignin has not aided in lignin processability and will likely be abandoned in this work.

Future work will focus on improving the metathesis of lignin and using combinations of fractionation, metathesis, and methacrylation to obtain optimum products for resin and carbon fiber production. The following major tasks will be completed in FY12 and FY13:

1. Focus on techniques four and five since the methacrylation of KPL and the methanol fraction of KPL have already been investigated using the methacrylation techniques (November 2011–March 2012).

2. Study the olefin metathesis degradation of KPL in collaboration with Dr. Bodine at Clemson University (November 2011–January 2013).

3. Utilize Dr. Bodine's expertise to characterize the KPL fractions in-depth (November 2011–January 2013).

4. Study the solubility of KPL and fractionated KPL in guaiacol, eugenol, and vanillin (November 2011–January 2012) as well as study the solubility of methacrylated versions of KPL and fractionated KPL (specifically the methanol fraction) in methacrylated guaiacol (MG) and methacrylated eugenol (ME) (January 2012–June 2012). If promising solubility results are revealed, polymerize and characterize the resins (January 2012–June 2013).

5. Use methacrylation and acetylation in one step to reduce the amount of processing steps and tailor the functionality of the lignin.

6. Perform methacrylation and methacrylation/acetylation of soda lignin.

7. Fractionate the chemically modified lignin after the chemical reaction to improve the ability to use the lignin in carbon fiber processing.

References

1. Wool, R. P.; Sun, X. S. *Biobased Polymer and Composites*, 1st ed.; Elsevier B. V.: New York, 2005.

2. Lora, J. H.; Glasser, W. G. *J. Polymers Environment* **2002**, *10*, 39–48.

3. Thielemans, W.; Wool, R. P. *Composites Part A: Applied Science and Manufacturing* **2004**, *35*, 327–338.

4. Li, Y.; Sarkanen, S. *Macromolecules* **2002**, *35*, 9707–9715.

5. Calvo-Flores, F. G.; Dobado, J. A.; *ChemSusChem* **2010**, *3*, 1227–1235.

6. Gandini, A. *Green Chemistry* **2011**, *13*, 1061–1083.

7. Voitl, T.; Rudolf von Rohr, P. *ChemSusChem* **2008**, *1*, 763–769.

8. Zakzeski, J.; Weckhuysen, B. M. *ChemSusChem* **2011**, *4*, 369–378.

9. Binder, J. B.; Gray, M. J.; White, J. F.; Zhang, Z. C.; Holladay, J. E. *Biomass and Bioenergy* **2009**, *33*, 1122–1130.

10. Jia, S.; Cox, B. J.; Guo, X.; Zhang, Z. C.; Ekerdt, J. G. *ChemSusChem* **2010**, *3*, 1078–1084.

11. Petrocelli, F. P.; Klein, M. T. *Industrial and Engineering Chem. Product Research and Development* **1985**, *24*, 635–641.

12. Silva, E. A. B. D.; Zabkova, M.; Araújo, J. D.; Cateto, C. A.; Barreiro, M. F.; Belgacem, M. N.; Rodrigues, A. E. *Chem. Engineering Research and Design* **2009**, *87*, 1276–1292.

13. Chakar, F.; Ragauskas, A. J. *Industrial Crops and Products* **2004**, *20*, 131–141.

14. Mialon, L.; Pemba, A. G.; Miller, S. A. *Green Chemistry* **2010**, *12*, 1704–1706.

15. Sergeev, A. G.; Hartwig, J. F.; *Science* **2011**, *332*, 439–443.

16. Marton, W. *In Lignins: Occurrence, Formation, Structure and Reactions*; Sarkanen, K. V.; Ludwig, C. H., Eds.; Wiley-Interscience: New York, 1971; pp 639–694.

17. Schrodi, Y.; Ung, T.; Vargas, A.; Mkrtumyan, G.; Lee, C. W.; Champagne, T. M.; Pederson, R. L.; Hong, S. H. *CLEAN - Soil, Air, Water* **2008**, *36*, 669–673.

18. Ferré-Filmon, K.; Delaude, L.; Demonceau, A.; Noels, A. F. *European J. Organic Chem.* **2005**, *2005*, 3319–3325.

19. Scholl, M.; Ding, S.; Lee, C. W.; Grubbs, R. H. *Organic Letters* **1999**, *1*, 953–956.

20. Gallivan, J. P.; Jordan, J. P.; Grubbs, R. H. *Tetrahedron Letters* **2005**, *46*, 2577–2580.

21. Bonini, C. *Industrial Crops and Products* **2004**, *20*, 243–259.

22. Bonini, C.; D'Auria, M.; Ferri, R. *Photochemical and Photobiological Sciences* **2002**, *1*, 570–573.

23. Lanzalunga, O.; Bietti, M. *J. Photochemistry and Photobiology B, Biology* **2000**, *56*, 85–108.

24. Holladay, J. E.; White, J. F.; Bozell, J. J.; Johnson, D. *Top Value-Added Chemicals From Biomass - Volume II - Results of Screening for Potential Candidates From Biorefinery Lignin*; PNNL-16983; Pacific Northwest National Laboratory: Richland, WA, 2007.

25. Mörck, R.; Yoshida, H.; Kringstad, K. *Holzforschung* **1986**, *40*, 51–60.

26. Hortling, B.; Turunen, E.; Eokkonen, P. *Handbook of Size Exclusion Chromatography and Related Techniques*, 2nd ed.; Wu, C., Ed.; Marcel Dekker, Inc.: New York, 2004; 355–383.

4. Development of Lignin-Based Carbon Fibers

4.1 Introduction

High-strength carbon fibers used in structural composite applications are almost exclusively derived from wet spinning of PAN precursor fibers (*1, 2*). This wet-spinning process suffers from two inherent limitations:

- Chemical conversion of PAN into carbon proceeds via generation of hydrogen cyanide (HCN) and other toxic gases during the thermal stabilization and carbonization steps.

- Wet-spinning process necessitates use of hazardous solvents.

Therefore, additional studies need to investigate the replacement of PAN by an environmentally sustainable precursor such as lignin, which is an abundant biorenewable hydrocarbon source (*3–5*). Numerous hydrocarbons can be converted to carbon, but very few have been actually converted to structural carbon fibers. Besides PAN, MP and rayon are the only other precursors that have produced carbon fibers. MP produces highly graphitic carbon fibers with high modulus and high thermal conductivity, but low strength. Rayon, on the other hand, uses naturally occurring cellulose, but its conversion to carbon is mechanistically limited to carbon fibers with poor strength and low thermal conductivity. Therefore, rayon-based carbon fibers cannot be used in primary reinforcement applications.

Among biobased alternatives, the aromatic encrusting material around cellulosic wood fibers is lignin, which confers rigidity and strength to wood. Lignin is abundantly available: over 3×10^{11} tons of lignin exist in the biosphere with $\sim 2 \times 10^{10}$ tons generated annually (*6*). Because of the aromatic nature of the compound, lignin may be used to generate a valuable source of aromatic precursors for processing into carbon fibers. However, because of its 3-D aromatic structure, lignin is intractable in its unmodified state and must be suitably modified into components or products that can be converted into fibers.

The processes involved in modifying lignin can be broadly identified as chemical and microbial. In general, chemical processes are typically not very selective in terms of the reaction products but may be accomplished at commercially viable (fast) reaction rates by adjusting reaction conditions and catalysts. In contrast, microbial mechanisms produce better selectivity, but such biological reactions may proceed at slow rates. Therefore, the project was designed to simultaneously investigate both chemical and biological mechanisms for obtaining suitable precursors to ultimately produce structural carbon fibers.

4.2   Literature Review

Since the 1960s, lignin has been studied as a precursor for carbon fiber. In 1969, Otani (*7*) patented a lignin-based carbon fiber produced by dry-spinning from an alkaline solution of lignin with polyvinyl alcohol added as a plasticizer. More recently, researchers have focused on producing carbon fiber from different types of lignin by melt spinning. Sudo and Shimizu (*8*) modified a steam-exploded birch wood lignin by hydrogenolysis and followed up with extraction. Uraki et al. (*9*) converted a lignin obtained from aqueous acetic acid pulping of hardwood into carbon fiber. The acetic acid pulping process partially acetylated the hydroxyl groups in the material and prevented condensation between hydroxyl groups. The resulting organosolv lignin has good melt spinnability. Kubo et al. (*10*) applied atmospheric acetic acid pulping on softwood and removed a large molecular weight fraction from it by fractionation with aqueous acetic acid to obtain a fusible material for melt spinning. Kadla et al. (*11*) produced carbon fiber directly from hardwood Kraft lignin and Alcell organosolv lignin. Poly(ethylene oxide) was also added into hardwood Kraft lignin to increase its processability. Indulin AT softwood Kraft lignin from MeadWestvaco was studied as well, but it was not able to be melt spun since it had a highly cross-linked structure and low thermal mobility. ORNL researchers studied a series of lignin from different sources as carbon fiber precursors. They found that a hardwood Kraft lignin from MeadWestvaco was melt spinnable (*12*). They also showed that softwood Kraft lignin cannot be melt spun without proper modification or plasticization. A softwood Kraft lignin from Kruger Wayagamack (Quebec, Canada) (*13*) was successfully melt spun by adding a certain percent of hardwood Kraft lignin as plasticizer, and this softwood Kraft lignin had a softening point of 190 °C.

Eckert and Abdullah (*14*) patented a softwood Kraft lignin–derived carbon fiber by acetylation of the hydroxyl group with acetic anhydride. A softwood Kraft lignin modified with or without catalyst resulted in 16%–22% acetyl content by weight and became fusible. In their example, a relatively small batch of acetylated lignin (200 mg) was subject to melt spinning.

Table 8 is a summary of tensile properties of carbon fibers obtained from different precursors from these studies. However, all the listed lignin-derived carbon fibers have relatively poor mechanical properties compared with pitch- or PAN-based carbon fiber.

The majority of these studies attempted to obtain low-cost carbon fibers, so performance was not necessarily emphasized. However, in the present study, we plan to investigate strategies to enhance the mechanical performance since the ultimate objective is to obtain structural carbon fibers.

Table 8. A summary of tensile properties of carbon fibers obtained from different precursors in prior studies.

Precursor Type	Diameter (µm)	Elongation (%)	Modulus (GPa)	Tensile Strength (MPa)	Electrical Resistivity (µΩ·m)	Reference
Steam exploded hardwood	7.6 ± 2.7	1.63 ± 0.19	40.7 ± 6.3	660± 230	NA	Sudo, 1992[8]
Organosolv hardwood	14–35	0.64–1.12	2.17–39.1	13.3–355	NA	Uraki, 1995[9]
Organosolv softwood	84 ± 15	0.74 ± 0.14	3.59 ± 0.43	26.4 ± 3.1	NA	Kubo, 1998[10]
Kraft hardwood	46 ± 8	1.12 ± 0.22	40 ± 11	422 ± 80	NA	Kadla, 2002[11]
Kraft softwood, acetylated	5–100	NA	NA	NA	NA	Eckert, 2008[14]
Rayon-based carbon fiber	5–25	—	172–690	117–3950	—	Various
PAN-based carbon fiber	5–15	2	100–500	3000–7000	—	Various
MP–based carbon fiber	5–15	0.6	200–800	1000–3000	1–15	Various

These studies also establish that spinning lignin precursor into thin fibers remains a technical barrier. Consequently, properties of the resulting carbon fibers from such lignin precursors have been rather low. Therefore, the goal of this research project is to produce carbon fiber from lignin precursors such as Indulin AT softwood Kraft lignin with enhanced properties such as those suitable for structural composites. The specific research objectives for this component of the project are as follows:

- Chemical modification of lignin to enable fiber spinning

- UV-thermal dual mechanism cross-linking/stabilization

- High-temperature thermal treatment

- Characterization of carbon fiber properties

4.3   Experimental

4.3.1 Material

Three grades of lignin were obtained:

- Softwood Kraft lignin, Indulin AT* (SKL), was obtained from Mead-Westvaco, Charleston, SC.

- Soda lignin Protobind 1000 was obtained from GreenValue Enterprises LLC in Media, PA, derived from wheat straw and grass.

---

*Indulin AT is a trademark of Mead-Westvaco.

- An organosolv hardwood lignin was provided by Energy Research Centre, Netherlands (ECN lignin). The ECN lignin was derived from poplar with an ethanol-organosolv process (<0.1% ash content).

4.3.2 Modified Lignin

Acetylated KPL and soda lignin, as well as methacrylated Kraft lignin, as previously described, were used throughout this work.

4.3.3 Analysis of Lignin

The softening point of lignin samples was measured with a METTLER TOLEDO FP900 Thermosystem using the Mettler Cup and Ball method according to ASTM D 3461. Ash content and elemental analysis determination were performed following ASTM D 5630 at the Agricultural Service Laboratory, Clemson University. FT-IR spectroscopy was performed in the transmission mode with a Nexus spectrophotometer using KBr pellets containing 1% samples.

4.3.4 Softening Point Analysis

The softening point of lignin samples was measured in accordance with the apparatus and procedures described in section 1.

4.3.5 Rheology

Rheological testing of lignin samples was carried out on an ARES rheometer (TA Instruments) using cone-and-plate fixture under a steady shear rate range of 1 to 10 1 s^{-1}. Lignin melts were tested at temperatures above their melting point under a nitrogen flow. The Ace_SKL solution was tested at room temperature without gas flow. We desire 30 min of stable viscosity to process the fibers. However, the material must also increase in viscosity significantly after 30 min, which would indicate that the precursor has some reactivity that is desired during fiber stabilization.

4.3.6 Fiber Spinning

Melt spinning of lignin precursors was performed using an Instron capillary rheometer equipped with a 0.25-mm-diameter die. The maximum take-up speed applied was around 3 m/s.

For solution spinning, 50 g of Ace_SKL dry powder was fully dissolved in 100 mL of acetone. The mixture was stirred continuously and solvent evaporated until the solution was concentrated to above 1.8-g solids per milliliter of solvent. The viscous solution was transferred into a spinning barrel equipped with a 12-hole die, with each hole having a 150-μm diameter. Spinning was performed with a batch unit from AJA Inc. (Greenville, SC). Warm air was blown on the extruded fibers in the spinning chamber during spinning to accelerate the evaporation rate of the solvent during the dry-spinning process. In this lab-scale process, the solvent was vented, but in the continuous commercial process, the solvent is routinely condensed and recycled.

4.3.7 Thermostabilization

Lignin fiber samples were placed in a programmable air oven and heated from room temperature up to 220 °C with a heating rate ranging from 0.01 to 0.5 °C/min for different batches of samples. Dwell time at a certain temperature was necessary to prevent fibers from melting and sticking.

4.3.8 Carbonization

After stabilization, the fiber was wrapped in graphite foil and placed into a RED DEVIL furnace. Carbonization was performed by heating at a rate of 4.5 °C/min up to 900 °C in a stream of argon and held at 900 °C for 1 h. Our labs are equipped with ultrahigh temperature furnaces (2700 °C), but such temperatures were not used in the present studies because the objective was to obtain higher tensile strength and strain-to-failure properties, which typically decrease at the ultrahigh temperatures.

4.3.9 Single Filament Tensile Testing

To measure tensile properties, individual fibers were tested in a Phoenix tensile testing device following the ASTM test method D-3379-5. The load cell of the MTS apparatus has a maximum capacity of 500 g, and the crosshead speed was set to 0.5 mm/min. Filaments 25 mm in length were mounted in the paper frame. The fiber diameter was measured by using an Olympus BX 60 optical microscope. The individual fibers were placed on the glass slide, and then images were obtained at a magnification of 50×. The diameter was measured with the aid of the image analysis program at three different spots on the fiber. Each paper tab was secured in the upper and lower jaws of the MTS. To prevent the accidental breakage of fiber prior to test failure, we used an electric hot wire (instead of scissors) to burn the paper tab.

4.4 Results and Discussion

4.4.1 Unmodified Lignin

As-received SKL showed no softening behavior during the entire heating procedure even when the temperature reached up to 300 °C (figure 48). The ball did not fall into the cup. Instead, degradation was observed, and the residue after heating was a foamed state, indicating the generation of volatiles during heating. These results are in agreement with those reported in previous literature studies in which softwood lignin has been shown to possess lower thermal mobility because it has a higher cross-linked structure than does hardwood lignin. The high content of hydroxyl groups results in dehydration reaction between molecules; thus, SKL cannot be melt spun without appropriate modification.
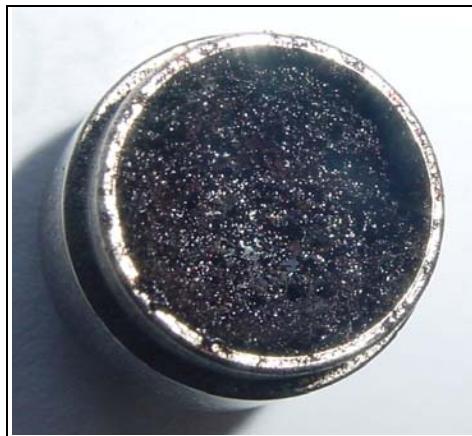
Figure 48. Unmelted, foamy residue
resulting from softening point
test of pure SKL (ball
removed).

The ash content of unmodified SKL and Protobind was measured as shown in table 9. A target
ash content to make high-performing carbon fibers is <0.1 wt% (*13*). Indulin AT SKL has a
higher ash content at 2.85%, and sulfur and sodium were the primary impurities in SKL.
Protobind also has a high ash content at 1.66% with, again, sulfur and sodium as the largest
concentration of impurities.

Table 9. Metal analysis and ash content of Indulin AT SKL and Protobind 1000 soda lignin

Sample	K (%)	Ca (%)	Mg (%)	S (%)	Na (%)	Al (%)	Ash (%)
Indulin AT	0.1032	0.0154	0.0167	1.1371	0.7057	0.0142	2.85 ± 0.04
Protobind 1000	0.2094	0.0193	0.0086	1.2303	0.2832	0.005	1.66 ± 0.03

4.4.2 Washing of SKL

To reduce the ash content in lignin, different washing methods were used (see table 10 for
results). SKL was washed in boiling water first. The filtered solution was brown because a
certain amount of SKL was dissolved in boiled water, which resulted in a yield of 61 wt%. The
solubility of SKL in room temperature deionized water was lower but also resulted in a higher
ash content. Washing with acidified water (using hydrochloric acid [HCl]) with a pH of 2 at
room temperature is the most typical method in literature to purify Kraft lignin. When SKL was
washed repeatedly up to 28 times, the ash content was reduced to 0.19%. In future studies,
boiled water and acidified water will be combined to reduce labor and the amount of water
consumed. It was assumed that washing with boiled water can lead to a larger average molecular
weight, since small molecular weight fractions will get dissolved in the boiled water together
with salts.

Table 10. Washing purification of SKL.

Washing Liquid	Ash Content (%)	Yield (%)
Boiled deionized water, 1 time	0.72	61
Room temperature deionized water, 1 time	1.42	85
Acidified water, 5 times	0.75	90
Acidified water, 11 times	0.30	64
Acidified water, 17 times	0.20	Not weighed
Acidified water, 28 times	0.19	62

The softening point of methanol fractionated SKL was measured. The lignin displayed no softening point. Thus, the reduction in molecular weight, as demonstrated in section 3, was not sufficient to enable flow of the lignin.

We are in the process of obtaining ash content of chemically modified lignin. The ash content can play a significant role in creating defects and weakening the resulting carbon fibers. In addition, molecular weight analysis using chromatography or mass spectrometry will be performed to assess how the chemical modification and purification steps affect the molecular weight.

4.4.3 Carbon Fiber From Highly Acetylated SKL

To modify SKL into a fusible material, acetylation was performed. Highly acetylated SKL was prepared by reacting SKL with acetic anhydride using procedure 1 as described in section 3.2.4.

4.4.3.1 Rheological Characterization of Modified Lignin Samples. The acetylated SKL showed a softening temperature between 156 and 167 °C (figure 49). To evaluate the melt viscosity of the acetylated sample, it was subjected to a shear rheology test at a shear rate of 1 s^{-1} at 170 °C, which is about 5 °C higher than its softening point. The viscosity of melted Ace_SKL increased from around 80 Pa·s to 8000 Pa·s within 30 min, as shown in figure 50, and the test finally ended because the torque transducer was overloaded. Overall, Ace-SKL had an unstable melt viscosity, as the viscosity build with time was too fast.

To obtain a material with relatively stable viscosity, Ace_SKL was extracted with 75% acetic acid, and a fraction with relatively large molecular weight was removed in this manner. The fraction soluble in 75% acetic acid had a softening point between 136 and 145 °C and was subject to a rheology test again, as shown in figure 50b. The viscosity still increased gradually but remained below 100 Pa·s for the first 20 min, which would enable subsequent melt spinning.

Figure 49. A consolidated melt resulting
from softening point test on
Ace_SKL (ball removed).
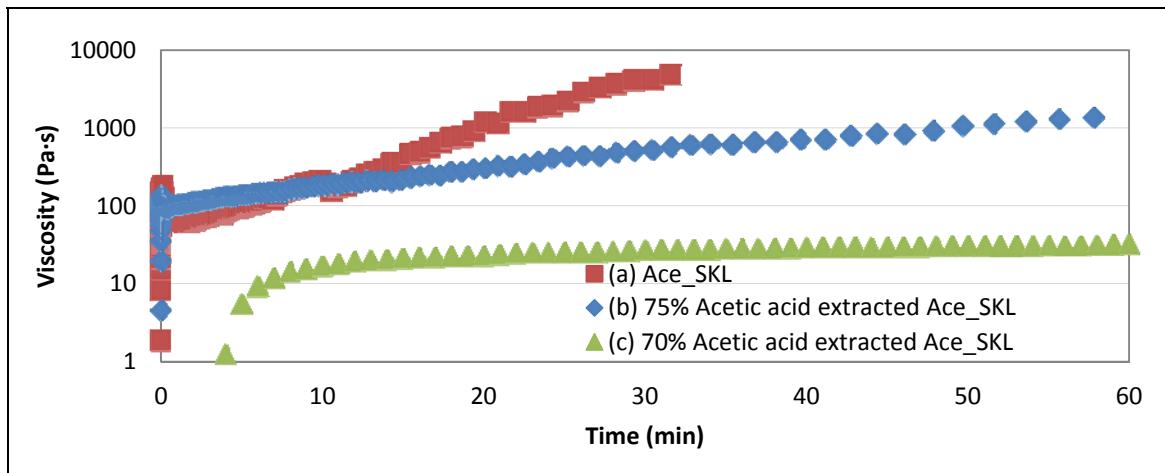
Figure 50. Transient shear viscosity of Ace_SKL and acetic acid extracted Ace_SKL.

Ace_SKL was extracted with 70% aqueous acetic acid first, and the soluble fraction had a softening point of 115–127 °C. When tested at 140 °C, it had a stable melt viscosity of about 70 Pa·s for 1 h (figure 50c). However, this melt stability also indicates the very stable chemical structure of this composition, which will hinder the thermo-oxidative stabilization step. We then used 75% aqueous acetic acid to extract Ace_SKL.

4.4.3.2 Fiber Spinning and Thermo-Oxidative Stabilization. The Instron capillary rheometer was preheated to 145 °C (for 75% acetic acid extract Ace_SKL), which was about 5 °C higher than the softening point for each batch of sample. When the temperature reached the target value, sample was loaded into the barrel. The plunger was fitted into the barrel, and the melt was extruded out of the capillary die. A take-up roll was positioned below to draw down the melt into fibers. The total heating time was controlled in this manner to prevent the formation of

82

high-viscosity material before spinning. Both Ace_Soda and 75% acetic acid extracted Ace_SKL were successfully spun into fiber. The lowest fiber diameter was 25 ± 4 μm for 75% acetic acid extracted Ace_SKL fiber, and 22 ± 3 μm for Ace_Soda fiber. Overall, excellent fibers were produced from Ace_SKL, as shown in figure 51. The fibers were 29.6 ± 1.6 μm in diameter and were spun continuously for 10 min before they began to break.
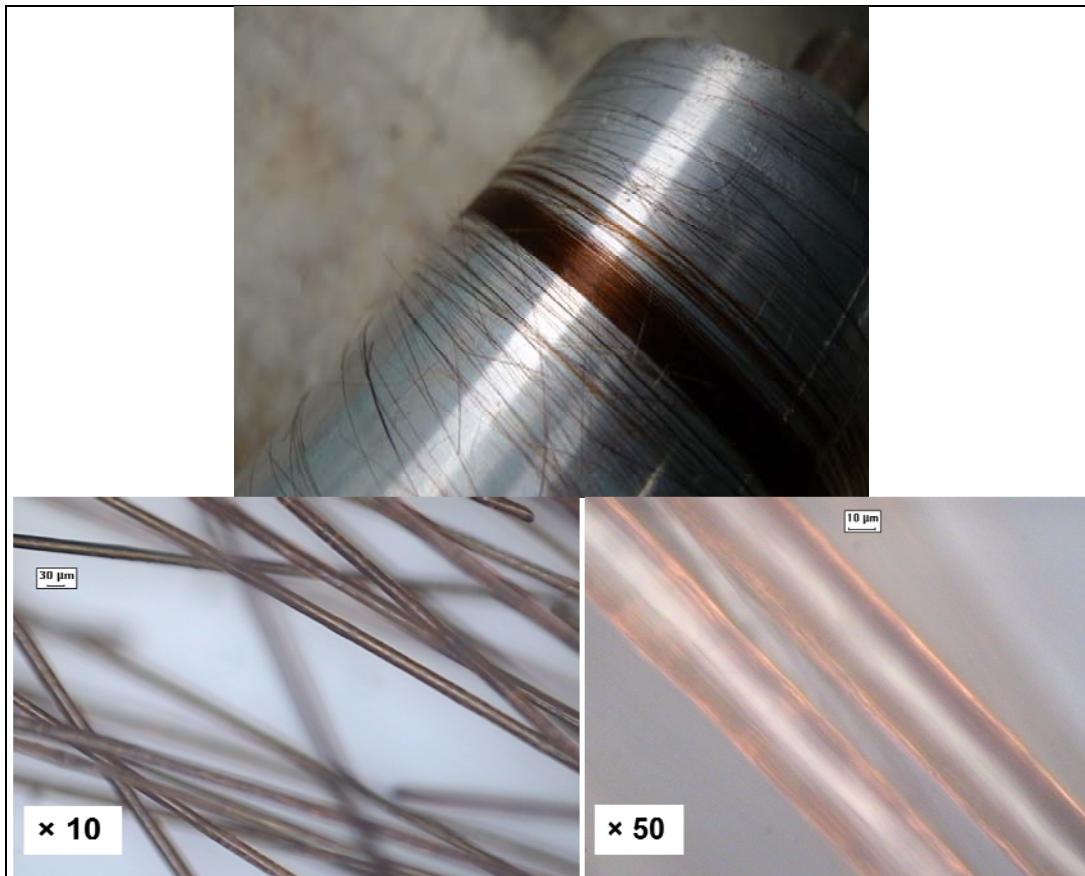
Figure 51. 75% acetic acid–extracted Ace_SKL as-spun fibers on spool (top) and magnified optical microscopy images (bottom).

Although the extracted Ace_SKL fiber was easy to melt spin, it was virtually impossible to stabilize by thermo-oxidative stabilization. Substitution of hydroxyl groups by the stable acetyl groups prevented any cross-linking and thermal stabilization of the macromolecules within the precursor fibers. Thus, although we did not attempt fiber formation and stabilization of 70% acetic extracted Ace_SKL, we believe that the resulting material will suffer the same limitations. We emphasize that molecular cross-linking within precursor fibers is an essential step in transforming the fiber into a thermoset before it can be carbonized. Although we applied a ramp program with a heating rate as low as 0.01 °C/min, the fibers could not be maintained in their glassy state and became tacky at around 150 °C. Once the precursor becomes tacky, it is not possible to retain individual precursor fibers; this shows that the composition is not well-suited for producing high-performance carbon fibers.

Figure 52 (left) shows as-spun Ace_SKL melt-spun fibers on the left (placed on a graphite sheet) before oxidative stabilization. The fibers were heated up to 150 °C at a ramp rate of 0.02 °C/min. The treated fibers became tacky and stuck to each other, as shown in figure 52 (right), during the thermo-oxidative stabilization. Although 1–2 days of dwell time at 140 °C was applied, fibers still became tacky when the temperature was raised above 150 °C. The same situation occurred on Ace_Soda fibers. This indicated that incomplete surface stabilization occurred, and there was not enough reaction occurring at the surface. Thus, another method of surface stabilization of these fibers is needed, otherwise these fibers will not produce high-performance carbon fibers. Nonetheless, the stabilized Ace_SKL fibers did not dissolve in acetone, indicating their cross-linked structure after thermo-oxidation.
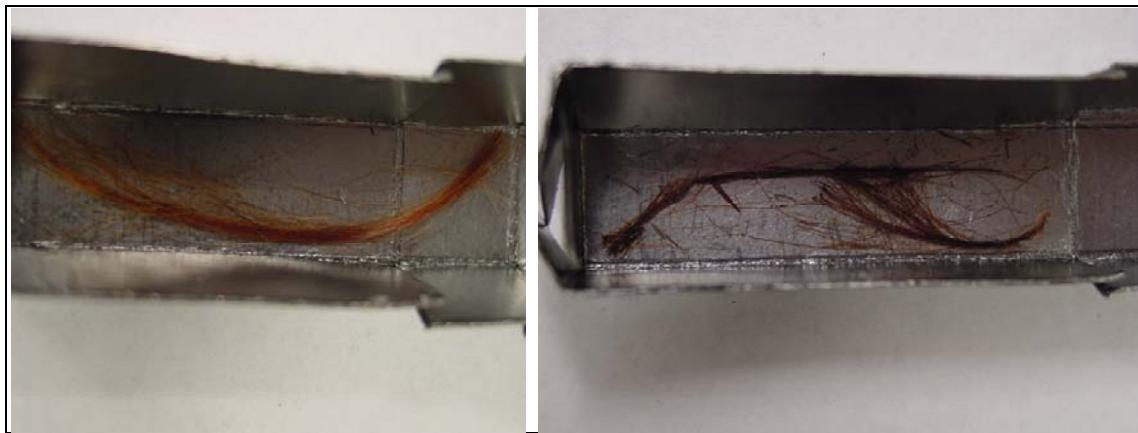
Figure 52. As-spun Ace_SKL fibers (left) and tacky Ace_SKL fibers after heat treatment (right).

The stabilized fibers were also tested with a lighter flame, as we typically do to test oxidized pitch fiber. Oxidized pitch fibers survive the flame test, but these fibers did not survive in the flame. However, in the inert environment used during carbonization, these fibers survived the heat treatment. Figure 53 is a photograph of the oxidized Ace_SKL fibers.

Figure 53. Oxidized Ace_SKL fiber.

To help the thermostabilization of 75% AA_Ace_SKL fibers, the material was heated in a vacuum oven for different hours to increase its T_g/softening point before spinning (figure 54). However, fibers spun with a high SP (~200 °C) material still could not be cross-linked.
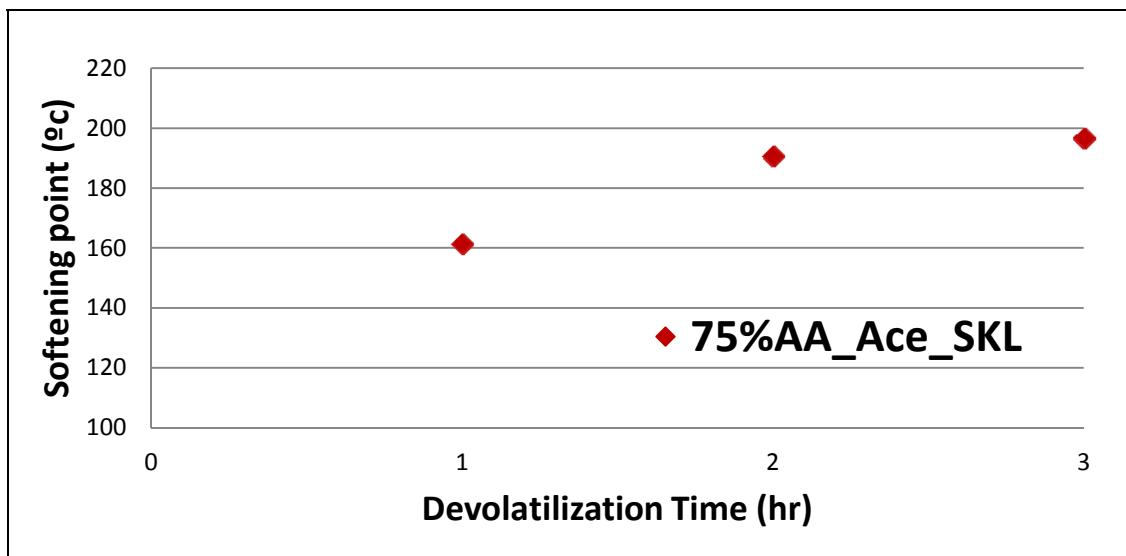
Figure 54. Softening point of Ace_SKL with different devolatilization time.

Although the extracted Ace_SKL fiber was easy to melt spin, it was virtually impossible to stabilize it by thermo-oxidative stabilization. Substitution of hydroxyl groups by the stable acetyl groups prevented any cross-linking and thermal stabilization of the macromolecules within the precursor fibers. We emphasize that molecular cross-linking within precursor fibers is an essential step in transforming the fiber into a thermoset before it can be carbonized. Although a ramp program with a heating rate as low as 0.01 °C/min was applied, the fibers could not be maintained in their glassy state and became tacky at around 150 °C. Once the precursor becomes tacky, it is not possible to retain individual precursor fibers; this shows that the composition is not well suited for producing high-performance carbon fibers. Thus, reduced acetylation or methacrylation of SKL may be useful in making a thermostabilized carbon fiber. In addition, a different type of lignin may result in improved properties. All of these methodologies are discussed in the following sections.

4.4.4 Carbon Fibers From Soda Lignin

Soda lignin is produced in a distinctly different process than Kraft lignin, as illustrated in figure 55. As a result, soda lignin is expected to have a different molecular structure and functionalization that can lead to enhanced properties for melt spinning and carbon fiber formation.
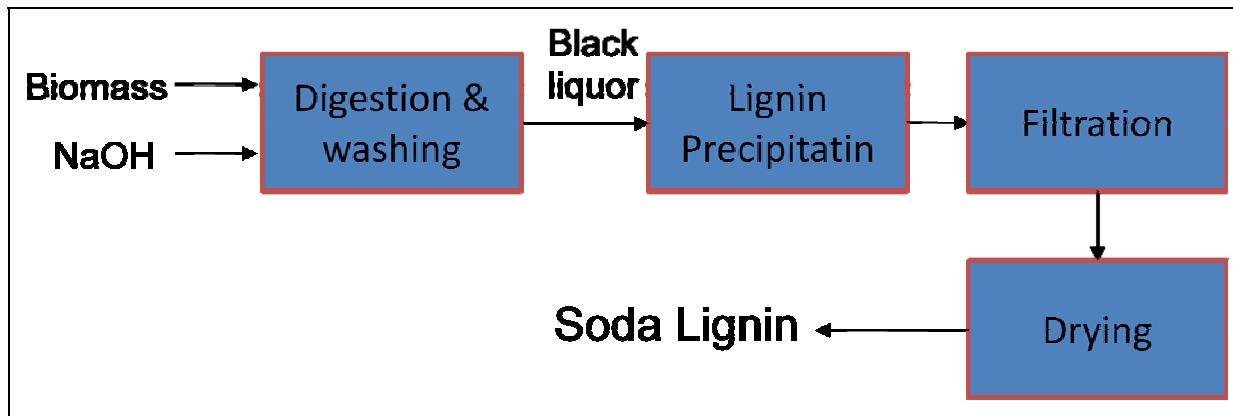
Figure 55. Soda pulping precipitation process.

The soda lignin Protobind 1000 showed a softening point of 245 °C. However, because of degradation, the residue was a foam (figure 56). According to a thermogravimetric analysis (TGA), it began to degrade at 200 °C (figure 57). Thus, melt spinning of soda lignin is unlikely to be successful because degradation will occur before and as the sample softens enough for spinning. As a result, it is necessary to decrease the softening point below 200 °C. Alternatively, solution spinning can be used to make lignin-based fibers and will be examined in future work.

Figure 56. Foamed soda lignin after heating to 250 °C.
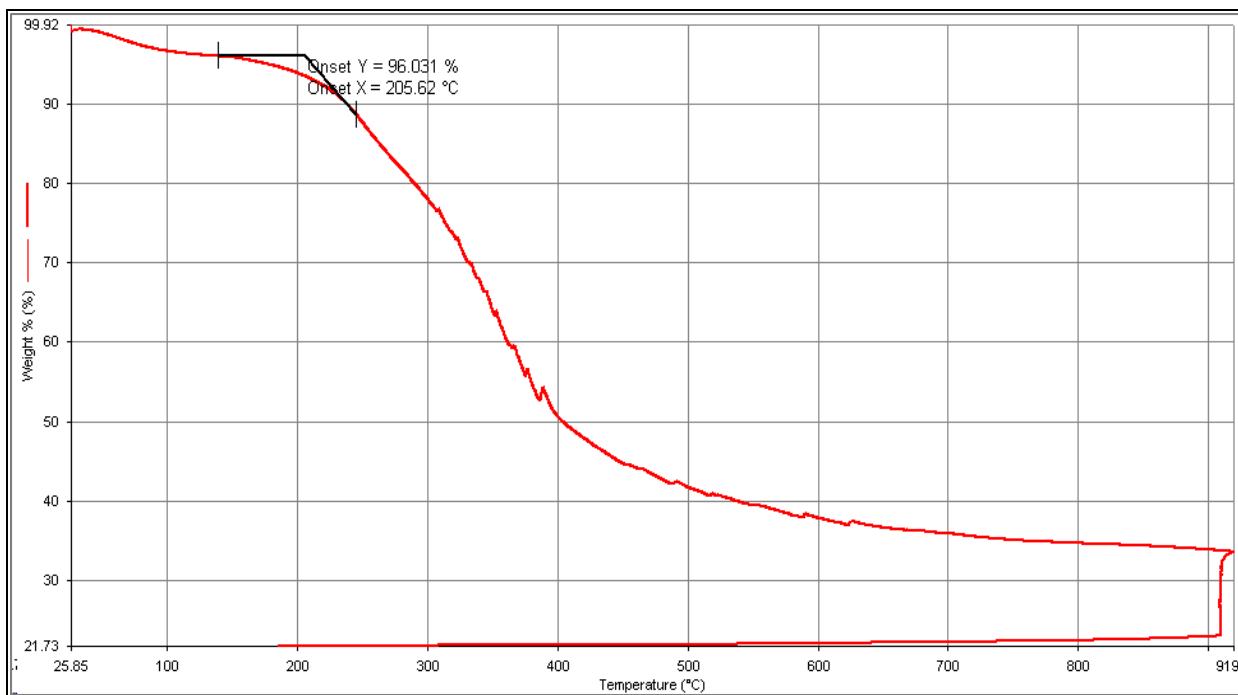
Figure 57. TGA of soda lignin.

Acetylation was carried out to enhance the flow characteristics of soda lignin as detailed in section 3. Unlike SKL, a fraction of soda lignin spontaneously precipitated from the reaction mixture after cooling. This fraction was regarded as a large molecular composition and removed. The recovered soluble fraction referred to as Ace_Soda had a softening point between 130 and 142 °C and a relatively stable melt viscosity when tested at 148 °C—again about 5 °C higher than the softening point (figure 58).
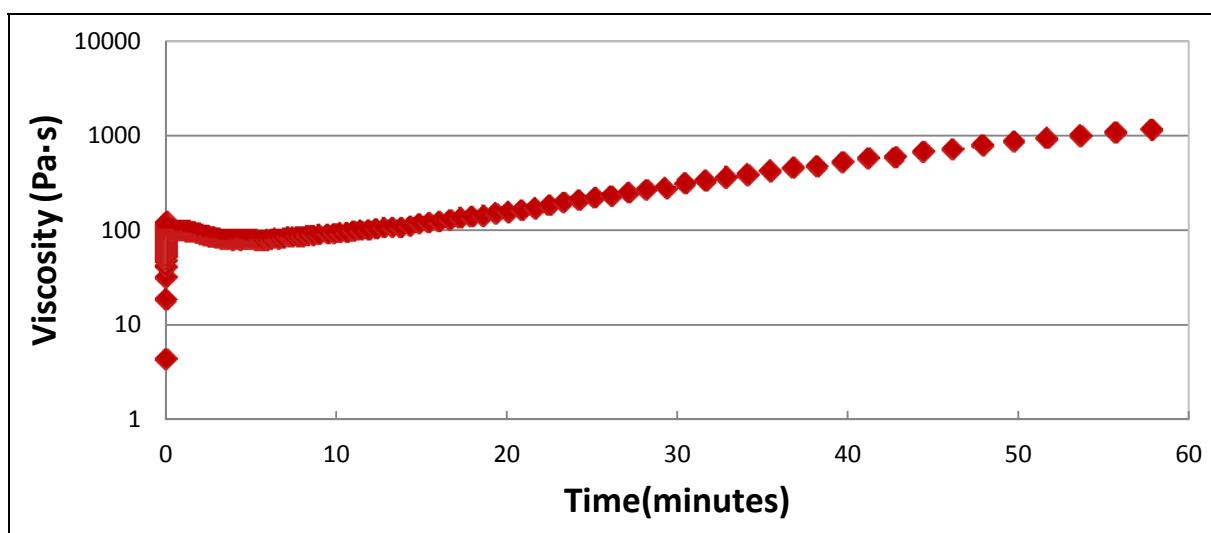
Figure 58. Transient shear viscosity of Ace_Soda at 148 °C.

The Ace_Soda was then melt spun into fibers. The Instron capillary rheometer was preheated to 148 °C (i.e., about 5 °C higher than the softening point for each batch of sample). When the temperature reached the target value, the sample was loaded into the barrel. The plunger was fitted into the barrel, and the melt was extruded out of the capillary die. A take-up roll was positioned below to draw down the melt into fibers. The take-up speed was 180 m/min and the spinneret diameter was 254 μm. The total heating time was controlled in this manner to prevent the formation of high-viscosity material before spinning. The resulting fibers were excellent, as shown in figure 59, and had a fiber diameter of 22 ± 3 μm.
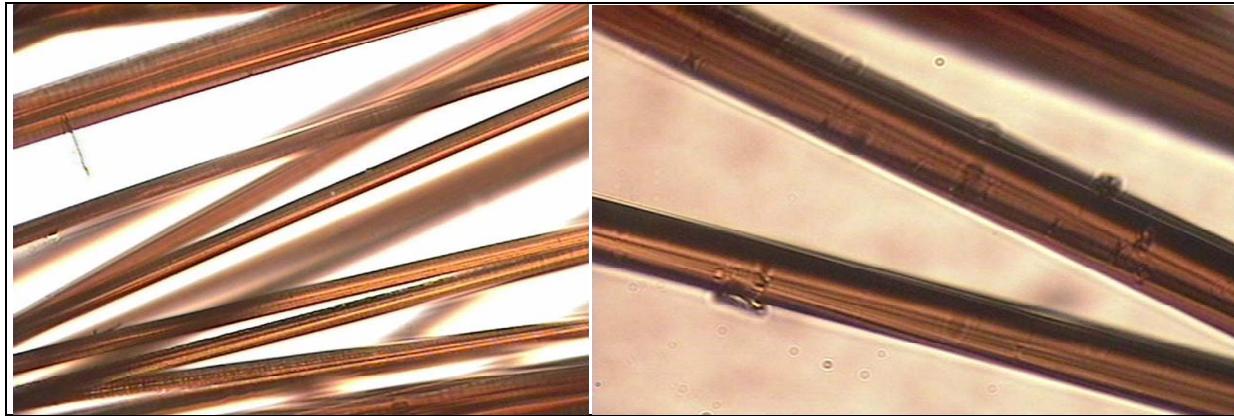
Figure 59. Polymer fibers of Ace–Soda.

These melt-spun Ace_Soda fibers were tacky during thermostabilization even with a heating rate as low as 0.01 °C/min. In retrospect, the stable melt viscosity (figure 58) indicates that little cross-linking of the lignin can occur upon heating, likely as a result of too much acetylation and too little hydroxylation to have enough dehydration cross-linking. To help the thermostabilization, the material was heated in a vacuum oven for different durations to increase its T_g. Softening points of both types of lignin increased from ~130 °C to around 190 °C after 2.5 h of devolatilization in a vacuum oven at 160 °C (figure 60).

The viscosity curve of Ace_Soda after different time periods of devolatilization was shown in figure 61. The results indicate long periods with a constant viscosity, allowing for significant duration for processing, followed by a significant rise in viscosity, indicating increased thermostabilization with increased devolatilization time. However, fibers spun with the highest SP (191 °C) material still could not be cross-linked. This is likely due to the lower concentration of alcohol groups on soda lignin, and thus less dehydration can occur.

Ace_Soda after heat treatment of 2.5 h and softening point of 190 °C was melt and spun into fibers. However, using the same slow thermostabilization program as Ace_SKL fibers, the Ace_Soda fibers still became tacky at around 145 °C. The main problem of Ace_SKL fiber and Ace_Soda fibers was the difficulty of cross-linking caused by acetylation.
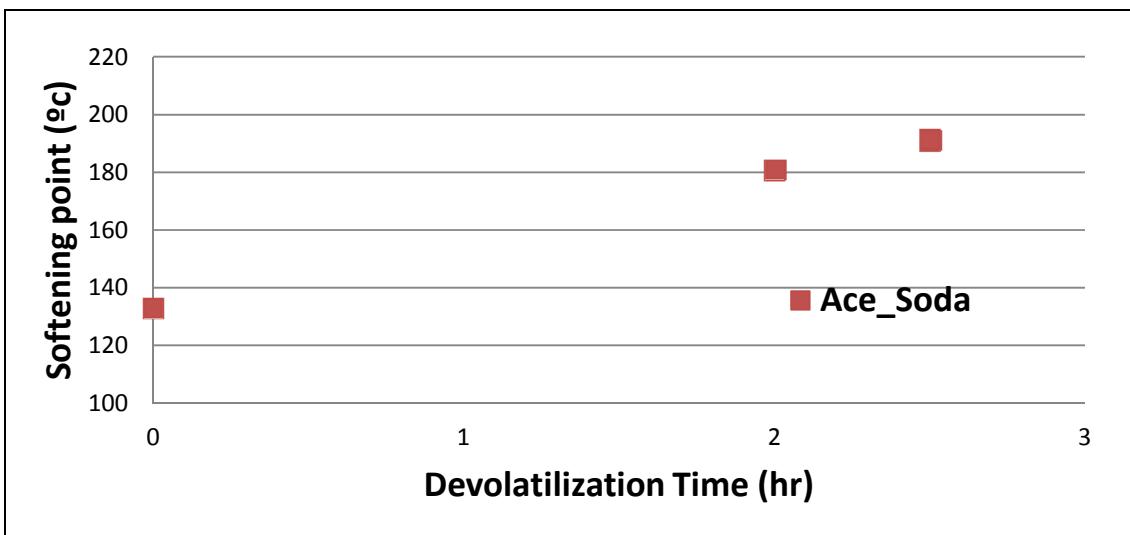
Figure 60. Softening point change with devolatilization time for Ace_Soda.
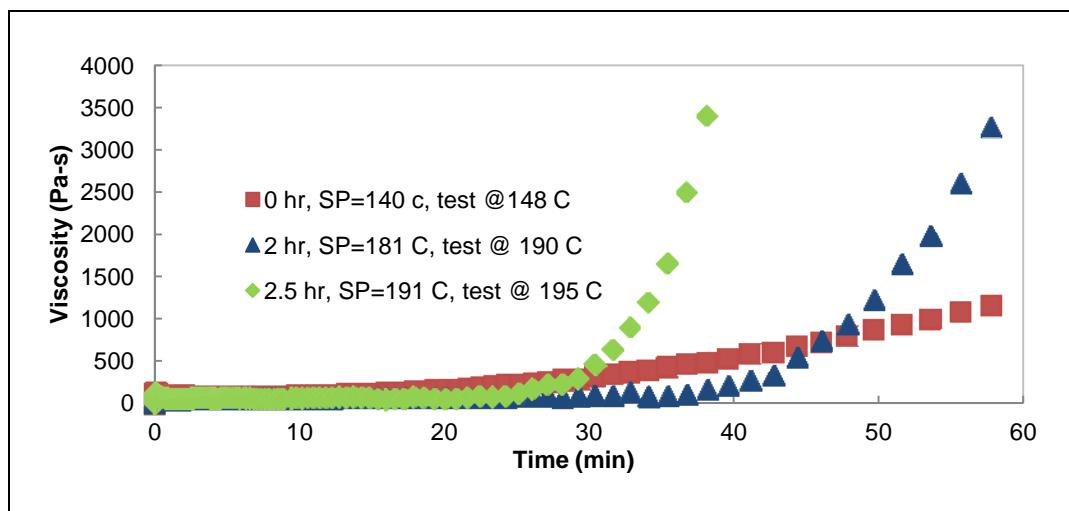
Figure 61. Transient shear viscosity of Ace_Soda with 0, 2, and 2.5 h of heat treatment.

Although the extracted Ace_Soda fiber was easy to melt spin, it was virtually impossible to stabilize by thermo-oxidative stabilization. Substitution of hydroxyl groups by the stable acetyl groups prevented any cross-linking and thermal stabilization of the macromolecules within the precursor fibers. We emphasize that molecular cross-linking within precursor fibers is an essential step in transforming the fiber into a thermoset before it can be carbonized. Although a ramp program with a heating rate as low as 0.01 °C/min was applied, the fibers could not be maintained in their glassy state and became tacky at around 150 °C. Once the precursor becomes tacky, it is not possible to retain individual precursor fibers; this shows that the composition is not well-suited for producing high-performance carbon fibers. Thus, methacrylation or reduced

89

acetylation could be used to improve the ability to melt spin or solution spin these fibers and will be attempted in the future.

4.4.5 Carbon Fibers From ECN Lignin

4.4.5.1 Rheological Characterization of ECN Lignin. ECN lignin has a softening point of 155 °C. The transient shear viscosity of ECN lignin tested at 160 °C was shown in figure 62. The viscosity increased gradually as time proceeded, but after 1 h, shear viscosity was not higher than 200 Pa·s, which indicates that the material is more thermally stable compared with the lignin materials described in the previous subsections. The result of TGA indicated a decomposition temperature of ECN lignin at around 280 °C.
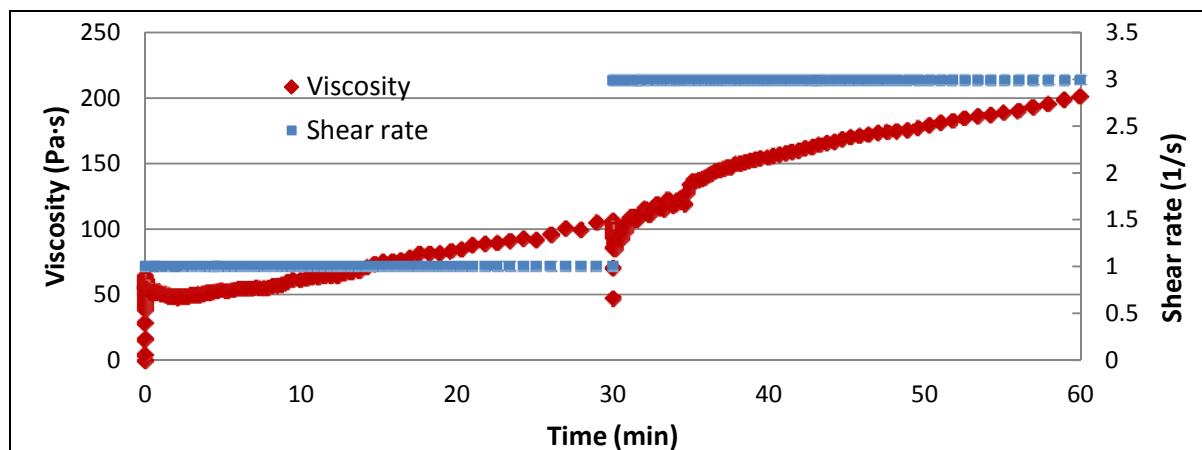
Figure 62. Transient shear viscosity of ECN lignin at 1 and 3 s^{-1}, 160 °C.

Spinning of ECN lignin was also performed on an Instron unit when heated at 160 °C with the winding rate as high as 190 m/min. Fiber was continuously spun on the roll for more than 2 min. The resulting fibers were uniform and defect-free with an average diameter of 29.3 ± 1.1 µm, as seen in figure 63.
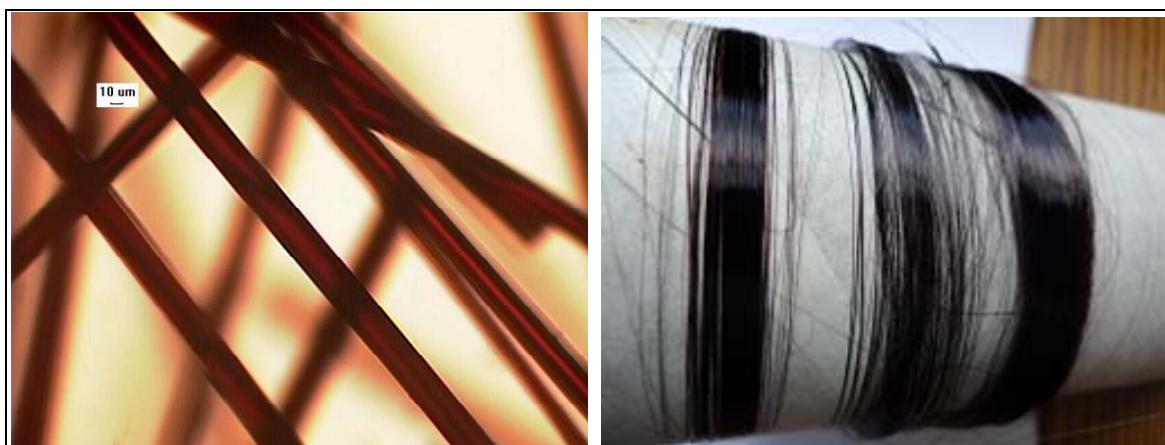
Figure 63. ECN lignin fibers at magnification (left) and as seen on the take-up wheel (right).

The first stabilization trial was performed with a heating rate of 0.1 °C/min. Fiber became tacky at around 125 °C. The second stabilization trial was performed carefully with a relatively long procedure. The temperature vs. time curve is shown in figure 64. The fiber survived during stabilization, and the final oxidation temperature was 240 °C. It takes more than 200 h (over 1 week) to stabilize to prevent fibers from being tacky, whereas most commercial processes require about 2 h. The slow oxidation rate was attributed to relatively low hydroxyl content in hardwood organosolv lignin.
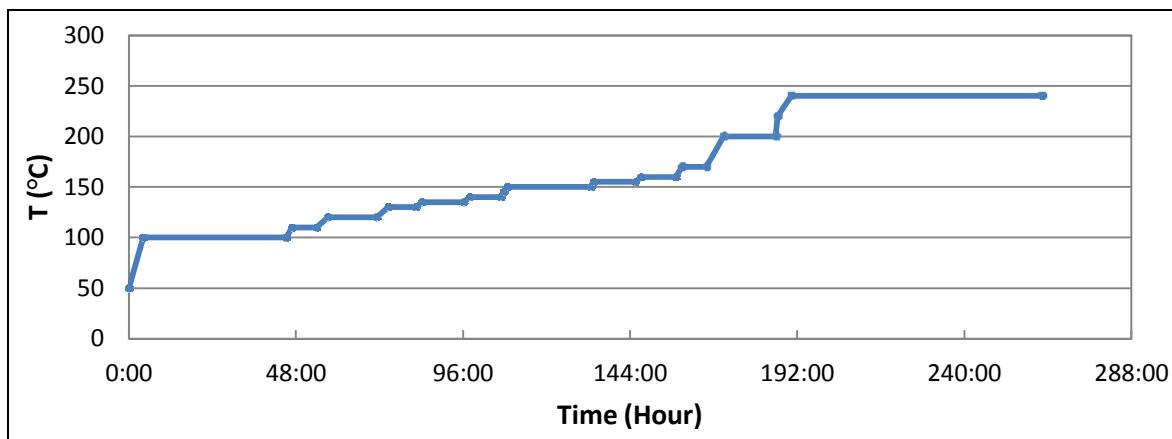
Figure 64. Thermostabilization of ECN lignin fiber.

The average fiber size after oxidation reduced to 23.5 ± 0.5 µm (figure 65). After stabilization, the ECN lignin fiber became infusible. The stabilized fibers did not dissolve in acetone, indicating their cross-linked structure after thermo-oxidation.

Figure 65. Oxidized ECN fiber.

The stabilized fibers were carbonized at 1000 °C. The resulting carbon fibers were nominally 14 ± 1 µm in diameter, as shown in figure 66. The results show that the carbon fibers had smooth surfaces and circular cross sections, both of which are good attributes to maintain high mechanical properties. Single fibers were mounted on a paper tap and tested with a Phoenix tensile testing device following the ASTM test method D-3379-5. The carbonized ECN fibers displayed a tensile modulus, strength, and strain-to-failure values of 34 ± 4 GPa, 450 ± 130 MPa, and 1.4 ± 0.4%, respectively. The electrical resistivity of these fibers was 60 µΩ-m. These results are similar to that of Rayon-based fibers. Although not ideal for structural applications, Rayon is no longer made in the United States because of the hazards and environmental regulations in processing. Rayon-based carbon fibers are used in missile casings where lightweight and low-thermal conductivity is desired. Note, the ash content of ECN was not measured and could be playing a role in the reduced properties. Future studies will investigate improvement in properties resulting from reduced ash content of the precursor lignin.
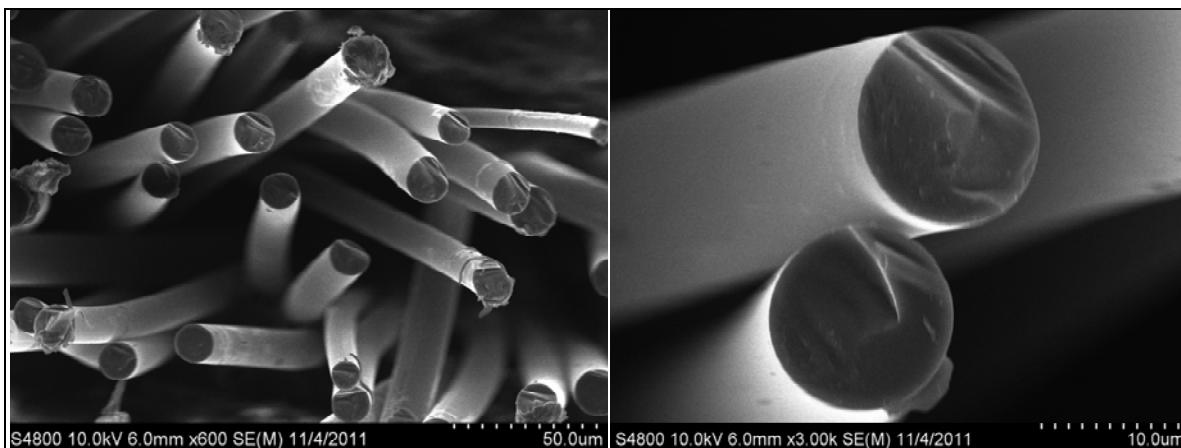
Figure 66. SEM micrographs of carbonized ECN lignin.

4.4.6 Carbon Fibers From Methacrylated SKL

Methacrylated lignin samples could not be melt spun because of the reactivity of the methacrylate groups. These become unstable at temperatures as low as 90 °C, which is considerably lower than the measured softening points of all lignin samples so far and any expected sample. Thus, only solution spinning is possible when using methacrylated lignin.

Methacrylated SKL was prepared as discussed in section 3, where the Indulin AT lignin was fractionated using methanol extraction and then methacrylated using methacrylic anhydride. Unfortunately, these samples did not have a measureable softening point. To test the stabilization potential of their methacrylated SKL composition (ethyl ether undissolved fraction), films with thicknesses around 0.5 to 1 mm were made by dissolving the sample in acetone and evaporating the acetone (figure 67, left). Heating in an oxidation oven from 50 to 160 °C at 0.2 °C/min resulted in cross-linked material, as the film chips did not dissolve in acetone after heating (figure 67, right).

Figure 67. Left: Film chips made from methacrylated SKL. Right: film chips of methacrylated SKL tested with acetone.

To test the potential of UV-assisted cross-linking for this sample, we made films with 1% 4,4 bis(dimethylamino)-benzophenone added as a PI. The experimental set included three types of films/chips: film 1 had no PI, film 2 had 1% PI, and film 3 had no PI and was shielded by an aluminum sheet on top to block the UV (figure 68). The films were processed in a Nordson UV chamber that can deliver up to 5 kW. After 5 min of UV exposure, the films were tested with acetone. A control film without any PI and without UV treatment was also produced. Because of the limited amount of samples available, the acetone-dissolution test was conducted with only films. Partial solubility of films can be deduced by the color of solution generated. In figure 69, film 1 and film 2 solutions had a very light color, indicating that only a tiny amount of treated film sample dissolved in acetone. Film 3 underwent the same thermal history as films 1 and 2 but was not exposed to any UV dissolved in acetone, as shown by the yellow color of the resulting solution. Control film without any PI or UV exposure also dissolved easily in acetone. Further, the chips of films 1 and 2 were fairly rigid and kept their shape well when exposed to acetone, but film 3 and the control samples decomposed into small particles after shaking the flask. The acetone tests indicated that both methacrylated samples, with or without PI, were capable of polymerizing in the UV chamber. Since film 1 had no PI, it can be inferred that it self-polymerized when exposed to UV radiation.

Although methacrylated SKL (ethyl ether undissolved fraction) could be dissolved in acetone, the concentrated solution did not have adequate elasticity to be stretched into filaments. In addition, methacrylated SKL displayed no softening point and thus could not be melt spun. Nonetheless, although 100% methacrylation of lignin is not useful for making fibers, partial methacrylation will enable UV stabilization of the fibers. Thus, partial methacrylation of acetylated SKL is assessed in the following section.

Figure 68. From left to right: film 1 had no PI, film 2 had 1% PI, and film 3 had no PI and was shielded by an aluminum sheet.
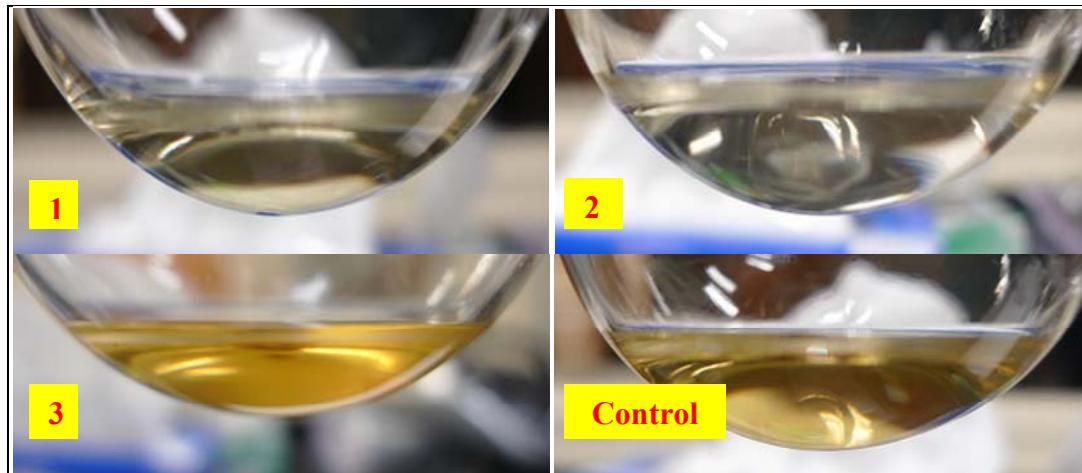
Figure 69. Acetone tests of film chips after UV exposure.

4.4.7 Methacrylated and Acetylated SKL

Methacrylated and acetylated SKL were prepared as discussed in section 3.2.7. Procedure 1 showed that 10 g/60 mL of MA_Ace_SKL can be fully dissolved in acetone. The concentrated solution can be drawn into short filaments with uneven thicknesses (figure 70). The short filaments were soft and tacky during thermostabilization. Thus, this particular sample and procedure were not ideal for carbon fiber formation.

Figure 70. MA_Ace_SKL (procedure 1) filaments.

In procedure 2 (section 3.2.7), 10 g of Ace_SKL + 25 mL of methacrylic anhydride + 0.5 mL of 1 MIM was prepared and used to make fibers. The resulting product was still soft when separated from the evaporation dish. The material can be dissolved into acetone and drawn into long filaments (figure 71), but the filaments were tacky. The filaments were dried for about 12 h at room temperature. Filaments melted and were tacky after thermostabilization; such filaments are not suitable for carbon fiber formation.
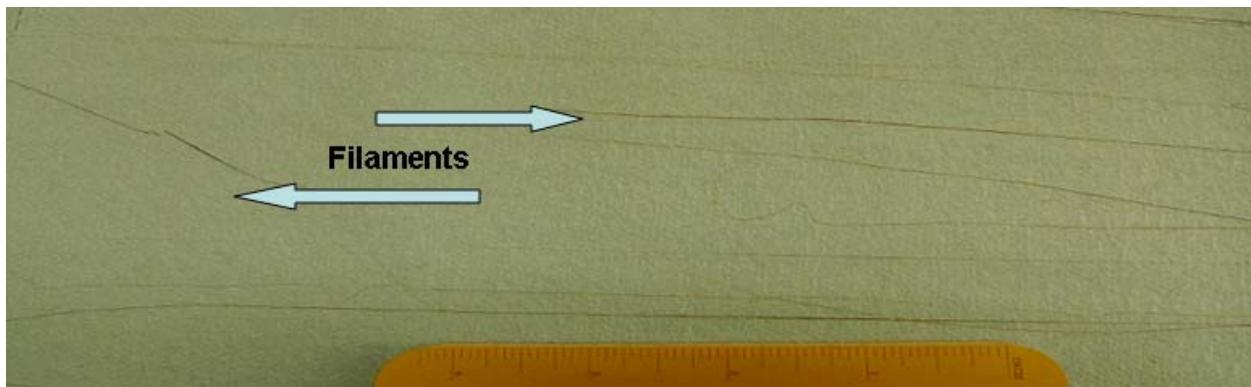
Figure 71. MA_Ace_SKL (procedure 2) filaments.

The 10 g/25 mL of MA_Ace_SKL was made into film chips to assess their ability to be UV stabilized (figure 72). After a 20-min UV (48–54 °C) treatment, some chips stuck to the surface of quartz or the aluminum sheet, indicating low T_g. UV-exposed film chips did not dissolve into acetone, but UV-blocked film chips dissolved. These results indicate that the MA groups are sensitive to UV stabilization and should help enable carbon fiber formation.
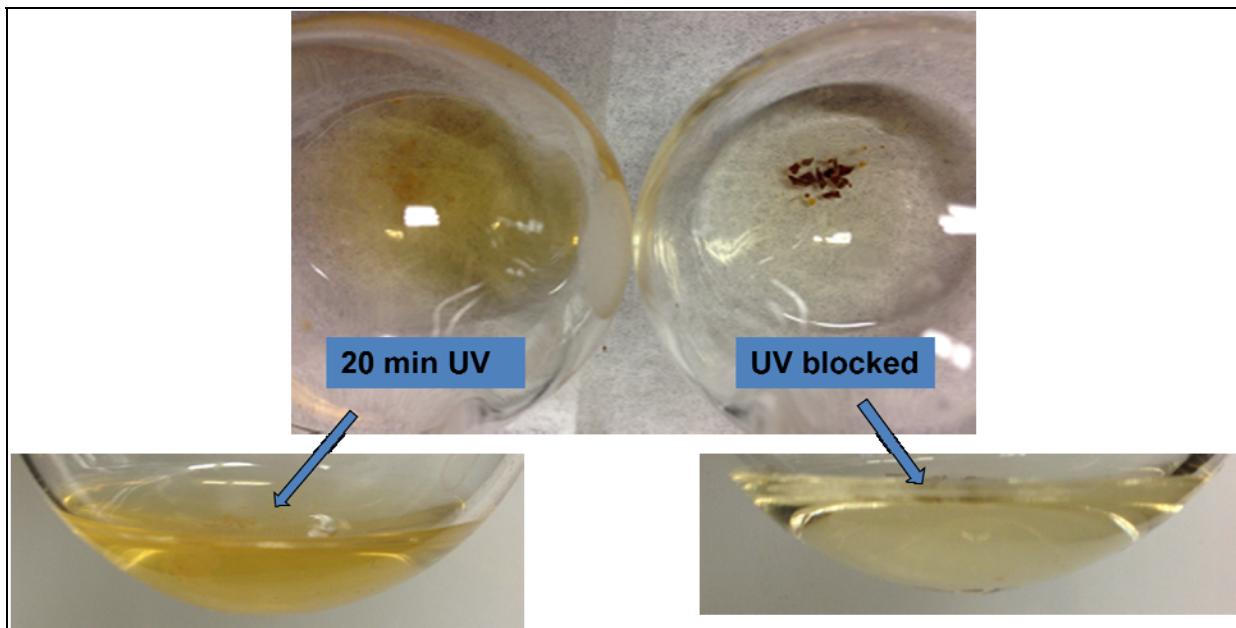
Figure 72. Photographs indicating UV stabilization of 10 g/25 mL MA_Ace_SKL.

In procedure 3, 10 g/10 mL of MA_Ace_SKL was prepared and tested for UV stabilization. As before, small pieces of the MA_Ace_SKL film were prepared. The film samples were either UV stabilized or not stabilized. The films samples were placed in a flask and acetone was added. The flask was shaken to help dissolve any sol components of the film. After 20 min, the UV-treated film partially dissolved and had a significant gel fraction, while the UV-blocked film fully dissolved in acetone (figure 73). Again, this indicates that UV stabilization can be an effective way to stabilize MA-modified lignin samples.
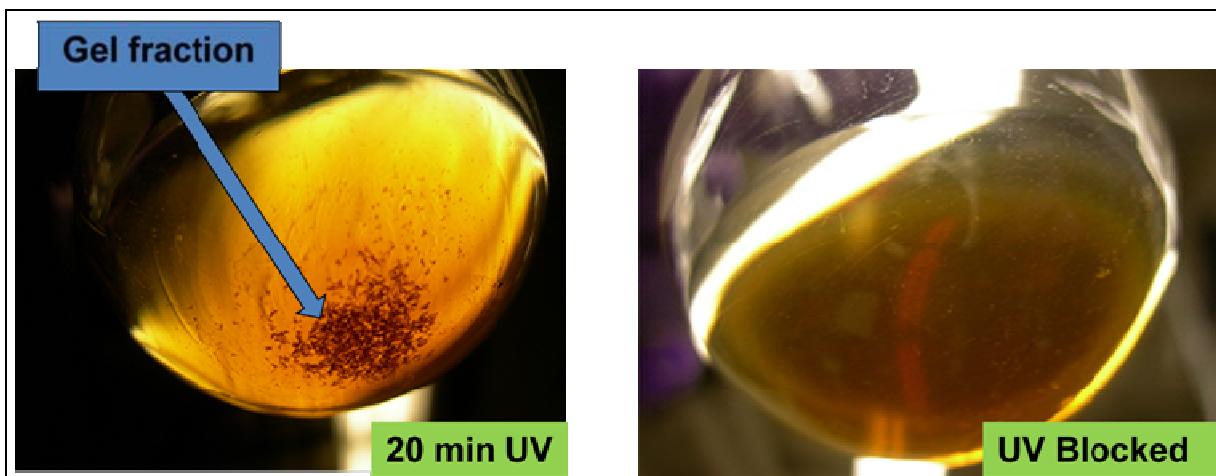
Figure 73. Photographs indicating UV stabilization of 10 g/10 mL MA_Ace_SKL.

To further test the stabilization, two pieces of film were placed face-to-face and pressed together (figure 74). The samples were then placed in an oxidation oven and heated from 40 to 150 °C at 0.2 °C/min. Both pairs of films (UV 20 min and UV blocked) can be separated without sticking. Since we were able to separate the UV-blocked samples, we are not sure if the films were close enough. Thus, filaments were prepared with MA_Ace_SKL (10 g/10 mL) and placed into an oxidation oven (40–150 °C, 0.2 °C/min). The non-UV-stabilized samples had some tackiness to them. The UV-stabilized samples will be tested soon to determine whether tackiness will be removed and a well-stabilized fiber can be prepared.
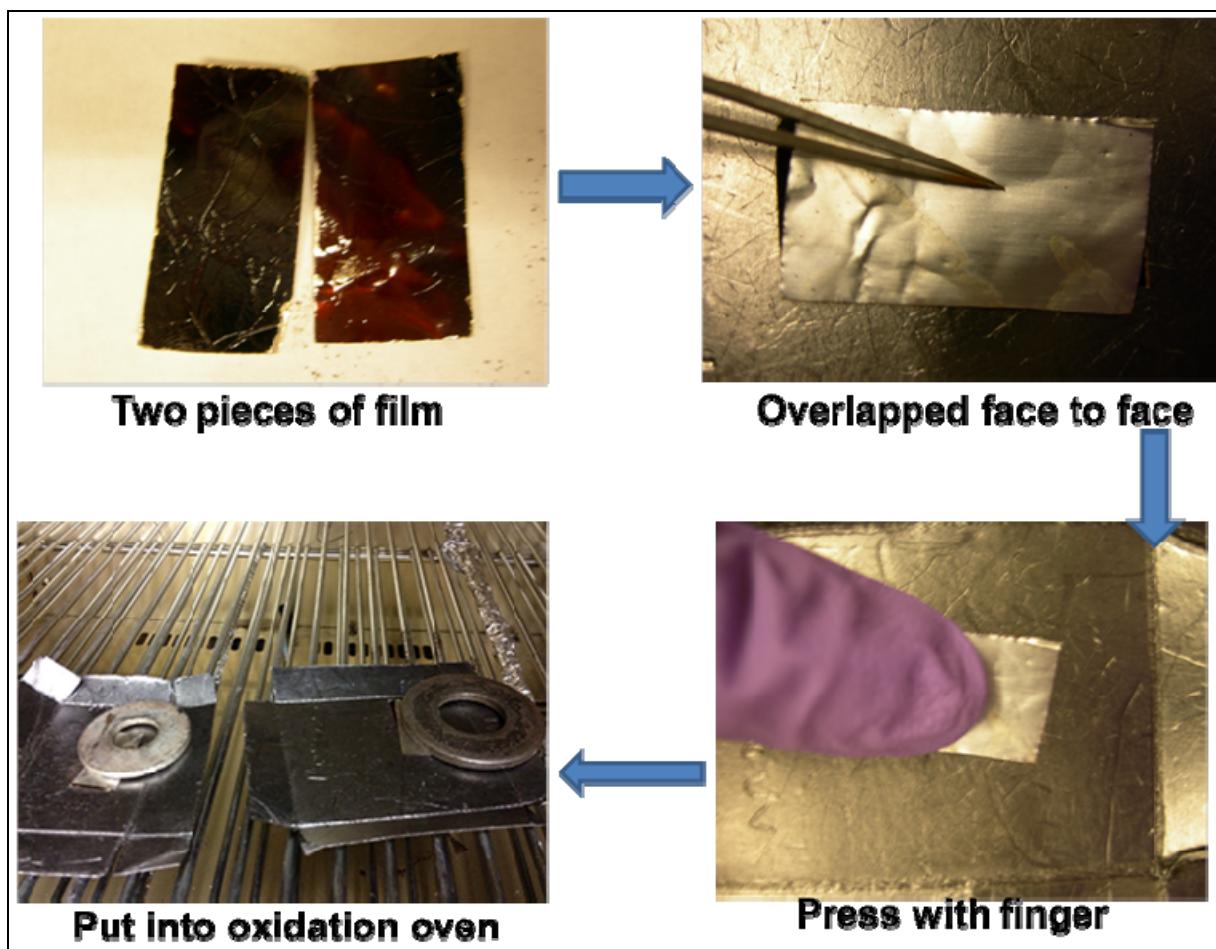
Figure 74. Thermostabilization test on the UV-treated 10 g/10 mL MA_Ace_SKL.

4.4.8 Carbon Fibers From Solution-Spinning of Ace_SKL

4.4.8.1 Solution Spinning of Highly Acetylated Ace_SKL. The acetylated SKL from the reaction of 10 g of SKL with 150 mL of acetic anhydride can be fully dissolved in acetone and manually drawn into filaments with minimum diameters as small as 20 μm, indicating its solution-spinning potential. Filaments had a diameter range from 20 to 70 μm (figure 75). The filaments kept their shape at around 145 °C while being tacky.

Figure 75. Solution spun Ace_SKL fibers.

4.4.8.2 Thermo-oxidative Stabilization of Highly Acetylated Ace_SKL. Thermo-oxidation was attempted to stabilize the fibers. The following general heating procedure was used to thermo-oxidatively stabilize the fiber:

- Heating from 25 to 140°C, with a heating rate of 0.1 °C/min

- Hold at 140 °C for 10 h

- Heating from 140 to 160 °C, with a heating rate of 0.05 °C/min

- Hold at 160 °C for 20 h

However, these filaments could not be thermo-oxidized even with the heating rate as low as 0.01 °C/min. The resulting filaments were still tacky (figure 76) after the process, indicating no ability to thermo-oxidatively stabilize due to the low amounts of hydroxyl groups remaining.
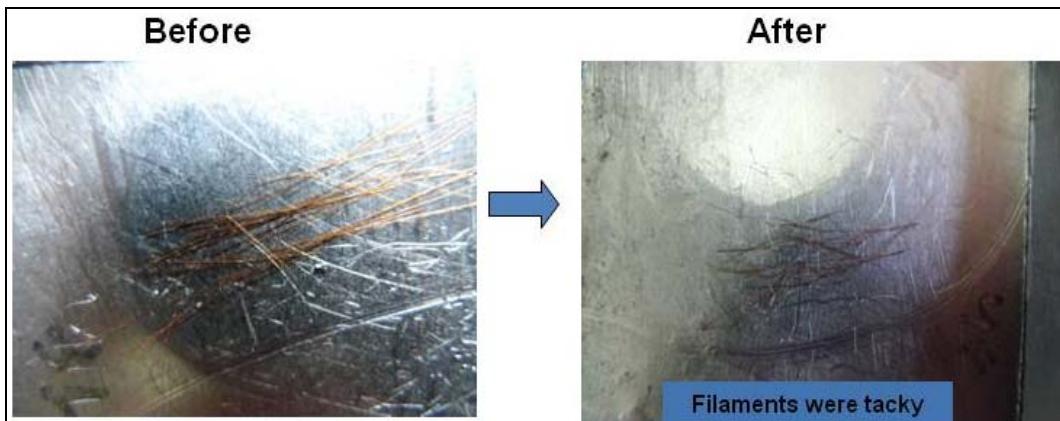
Figure 76. Thermostabilization of Ace_SKL solution-spun fibers produced tacky filaments.

4.4.8.3 Solution Spinning of Ace_SKL With Low Concentration of Acetate Groups. To reduce the degree of substitution, lower amounts of acetic anhydride were applied to preserve more hydroxyl group in SKL as detailed in the alternative procedures in section 3.4.2. A higher content of hydroxyl group is favorable for thermostabilization but is not amenable to melt spinning.

Since acetic anhydride less than 0.6 mL/g SKL was difficult to mix completely with SKL dry powder, a reaction product of 0.66 mL acetic anhydride per gram SKL react for 15 min was chosen as a precursor for the following solution spinning.

Ace_SKL (0.66 mL of acetic anhydride per gram SKL) was predissolved in excess acetone to obtain a homogeneous solution, which was later evaporated. A high concentration of solution was critical for spinning, since proper viscosity and elasticity were needed for the extension of filaments, and fast evaporation of acetone was necessary to prevent the filaments from becoming sticky when winding onto the take-up unit (figure 77). We found that when the concentration was between 1.70 and 1.90 g/mL, continuous filaments could be manually drawn out of the viscous solution. The viscosity of a 1.75-g/mL solution was measured at 1250 Pa·s.

Figure 77. Photograph showing sticking of
Ace_SKL to the roll surface due to
insufficient evaporation of acetone.

99

The first spinning trial used a solution with a concentration around 1.85 g/mL, without heating of the spinning barrel. Warm air in the spinning chamber assisted the evaporation of acetone in the filaments. The second trial had a solution concentration above 1.90 g/mL, and the spinning barrel was heated to 40 °C to increase the fluidity of solution. The drawdown was stable for take-up speeds up to about 50 m/min. The spinning temperature was 25 or 40 °C and the spinneret diameter was 150 μm (eight holes). At higher speeds, the fibers broke during drawing down. Fibers obtained from the two different batches had average diameters ranging from 32 to 45 μm, for an average of 39 ± 4 μm (figure 78, left). Figure 78 (right) shows dry and wet fibers while being spun onto the take-up roll. The inner part of the take-up wheel shows dry fibers. The outer part shows wet fibers without full evaporation of the acetone. This is not a significant issue and can be resolved by adjusting spinning parameters.
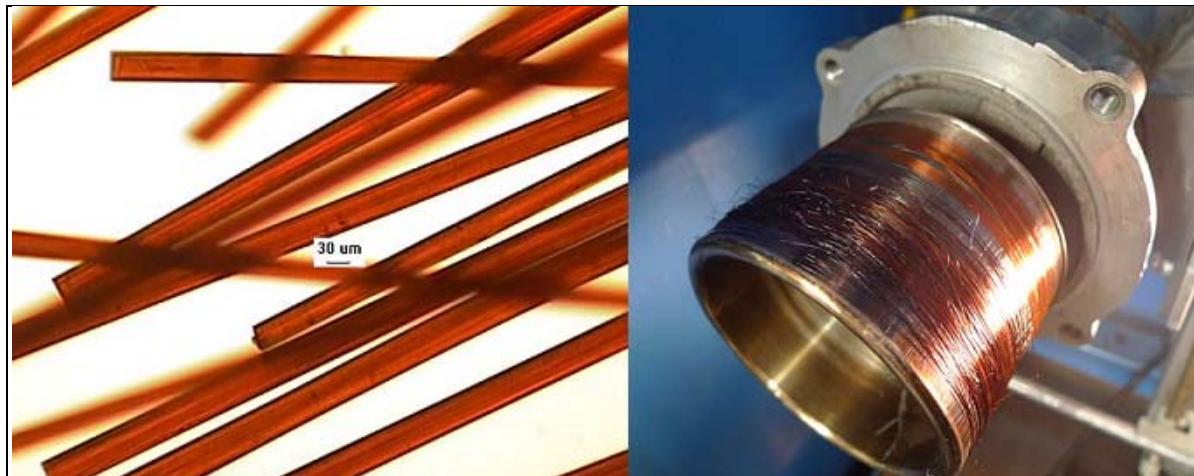
Figure 78. Solution-spun fibers of Ace_SKL fiber on the take-up roll (right) and micrographs of as-spun fibers (left).

The Ace_SKL fibers were thermal-oxidized with the following ramp heating program: heating from 50 to 140 °C with 0.25 °C/min, holding at 140 °C for 10 h, heating from 140 to 155 °C with 0.1 °C/min, holding at 155 °C for 10 h, heating from 155 to 220 °C with 0.1 °C/min, and holding at 220 °C for 24 h. The whole procedure took less than 72 h. Fibers could be stabilized and survived in this manner, and turned black after oxidative stabilization (figure 79).

Figure 79. Oxidized, solution-spun Ace_SKL with low
concentration of acetate groups.

The oxidized fibers were successfully carbonized. The fibers were heated up to 1000 °C at
4.5 °C/min and held at 1000 °C for 1 h in a furnace in a stream of argon. After carbonization,
the fiber size reduced to 31.7 ± 1.2 μm. The Ace_SKL carbon fibers had a rough surface and
noncircular shape due to evaporation of the acetone (figure 80). These carbon fibers displayed a
tensile modulus, strength, and strain-to-failure values of 27 ± 3 GPa, 230 ± 30 MPa, and 0.9 ±
0.1%, respectively. The electrical resistivity was quite low, ~14 μΩ-m, indicating a high
graphitic content in these fibers. Thus, optimizing the processing of these fibers is important to
achieving increased carbon fiber properties. Furthermore, ash content of Ace_SKL is in the
process of being measured and will be reduced to improve properties of resulting carbon fibers.
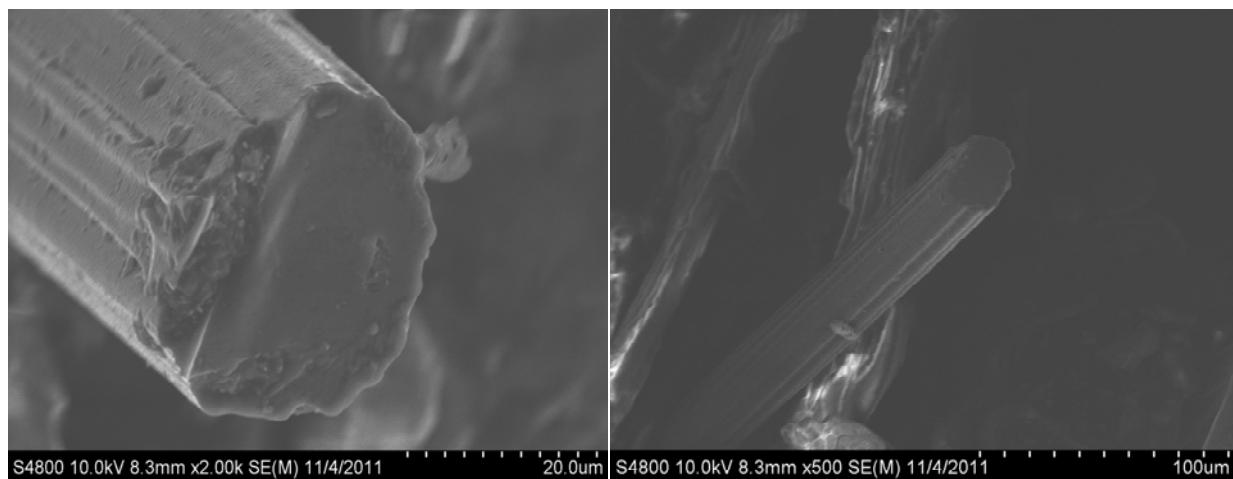
Figure 80. Carbonized, solution-spun Ace_SKL with low concentrations of acetate groups.

4.5   Summary and Conclusions

Table 11 summarizes the results observed for lignin-based fibers and carbon fibers. Overall, unmodified lignin is not ideal for preparing carbon fibers. Even ECN organosolv lignin, which we could convert to carbon fiber, had low properties and poor processing characteristics. In fact, one type of surface functionality—be it hydroxyls, acetates, or methacrylates—is not good for preparing carbon fibers. The results indicate that balance of these properties is desired. Low hydroxyl content is necessary to enable some oxidative stabilization, but high amounts reduce processing time unacceptably. High acetylation enables fiber spinning but prevents oxidative stabilization. High methacrylation enables UV stabilization but prevents spinning. In fact, using this balance, we recommend methacrylating ECN lignin to aid with thermostabilization. The colors in table 11 indicate the potential for the given method. Green indicates successfully made carbon fibers, although there are still aspects that need to be improved. Yellow indicates areas for significant amounts of future research. Red indicates the method was not successfully and is not worth additional effort.

It is evident from the results that suitable modification of lignin composition and spinning conditions has been achieved to obtain precursor fibers that could be thermo-oxidatively stabilized and carbonized. However, the tensile properties of carbon fibers still need to be improved significantly. This will be done by taking measurements to remove ash content from all lignin samples as well as improving processing. In addition, the processing techniques will be modified to enable attainment of improved properties.

In an effort to determine possible reasons for the flaw sensitivity of the fibers that lead to low tensile properties, the electrical resistivity of fibers was measured using a standard ASTM four-point technique. In a surprising development, the resistivity of ECN-derived carbon fibers was found to be about 80 $\mu\Omega$-m, whereas that of solution-spun Ace-SKL-based carbon fibers was 14 $\mu\Omega$-m. Literature studies have shown such values for PAN-derived carbon fibers to be about 18 $\mu\Omega$-m, whereas those for MP–derived carbon fibers are as low as 1.4 $\mu\Omega$-m when heat treated at 3000 °C. Higher resistivities mean less graphitic crystallinity, such as the turbostratic structure associated with PAN-derived carbon fibers, which does not result in high thermal conductivity but yields very high mechanical strength. In contrast, the ultra low electrical resistivity is a sign of highly developed graphitic crystallinity and order, which results in very high thermal conductivity but low mechanical properties. The relatively low electrical resistivity of 14 $\mu\Omega$-m found in Ace-SKL-derived carbon fibers (processed at only 900 °C) suggests that these fibers are developing a graphitic texture, which is good for thermal conductivity but not good for mechanical properties. In the next steps of the study, this structure will first be confirmed by wide-angle diffraction studies, and then spinning and oxidative stabilization steps will be modified to reduce the graphitic development to enhance mechanical properties.

Table 11. Softening point of different batches of lignin samples.

Lignin Type	Softening Point	Spinning Potential	Stabilization Potential	Carbon Fiber Potential?
SKL	No SP	Not spinnable	X	X
Soda lignin	245 °C	Not melt spinnable, degrades before it melts, solution spinning possible	High potential for thermo-oxidative	Potential
ECN organosolv lignin	155 °C	Melt spinnable	Very slow thermo-oxidative stabilization procedure	√ - can be heat treated to carbon fibers, methacrylation of ECN should help stabilization (solution spinning required)
Ace_SKL with high extent of substitution followed by fractionation	115–145 °C	Melt spinnable	Not able to cross-link	X
Ace_SKL with low extent of substitution followed by fractionation	187 °C	Not melt spinnable, can be solution spun	Thermo-oxidative stabilized	√ - made carbon fibers; tensile properties are low and need to be optimized
Methacryated SKL	No measurable SP	Not melt spinnable due to methacrylate reactivity; solution cannot be drawn into filament	Cross-links easily – UV and thermo-oxidiative stabilizable	X
Methacryated and acetylated SKL	No SP, cross-links during heating	Melt spinning not possible; solution spinnable and high likelihood of proper stabilization	UV and thermo-oxidiative stabilizable	High potential for making carbon fibers
Methacrylated (and MA/Ace) soda lignin	No SP, cross-links during heating	Not melt spinnable; potentially solution spinnable	UV and thermo-oxidiative stabilizable	Potential
Methacrylated (and MA/Ace) ECN	No SP, cross-links during heating	Not melt spinnable; potentially solution spinnable	UV and thermo-oxidiative stabilizable	Potential
Bacteria-modified lignin	Not available	Melt spinnable; solution spinnable	UV and thermo-oxidiative stabilizable	Potential

References

1. Fitzer, E.; Manocha, L. M. *Carbon Reinforcements and Carbon/Carbon Composites*; Springer: Berlin, 1998.

2. Buckley, J. D.; Edie, D. D. Eds. *Carbon-Carbon Materials and Composites*; Noyes Publishing: Park Ridge, NJ, 1993.

3. Naskar, A. K.; Walker, R. A.; Proulx, S.; Edie, D. D.; Ogale, A. A. UV Assisted Stabilization Routes for Carbon Fiber Precursors Produced From Melt-Processible Polyacrylonitrile Terpolymer. *Carbon* **2005**, *43*, 1065–1072.

4. Mukundan, T.; Bhanu, V. A.; Wiles, K. B.; Johnson, H.; Bortner, M.; Baird, D. G.; Naskar, A. K.; Ogale, A. A.; Edie, D. D.; McGrath, J. E. A Photocrosslinkable Melt Processible Acrylonitrile Terpolymer as Carbon Fiber Precursor. *Polymer* **2006**, *47*, 4163–4171.

5. Paiva, M. C.; Kotasthane, P.; Edie, D. D.; Ogale, A. A. UV Stabilization Route for Melt-Processible PAN-based Carbon Fibers. *Carbon* **2003**, *41*, 1399–1409.

6. Sandermann, H., Jr.; Scheel, D.; Trenck, T. Metabolism of Environmental Chemicals by Plants; Copolymerization Into Lignin. *J. Appl. Polymer Sci.* **1983**, *37*, 407–420.

7. Otani, S. Method for Producing Carbonized Lignin Fiber, U.S. Patent 3,461,082, 1969.

8. Sudo, K.; Shimizu, K. A New Carbon Fiber From Lignin. *J. Appl Polym Sci.* **1992**, *44*, 127–134.

9. Uraki, Y.; Kubo, S.; Nigo, N.; Sano, Y.; Sasaya, T. Preparation of Carbon Fibers From Organosolv Lignin Obtained by Aqueous Acetic Acid Pulping. *Holzforschung* **1995**, *49*, 343–350.

10. Kubo, S.; Uraki, Y.; Sano, Y. Preparation of Carbon Fibers From Softwood Lignin by Atmospheric Acetic Acid Pulping. *Carbon* **1998**, *36*, 1119–1124.

11. Kadla, J.; Kubo, S.; Venditti, R.; Gilbert, R.; Compere, A.; Griffith, W. Lignin-Based Carbon Fibers for Composite Fiber Applications. *Carbon* **2002**, *40*, 2913–2920.

12. Warren, C. D.; Paulauskas, F. L.; Baker, F. S.; Eberle, C.; Naskar, A. K. Development of Commodity Grade, Lower Cost Carbon Fiber-Commercial Applications. *SAMPE Journal* **2009**, *45*, 24–36.

13. Baker, F. S.; Visiting, O. Low Cost Carbon Fiber From Renewable Resources. EERE, U.S. Dept of Energy Project ID# lm_03_baker, 2009.

14. Eckert, R. C.; Abdullah, Z. Carbon Fibers From Kraft Soft Wood Lignin, U.S. Patent 7,678,358, 2010.

5.   Reactive Diluents From Lignin Model Compounds

5.1   Introduction

VE resins are used to produce polymer composites for commercial applications because they possess relatively high moduli, strength, and T_g's while maintaining low weight and cost (*1*, *2*). To facilitate the use of liquid molding techniques to fabricate large-scale composite parts, commercial VE resins typically contain high concentrations (>40 wt%) of a reactive diluent, such as styrene. In addition to lowering resin viscosity, styrene acts as a linear chain extender, thus improving the overall polymer performance by allowing for a higher degree of monomeric reactivity by delaying the onset of gelation and reducing diffusion limitations (*2*). However, despite its benefits, styrene has been designated a HAP and a VOC (*3*). In 2003, with an amendment in 2005, the Environmental Protection Agency (EPA) introduced legislation to limit styrene emissions from composite manufacturing (*1*, *3*, *4*). More recently, in June 2011, the Department of Health and Human Services through the National Toxicology Program in their 12th Report on Carcinogens has designated styrene as "reasonably anticipated to be a human carcinogen" (*5*). Moreover, styrene is emitted during metering, mixing, processing, and curing, and studies have shown that up to 40% of styrene can remain unreacted after curing and can continue to be released from composites during the remaining phases of their life cycle (*4*). With this significant drawback, new resins are required for the continued use of polymer composites. Therefore, the development of nonvolatile reactive diluents with styrene-like performance is gaining interest. Additionally, with the continued volatility of the petroleum industry and crude oil price fluctuations, the cost of styrene will eventually become a factor in the production of future resins if a suitable biobased replacement is not identified. These significant factors give impetus for the discovery and development of renewable, biobased reactive diluents that have styrene-like performance with minimal VOC emissions.

Previous work conducted by La Scala et al., in conjunction with the ACRES program at the University of Delaware, has demonstrated the potential of using methacrylated fatty acids (MFAs) as styrene replacements. These include methacrylated lauric acid (MLau), methacrylated hexanoic acid (MHex), and methacrylated octanoic acid (MOct) as styrene reducers in VE, soybean-based, and castor oil–based polymer matrices (*1*, *6–8*). These renewable, naturally occurring methacrylated plant oil derivatives exhibit low volatilities and viscosities (40–80 cP at 30 °C) and have the ability to act as acceptable chain extenders. These functionalized plant oil derivatives also demonstrate the ability to toughen polymer matrices via the flexible, long alkyl side chains. However, while showing promise, styrene, at a considerably reduced concentration, was still needed to produce biobased resins with comparable thermal and mechanical performance to commercial VE-styrene resins (*1*, *6*). Thus, lower-viscosity, nonvolatile, renewable reactive diluents with styrene-like performance are still being sought; particularly, reactive diluents that have similar T_g's to styrene when polymerized.

Lignin is a renewable biobased alternative rich in aromaticity with the capability to yield single aromatic chemicals when selectively broken down. Lignin is the second most abundant natural raw material, surpassed only by cellulose, with over 3×10^{11} tons existing in the biosphere and $\sim 2 \times 10^{10}$ tons generated annually (*9–11*). As of 2004, the pulp and paper industry alone produced roughly 50×10^6 tons of extracted lignin of which 95% was Kraft lignin (*11, 12*). The Kraft process, invented in 1879 by Carl F. Dahl, treats wood chips with a mixture of sodium hydroxide and sodium sulfide, known as white liquor, and separates the lignin from cellulose and hemicelluloses (*11, 12*). However, only ~2% of the available lignin is used commercially, with the remainder used as a low-value fuel to cover internal energy needs of the pulp and paper industry (*13*). Because of its very complex 3-D aromatic structure, lignin is largely intractable in its unmodified state and therefore is often sought to be broken down into smaller molecular weight aromatic components.

Nondegraded and chemically modified lignins have been successfully incorporated into various materials, including polymeric materials (*9, 11, 12, 14–16*). Additionally, much research has been conducted in selectively breaking down all types of lignin and multiphenolic LMCs to develop new chemicals and renewable sources of predominantly petroleum-derived chemicals (*10, 13, 15–23*). Recently, a modest yield of vanillin from Kraft lignin has been obtained using aqueous polyoxometalates in the presence of alcohols to oxidatively degrade lignin (*10*). Additionally, vanillin production via Kraft lignin oxidation using a NaOH alkaline medium has been reported (*21*). Moreover, a 70% yield of guaiacol has been achieved from common β-O-4 LMCs, guaiacylglycerol-β-guaiacyl and veratrylglycerol-β-guaiacyl ether, under catalytic hydrolysis using an acidic ionic liquid (*18*). In 2011, Zakzeski and Weckhuysen (*13*) reported 22.2% and 12% yields of guaiacol from aqueous phase reforming of a β-O-4 model compound and a 5-5' model compound, respectively, using a Pt/Al_2O_3 catalyst. Lastly, Sergeev and Hartwig (*23*) have reported yields as high as 99% of guaiacol from hydrogenolysis reactions of representative biphenyl LMCs.

In the work herein, vanillin, guaiacol, and eugenol have been selected as representative LMCs for the synthesis of novel reactive diluents as styrene replacements in polymer matrices. Specifically, these LMCs were selected based on extensive studies and the potential to obtain these chemicals in high yields from lignin as well as from clove oil in the case of eugenol (*17, 19, 24*). In order to chemically incorporate the selected LMCs into VE resins, polymerizable carbon-carbon double bonds need to be integrated onto the phenolic compounds. Methacrylated analogues of vanillin (*25, 26*), guaiacol (*27–30*), and eugenol (*24, 31*) have been reported in the literature but, to date, have not been studied as styrene replacements in polymer resins. We report the synthesis, relative volatilities, viscosities, and polymer T_g's of the methacrylated lignin model compounds (MLMCs) as well as viscosities and T_g's of a commercial VE resin that contains 50 wt% of an MLMC. The relative volatility of styrene and T_g of the commercial VE resin (bismethacryl glycidyl ether of bisphenol A epoxy, VE828) with 50 wt% styrene are also reported for direct comparison.

5.2 Experimental

5.2.1 Materials

All reagents, ampoules of dimethyl sulfoxide-d$_6$ (DMSO-d$_6$) (0.75 mL), 4-dimethylaminopyridine (DMAP), vanillin (99%), guaiacol (99 + %), and eugenol (99%) were obtained from Fisher Scientific and were used as recieved. Methacrylic anhydride (94%, inhibited with 2000 ppm Topanol A), chloroform-d (CDCl$_3$), methyl ethyl ketone peroxide (MEKP) (2-butanone peroxide), and styrene (St) (inhibited with 10-15 ppm 4-*tert*-butylcatechol) were purchased from Sigma Aldrich and used as received. Compressed argon was obtained from Keen Compressed Gas Co. (99.998%). Trigonox 239 (AkzoNobel Polymer Chemicals), containing 45% cumene hydroperoxide, was purchased and utilized as a free radical initiator.

VE cross-linking monomer was prepared as prescribed in the literature (*2*, *3*). Epon 828 was converted to the bismethacryl glycidyl ether of bisphenol A epoxy (Hexion Specialty Chemicals, Inc.) using standard literature procedures and is referred to as vinyl ester 828 (VE828). Characterization methods as described in La Scala et al. (*3*) were performed with similar results. The chemical structure of VE828 is shown in figure 81.
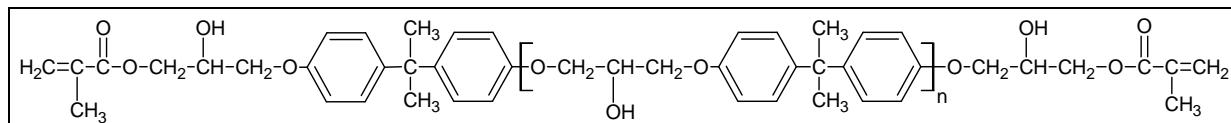
Figure 81. Chemical structure of VE monomer; VE828 contains a mixture of monomers that contain either two bisphenol units (*n* = 1) or one bisphenol unit (*n* = 0) with the majority of the mixture containing one bisphenol unit (*n* = 0).

5.2.2 Chemical Analysis of Lignin Model Compounds

Vanillin, guaiacol, and eugenol were purchased from Sigma Aldirch and used as received. Chemical structures of the LMCs are shown in figure 82. LMCs were characterized using ^{1}H NMR (400.13 MHz, 16 scans at 298.2 K) and ^{13}C NMR (100.6 MHz, 32 scans at 298.2 K) on a Bruker AV-400 spectrometer and showed peaks in agreement with the expected chemical shifts. Additionally, the LMCs were characterized using FTIR spectroscopy performed on a PerkinElmer Spectrum 400 FT-IR/FT-NIR Spectrometer. At room temperature, 16 cumulative scans were acquired with a resolution of 2 cm^{-1} in transmission mode in the mid-IR range. For liquids, a small amount of chemical was deposited between two NaCl discs (diameter = 25 mm; thickness = 5 mm) (International Crystal Laboratories, Garfield, NJ). For solids, a small amount of chemical was suspended in toluene and then deposited onto a NaCl disc. The toluene was evaporated in a vacuum oven prior to data spectral accumulation.
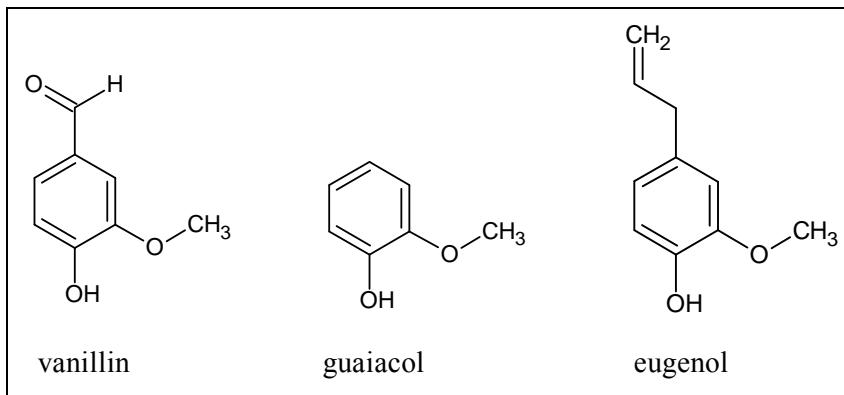
Figure 82. Chemical structures of LMCs, vanillin, guaiacol, and eugenol.

^{1}H NMR of vanillin (DMSO-d$_6$, 400 MHz): phenolic -OH, 10.27 ppm; -CHO, 9.76 ppm; ArH, 7.75-6.75 ppm, -OCH$_3$, 3.83 ppm. ^{13}C{^{1}H} NMR of vanillin (DMSO-d$_6$, 100 MHz): -CHO, 191 ppm; 6 aromatic carbons, 153, 148, 129, 126, 115, 110 ppm; -OCH$_3$, 55.6 ppm. ^{1}H NMR of guaiacol (DMSO-d$_6$, 400 MHz): phenolic –OH, 8.92 ppm; ArH, 7.75 – 6.75 ppm; -OCH$_3$, 3.82 ppm. ^{13}C{^{1}H} NMR of guaiacol (DMSO-d$_6$, 100 MHz): 6 aromatic carbons, 147.8, 146.7, 121, 119.3, 115.7, 112.3 ppm; -OCH$_3$, 55.6 ppm. ^{1}H NMR of eugenol (DMSO-d$_6$, 400 MHz): phenolic –OH, 8.75 ppm; ArH, 7.0-6.5 ppm; =CH-, 6.25 - 5.75 ppm; =CH$_2$, 5.25 – 4.75 ppm; -OCH$_3$, 3.74 ppm; -CH$_2$-, 3.30–3.20 ppm. ^{13}C{^{1}H} NMR of eugenol (DMSO-d$_6$, 100 MHz): 6 aromatic carbons, 147.5, 144.8, 130.5, 120.6, 115.4, 115.3 ppm; -CH$_2$CH=CH$_2$, 138.3 ppm; -CH$_2$CH=CH$_2$, 112.6 ppm; -OCH$_3$, 55.5 ppm; -CH$_2$CH=CH$_2$, 39.2 ppm. Notable FTIR spectral peaks of vanillin: phenolic -OH stretching vibration overlapped with the ArH, AlH, and -OCH$_3$ stretching vibrations due to the presence of residual H$_2$O, 3500-2800 cm^{-1}; -C=O wagging vibration; 1665 cm^{-1}; -OH bending vibration, 1265 cm^{-1}. Notable FTIR spectral peaks of guaiacol: phenolic -OH stretching vibration, 3510 cm^{-1}; ArH stretching vibrations, 3200–3000 cm^{-1}; -OCH$_3$ and AlH stretching vibrations, 3000-2800 cm^{-1}; -OCH$_3$ bending vibration, 1258 cm^{-1}; -OH bending vibration, 1216 cm^{-1}. Notable FTIR spectral peaks of eugenol: phenolic –OH stretching vibration, 3518 cm^{-1}; ArH stretching vibrations, 3200-3000 cm^{-1}; -OCH$_3$ and AlH stretching vibrations, 3000-2800 cm^{-1}; terminal double bond wagging vibration, 1638 cm^{-1}; -OCH$_3$ bending vibration, 1270 cm^{-1}; -OH bending vibration, 1233 cm^{-1}.

5.2.3 Synthesis of Methacrylated Lignin Model Compounds

Figure 83 depicts the synthetic route used to generate the MLMCs with the chemical structures of the MLMCs shown in figure 84. A catalytic amount of DMAP (2 mol% of methacrylic anhydride) was added to an LMC (20 g) and then placed in a 100-mL round bottom flask equipped with a magnetic stir bar. Prior to adding 1.2 LMC equivalents (adjustable to as low as 1.01) of methacrylic anhydride to the flask, the flask was sealed and subsequently purged with argon gas for 1 h to remove moisture and oxygen from the reaction vessel. For the first 3 h with stirring, the reaction progressed at room temperature. After 3 h, the flask was placed in a 45 °C silicon oil bath for a minimum of 24 h. The reaction mixture was then cooled to room
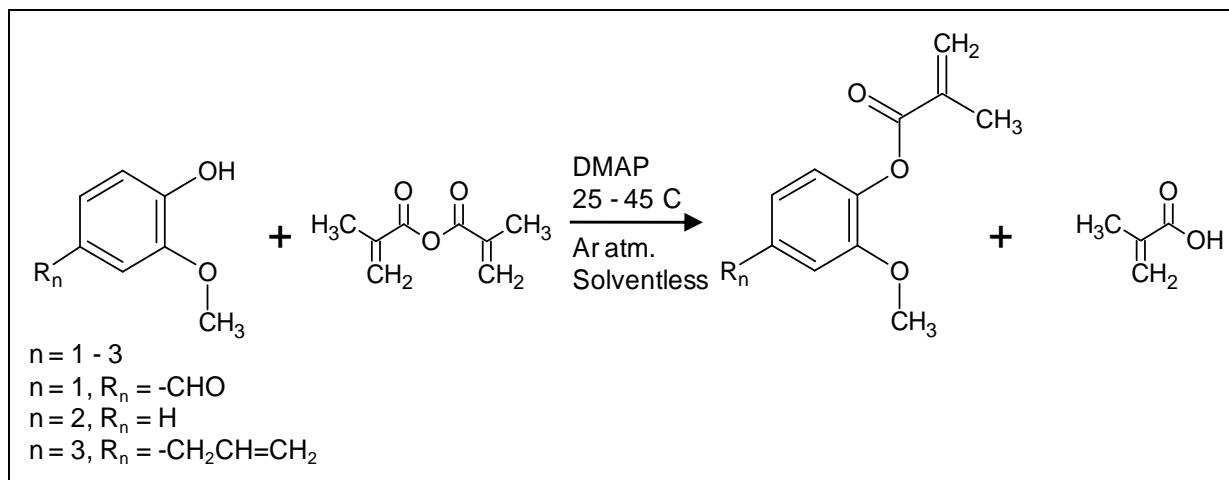
Figure 83. Reaction of methacrylic anhydride with an LMC to form an MLMC monomer.
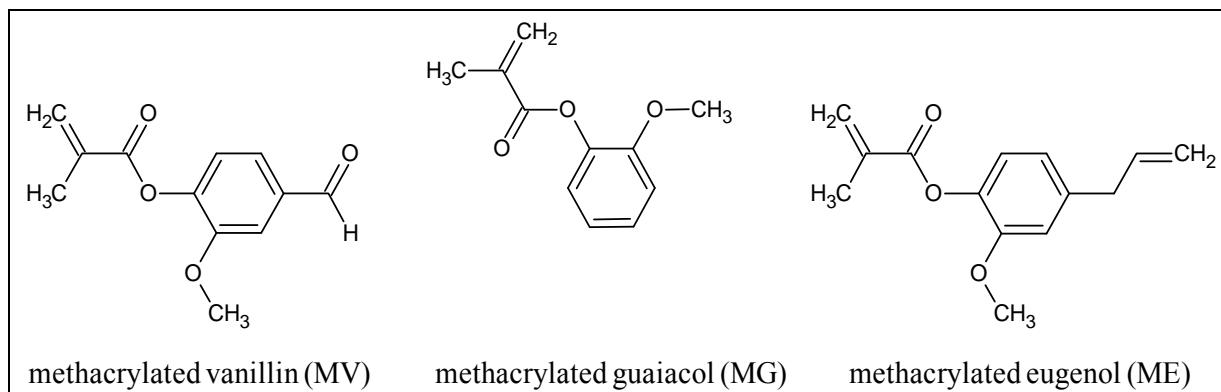
Figure 84. Chemical structures of the MLMCs, methacrylated vanillin (MV), methacrylated guaiacol (MG), and methacrylated eugenol (ME).

temperature and diluted with methylene chloride (150 mL) (ethyl acetate was also used as greener substitute). To remove unreacted methacrylic anhydride and methacrylic acid (MAA) product, the organic phase was washed repeatedly with a saturated sodium bicarbonate aqueous solution (150 mL) until carbon dioxide was no longer evolved. The organic phase was then washed with 1.0 M NaOH$_{(aq)}$ (150 mL), 0.5 M NaOH$_{(aq)}$ (150 mL), 1.0 M HCl$_{(aq)}$ (150 mL), and water (150 mL), dried over sodium sulfate, and then concentrated under reduced pressure.

Products were characterized using ^{1}H NMR (400.13 MHz, 16 scans at 298.2 K) and ^{13}C NMR (100.6 MHz, 32 scans at 298.2 K) on a Bruker AV-400 spectrometer and showed peaks in agreement with the expected chemical shifts. Additionally, the products were characterized using FTIR spectroscopy performed on a PerkinElmer Spectrum 400 FT-IR/FT-NIR Spectrometer. At room temperature, 16 cumulative scans were acquired with a resolution of 2 cm^{-1} in transmission mode in the mid-IR range. For liquids, a small amount of chemical was deposited between two NaCl discs (diameter = 25 mm; thickness = 5 mm) (International Crystal

Laboratories, Garfield, NJ). For solids, a small amount of chemical was suspended in toluene and then deposited onto a NaCl disc. The toluene was evaporated in a vacuum oven prior to data spectral accumulation.

MLMC melting points were measured using differential scanning calorimetry (DSC). A TA Instruments Discovery DSC was used with 40-μL hermetically sealed aluminum pans as sample holders and with sample masses of ~10 mg. With a continuous N_2 purge at a rate of 50 mL/min and for the room temperature liquid monomers (MG and ME), the samples were cooled down to –90 °C and then heated to 25°C at a rate of 10°C/min. For solids (MV), the samples were heated at a rate of 10 °C/min from 30 to 75°C. The experiments were run in duplicates to ensure reproducibility. Additionally, the melting temperature (T_m) of MV was measured using a Stuart melting point apparatus SMP10 with a heating rate of 2 °C/min and glass capillary tubes as sample holders.

MV (3-methoxy-4-methacryloyloxybenzaldehyde) (T_m = 55.4 °C; agreed with literature) (*32*): ^{1}H NMR (DMSO-d_6): δ 9.98 (s, 1H), 7.62–7.40 (bm, 7.62–7.40 (bm, 3H), 6.30 (s, 1H), 5.95 (t, 1H), 3.86 (s, 3H), 2.00 (s, 3H);^{13}C NMR (DMSO-d_6): δ 192.58, 164.74, 152.05, 144.76, 135.60, 135.07, 128.98, 124.28, 124.13, 112.32, 56.57, 18.50. Notable FTIR spectral peaks of MV: carbonyl wagging vibrations associated with the methacrylate and acetal groups, 1745 and 1702 cm^{-1}, respectively; terminal C=C wagging vibration, 1636 cm^{-1}; terminal C=CH$_2$ bending vibration, 947 cm^{-1}.

MG (2-methoxyphenyl methacrylate) (T_m = -59.9 °C): ^{1}H NMR (DMSO-d_6): δ 7.28–6.95 (bm, 4H), 6.28 (s, 1H), 5.89 (t, 1H), 3.76 (s, 3H), 2.00 (s, 3H); ^{13}C NMR (DMSO-d_6): δ 165.17, 151.38, 139.82, 135.49, 128.13, 127.42, 123.32, 121.03, 113.22, 56.15, 18.55. Notable FTIR spectral peaks of MG: carbonyl wagging vibraiton, 1737 cm^{-1}; terminal C=C wagging vibration, 1641 cm^{-1}; terminal C=CH$_2$ bending vibration, 945 cm^{-1}.

ME (4-allyl-2-methoxyphenyl methacrylate) (T_m = -58.2 °C): ^{1}H NMR (DMSO-d_6): δ 7.03–6.76 (bm, 3H), 6.25 (t, 1H), 6.03–5.93 (bm, 1H), 5.86 (t, 1H), 5.14–5.05 (bm, 2H), 3.73 (s, 3H), 3.38 (d, 2H), 1.98 (s, 3H); ^{13}C NMR (DMSO-d_6): δ 165.27, 151.13, 139.29, 138, 137.91, 135.51, 128.08, 123.06, 120.73, 116.48, 113.32, 56.12, 39.96, 18.58. Notable FTIR spectral peaks of ME: carbonyl wagging vibration, 1741 cm^{-1}; terminal C=C wagging vibrations associated with the methacrylate and allyl groups, 1638 cm^{-1}; terminal C=CH$_2$ bending vibrations associated with the methacrylate and allyl groups, 946 and 918 cm^{-1}, respectively (*33–37*).

5.2.4 Monomer and Resin Viscosity

Monomer and resin viscosities were obtained on a TA Instruments ARES-G2 rheometer. Measurements were performed isothermally at 25 °C controlled by a Peltier plate (+/– 0.1°C error). We used a 20-mm 1° steel cone with a truncation gap of 25 μm and a minimum sample volume of 0.04 mL. The shear rate was increased step-wise from 1 to 100 s^{-1} collecting 21 data points to observe any non-Newtonian behavior. At a given shear rate, the shear stress was

measured every 2 s. The shear rate and viscosity were recorded when the shear rate stabilized to within 5% tolerance for three consecutive points. Each monomer and resin was measured three times, and the viscosities at 50 s^{-1} were averaged and reported.

5.2.5 Thermogravimetric Evaporation Study

The evaporation behavior of MG, ME, and styrene was measured using a TA Instruments Q500 TGA. Approximately 50 mg of sample was placed in a platinum pan and held isothermally at 30 °C in a N_2 atmosphere (40 mL/min balance gas flow rate and 60 mL/min sample gas flow rate). Evaporation studies of MLMCs and styrene were performed for 18 and 3 h, respectively. Experiments were conducted three times to ensure reproducibility. MV was not measured because it is a solid at room temperature, and the sublimation rate would be orders of magnitude lower than the evaporation rates of styrene, MG, and ME.

5.2.6 Resin Curing

Homopolymers of MG and ME, poly(methacryl guaiacol) (PMG) and poly(methacryl eugenol) (PME), were prepared via bulk polymerization by adding 1.5 wt% MEKP to the monomer with curing at 90 °C for 4 h and subsequent postcuring at 130 °C for 2 h. Polymerizations were conducted in an argon atmosphere, whereby argon gas was purged through the oven for ~15 min at the beginning of cure. This purging technique was used for all subsequently described polymerizations as well. MV was not cured because it is a solid at standard temperature and pressure, therefore it is eliminated as a reactive diluent candidate. However, curing of resins containing MV is currently under investigation.

VE828 resins containing 5, 15, 30, 50, and 70 wt% MLMC monomers were prepared. VE828:St (styrene) resins were blended in similar concentrations (30, 50, and 70 wt% styrene) for use as standards equivalent to commercial resins. In an inert atmosphere, resins were cured at 90 °C using Trigonox 239 (1.5 wt% of the total resin mass) for 4 h and then postcured at 180 °C for 2 h.

5.2.7 In Situ FTIR Cure Kinetics Studies

In order to study the cure behavior of the VE resins that contained 30, 50, or 70 wt% reactive diluent, in situ FTIR cure kinetics studies were conducted on a PerkinElmer Spotlight 200 FTIR Microscope with a heating stage designed to hold 13-mm-diameter salt discs (heating stage controlled by a BriskONE Single-Zone Digital PID Thermocouple Temperature Controller with accuracy of ±0.25% of reading). At 90 °C for 4 h and 120 °C for 2 h, 32 cumulative scans were acquired with a resolution of 2 cm^{-1} in transmission mode in the mid-IR range with spectrum taken roughly every 1.1 min. A drop of well-mixed resin with 1.5 wt% Trigonox 239 was sandwiched between two 13-mm-diameter NaCl discs (International Crystal Labs) (the bottom NaCl disc was 2 mm thick while the top was 1 mm thick) prior to placement into the heating stage.

The conversion, α, of the VE828 and MLMC methacrylate groups, the styrene vinyl group, and the ME propene (allyl) group to single carbon-carbon bonds was calculated by measuring the heights of the associated peaks relative to an internal standard (i.e., a group that is not affected by the reaction). The equation used to calculate the conversions can be found elsewhere (3). VE828, MG, and ME contain methacrylate groups that appear at roughly 942 cm^{-1}. The methacrylate conversion was calculated by measuring the height of the peak relative to the VE aromatic C-H stretch at 830 cm^{-1}. Because of the TGA evaporation study results, it was deemed unnecessary to measure the peak heights of MG and ME relative to an MG and ME internal standard (evaporation of the reactive diluent deemed negligible). Styrene conversion was calculated by measuring the styrene carbon-carbon double bond peak height (910 cm^{-1}) relative to the styrene aromatic C-H stretch (700 cm^{-1}) (evaporation of styrene during curing deemed significant). ME allyl conversion was calculated by measuring the propene peak height (918 cm^{-1}) relative to the VE aromatic C-H stretch at 830 cm^{-1} (evaporation deemed negligible).

5.2.8 Polymer Properties

The thermogravimetric behavior of PMG, PME, and VE828 cured resins (30, 50, and 70 wt% reactive diluent) was measured using a TA Instruments Q500 TGA. Approximately 10 mg of sample was placed in a platinum pan and heated to 600 °C at 10 °C/min in a nitrogen atmosphere (40 mL/min balance gas flow rate and 60 mL/min sample gas flow rate).

Thermo-physical behavior of PMG, PME, and the VE828 cured resins (30, 50, and 70 wt% reactive diluent) were measured using DSC. A TA Instruments Discovery DSC was used with 40-μL aluminum pans as sample holders and with sample masses of ~10 mg. With a continuous N$_2$ purge at a rate of 50 mL/min, the samples were cooled to –90 °C and then heated to 225 °C at a rate of 10 °C/min. The cooling-heating cycle was repeated three times to eliminate any preexisting thermal history. The third heating cycle was used for T$_g$ acquisition.

Thermo-mechanical properties of the VE828 cured resins (5, 15, 30, 50, and 70 wt% reactive diluent) were measured using DMA. Rectangular samples with approximate dimensions of 35 × 13 × 3 mm^3 were tested using a TA Instruments Q800 DMA in single cantilever geometry. The samples were tested at an oscillation frequency and amplitude of 1 Hz and 7.5 μm, respectively, at a heating rate of 2 °C/min. The temperature at which the peak in the loss modulus occurred was considered the T$_g$ of the material (3). The storage modulus values in the rubbery plateau region at 175 °C for the VE828-styrene and VE828-MG cured resins and at 200 °C for the VE828-ME cured resins were used to calculate the molecular weight between cross-links, M$_C$. The densities of the cured resins were measured using Archimedes principle and were used to calculate M$_C$. The theory of rubber elasticity was used to calculate M$_C$ (3, 38).

5.3 Results and Discussion

5.3.1 Methacrylated Lignin Model Compound Monomer Properties

Methacrylated versions of vanillin, guaiacol, and eugenol, which were synthesized via an acid-catalyzed esterification, a Steglich esterification, or an esterification involving methacryloyl chloride, have been reported in the literature (*32–34*, *39–41*). The major disadvantage of the Steglich esterification is the requirement of a relatively large quantity of catalyst, 4-dimethylaminopyridine, and a large quantity of a reagent, *N,N'*-dicyclohexylcarbodiimde (15.3 and 153 wt% of total reactant mass, respectively) (*41*). Like the Steglich esterification, reported acid catalyzed esterifications of hydroxyls with an acid may require relatively large quantities of catalyst (*42*). While the reactivity of an acryl chloride is desirable, less desirable are the hazards associated with transporting and storing such unstable chemicals. To date, the utilization of methacrylic anhydride with catalytic amounts of DMAP has not been previously reported in synthesizing phenyl methacrylates. Despite acryl anhydrides being less stable than acryl acids, a significantly lower amount of catalyst is required than the Steglich and acid-catalyzed esterifications. An alternative phenolic methacrylation technique is a transesterification reaction involving methyl methacrylate catalyzed by *p*-toluenesulfonic acid with methanol, a classified green solvent (*43*), as the by-product. Currently, this reaction is being investigated as a potential scalable reaction to synthesize MLMCs.

ME and MG were low-viscosity liquids. MV was a solid at room temperature and thus was not used as a reactive diluent to replace styrene in this work. Average yields of 85.5% ± 4.5% were obtained for the MLMC esterification reactions. The purity of the MLMCs is estimated to be ≥94% based on ^{1}H NMR spectra. The impurities are believed to arise from the methacrylic anhydride, which is typically sold with 94%. In the methacrylic anhydride, Topanol A, 2-*tert*-butyl-4,6-dimethylphenol, was used as the free radical inhibitor in the amount of 2000 ppm. It is believed, though the hydroxyl of Topanol A is greatly hindered compared to the hydroxyls of the LMCs, that Topanol A participated in the phenolic methacrylation reactions and is collected with the desired product. However, methacrylated Topanol A contributes to no more than 0.2 wt% of the impurities. Despite this, further purification was not pursued and, after concentration under reduced pressure, the desired product was used as collected.

To determine the volatilities of MG and ME relative to styrene, TGA evaporation studies were performed with promising results (figure 85). Under the experimental conditions, styrene almost fully evaporated in about 3 h at 30 °C (only 6.3 wt% remained), whereas 99.04 and 98.95 wt% of ME and MG, respectively, remained after 18 h at 30 °C. This demonstrates that the MLMCs have a lower volatility than styrene and the potential to be environmentally friendly, low-VOC reactive diluents. The crossing of the MG and ME curves at roughly 600 min and other differences between the curves are within experimental error and are not representative of the difference between the evaporation behavior of MG and ME. However, because of the structure and molecular weight similarities of MG and ME, the evaporation behavior of these MLMCs was believed to behave similarly.

113
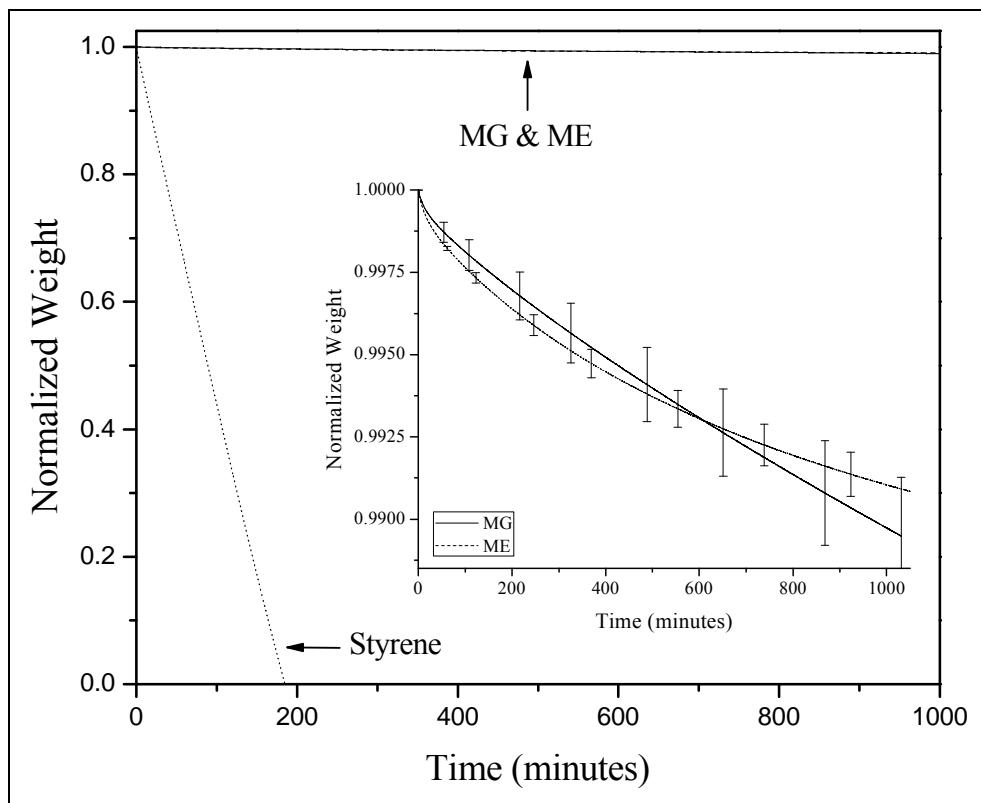
Figure 85. TGA normalized weight as a function of time for styrene, MG, and ME at T
= 30 °C; see inset for the MG and ME evaporation behavior. The maximum
standard deviation among the styrene TGA experiments was ± 0.17.

To elucidate the ability of MG and ME to replace styrene as reactive diluents in resins, MG, ME
(5, 15, 30, 50, and 70 wt% reactive diluent), and styrene (30, 50, and 70 wt% reactive diluent)
were blended with a standard VE resin, VE828. The viscosities of these blends as well as the
neat viscosities of MG and ME were evaluated. The results at 25 °C are shown in figure 86.
Included in figure 86 is the viscosity of styrene at 30 °C as reported in the literature (*3*). For all
samples, the viscosities exhibited Newtonian behavior. The neat MG and ME monomers have
higher viscosities than that of styrene (0.7 cP at 30 °C). This is attributed to the presence of
bulkier substituent groups on the phenyl ring of the neat MLMC monomers relative to just the
vinyl group on styrene, as van der Waals attractions are proportional to molecular weight (*44*).
Accordingly, the neat ME monomer has a slightly higher viscosity than MG as a result of the
slightly higher molecular weight of the ME attributed to the allyl group. In addition, MG and
ME have increased intermolecular attractions relative to styrene due to the ester linkages of MG
and ME (*44*).

As can be seen in figure 86, the viscosities of each VE828-reactive diluent resin system
decreased with reactive diluent molecular weight. The VE828-ME blend had a slightly higher
viscosity relative to the VE828-MG blend, while both have significantly higher viscosities
relative to the VE828-styrene blend. The observed order-of-magnitude higher viscosities of the
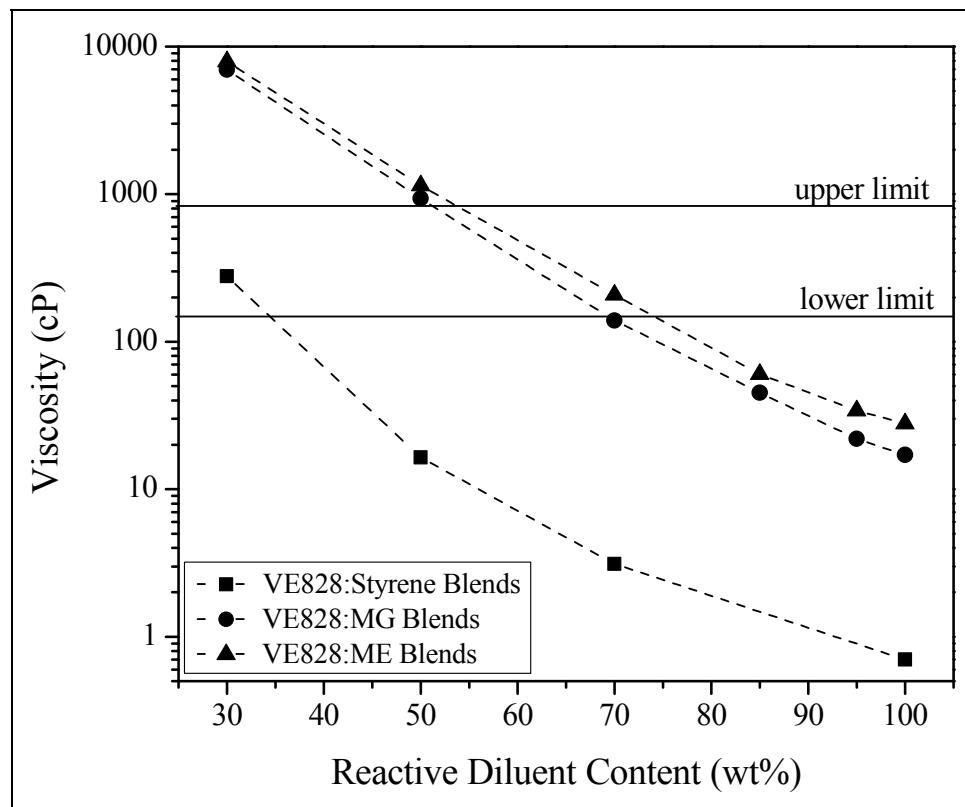
Figure 86. VE828 resin viscosities at 25 °C as a function of reactive diluent content in
weight percent. Upper (at 1000 cP) and lower (at 200 cP) limits of resin
viscosity for effective resin transfer are shown as black horizontal lines.
Maximum standard deviation for all resins = ±63 cP. Included is the viscosity
of styrene at 30 °C.

VE828-MLMC resins compared to the VE828-styrene resin are believed to be attributed to the
MLMC being able to hydrogen bond with the hydroxyls of VE828 via the methacrylate group.
Hydroxyl-ester hydrogen bonding has been show to increase resin viscosity of similar VE resin
systems that contained methacrylic-based reactive diluents (*2*, *3*). Yet, resins containing MG and
ME at reactive diluent concentrations between 50 and 70 wt% still maintain viscosities amenable
to molding applications (*1*). The VE828:St and VE828:MG blends exhibit exponential-like
viscosity behavior as a function of reactive diluent concentration. The VE828:ME blend also
exhibits similar behavior but with 15:85 VE828:ME and 5:95 VE828:ME acting as outliers.
Currently, the behavior of these outliers is being confirmed as well as modeling of the viscosity
behaviors.

5.3.2 In Situ FTIR Cure Kinetics Studies

The curing behavior of the VE828 resins was monitored using in situ FTIR spectroscopy with
curing at 90 °C for 4 h and a postcured at 120 °C for 2 h. The conversions of the methacrylate
groups of VE828 and of the vinyl groups of styrene in the VE828:St resins are shown as a
function of time in figures 87 and 88, respectively. As can be seen in figure 87, the conversion

rate and total conversion increased with increasing VE828 concentration. Similarly in figure 88, the conversion rate and total conversion of styrene vinyl bonds increased with increasing VE828 concentration. The curing behaviors of the methacrylate groups and styrene vinyl groups of 3:7 VE828:St are quite different and are thought to be influenced by styrene evaporation during curing.
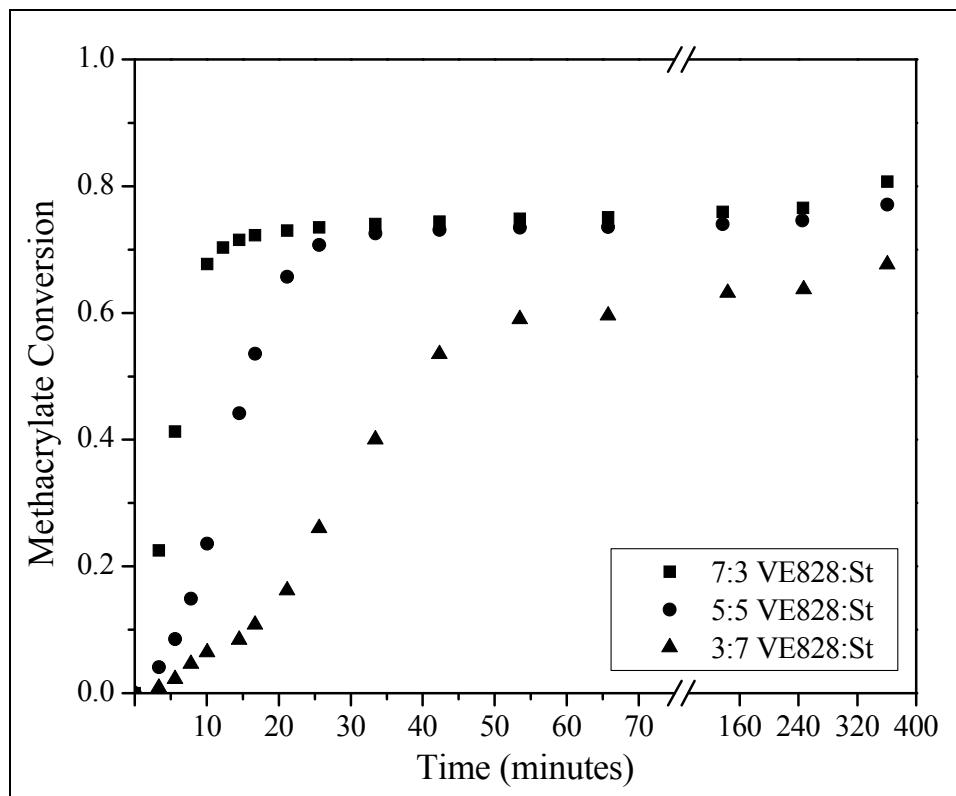
Figure 87. Methacrylate conversion as a function of time for the cure of VE828:St
resins. Samples were cured at 90 °C for 4 h and postcured at 120 °C for 2 h.
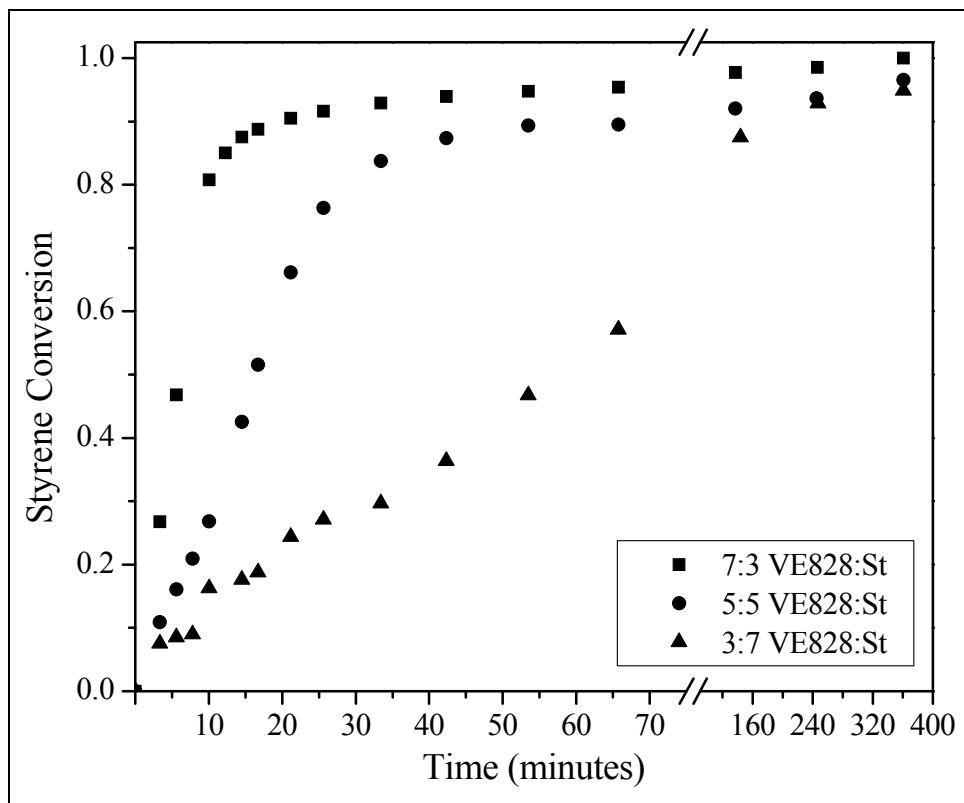
Figure 88. Styrene conversion as a function of time for the cure of VE828:St resins.
Samples were cured at 90 °C for 4 h and postcured at 120 °C for 2 h.

The conversion of the methacrylate groups of VE828 and MG of the VE828:MG resins as a
function of time is shown in figure 89. As can be seen in figure 89, the conversion rate and total
conversion of 3:7 VE828:MG are higher than 7:3 VE828:MG and 5:5 VE828:MG. This is
believed to be a result of the higher resin viscosities of 7:3 VE828:MG and 5:5 VE828:MG.
With increased resin viscosity, molecular mobility during curing is suppressed, decreasing the
propagation efficiency and overall curing. Additionally, the onset of gelation increases with
increasing cross-linker concentration. The exact point of gelation is currently unknown;
however, it is suspected to aid in the overall curing behavior.
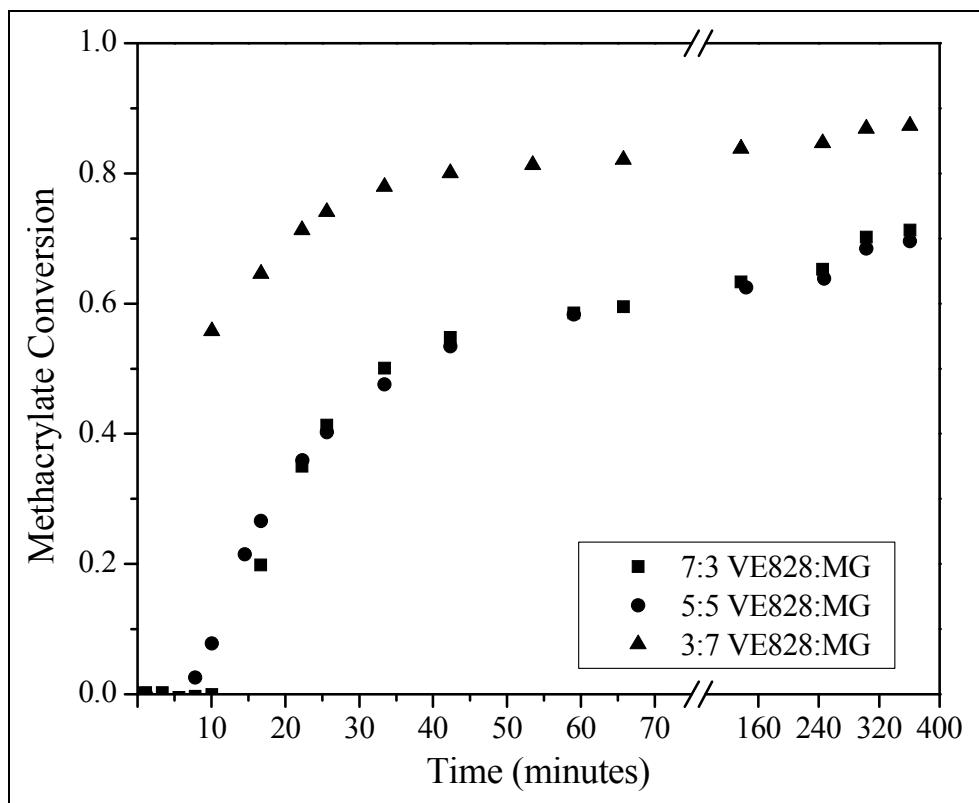
Figure 89. Methacrylate conversion as a function of time for the cure of VE828:MG
resins. Samples were cured at 90 °C for 4 h and postcured at 120 °C for 2 h.

The conversion of the methacrylate groups of VE828 and the allyl groups of ME of the
VE828:ME resins as a function of time is shown in figures 90 and 91, respectively. As can be
seen in figure 90, the overall methacrylate conversion of 3:7 VE828:ME is higher than 7:3
VE828:ME and 5:5 VE828:ME. Figure 91 shows that, interestingly enough, the conversion rate
and overall conversion of the ME allyl groups increased with increasing VE828, essentially an
increased concentration of methacrylate groups. These results confirm the ability of ME to
partially act as a cross-linker in VE resin systems with the extent of allyl conversion greatly
influenced by the methacrylate group concentration.
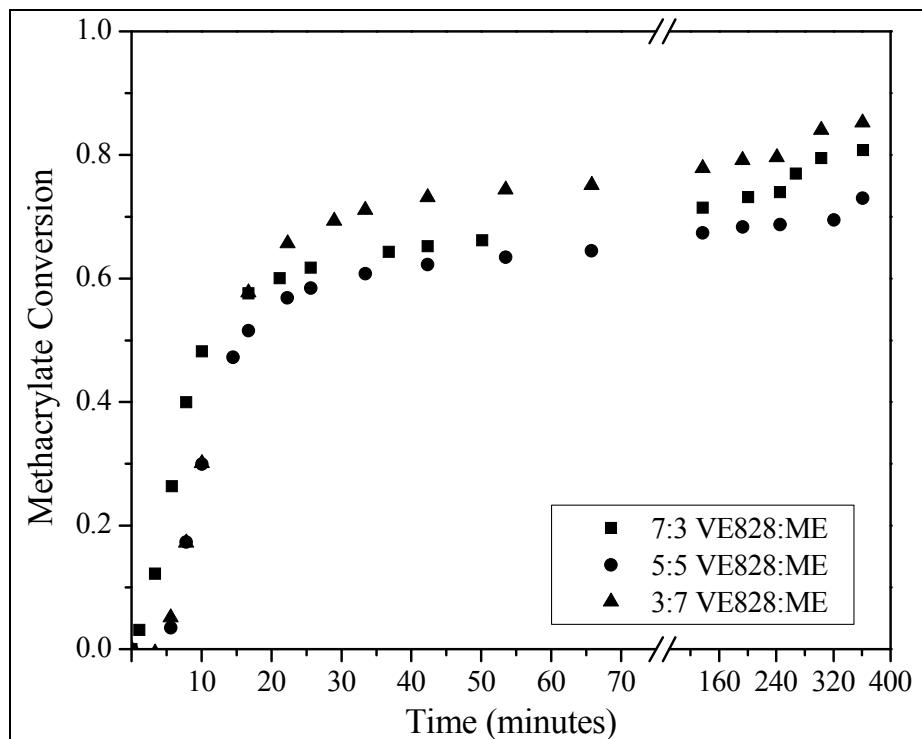
Figure 90. Methacrylate conversion as a function of time for the cure of VE828:ME resins. Samples were cured at 90 °C for 4 h and postcured at 120 °C for 2 h.
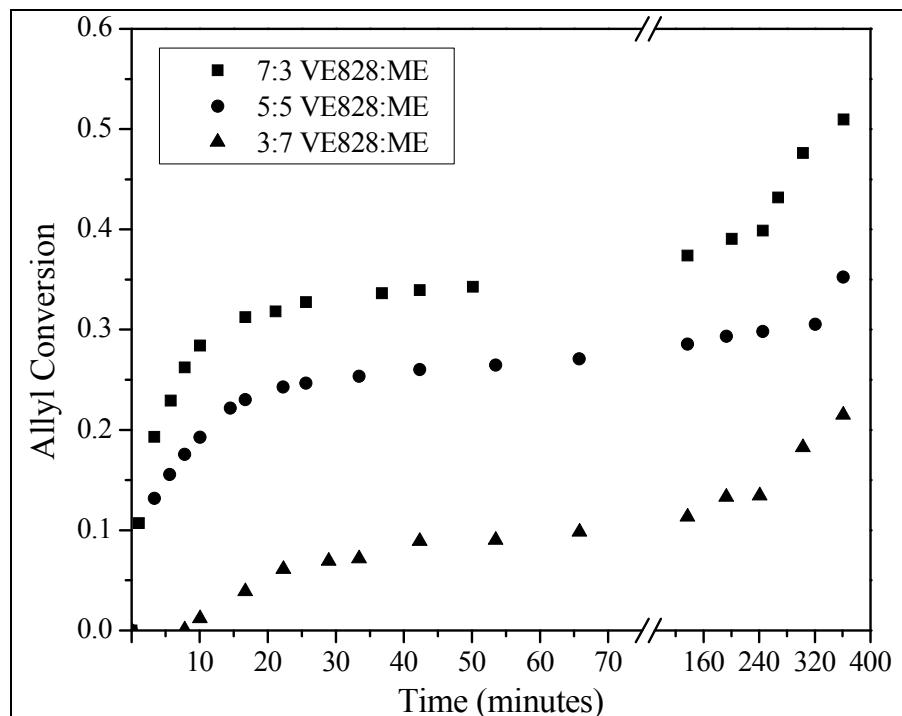
Figure 91. Allyl conversion as a function of time for the cure of VE828:ME resins. Samples were cured at 90 °C for 4 h and postcured at 120 °C for 2 h.

In all of these conversion figures, changes in conversion profiles can be seen at time = 240 min. This is attributed to increasing the reaction temperature from 90 to 120 °C. As the T_g's are approached, molecular mobility greatly increases; therefore, any unreacted monomers have a greater chance to react into the polymer network. Postcuring temperature was limited because of the FTIR owner's request. Since the overall conversion increased with increasing temperature, it is believed that a postcure at 180 °C would greatly enhance the overall conversion. Currently, this is being investigated.

5.3.3 Polymer Glass Transition Temperature via DSC

Polystyrene has a relatively high T_g (~100 °C) (*38*). The aromatic side chain of styrene via π-bond stacking provides structural rigidity, thermal stability, limited "free volume," and brittleness. According to a new theory of the glass transition entitled "the twinkling fractal theory" (TFT), the glassiness of polystyrene at room temperature is attributed to the rigid aromatic side chains rapidly slowing down the twinkling fractal dynamics and thus enhancing vector percolation of solid fractal clusters and ultimately fractal cavitation (*45, 46*). The enhancement of vector percolation and fractal cavitation occurs despite a considerable amount of liquid-like clusters still existing, ≈0.40, at 298 K (*45, 46*). However, the liquid-like clusters exhibit characteristics of "free volume," but because of the closeness of the aromatic side chains to the polymer backbone, they lack the normal alkyl chain-like mobility. Thus, they contribute to the relatively high onset temperature of vector percolation, T_{cv}, and fractal cavitation at T_g = 100 °C (*45, 47*). The similarities between the MLMCs and styrene are evident through the aromatic ring and the presence of a reactive terminal carbon-carbon double bond. Additionally, it is interesting to note the similarities between the MLMCs and methyl methacrylate, which has a T_g ~ 104 °C when homopolymerized (*38*). Despite the fact that there are alkyl substituent groups on the phenol groups that increase the bulkiness of polymer side chains, the MLMCs, when polymerized, are expected to possess T_g's close to that of polystyrene and poly(methyl methacrylate) (PMMA) and exhibit twinkling dynamics similar to that of polystyrene and PMMA. Furthermore and prior to methacrylation, eugenol contains a terminal allyl group that is in the para position to the hydroxyl group on the aromatic ring. However, eugenol itself is not easily polymerized because of the presence of a phenolic hydroxyl that acts as a free radical scavenger and the allylic nature of the propene substituent group (*33, 34*). The reactivity of the allyl group of eugenol, which determines whether the ME behaves as a monofunctional reactive diluent or as a cross-linker in VE resin systems, is currently under investigation.

T_g's of the cured resins have been determined by DSC analysis. The DSC thermograms and the measured T_g's are shown in figures 92–94. As can be seen, all T_g's of the VE828 cured resins are above 100 °C, the T_g's of PMG and PME are 92 and 103 °C, respectively, and, as expected, the T_g's decreased with increasing reactive diluent content. The VE828:MG T_g's are lower than the VE828:St T_g's; however, the VE828:ME T_g's are either higher or only a fewer degrees lower than the VE828:St T_g's. Wesslén et al. (*39*) have reported a PMG T_g of 110 °C via DSC, while Rojo et al. (*33*) have reported a PME T_g of 96 °C via DSC at a heating rate of 10 °C/min.
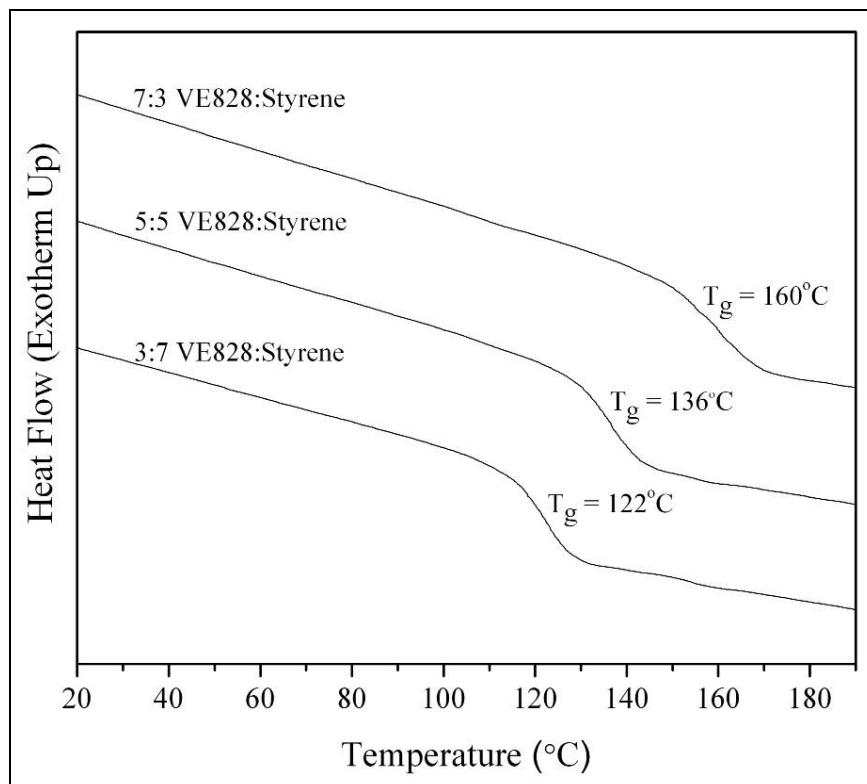
Figure 92. DSC thermograms of VE828:St cured resins.
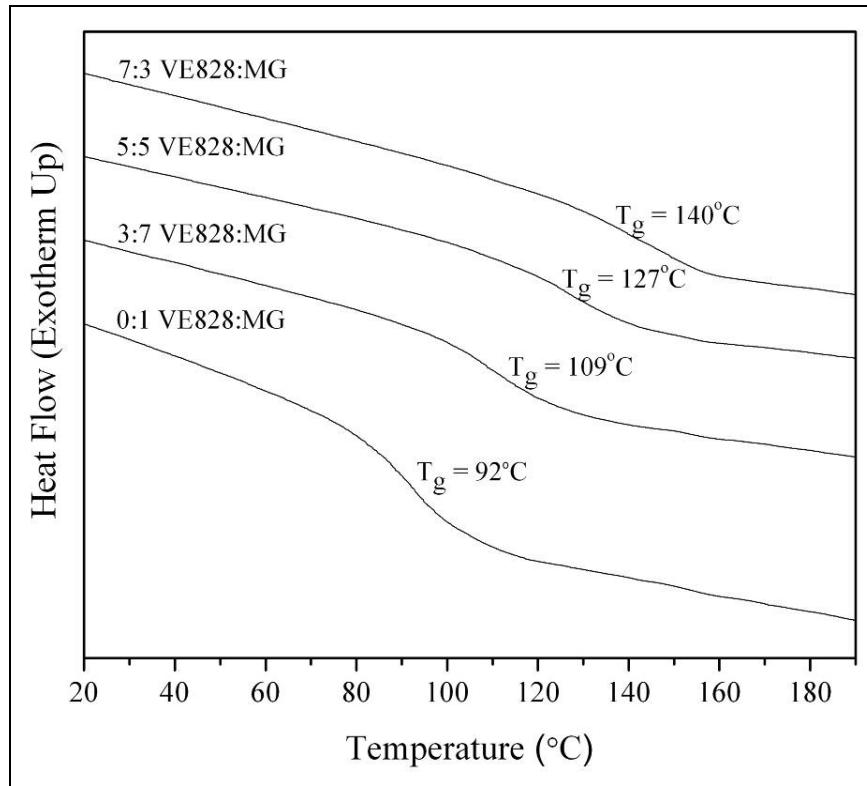
Figure 93. DSC thermograms of VE828:MG cured resins.
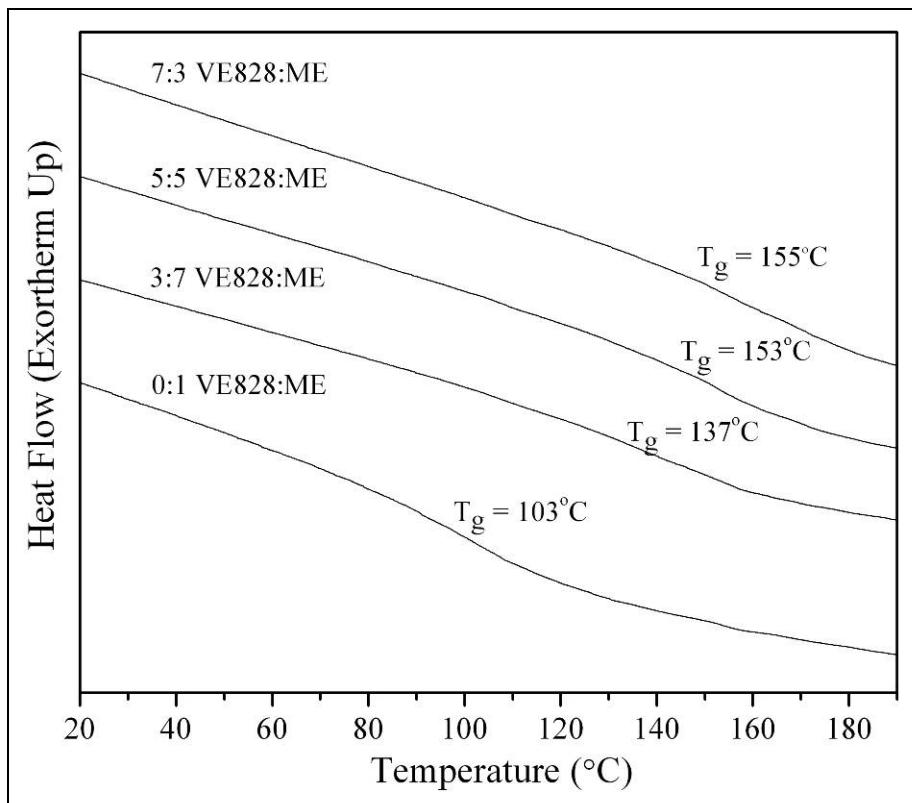
Figure 94. DSC thermograms of VE828:ME cured resins.

Despite the discrepancies between the homopolymer T_g's reported in this report and those reported previously, which could be a function of differences in polymerization conditions, molecular weights, and DSC techniques, it is encouraging to find that PMG and PME have similar T_g's to that of polystyrene and poly(methyl methacrylate), and that the cured VE resins have similar T_g's to those that contain styrene. Additionally, glass transition broadness increased with decreasing reactive diluent content and with reactive diluent type (styrene < MG < ME). This may be a result of an increased amount of relaxation modes present in the cross-linked network, which, according to the TFT, arises when there exists a broad distribution of solid fractal clusters that twinkle into the liquid upon heating (*45–47*). With increasing resin viscosity, molecular mobility is suppressed during curing, leading to a greater chance of an irregular cross-linked network formation, and, in turn, a broader distribution of solid fractal clusters and relaxation dynamics. Moreover, and unlike styrene, MG and ME contain methacrylate groups that are capable of hydrogen bonding with the hydroxyls of VE828. Hydrogen bonding may influence the relaxation dynamics of the cross-linked network and the ability of the solid fractal clusters to transition into liquid-like behavior. Furthermore, irregularity of the cross-linked network may further increase because of the ability of ME to cross-link, imparting a higher degree of rigidity and lowering molecular mobility during polymerization. Allylic monomer reactivity in the presence of methyl methacrylate has been reported to be 4 orders of magnitude

122

lower than the comonomer (*48*). Additionally, Rojo et al. (*33*, *34*) have reported thermosetting-type behavior of PME, which is attributed to pendant allyl groups contributing to grafting and cross-linking when polymerization reaches high conversion. Intentionally breaking PMG and PME specimens, PME exhibited greater qualitative brittleness compared to PMG, indicating a potential degree of cross-linking. This is consistent with the fact that increased cross-linking is known to increase the breadth of the glass transition (*44*).

5.3.4 Polymer Properties via TGA and DMA

Thermo-gravimetric behavior of VE828:St, VE828:MG, and VE828:ME cured resins that contain 30, 50, and 70 wt% reactive diluent as well as PMG and PME were measured and are illustrated in figures 95–97, respectively. In all three figures, the normalized sample weight (left y-axis) and the derivative of the normalized sample weight (right y-axis) are plotted as a function of temperature. Additionally, values of the temperature for the maximum rate of decomposition, T_{max}, and temperature for 50% weight loss, $T_{50\%}$, are shown in table 12. As can be seen, all cured resins are thermally stable (<3 wt% mass loss) above 225 °C with the VE828:St and VE828:ME cured resins exhibiting greater thermal stability than the VE828:MG cured resins. For all resins, T_{max} occurred near 400 °C. The degradation that occurs around 400 °C is attributed to aliphatic carbon-carbon bond breakage (*49*). Despite conducting the TGA experiments in the presence of air, similar thermograms of VE:St cured resins have been reported in the literature with char contents considerably less than that shown in figure 95.
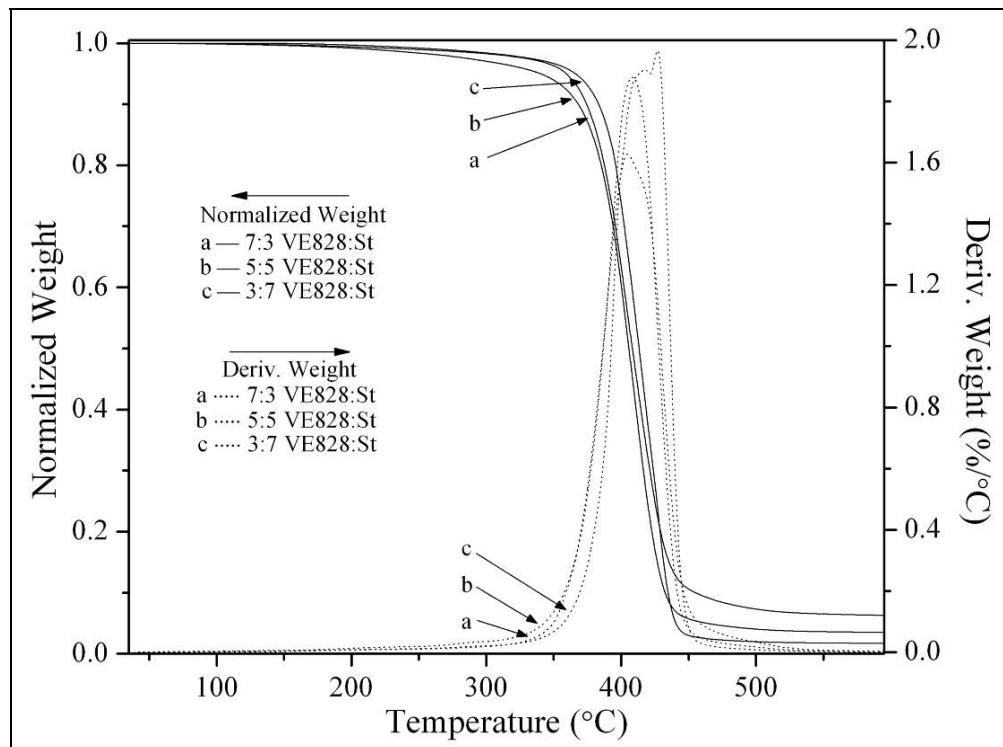
Figure 95. TGA normalized weight (left y-axis) and derivative of normalized weight (right y-axis) as a function of temperature for VE828:St cured resins.
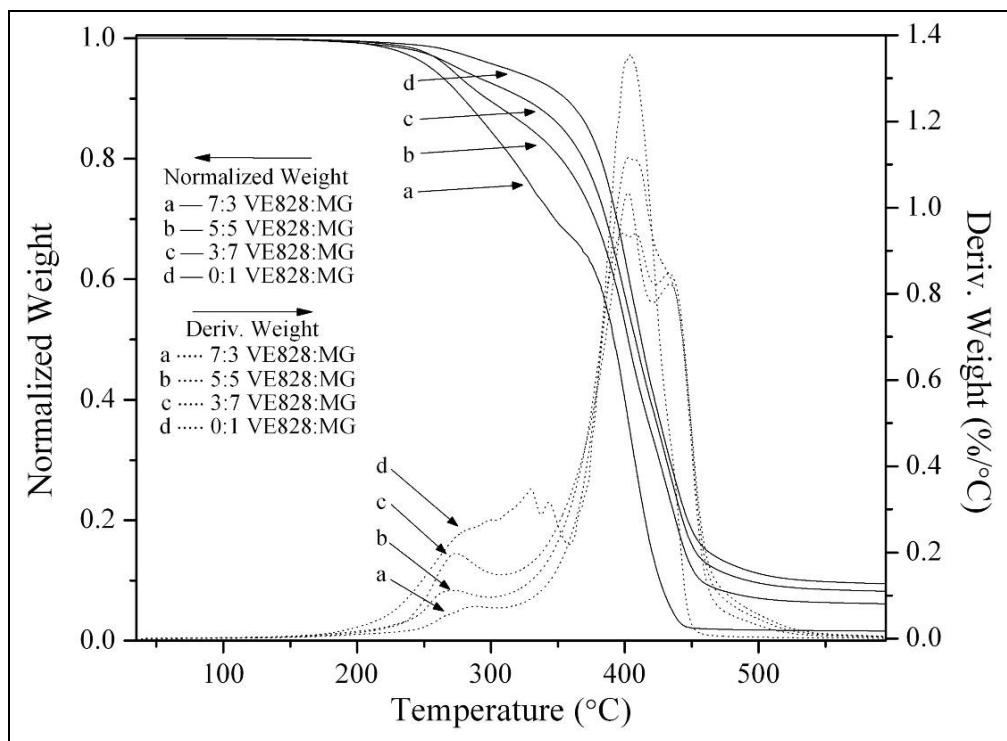
Figure 96. TGA normalized weight (left *y*-axis) and derivative of normalized weight (right *y*-axis) as a function of temperature for VE828:MG cured resins.
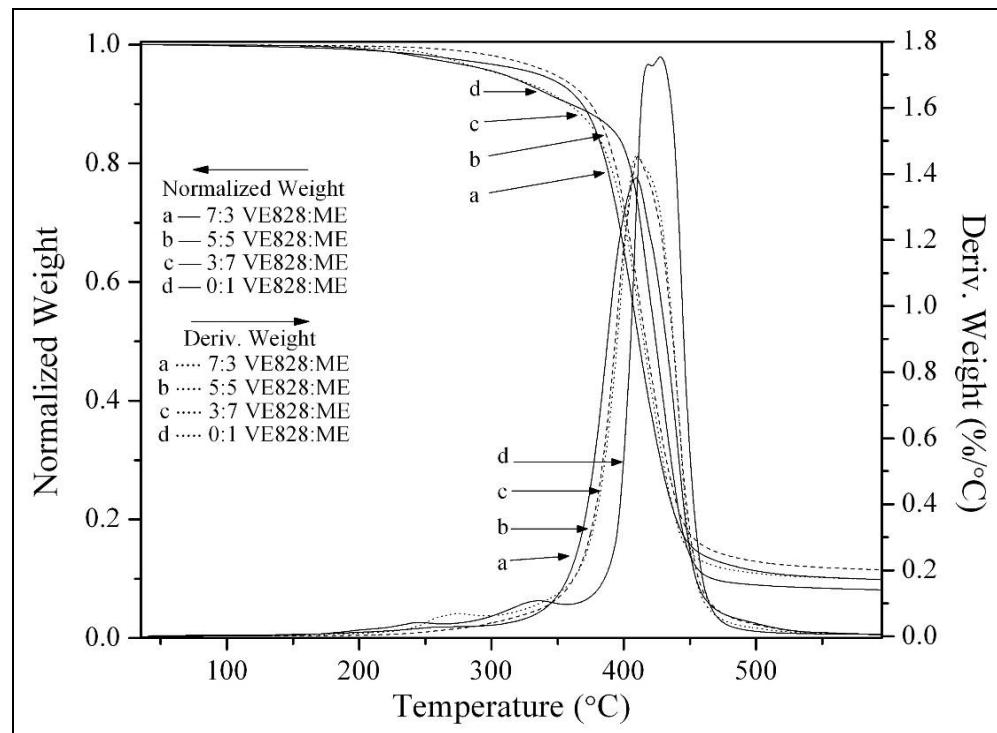
Figure 97. TGA normalized weight (left *y*-axis) and derivative of normalized weight (right *y*-axis) as a function of temperature for VE828:ME cured resins.

124

Table 12. Values of temperature for maximum rate
of decomposition (T_{max}) and temperature
for 50% weight loss ($T_{50\%}$) obtained
from TGA curves of the cure VE resins.

System	T_{max} (°C)	$T_{50\%}$ (°C)
7:3 VE828:St	404.7	408.3
5:5 VE828:St	408.5	405.7
3:7 VE828:St	427.0	413.3
7:3 VE828:MG	404.3	407.1
5:5 VE828:MG	392.7	402.7
3:7 VE828:MG	399.0	398.9
0:1 VE828:MG	404.2	391.8
7:3 VE828:ME	409.1	411.3
5:5 VE828:ME	410.8	416.6
3:7 VE828:ME	409.9	414.9
0:1 VE828:ME	427.7	424.1

Charring occurs because of inhibition of thermal oxidative degradation and, thus, an increased cyclization potential when studies are conducted in an inert atmosphere. In addition, the char content increased as the amount of styrene decreased. This resulted because VE828 contains four or more aromatic rings per molecule, whereas styrene contains only one aromatic ring per molecule. Thermal degradation of aromatic carbon-hydrogen bonds in the presence of air is reported to commence at temperatures >500 °C (*49*). Therefore, the greater the aromatic content of the resin, the higher the char content. Grishchuk and Karger-Kocsis (*50*) observed similar char contents upon conducting thermogravimetric studies on VE resins in the presence of a nitrogen atmosphere.

Table 12 shows that the T_{max} and $T_{50\%}$ values of VE828:MG are less than that of VE828:St but not by an appreciable amount. A more noticeable difference between the thermal behavior of VE828:St and VE828:MG can be observed when comparing figures 95 and 96. Unlike VE828:St, VE828:MG exhibits a two-stage thermal decomposition (first stage between 200 and 350 °C and the second stage between 350 and 600 °C). This two-stage behavior was also observed by Zulfiqar et al. (*51*) in thermograms of poly(phenyl methacrylate). According to Zulfiqar et al. (*51*), the first stage is believed to be depolymerization initiated at unsaturated chain ends, and the second stage is depolymerization by random scission. However, unlike Zulfiqar et al. (*51*) who observed that the copolymers of methyl methacrylate and styrene with phenyl methacrtylate were more thermally stable than their homopolymers, PMG exhibited more thermal stability than the copolymers (figure 96). Furthermore, as can be seen in figure 96, the thermal stability decreases with increasing VE828 content. The observed opposite trend may be

a result of increased resin viscosity as the amount of VE828 increases, decreasing monomer mobility and decreasing the extent of polymerization (see figure 89). In turn, this increases the amount of unsaturated chain ends created during polymerization. Additionally, in figure 96, the char content increases with increasing MG content. Because of the abundance of methacrylate groups, anhydride ring formation may occur during thermal treatment, which, in turn, interferes with polymer chains unzipping to monomers (*51*).

Unlike VE828:MG thermograms shown in figure 96, VE828:ME thermograms shown in figure 97 demonstrate similar thermal behavior to that of VE828:St. PME does exhibit a two-stage thermal decomposition profile; however, the blends demonstrate single-stage thermal decomposition profiles with no clear trend. Again, charring is present in figure 97 with PME possessing the least amount of char but possessing more char than PMG (figure 96). The fact that PME possesses the least amount of char and that the VE828:ME cured resins show very similar thermal behavior to the VE828:St cured resins may be a function of the allyl group reactivity (*48*). Despite the relatively high viscosities of the VE828:ME resins, the allylic groups may be forming cross-links and therefore creating a tighter cross-linked network with greater thermal stability (figure 91).

Thermo-mechanical properties of the cured VE resins were measured using DMA. Similar to polymers using styrene as a reactive diluent, polymers using MG and ME as reactive diluents produced hard and rigid polymers. Table 13 lists the properties of the VE828:St, VE828:MG, and VE828:ME cured resins that were cured at 90 °C for 4 h and postcured at 120 °C for 2 h. As can be seen in table 13, the DMA measured T_g's and trends are similar to those obtained via DSC. All resins are glassy at room temperature and possess storage moduli at 25 °C to be ≥2.0 GPa. Additionally, the rubbery moduli of the polymers are between 1.9 and 192 MPa, indicating the molecular weight between cross-links, M_C, of 8100 to 74 g/mol. With respect to reactive diluent concentration, the M_C of the polymers that contain ME as the reactive diluent is lower than those that contain styrene or MG as reactive diluents, confirming that the allyl groups of ME are indeed partially polymerizing during curing.

Table 13. Properties of the cured VE resins that were cured at 90 °C for 4 h and postcured at 180 °C for 2 h in an inert atmosphere.

Sample	T_g (°C)	E' at 25°C (GPa)	Rubbery E' (MPa) [a]	ρ at 25°C (g/cm^{-3}) [b]	M_c (g/mol) [c]
7:3 VE828:St	143	3.0	52.1	1.165	250
7:3 VE828:MG	127	3.2	55.4	1.225	247
7:3 VE828:ME	151	2.8	192	1.208	74
5:5 VE828:St	134	2.2	24.6	1.136	516
5:5 VE828:MG	116	3.3	30.6	1.228	449
5:5 VE828:ME	141	2.8	128	1.205	111
3:7 VE828:St	119	2.0	10.7	1.095	1144
3:7 VE828:MG	105	3.3	14.4	1.227	952
3:7 VE828:ME	128	2.9	51.8	1.192	272
15:85 VE828:MG	93	3.0	4.0	1.228	3432
15:85 VE828:ME	120	2.3	43.8	1.179	318
05:95 VE828:MG	91	3.2	1.7	1.232	8101
05:95 VE828:ME	108	2.7	12.5	1.175	1109

[a] For VE828:St, VE828:MG, and VE:MG:St, E' taken at $T = 175$°C. For VE828:ME and VE828:ME:St E' taken at $T = 200$°C.

[b] Max standard deviation for all densities $= \pm 0.009$ g/cm^{-3}.

[c] Maximum standard deviation for all M_c's $= \pm 2.8$ g/mol.

5.4 Conclusions and Future Work

Lignin is a copious paper and pulping waste product that is primarily burned for energy recovery. Despite being considered intractable, novel methods to selectivity that break down lignin into valuable, lower molecular weight chemicals, often referred to as LMCs, are being developed. The major highlights of the research to date are as follows:

1. LMCs, vanillin, guaiacol, and eugenol have been successfully methacrylated in modest yields (85.5% ± 4.5%).

2. MV was a solid at room temperature while MG and ME were low-viscosity liquids (17 and 28 cP, respectively) at room temperature.

3. MG and ME were successfully blended with VE828 with the majority of the resin mixtures having room temperature viscosities acceptable for liquid molding applications (<1000 cP at 25 °C).

4. Relative to styrene, the volatilities of MG and ME were shown to be much lower, ultimately showing that they have potential to be environmentally friendly, low-VOC reactive diluents.

5. Homopolymerizations of MG and ME produced transparent and hard polymers that possess T_g's (92 and 103 °C) that are similar to polystyrene (100 °C) and PMMA (104 °C).

6. VE828:MG and VE828:ME cured resins were shown to have T_g's (via DSC and DMA) and room temperature storage moduli values comparable to VE828:St cured resins. Additionally, the molecular weights between cross-links of cured resins containing ME were higher than cured resins that contained MG and St, indicating that ME partially acts as a cross-linker. This was further confirmed via in situ FTIR cure kinetics studies, which showed that a significant percentage of ME allyl groups polymerize during curing.

7. TGA studies of the cured VE828 resins showed that the polymers containing MG and ME have comparable thermal resistivity to polymers containing styrene, with VE828:MG polymers exhibiting a slightly lower thermal resistivity than VE828:ME polymers.

In writing this midterm report, it was revealed that progress has been made utilizing lignin and LMCs in biobased composite applications. However, many holes and gaps were also revealed. The following list outlines future tasks that are currently being accomplished and will hopefully be accomplished in the near future at the University of Delaware in order to fill in the revealed holes:

1. Currently, we are performing a more in-depth analysis of the FTIR cure kinetics studies and polymer properties of the cured VE828:MG, VE828:ME, and VE828:St resins. This includes potentially repeating some experiments as well as modeling the observed behaviors (i.e., applying the autocatalytic model to the FTIR conversion data, modeling the resin viscosities as a function of reactive diluent type and concentration, and applying polymer physics models to the T_g trends). Additionally, we plan to perform tensile and flexural tests on the cured resins (November 2011–January 2012).

2. Model the volatility behavior of MG and ME relative to styrene (November 2011–January 2012).

3. Continue with TGA experiments of the VE828 resins and model the VE828 resin decompositions (December 2011–July 2012).

Acknowledgments

References

1. Wool, R. P.; Sun, X. S. *Bio-based Polymer and Composites*, 1st ed. Elsevier B.V.: New York, 2005.

2. La Scala, J. J.; Orlicki, J. A.; Winston, C.; Robinette, E. J.; Sands, J. M.; Palmese, G. R. *Polymer* **2005**, *46*, 2908–2921.

3. La Scala, J. J.; Sands, J. M.; Orlicki, J. A.; Robinette, E. J.; Palmese, G. R. *Polymer* **2004**, *45*, 7729–7737.

4. Environmental Protection Agency. National Emissions Standards for Hazardous Air Pollutants: Reinforced Plastic Composites Production. 40 CFR Part 63; *Federal Register* **2003**, *68* (76), 19375–19443.

5. U.S. Department of Health and Human Services, Public Health Service, National Toxicology Program. *Report on Carcinognes*, 12th ed.; Washington, DC, 2011.

6. La Scala, J. J.; Ulven, C. A.; Orlicki, J. A.; Jain, R.; Palmese, G. R.; Vaidya, U. K.; Sands, J. M. *Clean Technologies and Environmental Policy* **2007**, *9*, 265–279.

7. Campanella, A.; La Scala, J. J.; Wool, R. P. *Polymer Engineering and Science* **2009**, *49*, 2384–2393.

8. Campanella, A.; La Scala, J. J.; Wool, R. P. *Journal of Applied Polymer Science* **2011**, *119*, 1000–1010.

9. Palmese, G. R.; La Scala, J. J.; Sands, J. M. Fatty Acid Monomers to Reduce Emissions and Toughen Polymers. U.S. Patent 7,525,909, April 28, 2009.

10. Lora, J. H.; Glasser, W. G. *Journal of Polymers and the Environment* **2002**, *10*, 39–48.

11. Voitl, T.; Rudolf von Rohr, P. *ChemSusChem* **2008**, *1*, 763–769.

12. Thielemans, W.; Wool, R. P. *Composites Part A: Applied Science and Manufacturing* **2004**, *35*, 327–338.

13. Zakzeski, J.; Weckhuysen, B. M. *ChemSusChem* **2011**, *4*, 369–378.

14. Binder, J. B.; Gray, M. J.; White, J. F.; Zhang, Z. C.; Holladay, J. E. *Biomass and Bioenergy* **2009**, *33*, 1122–1130.

15. Jia, S.; Cox, B. J.; Guo, X.; Zhang, Z. C.; Ekerdt, J. G. *ChemSusChem* **2010**, *3*, 1078–1084.

16. Li, Y.; Sarkanen, S. *Macromolecules* **2002**, *35*, 9707–9715.

17. Calvo-Flores, F. G.; Dobado, J. A. *ChemSusChem* **2010**, *3*, 1227–1235.

18. Gandini, A. *Green Chemistry* **2011**, *13*, 1061–1083.

19. Petrocelli, F. P.; Klein, M. T. *Industrial and Engineering Chem Product Research and Development* **1985**, *24*, 635–641.

20. Silva, E. A. B. D.; Zabkova, M.; Araújo, J. D.; Cateto, C. A.; Barreiro, M. F.; Belgacem, M. N.; Rodrigues, A. E. *Chemical Engineering Research and Design* **2009**, *87*, 1276–1292.

21. Chakar, F.; Ragauskas, A. J. *Industrial Crops and Products* **2004**, *20*, 131–141.

22. Mialon, L.; Pemba, A. G.; Miller, S. A. *Green Chemistry* **2010**, *12*, 1704–1706.

23. Sergeev, A. G.; Hartwig, J. F. *Science* **2011**, *332*, 439–443.

24. Sarkanen, K. V.; Ludwig, C. H. Lignins: Occurrence, Formation, Structure and Reactions; John Wiley & Sons, Inc., New York, 1971; pp 639–694.

25. Schrodi, Y.; Ung, T.; Vargas, A.; Mkrtumyan, G.; Lee, C. W.; Champagne, T. M.; Pederson, R. L.; Hong, S. H. *CLEAN - Soil, Air, Water* **2008**, *36*, 669–673.

26. Ferré-Filmon, K.; Delaude, L.; Demonceau, A.; Noels, A. F. *European J. Organic Chem.* **2005**, *2005*, 3319–3325.

27. Scholl, M.; Ding, S.; Lee, C. W.; Grubbs, R. H. *Organic Letters* **1999**, *1*, 953–956.

28. Gallivan, J. P.; Jordan, J. P.; Grubbs, R. H. *Tetrahedron Letters* **2005**, *46*, 2577–2580.

29. Bonini, C. *Industrial Crops and Products* **2004**, *20*, 243–259.

30. Bonini, C.; D'Auria, M.; Ferri, R. *Photochemical and Photobiological Sciences* **2002**, *1*, 570–573.

31. Lanzalunga, O.; Bietti, M. *Journal of Photochemistry and Photobiology. B, Biology* **2000**, *56*, 85–108.

32. Imoto, M.; Maeda, T.; Ouchi, T. *Chem. Letters* **1978**, *7*, 153–156.

33. Rojo, L.; Borzacchiello, A.; Parra, J.; Deb, S.; Vázquez, B.; San Román, J. *Journal of Materials Science: Materials in Medicine* **2008**, *19*, 1467–1477.

34. Rojo, L.; Vazquez, B.; Parra, J.; López Bravo, A.; Deb, S.; San Roman, J. *Biomacromolecules* **2006**, *7*, 2751–2761.

35. Olbert-Majkut, A.; Wierzejewska, M. *Journal of Physical Chemistry A* **2008**, *112*, 5691–5699.

36. Rahim, E. A.; Sanda, F.; Masuda, T. *Journal of Macromolecular Science, Part A* **2004**, *41*, 133–141.

37. Dhoot, G.; Auras, R.; Rubino, M.; Dolan, K.; Soto-Valdez, H. *Polymer* **2009**, *50*, 1470–1482.

38. Sperling, L. H. *Introduction to Physical Polymer Science*, 4th ed.; John Wiley and Sons, Inc.: Hoboken, NJ, 2006.

39. Wesslén, B.; Gunneby, G.; Hellström, G.; Svedling, P. *Journal of Polymer Science: Polymer Symposia* **1973**, *42*, 457–465.

40. Yamada, B.; Tanaka, T.; Otsu, T. *European Polymer Journal* **1989**, *25*, 117–120.

41. Renbutsu, E.; Okabe, S.; Omura, Y.; Nakatsubo, F.; Minami, S.; Saimoto, H.; Shigemasa, Y. *Carbohydrate Polymers* **2007**, *69*, 697–706.

42. Hatakeyama, S.; Satoh, K.; Sakurai, K.; Takano, S. *Tetrahedron Lett.* **1987**, *28*, 2713–2716.

43. Alfonsi, K.; Colberg, J.; Dunn, P. J.; Fevig, T.; Jennings, S.; Johnson, T. A.; Kleine, H. P.; Knight, C.; Nagy, M. A; Perry, D. A; Stefaniak, M. *Green Chem* **2008**, *10*, 31.

44. La Scala, J. J. Ph.D. Dissertation, The Effects of Triglyceride Structure on the Properties of Plant Oil-Based Resins, University of Delaware, Newark, DE, 2002.

45. Wool, R. P. *Journal of Polymer Science Part B: Polymer Physics* **2008**, *46*, 2765–2778.

46. Stanzione, J. F., III; Strawhecker, K. E.; Wool, R. P. *Journal of Non-Crystalline Solids* **2011**, *357*, 311–319.

47. Wool, R. P. *Soft Matter* **2008**, *4*, 400–418.

48. Heatley, F.; Lovell, P.; Mcdonald, J. *European Polymer Journal* **1993**, *29*, 255–268.

49. Can, E.; La Scala, J. J.; Sands, J. M.; Palmese, G. R. *Journal of Applied Polymer Science* **2007**, *106*, 3833–3842.

50. Grishchuk, S.; Karger-Kocsis, J. *eXPRESS Polymer Letters* **2011**, *5*, 2–11.

51. Zulfiqar, S.; Zulfiqar, M.; Kausar, T. *Polymer Degradation and Stability* **1987**, *17*, 327–339.

5.5   Appendix

5.5.1   Spectra of Guaiacol and Eugenol
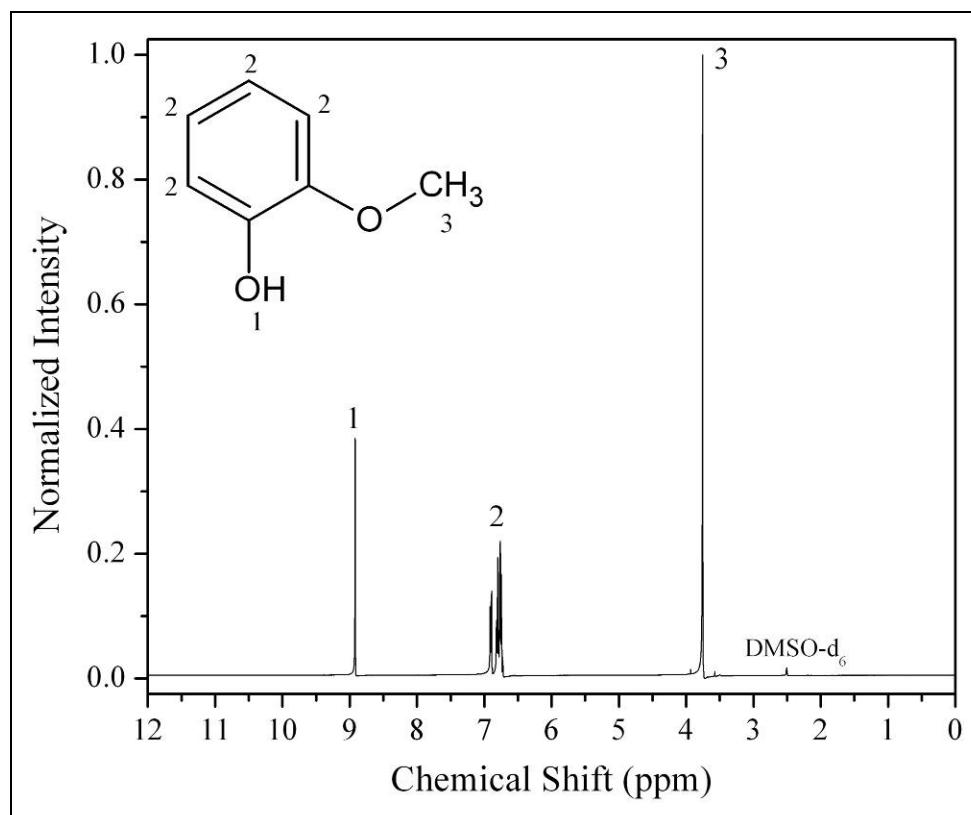
Figure 98. ^{1}H NMR spectrum of guaiacol in DMSO-d$_6$.
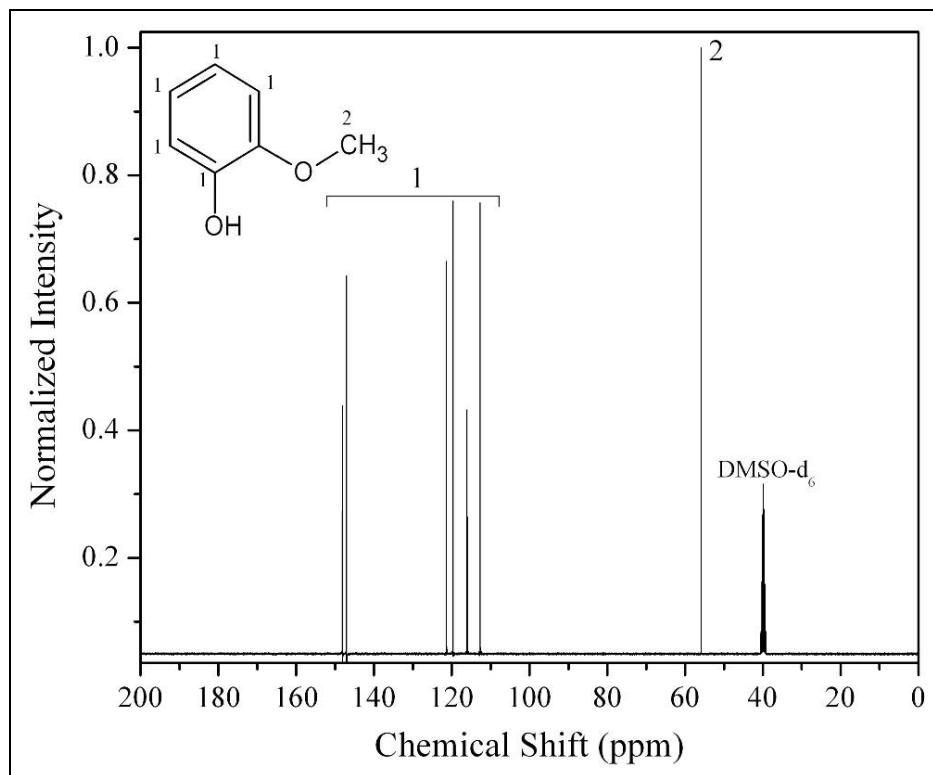
Figure 99. ^{13}C NMR spectrum of guaiacol in DMSO-d$_6$.
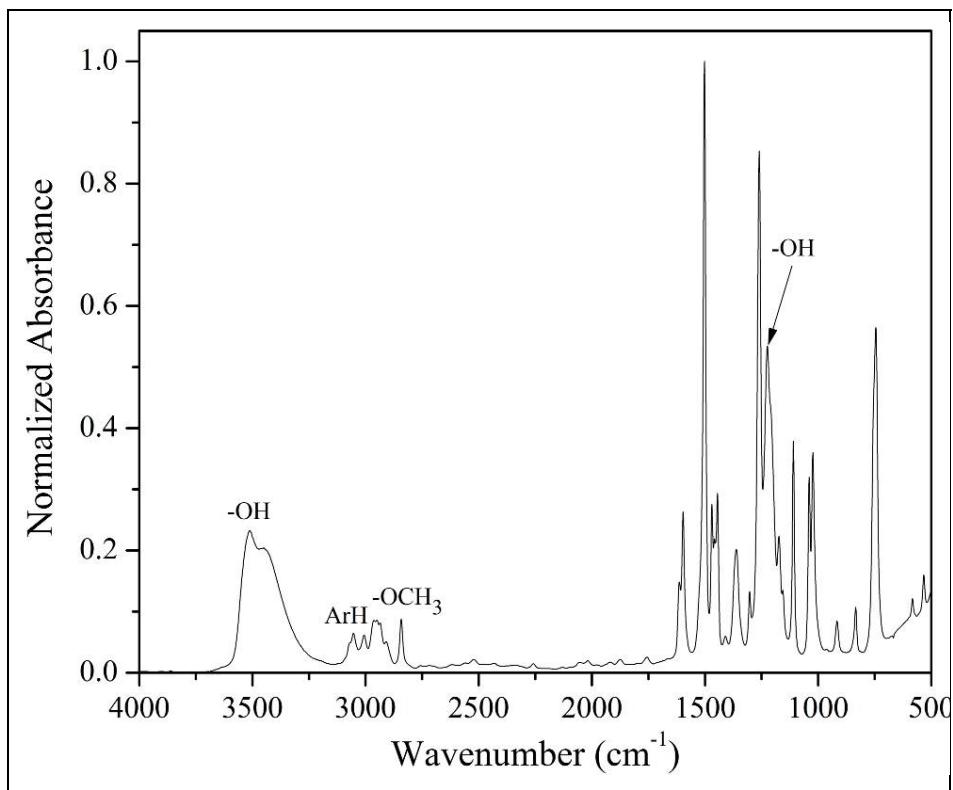
Figure 100. FTIR spectrum of guaiacol.
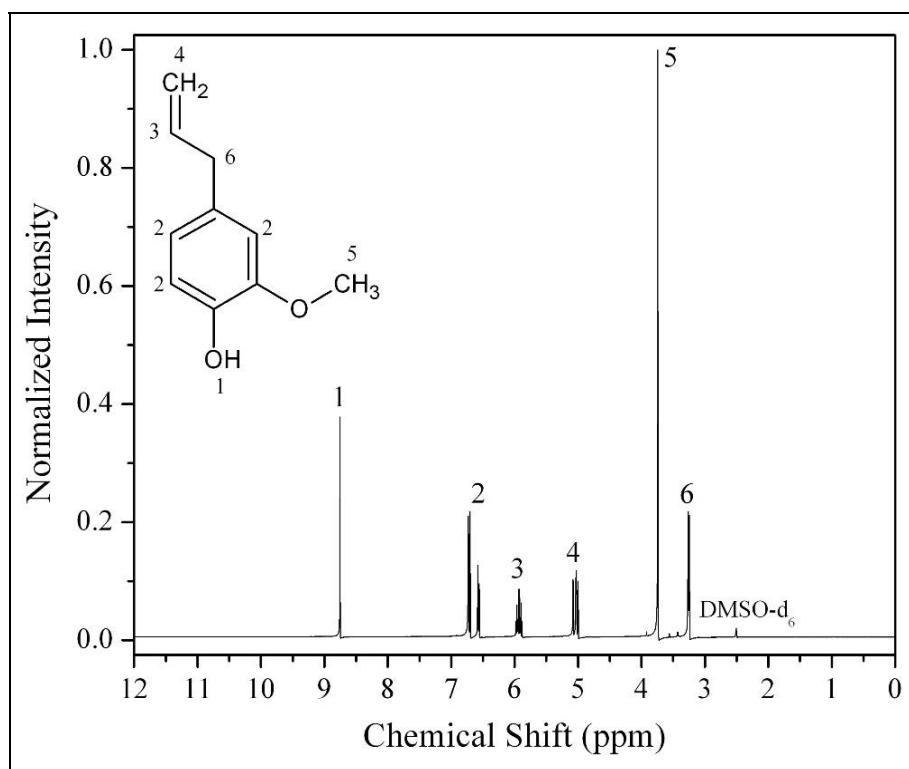
Figure 101. ^{1}H NMR spectrum of eugenol in DMSO-d$_6$.
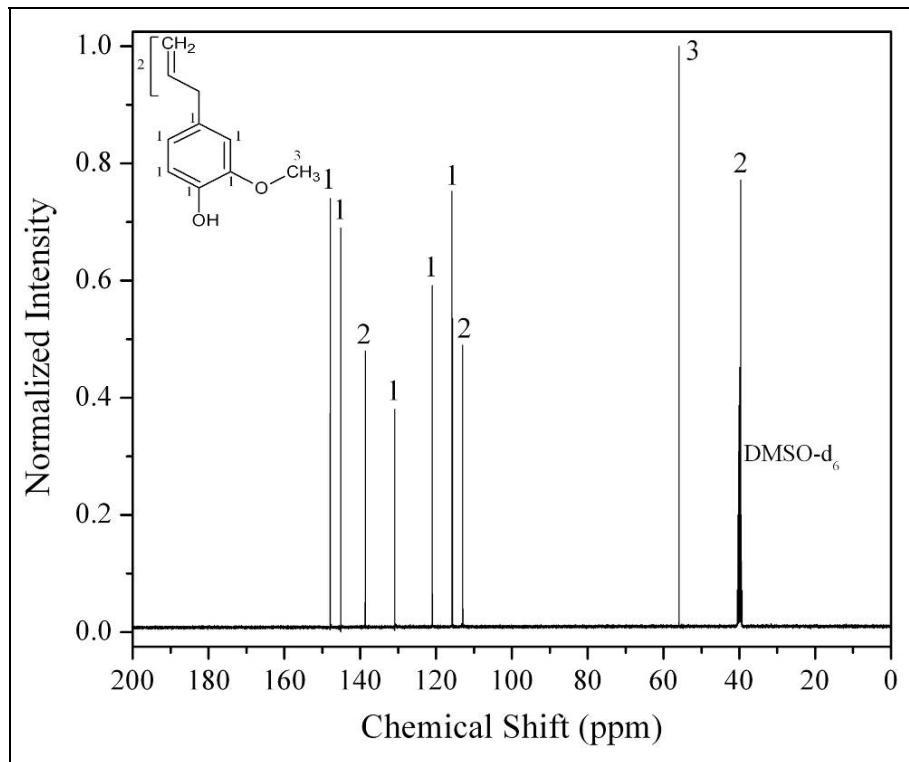
Figure 102. ^{13}C NMR spectrum of eugenol in DMSO-d$_6$.
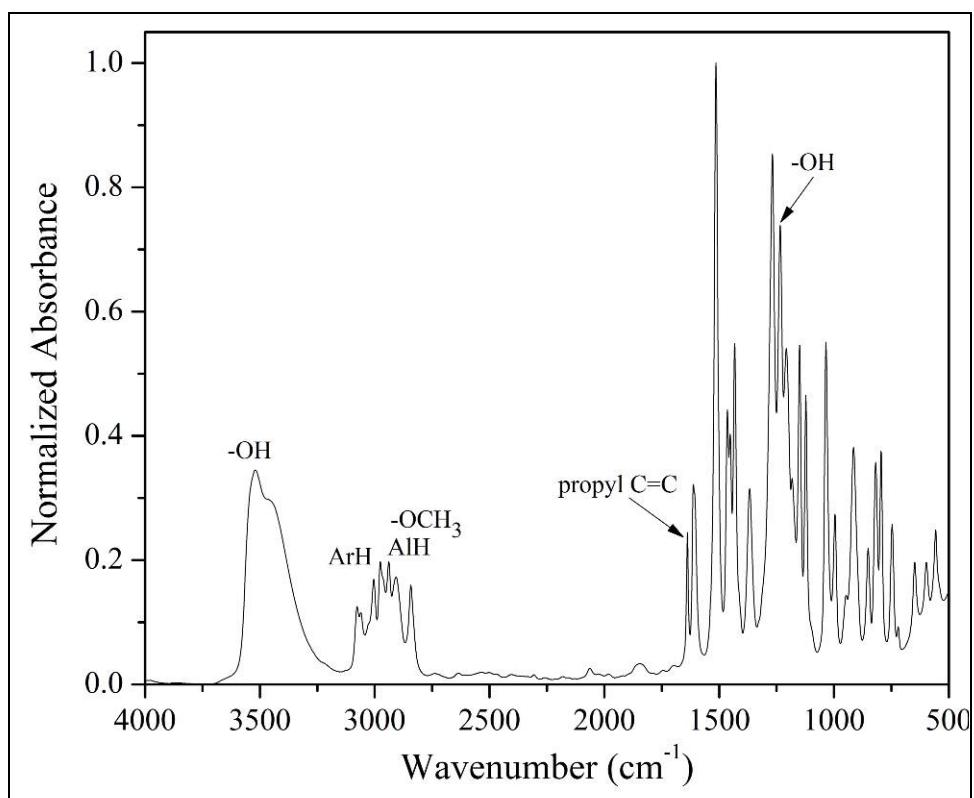
Figure 103. FTIR spectrum of eugenol.

5.5.2   Spectra of Methacrylated Guaiacol and Methacrylated Eugenol
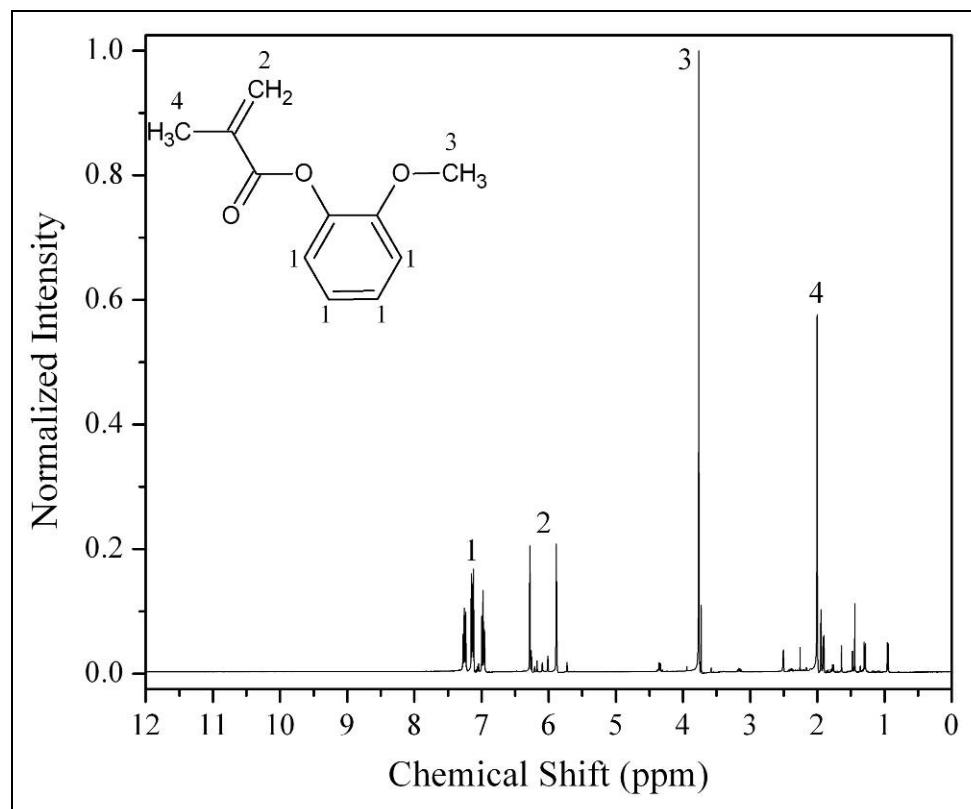
Figure 104. ^{1}H NMR spectrum of MG in DMSO-d$_6$.
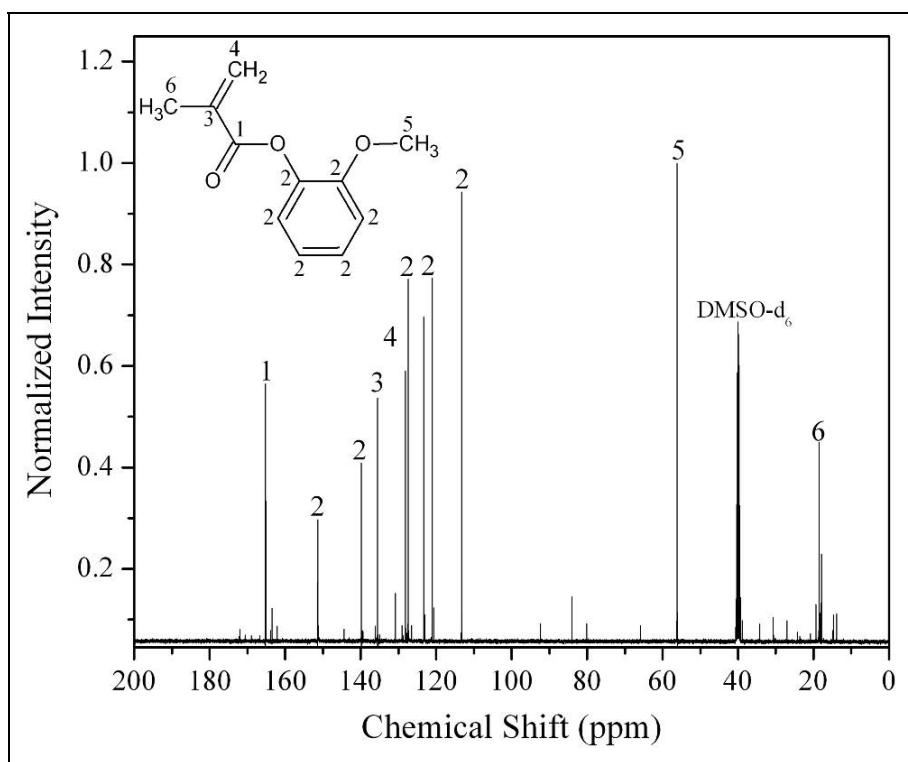
Figure 105. ^{13}C NMR spectrum of MG in DMSO-d$_6$.
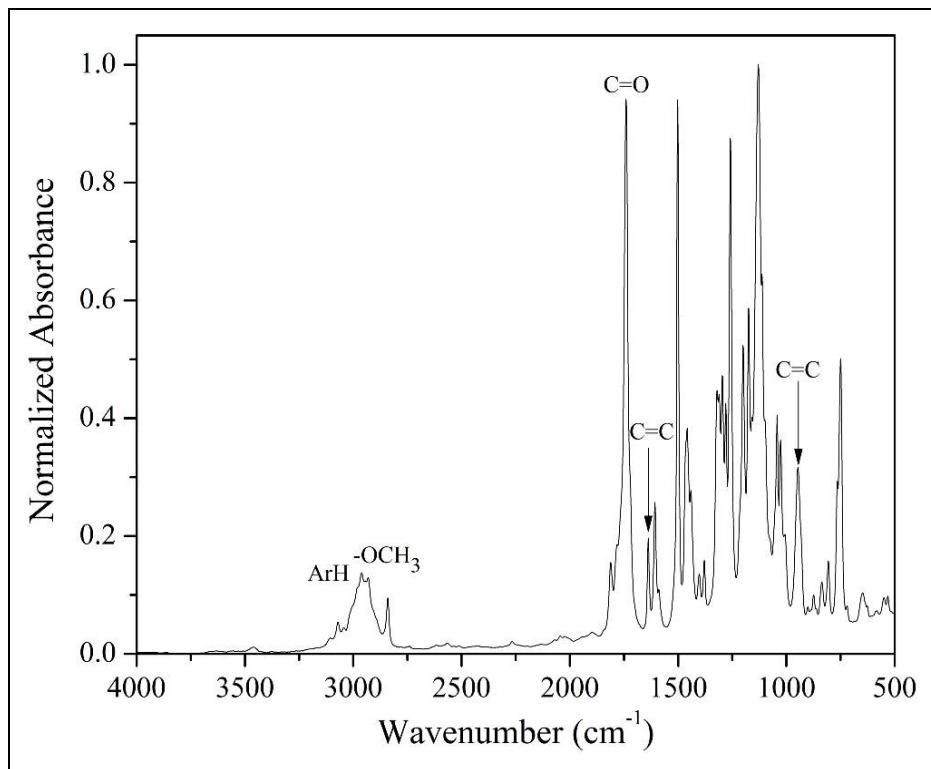
Figure 106. FTIR spectrum of MG.
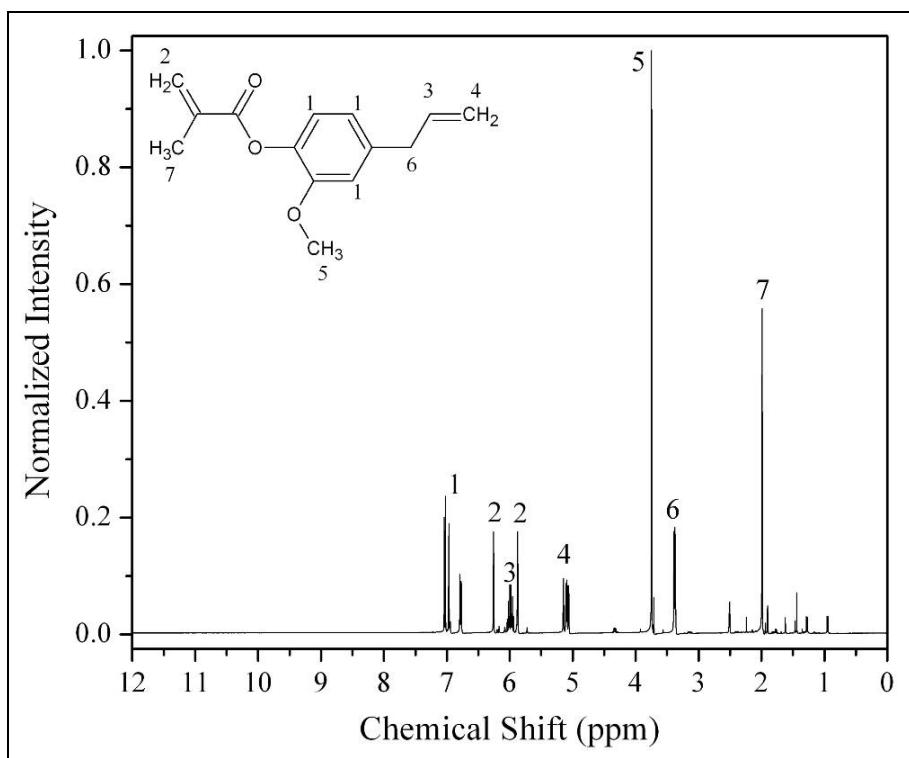
Figure 107. ^{1}H NMR spectrum of methacrylated eugenol in DMSO-d$_6$.
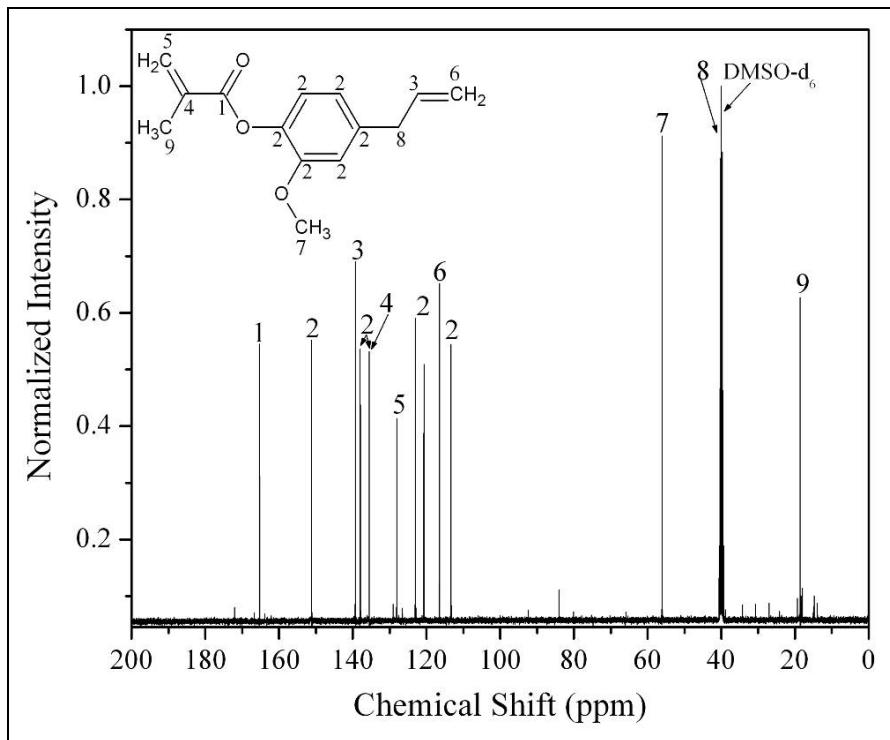
Figure 108. ^{13}C NMR spectrum of methacrylated eugenol in DMSO-d$_6$.

138
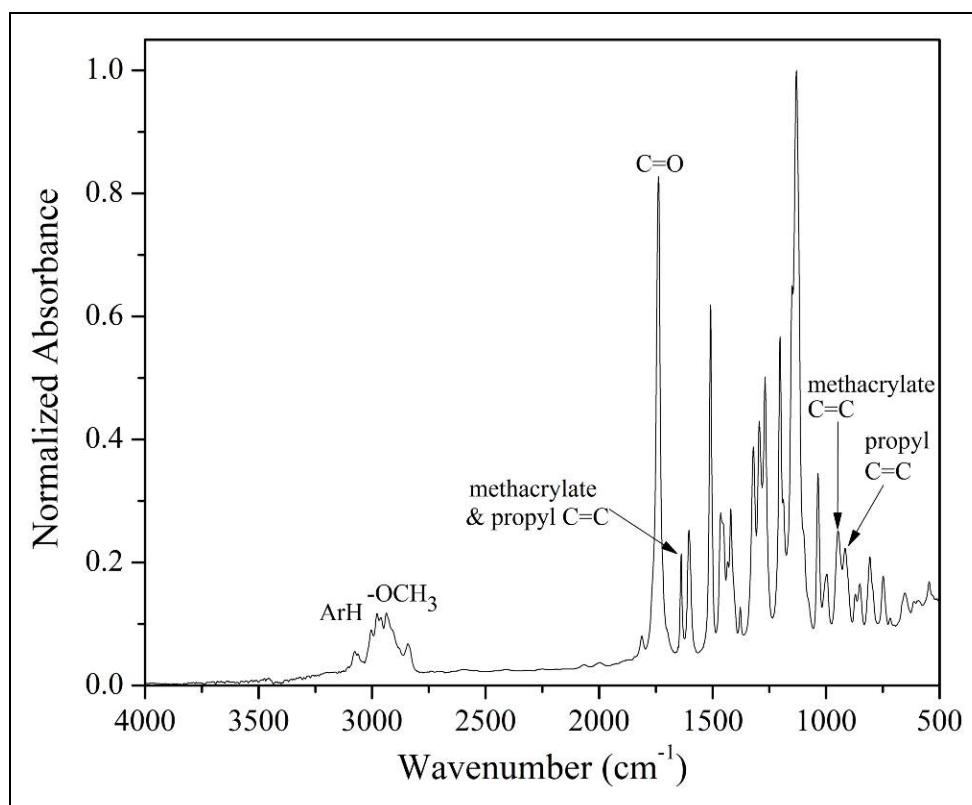
Figure 109. FTIR spectrum of methacrylated eugenol.

5.5.3 DMA Curves

Figures 110–115 show the DMA storage moduli, loss moduli, and tan delta curves of cured VE828 resins that contain styrene, MG, and ME as reactive diluents.
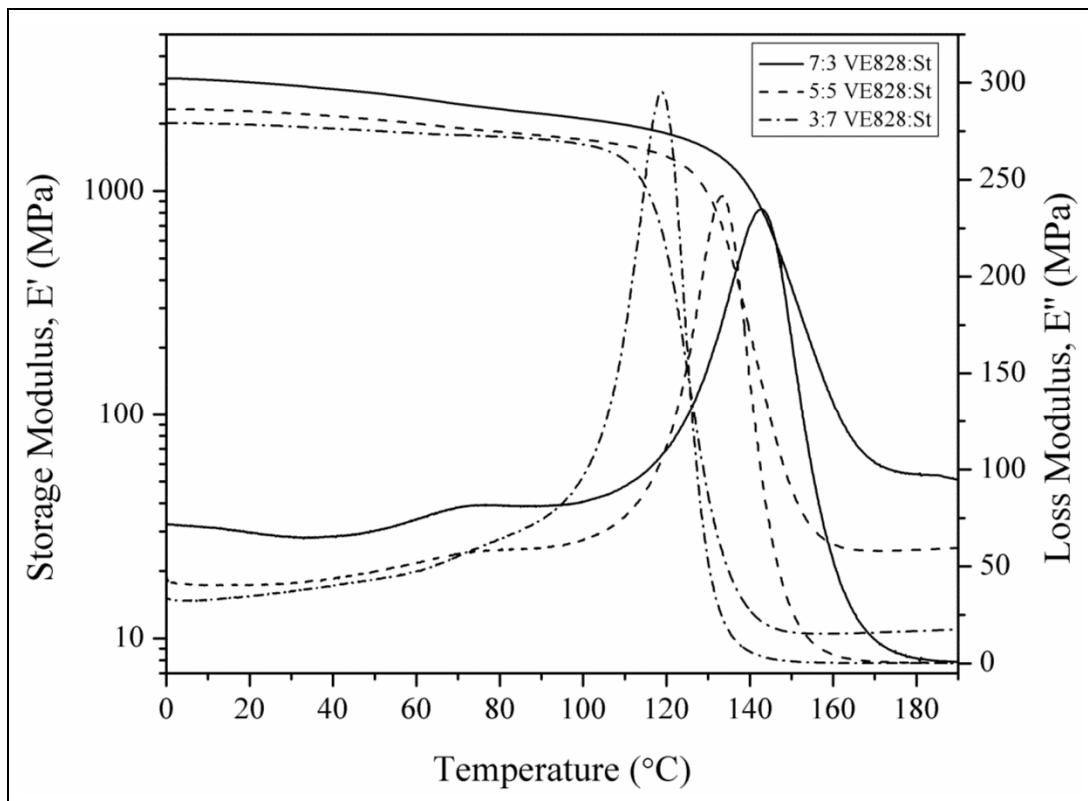
Figure 110. Storage and loss moduli of VE828:St cured resins as a function of temperature.
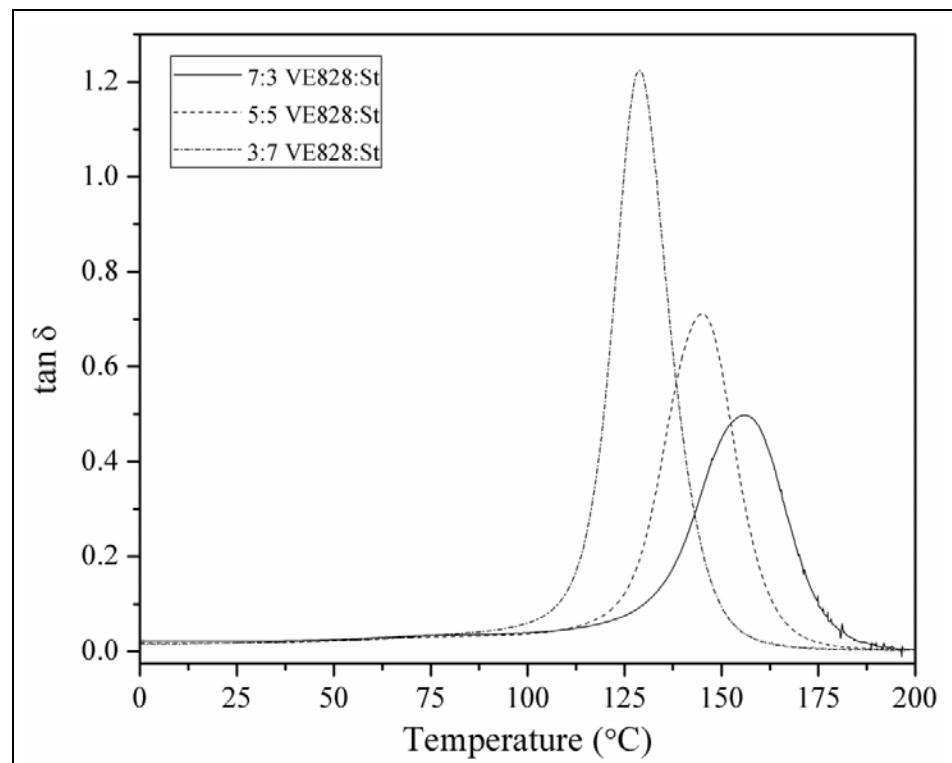
Figure 111. Tan deltas of VE828:St cured resins as a function of temperature.
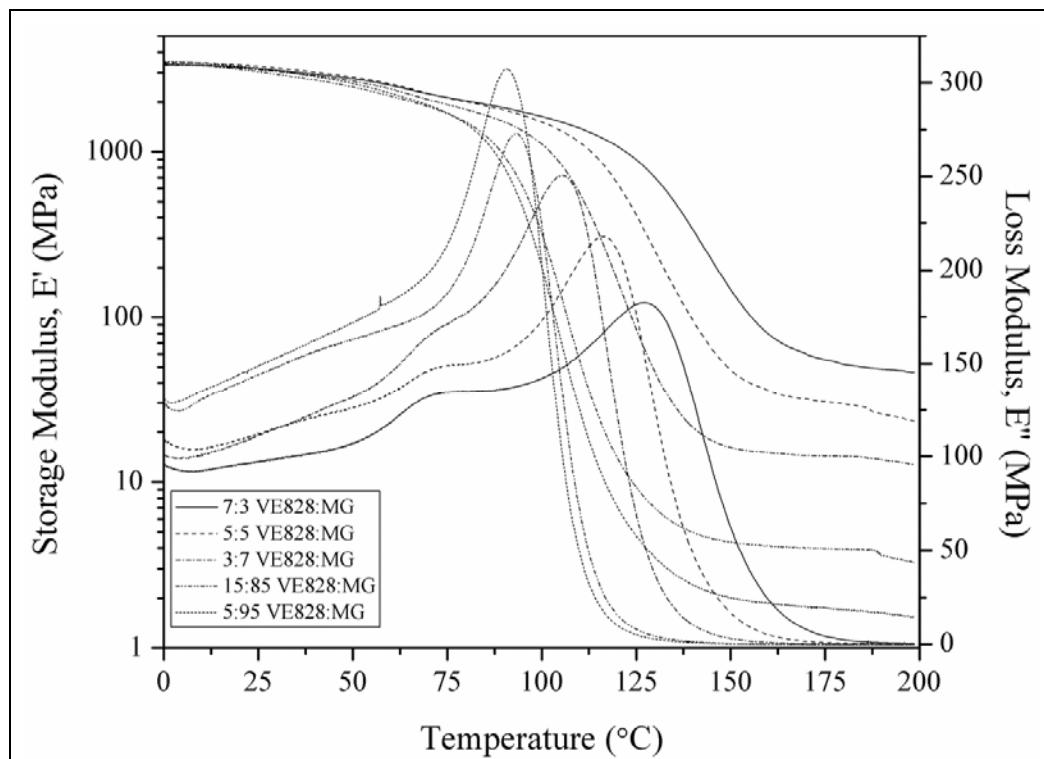
Figure 112. Storage and loss moduli of VE828:MG cured resins as a function of temperature.

141
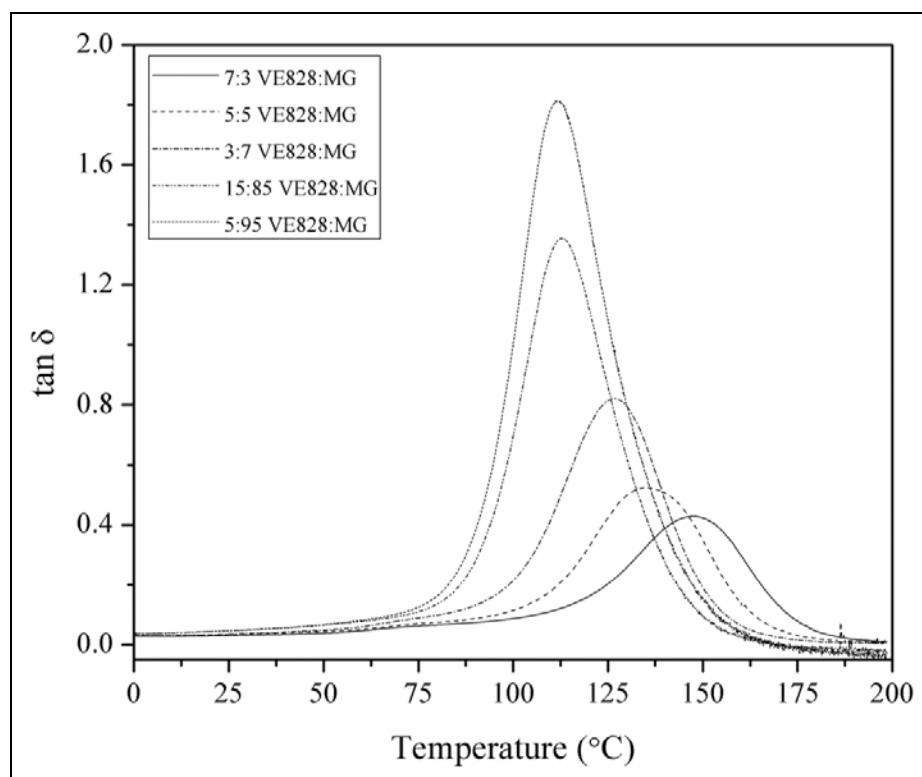
Figure 113. Tan δ of VE828:MG cured resins as a function of temperature.
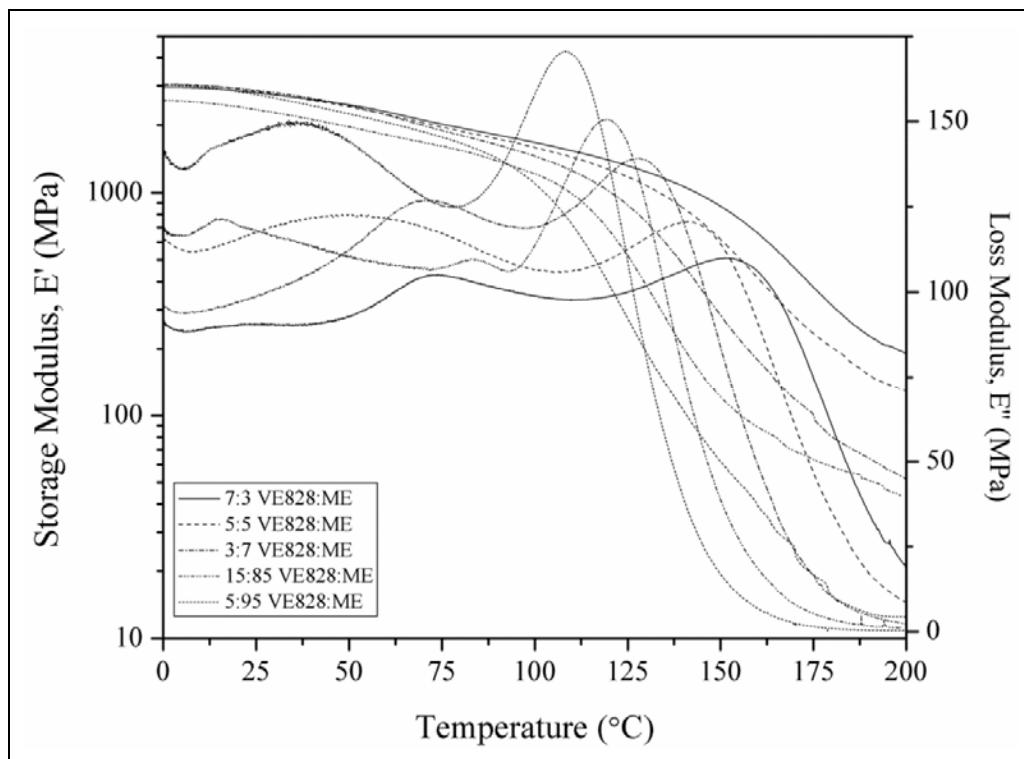
Figure 114. Storage and loss moduli of VE828:ME cured resins as a function of temperature.

142
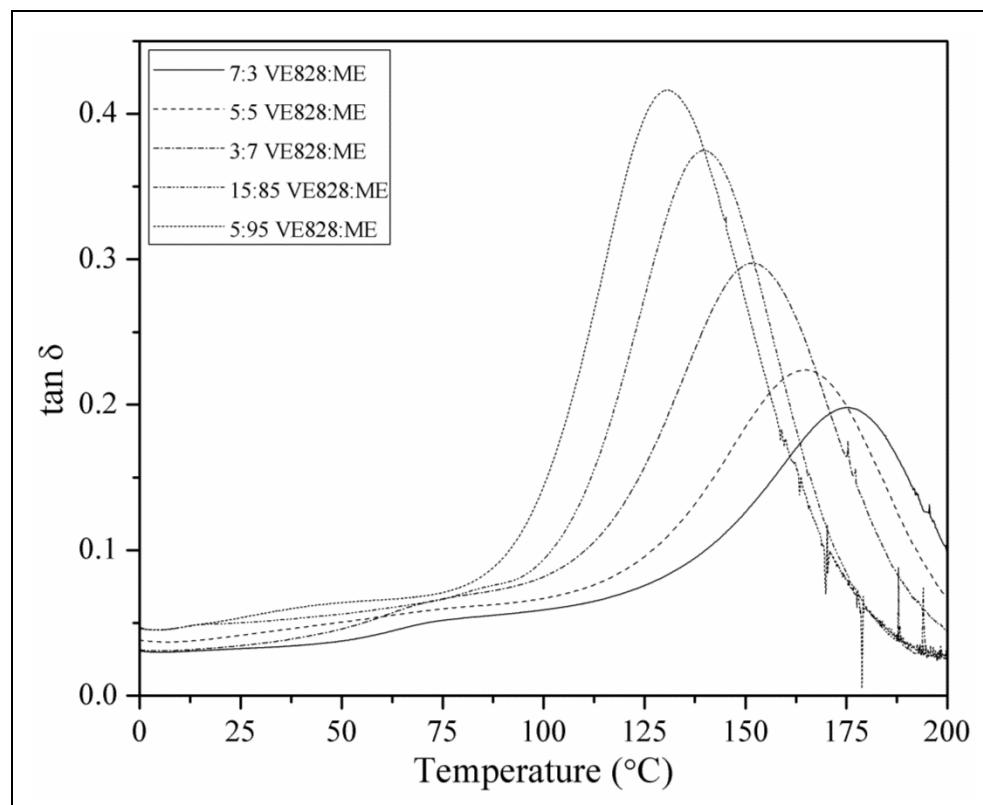
Figure 115. Tan δ of VE828:ME cured resins as a function of temperature.

6. Vanillin-Based Resins Derived From Lignin

6.1 Introduction

Petroleum-based VE resins are used to produce polymer composites for a wide variety of commercial applications because they possess relatively high moduli, strength, and T_g's while maintaining low weight and cost (*1*, *2*). Additionally, commercial VE resins typically contain high concentrations of a reactive diluent, such as styrene, to facilitate the use of liquid molding techniques to fabricate composite parts; however, these reactive diluents are often considered HAPs and/or VOCs (*2*, *3*). With the continued volatility of the petroleum industry and crude oil price fluctuations, the cost of petroleum-based chemicals will eventually become a factor in the production of future resins if suitable renewable biobased replacements are not identified.

Vanillin (figure 116) has been identified as a suitable renewable biobased replacement to use in VE resins mainly because of its aromatic character. The incorporation of aromaticity in cured resins is known to provide structural rigidity (high moduli and strength) and thermal stability (high T_g's) via π-bond stacking. Vanillin is an important aroma compound that is used primarily by flavor and fragrance companies, chocolate and ice cream producers, and pharmaceutical manufacturers (*4*, *5*). Roughly 85% of the world's supply of vanillin is produced synthetically from petrochemical guaiacol and 15% from lignin (*5*). Only 0.2% of the overall vanillin market uses natural vanillin from beans of *Vanilla plantifolia* (*4*). As a flavoring and fragrance ingredient, the current global demand for synthetic vanillin is estimated to be roughly 16,000 ton/year (*5*). Vanillin is a valuable, versatile fine chemical that can be obtained from an economically feasible, future lignocellulosic biorefinery. In order to increase the production of vanillin from current pulp and paper mills, scientists have researched sustainable methods for obtaining vanillin from lignin (*4–9*). Lignin, the second most abundant natural raw material surpassed only by cellulose, is abundantly available, with over 3×10^{11} tons existing in the biosphere, $\sim 2 \times 10^{10}$ tons generated annually, and $\sim 70 \times 10^6$ tons extracted from biomass by the pulp and paper industry annually (*7*, *10*, *11*).
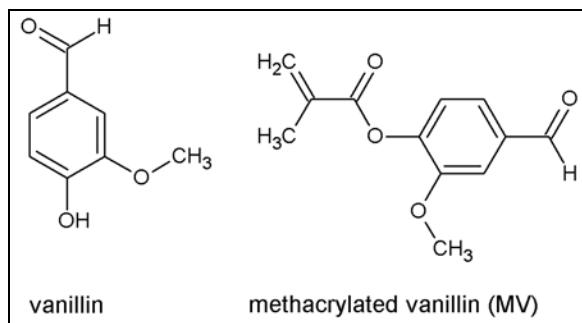
Figure 116. Chemical structures of an LMC, vanillin, and MV.

144

Vanillin and modified vanillin have been successfully incorporated into novel polymeric materials (*3, 12–14*). Recently, Mialon et al. (*12*) have developed a sustainable polyethylene terephthalate mimic that was synthesized from vanillin and acetic anhydride. Additionally, Peng et al. (*13*) cross-linked chitosan microspheres with vanillin for the controlled release of resveratrol. Moreover, Renbutsu et al. (*14*) have synthesized 3-methoxy-4-methacryloyloxybenzaldehyde (methacrylated vanillin, MV, figure 116) via a Steglich esterification of vanillin with MAA in the development of UV-curable palladium-chelating chitosan derivatives. Lastly, in our laboratory, MV has been synthesized via an esterification reaction of vanillin with methacrylic anhydride in the investigation of methacrylated LMCs as potential styrene replacements in liquid molding VE resins (*3*). However, MV was not pursued as a viable reactive diluent because it is a solid at room temperature.

In the work herein, we present an alternative vanillin-based VE resin for use in commercial polymer composite applications. Also described is a green conscientious two-part reaction scheme to generate a VE resin consisting of a 1:1 mole ratio of a monofunctional monomer (MV) and a cross-linking agent (glycerol dimethacrylate, GDM) (figure 117) along with resin properties, polymerization, cure kinetics, and polymer properties.
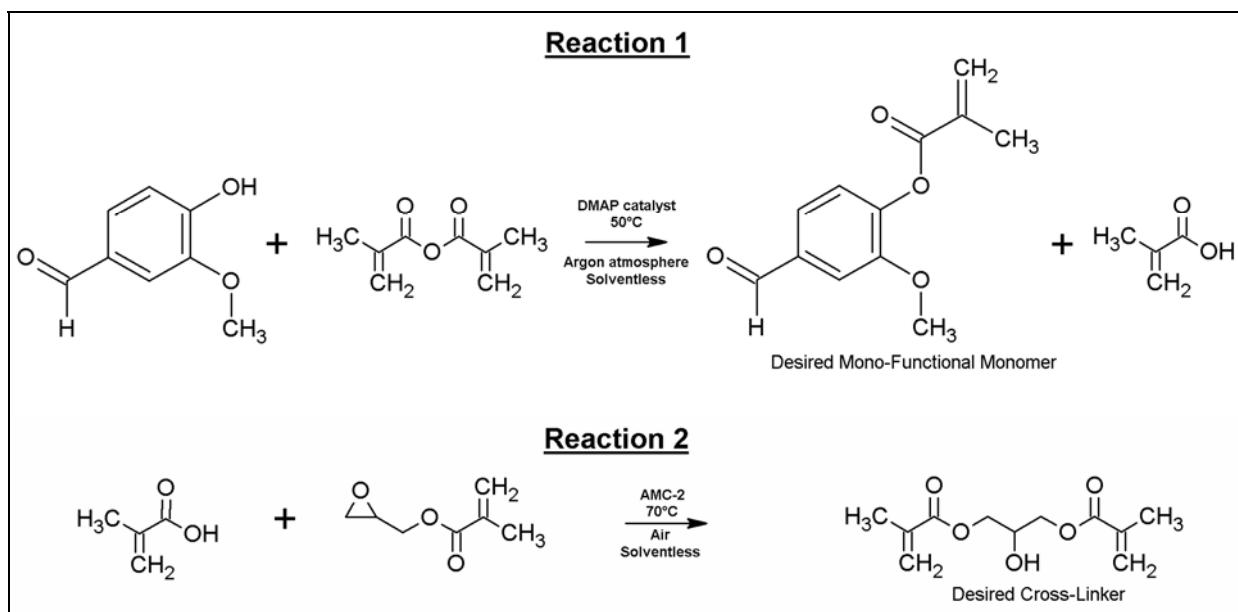
Figure 117. Two-part reaction scheme to produce a resin that contains a 1:1 mole ratio of MV (desired mono-functional monomer of reaction 1) and GDM (desired cross-linker of reaction 2). The MAA produced in reaction 1 is consumed in reaction 2.

6.2 Experimental

6.2.1 Materials

All reagents, 0.75-mL ampoules of dimethyl sulfoxide (DMSO-d$_6$), tetrahydrofuran (THF) (Optima, submicron filtered), DMAP, phenolphthalein (99+%), and vanillin (99%) were

obtained from Fischer Scientific and used as received. Methacrylic anhydride (94%, inhibited with 2000-ppm Topanol A), and glycidyl methacrylate ($\geq$97%, stabilized with ~ 0.0005% hydroquinone monomethyl ether [Mequinol, MEHQ]) were purchased from Sigma Aldrich and used as received. Compressed argon was obtained from Keen Compressed Gas Co. (99.998%). AMC-2, which is a mixture of 50% trivalent organic chromium complexes and 50% phthalate esters, was purchased from AMPAC Fine Chemicals (Rancho Cordova, CA) and used as received. Trigonox 239 (AkzoNobel Polymer Chemicals), containing 45% cumene hydroperoxide, was purchased and used as a free radical initiator.

6.2.2 Synthesis of Vanillin-Based Resin

The two-step, one-pot reaction scheme for production of this resin is shown in figure 117 and described in the following sections.

6.2.2.1 Reaction 1. A catalytic amount of DMAP (2 mol% of methacrylic anhydride) was added to vanillin (10 g) and placed in a 100-mL round bottom flask equipped with a magnetic stir bar. Prior to adding 1.01 vanillin equivalents of methacrylic anhydride to the flask, the flask was sealed and subsequently purged with argon gas for an hour to remove moisture and oxygen from the reaction vessel. For the first 15 min with stirring, the reaction progressed at room temperature, after which the flask was placed in a 50 °C silicon oil bath for a minimum of 24 h. After confirming that the reaction went to near completion via ^{1}H NMR, we cooled the reaction flask to room temperature.

6.2.2.2 Reaction 2. At room temperature, 1.01 MAA equivalents (assuming 100% theoretical conversion of methacrylic anhydride to MAA) of glycidyl methacrylate (GM) and AMC-2 (0.1 wt% of GM and MAA) were added to the reaction flask. After stirring vigorously at room temperature for 10 min, we placed the reaction flask in a 70 °C silicon oil bath. Reaction was followed by acid number titration and allowed to progress until an acid number of 10 or less, corresponding to ~3% free acid, was achieved. The acid number titration method described in La Scala et al. (*1*) was performed with success.

6.2.3 Resin Characterization

The methacrylated vanillin–glycerol dimethacrylate (MVGDM) resin was characterized using ^{1}H NMR (400.13 MHz, 16 scans at 298.2 K) on a Bruker AV-400 spectrometer. Additionally, MVGDM was characterized using FTIR spectroscopy performed on a PerkinElmer Spectrum 400 FT-IR/FT-NIR Spectrometer. At room temperature, 32 cumulative scans were acquired with a resolution of 2 cm^{-1} in transmission mode in the mid-IR range.

SEC was performed on the resin to determine if extensive methacrylation and/or epoxy homopolymerization occurred. A Viscotek 270max – Modular Advanced GPC/SEC System fitted with Waters Styragel HR1 and HR4 columns in series was used, operated with THF (1 mL/min) as the mobile phase, and calibrated with polystyrene standards. Samples were

146

prepared by dissolving 2 mg of resin in 1 mL of THF. Refractive index data were used to determine the occurrence of extensive methacrylation and/or epoxy homopolymerization.

Resin viscosity was obtained on a TA Instruments ARES-G2 rheometer. Measurements were performed isothermally at 25 °C controlled by a Peltier plate (+/– 0.1°C error). A 20-mm 1° steel cone with a truncation gap of 25 µm and a minimum sample volume of 0.04 mL was utilized. The shear rate was increased step-wise from 1 to 100 s^{-1} collecting 21 data points to observe any non-Newtonian behavior. At a given shear rate, the shear stress was measured every 2 s. The shear rate and viscosity were recorded when the shear rate stabilized to within 5% tolerance for three consecutive points. Resin was measured three times, and the viscosities at 50 s^{-1} were averaged and reported.

6.2.4 Resin Curing

Free-radically cured MVGDM resin was prepared via bulk polymerization by adding 1.5 wt% Trigonox 239 to the monomer with curing at 90 °C for 4 h and subsequent postcuring at 130 °C for 2 h. Polymerization was conducted in an argon atmosphere, whereby argon gas was purged through the oven for ~15 min at the beginning of cure.

6.2.5 Cure Kinetics

In order to determine the overall extent of polymerization of the cured resin, cure kinetics studies were performed on a PerkinElmer Spotlight 400 FTIR Microscope with a heating stage designed to hold 13-mm-diameter salt discs (heating stage controlled by a BriskONE Single-Zone Digital PID Thermocouple Temperature Controller with accuracy of ±0.25% of reading). At 70 °C for 4 h and 130 °C for 2 h, 32 cumulative scans were acquired with a resolution of 2 cm^{-1} in transmission mode in the mid-IR range, with spectrum taken roughly every 1.1 min. A drop of resin with 1.5 wt% Trigonox 239 as the free radical initiator was sandwiched between two 13-mm-diameter NaCl discs (the bottom NaCl disc was 2 mm thick while the top was 1 mm thick) prior to placement into the heating stage.

The fractional conversion of monomer carbon-carbon double bonds (C=C) to polymer carbon-carbon single bonds (-C-C-), α, was calculated by measuring the absorbance intensity of a peak (i.e., a group that is affected by the reaction) relative to an internal standard (i.e., a group that is not affected by the reaction) (equation 2) (*2*):

$$\alpha = 1 - \left(\frac{ABS(t)_{947cm^{-1}}}{ABS(t=0)_{947cm^{-1}}} \right)\left(\frac{ABS(t=0)_{3510cm^{-1}}}{ABS(t)_{3510cm^{-1}}} \right). \qquad (2)$$

In the MVGDM resin, both MV and GDM contain methacrylate groups that appear at 947 cm^{-1}, specifically corresponding to the out-of-plane bending of C-H bonds in the vinyl group (*2, 15*). Since the decrease in absorbance intensity can result from not only polymerization but also physical changes, such as changes in sample film thickness and/or component evaporation, the

vinyl group conversion was calculated by measuring the peak absorbance intensity relative to the peak absorbance intensity of the hydroxyl stretch of GDM at 3510 cm^{-1} (*16*). The conversion as a function of time data was fitted to an empirical autocatalytic kinetic model in order to determine the reaction rate constant, *k*, and reaction order, *m* (*17*).

6.2.6 Polymer Properties

Thermogravimetric behavior of the MVGDM cured resin was measured using a TA Instruments Q500 TGA. Approximately 10 mg of sample was placed in a platinum pan and heated to 650 °C at 10 °C/min in a N$_2$ atmosphere (40 mL/min balance gas flow rate and 60 mL/min sample gas flow rate).

Thermomechanical properties of the MVGDM polymer were measured using DMA. Rectangular samples with approximate dimensions of $35 \times 12 \times 3$ mm^3 were tested using a TA Instruments Q800 DMA in single cantilever geometry. The samples were tested at 1 Hz with a deflection of 7.5 μm while ramping the temperature from –50 to 250 °C at a rate of 2 °C/min. The point at which the modulus in the rubbery plateau began to increase with increasing temperature was used to calculate the molecular weight between cross-links, M$_C$. M$_C$ was estimated using the theory of rubber elasticity and the polymer density (measured using Archimedes' principle) (*2*, *18*, *19*).

6.3   Results and Discussion of Vanillin-Based Thermosetting Resin Properties

6.3.1 Resin Characterization

The two-step reaction mechanism shown in figure 117 possesses many green chemistry and engineering characteristics, including the following:

- Uses a renewable, lignin-derived chemical vanillin.

- Uses potential renewable reactants methacrylic anhydride and glycidyl methacrylate.

- Produces no by-products (MAA, the by-product of the first reaction, is consumed in the second reaction).

- Utilizes neat chemical reactions that produces the desired product with potentially 100% atomic efficiency.

- Requires relatively small quantities of catalysts.

- Requires relatively low reaction temperatures.

MAA, which can be condensed to produce methacrylic anhydride, is currently produced via ethylene, propylene, isobutylene, and isobutane routes of which ethylene can be derived from bioethanol; propylene can be derived from bioethanol, biobutanol, and glycerol; isobutylene can be derived from bioisobutanol; and isobutane can be derived from catalytic cracking of biomass (*20–22*). Additionally, gasification of biomass to syngas with subsequent conversion of syngas

148

to alcohols and then to olefins is another attractive pathway (*20*). Moreover, glycidyl methacrylate is currently synthesized using epichlorohydrin and MAA of which epichlorohydrin can be produced via glycerol chlorination routes (*23*). Therefore, the MVGDM resin has the potential to be 100% biobased.

Despite the first reaction being a substitution reaction that generates stiochiometric amounts of waste, the overall two-step reaction scheme generates no waste with a 100% mass efficiency due to the second reaction being an addition reaction which utilizes the by-product MAA from the first reaction in order to synthesis the desired cross-linking agent GDM. Interesting to note, glycerol dimethacrylate has been reported in the literature to be biocompatible (*24*). The final product mixture is a ready-to-use resin that consists of a 1:1 mole ratio of a monofunctional monomer, MV, and a cross-linker, glycerol dimethacrylate. The third reaction required to produce the thermoset is polymerization. Polymerization requires a small quantity of initiator, moderate curing temperatures, and an inert atmosphere while generating no waste.

After the two-step reaction, MVGDM resin exhibited no epoxy homopolymerization (confirmed by GPC), possessed an acid number of 9.00 ± 0.01, indicating that less than 3% free acid remains, and a viscosity of 87.25 ± 0.5 cP at 25 °C—a viscosity that is slightly lower than the recommended lower limit for effective liquid molding applications but, nevertheless, a viscosity that is workable (*10*). ^{1}H NMR spectrum of the MVGDM (figure 118, top) possessed peaks indicative of MV (3-methoxy-4-methacryloyloxybenzaldehyde, 220.21 g/mol) and glycerol dimethacrylate (2-hydroxy-1,3-propanediyl bismethacrylate, 228.23 g/mol). Additionally, a peak at 907 cm^{-1} indicative of epoxy group vibrations was not present in the FTIR spectrum of the MVGDM resin (figure 118, bottom), indicating a complete conversion of glycidyl methacrylate to glycerol dimethacrylate (*25*). The resin is a transparent liquid with a brownish-green hue. The resin smell was a combination of methacrylates and vanilla.
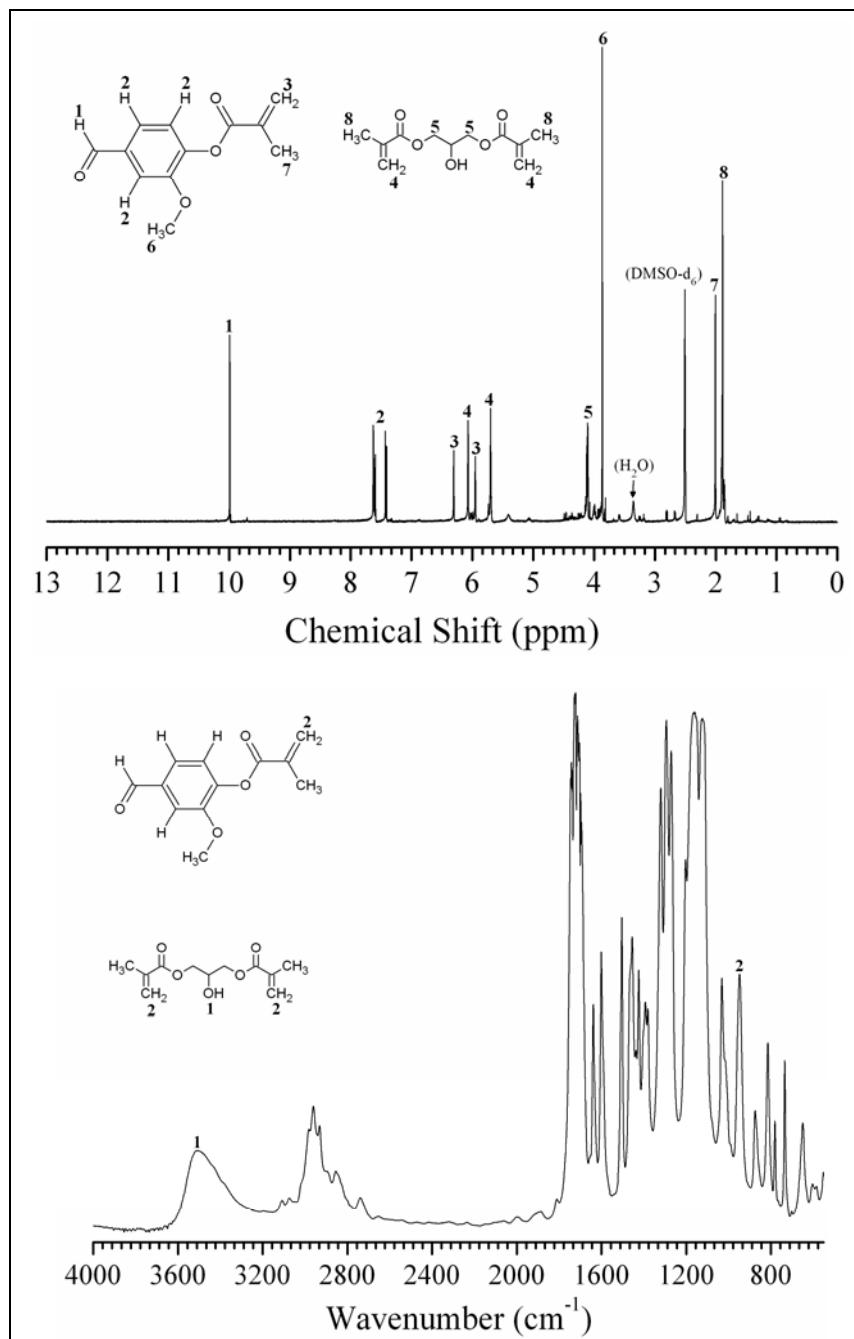
Figure 118. ^{1}H NMR spectrum (top) of the MVGDM resin with proton assignments. FTIR spectrum (bottom) of the MVGDM resin with two notable peaks assigned, specifically, the hydroxyl stretch (1) and C-H vinyl group bending (2).

6.3.2 Cure Kinetics

Free-radical curing of thermosetting resins generally follow three polymerization stages: initiation, propagation, and termination. Initiation begins via thermal decomposition of a peroxide initiator followed by the formation of monomer radicals. In curing of the MVGDM resin, Trigonox 239, which contains 45% cumene hydroperoxide, was used as the peroxide. The formed monomer radicals provide active sites for polymer chain growth. During chain propagation, the polymerization initially accelerates because of the Tromsdorff Effect (*16*). In the latter chain propagation stages, the polymerization rate decreases rapidly because of large molecule mobility limitations as the vitrified cross-linked network formation leads to entrapment of unreacted species in a cross-linked polymer matrix and results in a less than unity final fractional conversion (*16*).

Typical FTIR spectral behavior in the region of interest is shown in figure 119, where the normalized intensity is plotted as a function of wave number, from 1350 to 700 cm^{-1}, and as a function of time. As can be seen in figure 119, the 947 cm^{-1} peak associated with the out-of-plane bending of C-H bonds in vinyl groups decreases with increasing time (*15*, *16*). Furthermore, the appearance of a left shoulder increases with increasing time. Brill and Palmese (*16*) have shown that the 947 cm^{-1} includes contributions from underlying peaks of absorbances associated with the monomers and the cure reaction products. Upon deconvolution, the 947 cm^{-1} peak was a combination of three absorbances with the out-of-plane bending of C-H bonds in vinyl groups being the prominent peak (*16*). This fact, which results in a slight difference between the fitted and unfitted prominent peak height, corresponded to an underestimation of the final fractional conversion of double bonds of about 5%. The shoulder that increasingly appears with increasing cure time at 954 cm^{-1} is believed to be from the backbone mode of GDM (*16*).
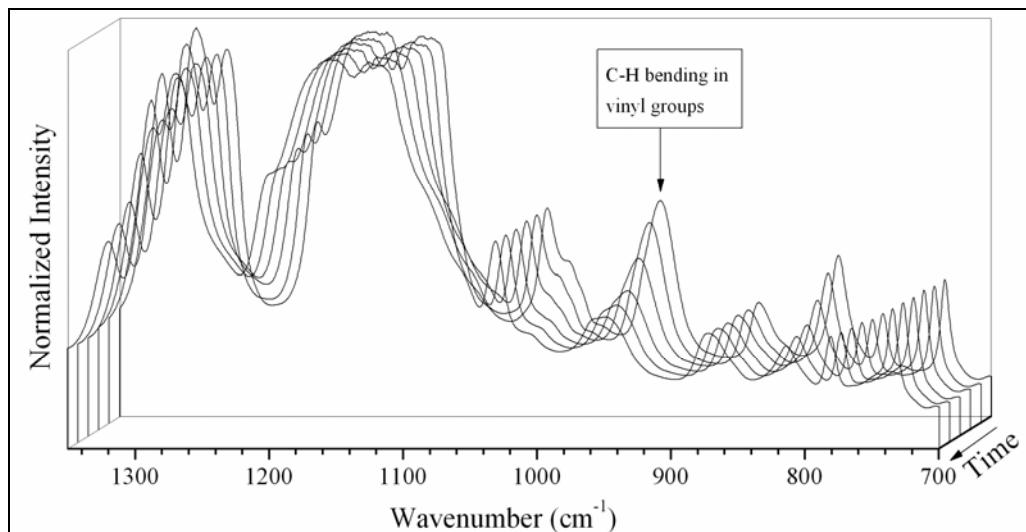
Figure 119. FTIR spectra of the MVGDM during curing as a function of reaction time at 70 °C. The height of the C-H bending in vinyl groups peak (947 cm^{-1}) was used to monitor and calculate monomer conversion to polymer. The height of the OH stretching peak (3510 cm^{-1}) (not shown) was used as an internal reference.

151

Equation 2 was used to calculate the fractional conversion of C=C to -C-C-, α, for the MVGDM resin as a function of time, shown in figure 120. In general, the polymerization reaction follows typical behavior associated with free-radical curing, including the presence of an initial inhibition period and a period of accelerated propagation that is followed by a reduction in cure rate due to vitrification. After a 70 °C cure for 4 h, a fractional conversion of 0.66 ± 0.06 was achieved (figure 120). The fractional conversion increased to 0.78 upon subsequent postcuring at 130 °C for 2 h (data not shown). Since the fractional conversions were calculated using unfitted peaks, the reported values, based on the work of Brill and Palmese (*16*), could be underestimated by about 5%. Prior to postcuring, the 66% conversion is in agreement with reported conversions of similar VE resins that contain methacrylate groups (*2*). The seemingly low conversion is partially attributed to the inherent low reactivity of methacrylate groups with themselves (*2*). In addition, because of the chemical structure differences between MV and GDM, particularly the aromaticity of MV and the hydroxylated alkyl backbone of GDM, there is potential for micron or submicron domain formations, which can affect reactivity and ultimately the extent of cure (*15*). Moreover, the polymerization rate may have decreased early and rapidly because of entrapment of unreacted species. This may have been a result of GDM having a relatively low molecular weight (228.23 g/mol) and having the potential to hydrogen bond with carbonyl groups present on MV and other GDM molecules, which are both factors that can lead to a high cross-link density and mobility limitations.

Since the polymerization followed the typical behavior associated with free-radical curing, the empirical autocatalytic kinetic model was able to fit the experimental data with a sum of the squares error of 5.0×10^{-5} (figure 120). A reaction order, $m = 0.63$, and a reaction rate constant, $k = 0.175$, were obtained from the kinetic model and are similar to values reported in the literature for the curing of VE resins (*16*).
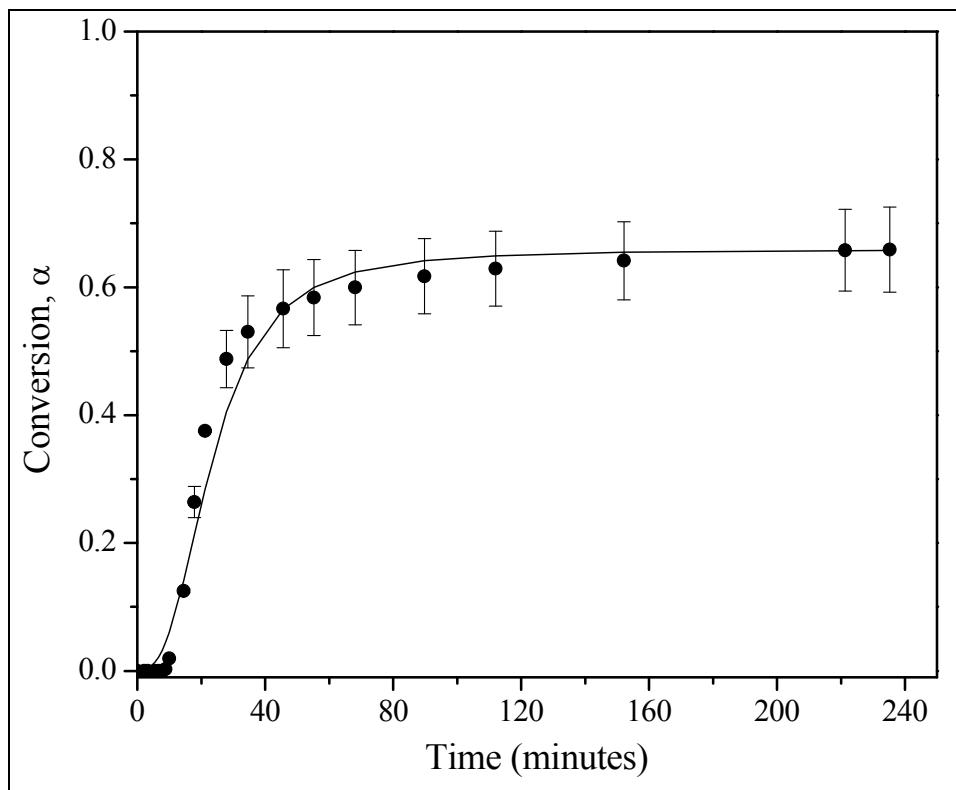
Figure 120. The conversion as a function of time for the cure of MVGDM resin.
Samples were cured at 70 °C for 4 h and then postcured at 130 °C for 2 h.
Autocatalytic kinetic model fit is shown as the solid, black line.

6.3.3 Polymer Properties

After the resin was cured with 1.5 wt% Trigonox 239, it became a transparent, hard polymer that still possessed a weak hint of vanilla. In order to elucidate the thermogravimetric behavior and thermomechanical properties of the polymer, TGA and DMA experiments, respectively, were performed. Figure 121 shows the TGA thermogram and the derivative of the thermogram of the MVGDM polymer. From the TGA data, thermal stability factors, including the initial decomposition temperature, IDT, the temperature of 50% weight loss, $T_{50\%}$, the temperature of maximum decomposition rate, T_{max} (tallest peak of the derivative thermogram), and the decomposition activation energy, E_D, were determined and are presented in table 14. E_D was calculated using the Horowitz and Metzger integral method (*26, 27*). The results show that the MVGDM polymer is thermally stable up to about 244 °C (the IDT) with $T_{max} = 426$ °C. In addition, the MVGDM cured resin exhibited a two-stage thermal decomposition (first stage between 200 and 330.5 °C and the second stage between 330.5 and 650 °C) (figure 121). This two-stage behavior was also observed by Zulfiqar and Zulfiqar (*28*) in thermograms of poly(phenyl methacrylate). According to Zulfiqar and Zulfiqar (*28*), the first stage is believed to be depolymerization initiated at unsaturated chain ends, and the second stage is depolymerization by random scission. Evaporation of unreacted monomer may also be occurring as evidenced by this first peak in the derivative curve.

153
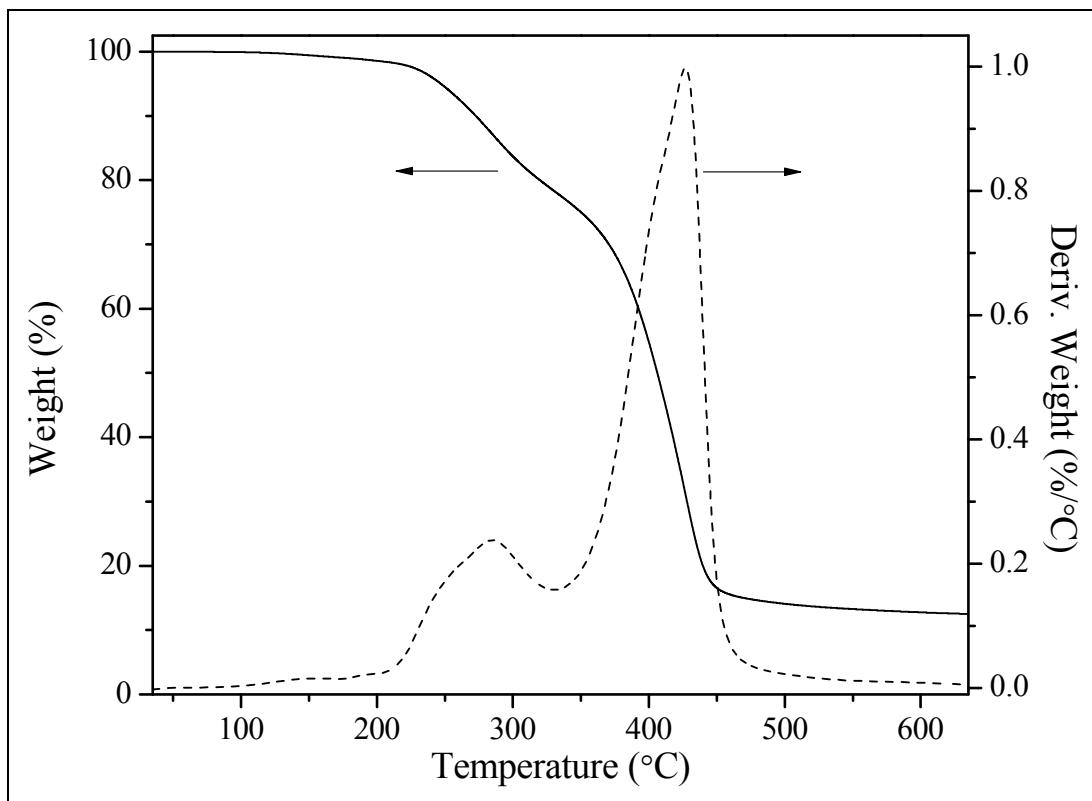
Figure 121. TGA weight (left *y*-axis) and the derivative of the weight (right *y*-axis) as a function of temperature for MVGDM cured resin.

Table 14. Thermogravimetric and thermomechanical properties as well as the density of the MVGDM cured resin.

IDT	244 ± 3.6 °C
$T_{50\%}$	405 ± 0.4 °C
T_{max}	426 ± 1.4 °C
E_D	110.9 kJ/mol
E′ at 25 °C	3.6 ± 0.3 GPa
E′ at 237.5 °C	17.4 ± 0.5 MPa
ρ at 25 °C	1.284 ± 0.002 g/cm^3
M_C	825 ± 26 g/mol

decomposition stage. Referring to figure 121, at 330.5 °C, which is the temperature where the second derivative of the TGA thermogram is equal to zero, indicating the transition from the first thermal decomposition stage to the second, 78% ± 0.06% of the polymer remains. This result is in agreement with the FTIR cure study result of reaching 78% conversion of monomer C=C to polymer -C-C- after postcuring. The 22% of unreacted C=C is most likely a combination of unreacted MV and partially reacted GDM where one end is connected to the polymer network and the other remains as an unsaturated chain end. Therefore, the first thermal decomposition stage is most likely due to a combination of unreacted MV evaporation and depolymerization initiated at GDM unsaturated chain ends. Because of the abundance of methacrylate groups, anhydride ring formation may also occur during thermal treatment, which, in turn, interferes with polymer chains unzipping to monomers causing appreciable charring (12.61 ± 0.04 °C char content at 625 °C) (*28*).

Thermomechanical properties were measured using DMA and are shown in figure 122. In this figure, the storage modulus (E') and tan δ are plotted as a function of temperature. The stiffness of a viscoelastic material is represented by E' and is proportional to the energy stored during a loading cycle (*29*). E' at 25 °C was measured to be 3.6 ± 0.3 GPa (table 14), which is comparable to cured commercial VE resins (*2*, *30*, *31*). Referring to figure 122 and table 14, the rubbery E' was ~17.4 MPa, indicating a M_C of 825 g/mol as per the theory of rubber elasticity, which suggests a reasonable average of 3.75 MV units between cross-links.
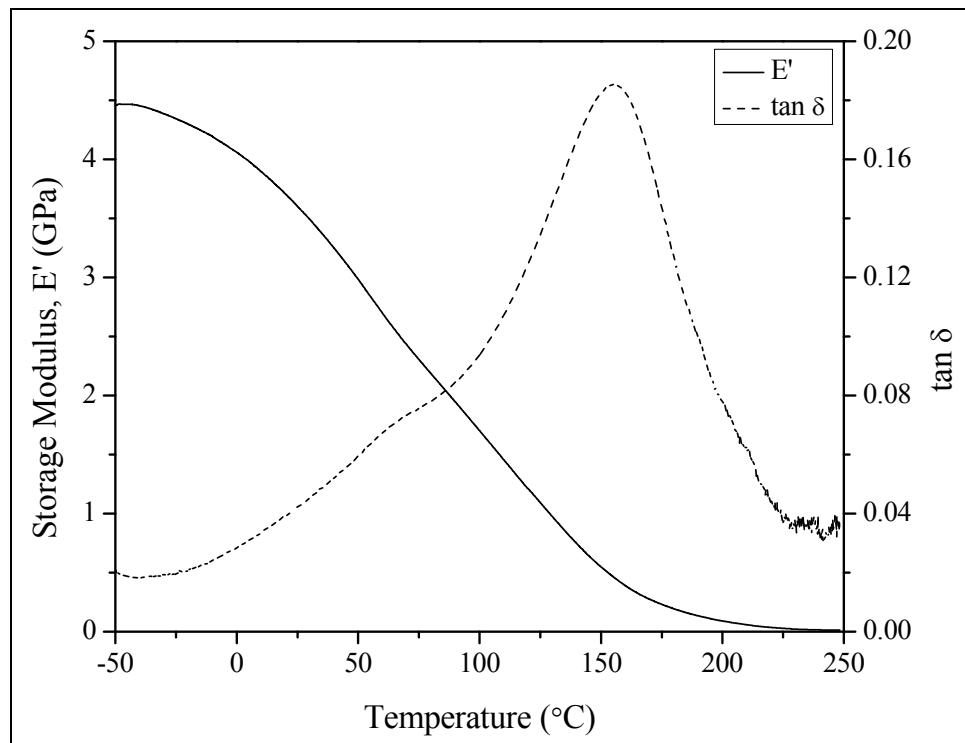
Figure 122. Storage modulus (E') and tan δ of MVGDM as a function of temperature.

Tan δ, also known as the damping factor or loss tangent, is the ratio of the loss modulus (E″) to E′, where E″ represents the energy lost as heat during a loading cycle (*23*, *29*). The width of the tan δ peak reflects polymer network heterogeneity with a broader peak implying a more heterogeneous polymer (*29*, *32*). According to a new theory of the glass transition entitled the twinkling fractal theory (TFT), an increased amount of relaxation modes present in the polymer network arises when there exists a broad distribution of solid fractal clusters that twinkle into the liquid upon heating, thus exhibiting heterogeneity (*33*, *34*). The tan δ peak in figure 122 is considered a broad peak, indicating the formation of a rather heterogeneous polymer network that contains a very broad distribution of relaxation modes and twinkling solid fractal clusters. Thus, a glass transition region occurs over a wide temperature range with a broad distribution of solid fractal clusters percolating with eventual fractal cavitation occurring upon cooling (*33*, *34*). This result may be attributed to the formation of regions that are highly cross-linked to regions that may contain unreacted monomer pools (*29*, *32*). The heterogeneity of the polymer network captured by the broadness of the tan δ coincides with the FTIR cure study and TGA results via the results that revealed the presence of unreacted C=C and the two-stage thermal decomposition profile. The designation of a specific temperature as T_g is difficult to provide because of the broadness of the glass transition region. However, in using the maximum peak intensity of the tan δ curve, $T_g = 155 \pm 1.7$ °C.

The extent of polymer chain segmental mobility at the temperature of maximum tan δ peak intensity is reflected by the intensity value, with higher values indicating higher energy loss and more viscous behavior, whereas lower values indicate higher elastic behavior (*29*). Having a maximum tan δ peak intensity value <0.2 is reflective of high elastic behavior and the presence of a highly cross-linked polymer network, which was expected with a monofunctional monomer to cross-link monomer ratio of 1:1. Additionally, the viscous behavior may be further restricted, and the elastic behavior enhanced by the ability of polymer chains to hydrogen bond, which may influence the relaxation dynamics of the cross-linked network and the ability of the solid fractal clusters to transition into the liquid upon heating (*33*, *34*).

6.4 Conclusions

In this work, a low-viscosity polymer resin consisting of a 1:1 mole ratio of MV to GDM was synthesized using a two-step, one-pot reaction scheme. The reaction scheme utilized the renewable, lignin-derived chemical vanillin and potential biobased reactants methacrylic anhydride and glycidyl methacrylate. Additionally, the reaction scheme generated no by-products, required small quantities of catalyst and relatively low reaction temperatures, and produced the biocompatible cross-linking agent glycerol dimethacrylate. Resin curing generated a hard, transparent thermoset that possessed a broad glass transition and $T_g = 155$ °C (based on the tan δ maximum). An overall fractional conversion of monomer C=C to polymer -C-C- during cure of 0.78 was elucidated from a FTIR cure study, while thermogravimetric analysis revealed a two-stage thermal decomposition profile with a T_{max} occurring at 426 °C. Overall, a

potentially 100% biobased resin was synthesized for use in composite applications and, when cured, possessed comparable thermogravimetric and thermomechanical properties to commercial VE resins. However, optimization of cure and postcure temperatures and durations as well as initiator concentration is recommended to improve overall conversion, thus reducing the concentration of unreacted monomer that could potentially leech into the environment.

Acknowledgments

References

1. La Scala, J. J.; Orlicki, J. A.; Winston, C.; Robinette, E. J.; Sands, J. M.; Palmese, G. R. *Polymer* **2005**, *46*, 2908–2921.

2. La Scala, J. J.; Sands, J. M.; Orlicki, J. A.; Robinette, E. J.; Palmese, G. R. *Polymer* **2004**, *45*, 7729–7737.

3. Stanzione, J. F., III; Sadler, J. M.; La Scala, J. J.; Wool, R. P. *ChemSusChem*, submitted for review, 2011.

4. Brazinha, C.; Barbosa, D. S.; Crespo, J. G. *Green Chemistry* **2011**, *13*, 2197.

5. Borges da Silva, E. A.; Zabkova, M.; Araújo, J. D.; Cateto, C. A.; Barreiro, M. F.; Belgacem, M. N.; Rodrigues, A. E. *Chemical Engineering Research and Design* **2009**, *87*, 1276–1292.

6. Gandini, A. *Green Chemistry* **2011**, *13*, 1061–1083.

7. Voitl, T.; Rudolf von Rohr, P. *ChemSusChem* **2008**, *1*, 763–769.

8. Holladay, J. E.; White, J. F.; Bozell, J. J.; Johnson, D. *Top Value-Added Chemicals From Biomass - Volume II - Results of Screening for Potential Candidates From Biorefinery Lignin*; PNNL-16983; Pacific Northwest National Laboratory: Richland, WA, 2007.

9. Araújo, J. D. P.; Grande, C. A; Rodrigues, A. E. *Chemical Engineering Research and Design* **2010**, *88*, 1024–1032.

10. Wool, R. P.; Sun, X. S. *Bio-based Polymer and Composites*, 1st ed.; Elsevier B.V.: New York, 2005.

11. Lora, J. H.; Glasser, W. G. *Journal of Polymers and the Environment* **2002**, *10*, 39–48.

12. Mialon, L.; Pemba, A. G.; Miller, S. A. *Green Chemistry* **2010**, *12*, 1704–1706.

13. Peng, H.; Xiong, H.; Li, J.; Xie, M.; Liu, Y.; Bai, C.; Chen, L. *Food Chemistry* **2010**, *121*, 23–28.

14. Renbutsu, E.; Okabe, S.; Omura, Y.; Nakatsubo, F.; Minami, S.; Saimoto, H.; Shigemasa, Y. *Carbohydrate Polymers* **2007**, *69*, 697–706.

15. Ziaee, S.; Palmese, G. R. *Journal of Polymer Science Part B: Polymer Physics* **1999**, *37*, 725–744.

16. Brill, R. P.; Palmese, G. R. *Journal of Applied Polymer Science* **2000**, *76*, 1572–1582.

17. Lam, P. W. K.; Plaumann, H. P.; Tran, T. *Journal of Applied Polymer Science* **1990**, *41*, 3043–3057.

18. Palmese, G. R.; McCullough, R. L. *Journal of Applied Polymer Science* **1992**, *46*, 1863–1873.

19. Sperling, L. H. *Introduction to Physical Polymer Science*, 4th ed.; John Wiley and Sons, Inc.: Hoboken, NJ, 2006.

20. Mathers, R. T. *Journal of Polymer Science Part A: Polymer Chem* **2011**, *50* (1), 1–15; DOI: 10.1002 /pola.24939.

21. Nagai, K. *Applied Catalysis A: General* **2001**, *221*, 367–377.

22. Kamm, B., Gruber, P. R., Kamm, M., Eds.; *Biorefineries - Industrial Processes and Products: Status Quo and Future Directions*; Wiley-VCH Verlag GmbH and Co. KGaA: Weinheim, Germany, 2012.

23. Santacesaria, E.; Tesser, R.; Di Serio, M.; Casale, L.; Verde, D. *Industrial & Engineering Chem Research* **2010**, *49*, 964–970.

24. Restani, R. B.; Correia, V. G.; Bonifácio, V. D. B.; Aguiar-Ricardo, A. *Journal of Supercritical Fluids* **2010**, *55*, 333–339.

25. Juntuek, P.; Ruksakulpiwat, C.; Chumsamrong, P. *Journal of Applied Polymer Science* **2011**, *122*, 3152–3159.

26. Park, S. J.; Jin, F. L. *Polymer International* **2005**, *54*, 705–709.

27. Horowitz, H. H.; Metzger, G. *Analytical Chem* **1963**, *35*, 1464–1468.

28. Zulfiqar, S.; Zulfiqar, M.; Kausar, T. *Polymer Degradation and Stability* **1987**, *17*, 327–339.

29. Park, J.; Eslick, J.; Ye, Q.; Misra, A.; Spencer, P. *Dental Materials* **2011**, *27*, 1086–1093.

30. La Scala, J. J.; Logan, M. S.; Sands, J. M.; Palmese, G. R. *Composites Science and Technology* **2008**, *68*, 1869–1876.

31. Scott, T. F.; Cook, W. D.; Forsythe, J. S. *European Polymer Journal* **2008**, *44*, 3200–3212.

32. Kannurpatti, A. R.; Anseth, J. W.; Bowman, C. N. *Polymer* **1998**, *39*, 2507–2513.

33. Stanzione, J. F., III; Strawhecker, K. E.; Wool, R. P. *Journal of Non-Crystalline Solids* **2011**, *357*, 311–319.

34. Wool, R. P. *Journal of Polymer Science Part B: Polymer Physics* **2008**, *46*, 2765–2778.

7. Synthesis and Characterization of a Novel Bio-Based Reactive Diluent as a Styrene Replacement*

7.1 Introduction

Fiber reinforced composites are quickly becoming the preferred building material in applications ranging from marine hulls, to aerospace components and commercial construction due to their ability to outperform traditional materials (*1–4*). High performance composites utilize thermosetting epoxy resins, vinyl ester (VE) or unsaturated polyester (UPE) resins for the polymer matrix with vinyl ester and UPE resins being preferred for large scale manufacture due to their low cost despite reduced glass transition temperature and fracture toughness (*1*). However, VE and UPE resins must be blended with reactive diluents, such as styrene (figure 123) and methyl methacrylate, which reduce their viscosity in order for them to be used in commercial liquid molding techniques. These reactive diluents are hazardous air pollutants (HAPs) and volatile organic compounds (VOCs) and are emitted during and after manufacture of these composites (*5*). Composites emit these pollutants at each stage of production: creation, molding, curing and throughout their life time during utilization (*5*).
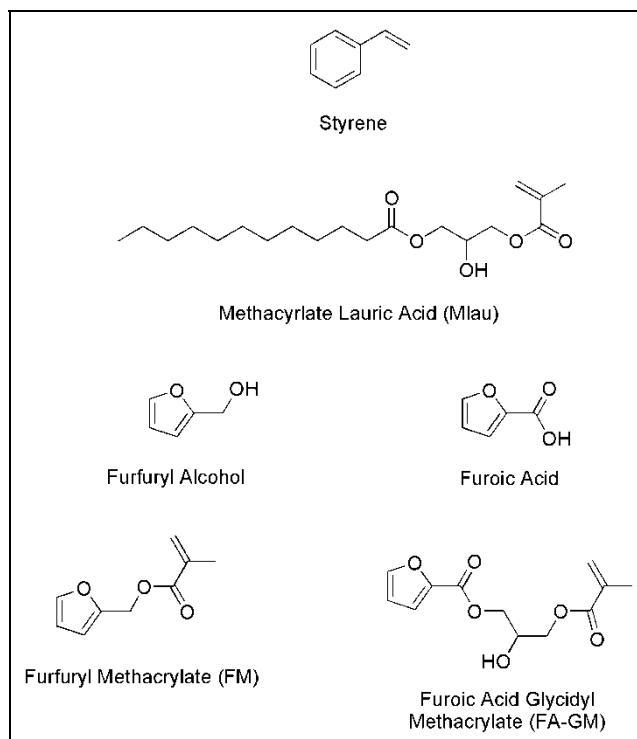
Figure 123. Reactive diluents and bio-based materials.

Another drawback that commercially available thermosetting resins suffer from, including VE and UPE resins, is the fact they are derived from crude oil. The cost of petroleum fluctuates dramatically due to a number of factors such as the current economic climate, the cost associated with processing, the worldwide demand, and the dwindling reserves that can be tapped for future use (6). Due to of these factors, the cost of thermosetting resins is directly tied to the cost of crude oil and the limited supply will eventually cause these resins to become more expensive and more difficult to obtain (6, 7).

Resins derived from renewable, bio-based resources are a potential means for reducing the impact of the issues associated with petroleum-derived resins. Fatty acid and triglyceride modification has been studied extensively and the results have been used in applications ranging from toughening agents and plasticizers (modified soybean oil derivatives) (8–10) to reactive diluents replacements (methacrylated fatty acids, MFAs) that have limited HAP and VOC emissions (11). Fatty acid monomers have been used to successfully reduce the HAP content in vinyl ester resins, but have been unable to completely replace styrene (11). These fatty acid vinyl ester resins have viscosities less than 1000 cP, glass transition temperature (T_g) greater than 100 °C and strength over 100 MPa, but only use 10–25 wt% renewable component and contain 10–25 wt% styrene. Higher renewable components and lower styrene contents result in viscosities over 1000 cP and T_g below 100 °C (12). While methacrylated fatty acids (MFA) have not been able to completely replace styrene in the formation of high performance resins, they have been shown to lower the overall styrene content and produce materials with lower emissions while retaining comparable physical properties (11, 12).

The escalation of the bio-refining industry to produce fuels has also resulted in the production of a wealth of new fine chemicals that can be used to produce monomers, polymers, and resins (13). The strategy that will be described herein will focus on the use of new carbohydrate based compounds that possess ring structures that offer a scaffold to build new monomers that are analogous to styrene (figure 123). The first logical step in designing a replacement for styrene that possesses similar attributes is to find a core molecule that is structurally similar. Of the compounds produced from biorefining industry, furanics are common, many of which are monosubstituted which can be easily modified to generate compound with a single polymerizable site. Compounds such as furfuryl alcohol and furoic acid are two such candidates that can be methacrylated in order to yield monomers, furfuryl methacrylate (FM) and furoic acid glycidyl methacrylate (FA-GM), that fulfill the desired structural features. Blending with these novel reactive diluents with a commercial vinyl ester resin and then copolymerization at room temperatures with peroxide initiator (Trigonox 239-A) and an accelerator (cobalt (II) naphthenate) yield quantifiable results that can be directly compared to an equivalent styrene blend. These furan based molecules, furfuryl methacrylate (FM) and furoic acid gylcidyl methacrylate (FA-GM), provide the ring structure that is usually associated with stiffness and should have viscosities that are reasonable for blending as a reactive diluent without sacrificing Tg.

7.2 Experimental

7.2.1 Materials

Furoic Acid (98%, Sigma-Aldrich), Tetrabutylammonium bromide (TBAB, NBu$_4$Br, ACS reagent grade $\geq$ 98%, Sigma-Aldrich), glycidyl methacrylate (97%, Sigma-Aldrich), acetonitrile (HPLC grade $\geq$ 99.9%, Sigma-Aldrich), furfuryl methacrylate (FM, 97%, Sigma-Aldrich), potassium hydroxide (KOH, ACS reagent grade $\geq$ 85% pellets, Sigma-Aldrich), Cobalt (II) Naphthenate (CoNap, 6% Cobalt Naphthenate, Sigma-Aldrich), styrene (Reagent Plus > 99.9%, Sigma-Aldrich), Tetrahydrofuran (THF, HPLC Grade $\geq$ 99.9%, Sigma-Aldrich) were all used as received.

RDX-26936 (methacrylated epoxy) vinyl ester was provided by Cytec Industries. Bio-based reactive diluent, methacrylated lauric acid (Mlau) was provided by Applied Poleramics, Inc. (API, Benicia, CA). Free radical polymerization initiator Trigonox 239-A was purchased from Akzo Nobel.

7.2.2 Preparation of Furoic Acid Glycidyl Methacrylate (FA-GM)

FA-GM was prepared using a mild proton transfer catalyst system that promotes ring opening of the epoxide found on glycidyl methacrylate. Furoic acid (solid) and glycidyl methacrylate (liquid) are only partly soluble without use of a solvent. In this particular reaction, acetonitrile not only functions as the solvent, but it is also necessary to facilitate the reaction in conjunction with tetrabutyl ammonium bromide (TBAB) (*14*). In this reaction, a slight excess of furioc acid (1.05 mol) is suspended in a solution of glycidyl methacrylate in acetonitrile with 1–2.5 wt% of TBAB. The suspension was refluxed over a period of 3–5 h, monitoring the reaction by acid number titrations of aliquots taken at 30–60 min intervals. As the reaction progressed, the solid dissolved and slowly became a pale yellow solution. After the decaying AN stabilized, the reaction mixture was cooled and the solvent removed using rotatory evaporation. The resulting residue was dissolved in diethyl ether and washed with water (3 × 100 mL), brine (100 mL), dried over MgSO$_4$ and evaporated to dryness resulting in a bright yellow oil (88–95%). The crude yellow oil was purified by silica gel chromatography eluting with 5.0% ethyl acetate in hexanes. The product was characterized using ^{1}H NMR (250.13 MHz, spectral window of G2000 Hz, 0.427 Hz/pt digital resolution, 16 scans at 293 K, 908 pulse width) on a Bruker (Billerica, MA) AC250 Spectrometer and showed peaks in agreement with the expected chemical shifts. ^{1}H NMR (CDCl$_3$): δ 7.57 (dd, 1H), 7.18 (dd, 1H), 6.50 (m, 1H), 6.13 (d, 1H), 5.59 (d, 1H), 4.54-4.24 (bm, 5H), 1.94 (t, 3H). ^{13}C NMR (CDCl$_3$): δ 167.50, 147.04, 146.94, 146.93, 135.87, 126.50, 119.02, 118.87, 118.77, 68.44, 65.61, 18.40. Elemental analysis: Calculated C$_{12}$H$_{14}$O$_6$·0.05 mol hexanes: C 58.11%, H 5.83%; found, C 57.91%, H 5.98%.

7.2.3 Acid Number Titration

Aliquots (0.25–0.80 g) of the reaction mixture were taken at regular intervals and titrated to monitor the progression of the reaction. The acid number for each sample was determined by dissolving each aliquot in 10 mL of 2-propanol and titrated using an aqueous 0.1 KOH solution (standardized with potassium hydrogen phthalate) in the presence of phenylphalene as an indicator in order to calculate the corresponding AN.

$$AN = V_t M \frac{56.1}{W_s} \qquad (3)$$

Where V_t is the volume of titrant, M is the molarity of the titrant, and W_s is the mass of the sample being titrated (*15*).

7.2.4 Size Exclusion Chromatography

Size exclusion chromatography (SEC) was used to evaluate the resulting reaction mixtures from the methacrylation reactions to determine the quality of the product and to establish to what degree, if any, epoxy polymerization or other molecular weight building side reactions had taken place. Samples were processed using a Waters 515 GPC with two 30 cm × 7.5 mm columns packed with 5 μm (poly)styrene-divinyl benzene in succession. The columns were equilibrated at 45 °C before elution with tetrahydrofuran (THF) at a rate of 1.0 mL/min. The eluent was monitored using a Waters 2487 dual channel absorbance detector at 270 nm and 254 nm at 25 °C. Samples were prepared by dissolving 3 mg product in 1 mL of THF.

7.2.5 Blending of Bio-Based Reactive Diluents and Free-Radical Curing Process

Resin systems were blended so that their composition consisted of 65 wt% of cross-linker and 35 wt% reactive diluent. All resin systems were blended using an ARE-250 Thinky planetary mixer at 2000 rpm for 5 to 10 min until the sample was homogenous. All samples were purged with N_2 prior to free radical polymerization to minimize oxygen inhibition. Free radical polymerization of each resin was initiated with 1.5 wt% Trigonox with 0.375 wt% CoNap added as a promoter. Resins were cured over night in RTV mold at room temperature in an oven with a constant purge of N_2. Samples were then post-cured at 110 °C for 2 h before any analysis was carried out.

7.2.6 Rheological Characterization

A steady state flow procedure was used to obtain viscosity in the formulated blends before polymerization and without initiator and catalyst using an AR 2000 Rheometer (TA Instruments). A Peltier Plate was utilized for temperature control with a 40-mm parallel plate geometry (TA Instruments). The resin samples were placed between the plates and a 1000 μm gap spacing (i.e., sample thickness) was used. A TA Instruments double concentric cylinder with 21.96-mm rotor outer radius, 20.38-mm rotor inner radius, 20.00-mm stator inner radius, and 59.5-mm cylinder immersed height was used to characterize neat furfuryl methacrylate

monomer. The sample rheology was measured in steady shear flow experiments at 25 °C. The shear rate was increased from 0.001 s^{-1} to 100 s^{-1} and then decreased back to 0.001 s^{-1}, and 10 measurements were taken per decade. At a given shear rate, the shear stress was measured every two s. The shear rate and viscosity were recorded when the shear rate stabilized to within 5% tolerance for three consecutive points. For low viscosity samples, low shear rates generally produce too little torque for accurate measurement while high shear rates produce too much torque for viscous samples. This was ascertained by torque maps at each shear rate. Viscosity was determined as the average viscosity across the shear rate range where appropriate torque maps were produced.

7.2.7 Dynamic Mechanical Analysis

The thermomechanical properties of the polymer samples were measured using TA Instruments Q800 dynamic mechanical analysis (DMA) in a 35-mm dual cantilever clamp geometry. Bars were cut into nominal dimensions of $60 \times 12 \times 3$ mm^3 and were sanded on both sides to ensure uniform cross-sectional area. The samples were tested at 1 Hz with a deflection of 7.5 μm while subjected to a temperature sweep at a rate of 2 °C/min. The temperature for all samples began at –50 °C, while VE/FM initial temperature started at 25 °C, and went to 200 °C for VE/FM and VE/Mlau whereas an end temperature of 250 °C was used for VE/styrene and VE/FA-GM. Deflection amplitude was reduced from 7.5 μm to 3.5 μm for RDX/FA-GM blend due to its brittle nature. Two temperature ramp experiments were run for each sample. The temperature at the loss modulus peak was considered as the glass transition temperature of the material (*16*).

7.2.8 Extent of cure

The extent of cure was characterized using Thermo Nicolet Nexus 870 Fourier transform infrared spectrometer (FT-IR). The Near–Infrared spectroscopic (NIR) details were recorded in the 4000–7000 cm^{-1} range for samples before and after curing. A 3.5-mm thick glass cell was used for NIR studies of liquid resin. Cured samples have a typical thickness of 3 mm. NIR experiments were carried out at room temperature. Each spectrum was obtained using 64 scans at 4 cm^{-1} resolution. Conversion rate was calculated by observing the vinyl (6135 cm^{-1}) and methacrylate (6166 cm^{-1}) double bonds before and after curing (*17–19*). In our case, vinyl and methacrylate peaks are superimposed making it difficult to distinguish between the two. Therefore the total vinyl and methacrylate (6135 – 6166 cm^{-1}) bands were taken into account for a global conversion calculation using the equation below:

$$X = \frac{\left(^{H}6135 - 6166\,cm^{-1}\right)_{Unreacted} - \left(^{H}6135 - 6166\,cm^{-1}\right)_{Reacted}}{\left(\dfrac{^{H}6135 - 6166cm^{-1}}{H_{ref}}\right)_{Unreacted}} \tag{4}$$

The reference bands were chosen at 4623 cm^{-1} and 4681 cm^{-1} as they are widely reported in literature as the internal phenyl groups (*18*). Figure 124 displays a typical NIR spectrum of the styrenated and bio-based resin blends. The vinyl and methacrylate bands (6135 – 6166 cm^{-1}) and the phenyl bands (4623cm^{-1} and 4681 cm^{-1}) consistently exist in similar wave number region for all of the VE resin blends.
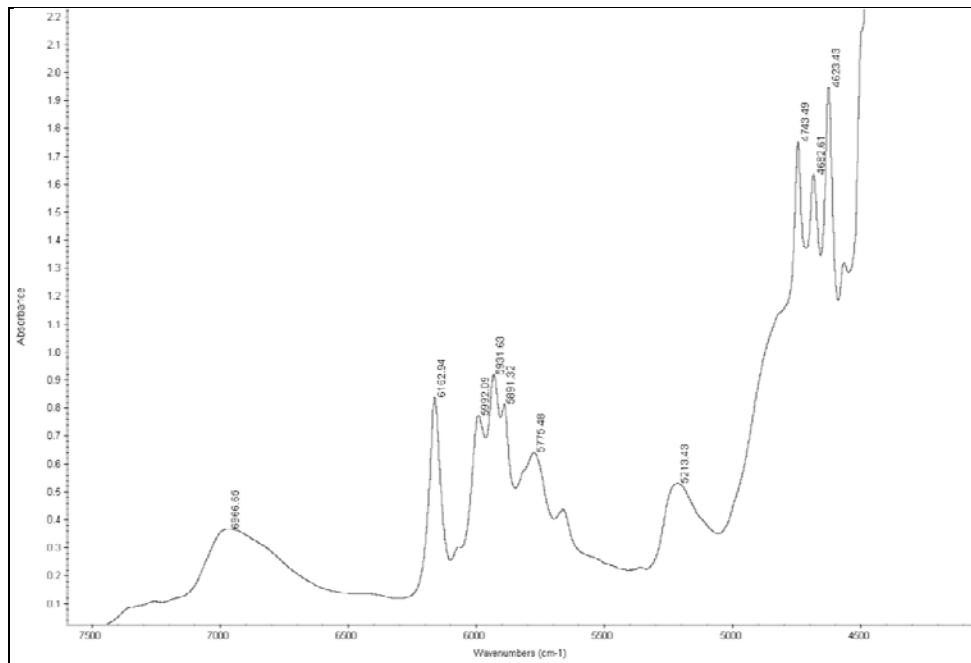
Figure 124. NIR spectrum of styrenated and bio-based resin blends.

7.3   Results and Discussion

Investigation of bio-based reactive diluents initially seemed to be straight forward. FM is commercially available from a number of sources, and resin blends were easily produced in order to evaluate its potential as a reactive diluent. The synthesis of FA-GM was envisioned using a similar methodology to that was previously employed in our laboratories to produce methacrylated fatty acids, such as Mlau (*11*). Furioc acid contains a single terminal carboxylic acid that can be use to react with glycidyl methacrylate. Based on the production of Mlau, we attempted to run this reaction in the presence of 1–3 wt% AMC-2 catalyst at ~70 °C without solvent to form the desired product. However, it was found that the reaction did not proceed as expected; instead of forming low viscosity oil, a tacky, high viscosity semi-solid was obtained which was not amiable to any further formulation. Analysis by ^{1}H NMR showed that both the furoic acid and glycidyl methacrylate starting materials had been consumed, however the peaks indicating the presence of the expected product were found in extremely small concentrations. Using size exclusion chromatography (SEC) it was determined that the resulting product was composed mainly of polymeric material, figure 125, with retention time between 12.0 and 15.0 min. The peak just after 15 min is indicative of the desired product and the broad peak after 17.8 is unreacted starting material.

165
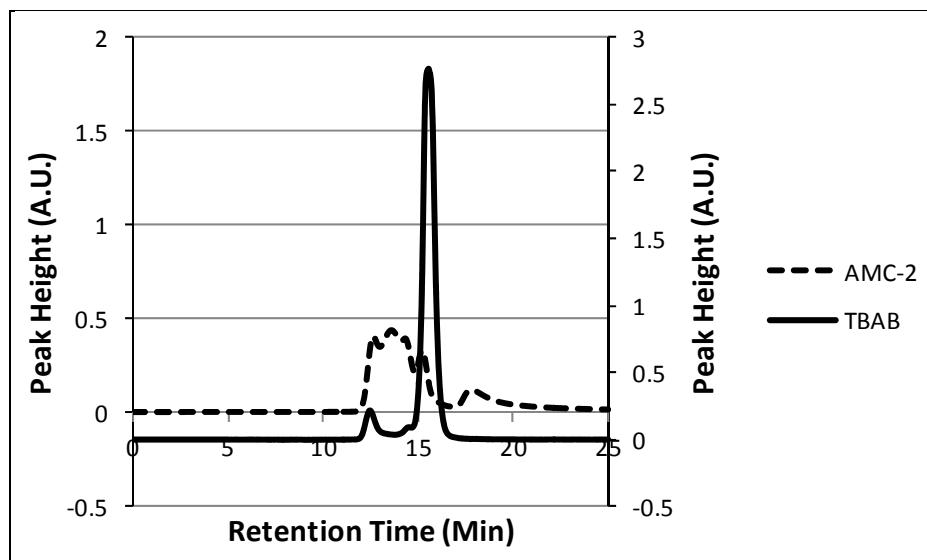
Figure 125. SEC chromatogram comparison of products via TBAB catalyzed and
AMC-2 catalyzed reactions. (Axis offset for clarity.)

7.3.1 Synthesis and Optimization of FA-GM

After reevaluating our synthetic methodology, we decided that it would be prudent to use a
reaction that was both milder and utilized a solvent to disperse the reactants and aid in
dissolution of the solid furoic acid. There are examples in the literature of epoxidations of
aromatic acids using tetrabutylammonium bromide (TBAB) in catalytic quantities that possessed
high rates of conversion, figure 126 (*14*). Dissolving furoic acid and glycidyl methacrylate in
acetonitrile and refluxing with 1–2.5 wt% TBAB resulted in the desired product, FA-GM, in near
quantitative yields. Analysis by ^{1}H and ^{13}C NMR showed distinct peaks indicative of FA-GM
with minimal amounts of byproducts. SEC was used for comparison to ensure that minimal
polymer was formed during the course of the reaction, figure 125. The dominant component of
the TBAB catalyzed synthesis is the monomeric product, with the starting material being
completely consumed with a relatively small percentage making up the unwanted polymer that
was seen using the AMC-2 catalyzed reaction, figure 125.
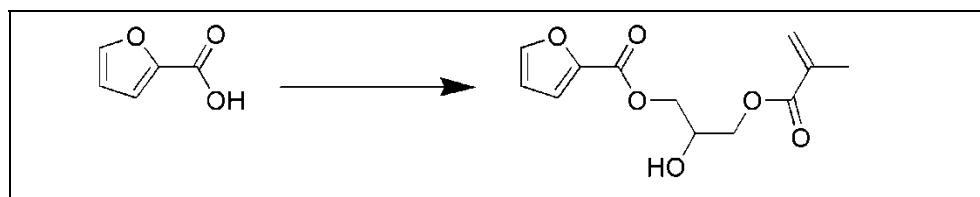
Figure 126. Synthesis of FA-GM. Reagents and conditions: Bu$_4$NBr, Acetonitrile,
glycidyl methacrylate, reflux, 4 h.

166

In an effort to optimize the synthesis of this novel reactive diluent, we studied the effect of catalyst and solvent concentrations on reaction time to make the process as efficient as possible. A series of reactions was carried out, first varying the catalyst concentration and then the solvent concentrations to determine the minimum quantities necessary to achieve complete conversion in a minimal time frame. The progress of the reaction was monitored by Acid Number (AN) titrations and the reaction was quenched when the AN value began to plateau. The results of this study have been summarized in table 15. As expected, the rate of the reaction increased as the catalyst concentration increased; however, when the solvent concentration was reduced, the products that were recovered had a similar composition to that of the AMC-2 catalyzed reaction. For this method, the reaction was optimized with 2.5 mol % catalyst and ~14 wt% percent solvent to achieve maximum turnover in least amount of time. Using lower catalyst concentrations resulted in protracted reaction times, and lower solvent concentrations resulted in the formation of a highly viscous polymerized species.

Table 15. Optimization of TBAB/acetonitrile reaction.

Catalyst Concentration (wt%)	Solvent Concentration (wt%)	Reaction Time (h)	Final Acid Number
2.5	50.0	6	6.42
1.0	50.0	6	20.68
2.5	35.0	4	4.77
2.5	14.0	5	1.23
2.5	10.0	1	<10[a]
2.5	5.0	1	<12[a]

[a]Polymerization occurred in the first hour of the reaction, similar to the AMC-2 catalyzed reaction.

7.3.2 Neat Viscosities of FM and FA-GM

The viscosities of the furanic based reactive diluents were evaluated in comparison to styrene, and methacrylated fatty acids, such as Mlau, which has been shown in the literature to be an acceptable styrene replacement (*11*). The results of which are summarized in table 16.

Table 16. Absolute viscosities of furanic reactive diluents.

Monomers	Viscosity (cP) at 25 °C
Styrene	~0.8
Furfuryl methacrylate	4 ± 0
MLau	72 ± 2
FAGM	234 ± 25

Furfuryl methacrylate has a slightly higher molecular weight of 166.17 g/mol relative to 104.15 g/mol for styrene. It is architecturally similar to styrene, although the ester group results in a slightly higher viscosity; but also maintains a much higher boiling point (87 °C/5 mmHg),

making it much less likely to be listed as either a HAP or VOC. The Mlau monomer consists of a long hydrocarbon fatty acid coupled to a methacrylate terminal end group through a glycidyl linker and has the highest molecular weight of 332.54 g/mol. These additional functionalities contribute to a higher viscosity compared to styrene and furfuryl methacrylate. FA-GM has a molecular weight (242.25 g/mol) between that of FM and Mlau. The structure of FA-GM is similar to that of Mlau, and both possess free hydroxyl functionalities on the glycidyl linker that allows for intermolecular hydrogen bonding with neighboring molecules. This results in a drastic viscosity increase, but also allows for improved solubility in more polar cross-linkers. Additionally, the observed viscosity of Mlau is three times less than FA-GM because it is likely that the furan ring exacerbates the hydrogen bonding effect relative to the long aliphatic chain of Mlau.

7.3.3 Resin Blends Using Furanic Reactive Diluents

The formulated resin systems used the aforementioned reactive diluents in conjunction with RDX–26936 (Cytec) as a model vinyl ester crosslinker. Previous work shows that RDX-26936 is similar to dimethacrylated vinyl esters of Epon 828 (VE 828), and is a low molecular weight VE monomer of approximately 600 g/mol (*11*, *20*). All resins were formulated with 65 wt% RDX-26936 (VE) and 35 wt% reactive diluents, which is a ratio commonly used in VE resins (*21*). All VE blends displayed Newtonian behavior, as depicted in figure 127, showing viscosity as a function of shear rate. The VE blend with styrene has the lowest viscosity (0.2 Pa·s ± 0.1 Pa·s), whereas using furfuryl methacrylate as reactive diluent resulted in a higher viscosity (0.7 Pa·s ± 0.0 Pa·s) roughly three and half times higher than that of the styrene blends. Resin systems using Mlau as the reactive diluents result in even higher viscosities (5.3 Pa·s ± 0.0 Pa·s) due to the higher monomer viscosity caused by the hydroxyl functionality. FA-GM resulted in viscosities significantly higher (30.6 Pa·s ± 0.2 Pa·s) due to the dominant effect in hydrogen bonding relative to using Mlau.

Dynamic mechanical properties of VE blends using bio-based reactive diluents were compared to a conventional blend using styrene. A representative plot of storage and loss moduli as a function of temperature is illustrated. VE/Mlau blend has the lowest storage modulus, E', in the glassy region compared to furanic based and conventional reactive diluents. Regarding the furan-based resins, the VE/FA-GM resin has a higher modulus in the glass and rubbery regions relative to the VE/FM resin. Another observation is that all blends had the same glassy modulus when cooled well below Tg except for VE/Mlau, which had a lower modulus. The rubbery modulus of VE/styrene blend (i.e., plateau modulus at high temperatures) was the lowest relative to the other three blends. In fact, the trends in rubbery modulus were exactly opposite that of the glassy modulus, as VE/Mlau had the highest value, followed by VE/FM, VE/FA-GM, and lastly VE/styrene.
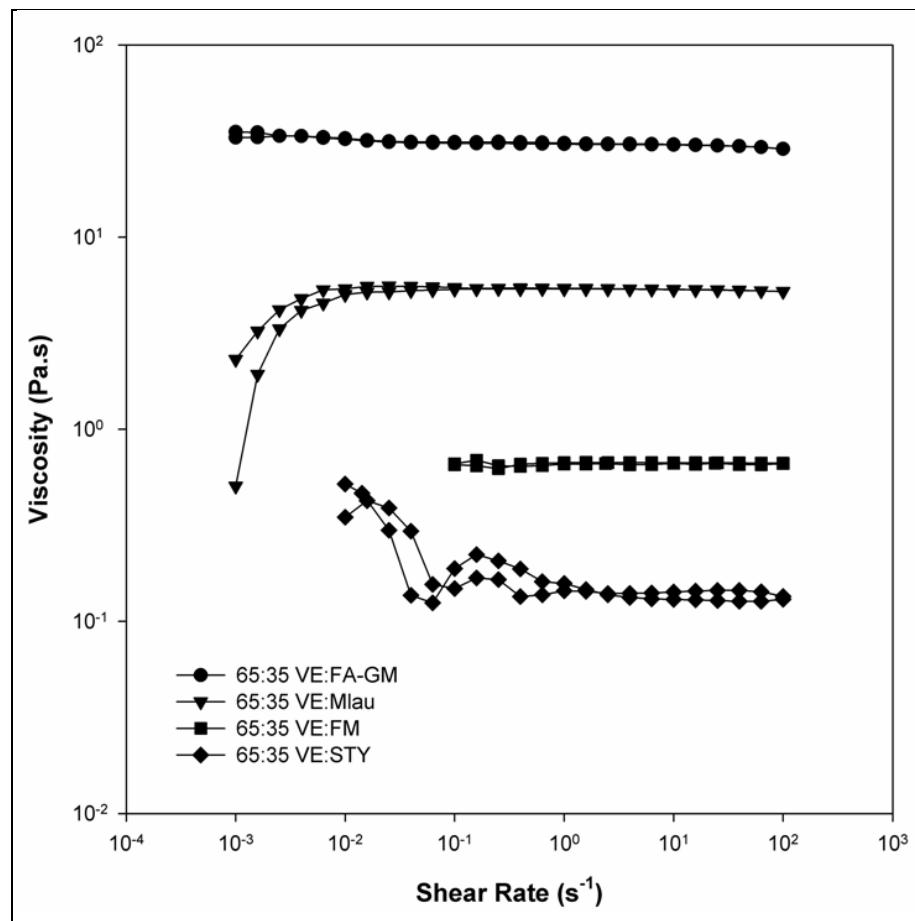
Figure 127. Viscosities of vinyl ester resins as a function of shear rate at 25 °C.
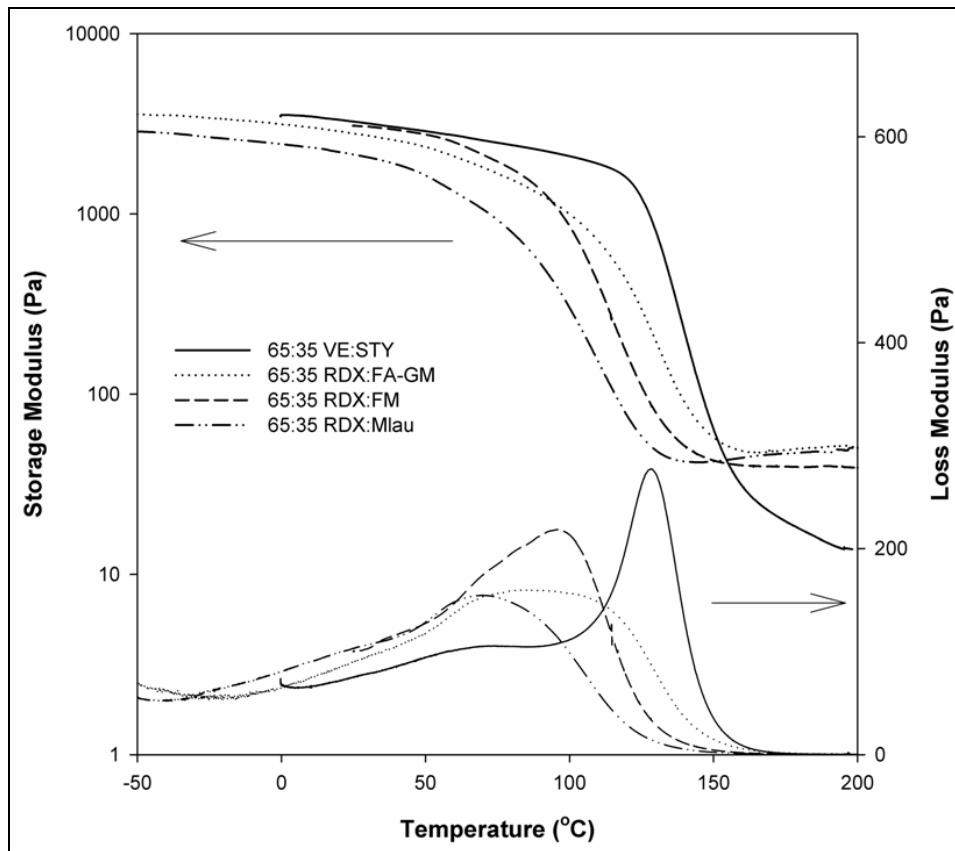
Figure 128. Storage and loss moduli bio-based resin systems.

The cross-link density of the VE resin blends was measured using DMA. The theory of rubbery elasticity was utilized to determine the molecular weight between cross-link (M_C):

$$M_c = \frac{3RT\rho}{E} \qquad (5)$$

Where E is the rubbery modulus, R is the universal gas constant, T is the absolute temperature and ρ is the sample density (22–24). The temperature T and rubbery modulus E are collected at which point where the rubbery modulus no longer decreased with temperature (12). The samples density ρ was measured at 18 °C according to (ASTM D792-00) and is tabulated in table 17. The sample density ρ divided by M_C is the cross-link density of the polymer, making M_C inversely proportional to the cross-link density. The crosslink density among VE polymer samples changed significantly as styrene (104.15 g/mol) is replaced with furan-based and modified fatty acid reactive diluents, this is mainly due to the molecular weight of the reactive diluents (FM: 166.17 g/mol, FA-GM: 242.25 g/mol, MLau: 332.54 g/mol). However, the density of VE/Mlau polymer is much lower relative to polymers that were blended with furan based reactive diluents. The molecular weight of Mlau is considerably higher compared to the other reactive diluents, and as a result the lower density is not due to molecular weight but rather the chemical packing and free volume formed from the hydrocarbon chain. This analysis shows

170

Table 17. Thermomechanical properties of VE/reactive diluents blends.

Blends	E' at 25 °C (MPa)	Peak of E" (°C)	Peak of Tan Delta (°C)	Rubbery E (MPa)	Rubbery T (°C)	M_c (g/mol)	Polymer Density (g/cm³)
VE/Sty	3,394 ± 488	129 ± 0	147 ± 4	21 ± 4	178 ± 19	726 ± 238	1.170 ± 0.003
VE/Mlau	2,319 ± 257	71 ± 1	115 ± 1	43 ± 5	147 ± 2	311 ± 31	1.184 ± 0.003
VE/FM	2,862 ± 609	98 ± 4	124 ± 6	35 ± 7	211 ± 11	398 ± 20	1.233 ± 0.004
VE/FA-GM	3,193 ± 356	85 ± 3	134 ± 2	50 ± 2	166 ± 0	289 ± 2	1.258 ± 0.008

that VE/FA-GM resins have the lowest M_C (i.e., highest crosslink density) closely followed by VE/Mlau, then VE/FM, while VE/styrene had by far the highest M_C. Previous analysis of VE/styrene and VE/Mlau cure indicates that the cure is highly dependent on the diluents used (*11*, *25*). In VE/styrene resins, the VE vinyl groups only react to about 70% extent of cure, while styrene can react up to 95% after postcure. In VE/Mlau, the VE crosslinkers react to a slightly higher content (75%–80%), while the Mlau reacts to a lower extent (80%–85%) relative to styrene. Both of these changes result in a higher crosslink density as they result in more VE monomer crosslinking and less reactive diluent incorporated into the network. The same trend applies to the other bio-based reactive diluents for that both the VE and diluents have methacrylate functionality. NIR was used to approximate the total reactivity of the bio-based resin. VE/FM has 73%–80% total conversion whereas VE/FA-GM has the lowest total conversion of 58%–67% thus strongly indicating that there is less reactive diluent incorporation in the polymer network. Two factors would thus affect extent of cure: vitrification (i.e., glass transition temperature of curing polymer rises above cure temperature to essentially freeze molecular motions and thus cure) and diluent molecular weight. FM is the smallest molecule and thus would have the highest diffusivity in the curing polymer. As a result, it likely has the highest level of incorporation into the polymer network, causing it to have the highest M_c of the bio-based resins. While Mlau has the highest molecular weight of the bio-based diluents studied, it did not have the lowest M_c. Thus, it is likely that the lower M_c for VE/FA-GM was a result of vitrification, as VE/FA-GM has a higher T_g than that of VE/Mlau.

The temperature at which peak of the loss modulus, E", occurs is indicative of the T_g and generally matches the temperature of the inflection point of E'(T) (*22–24*). Alternatively, the temperature at which the peak of the tan δ occurs (E"/E') has been considered the T_g for many samples, but generally this occurs at well higher temperature relative to the inflection point of the E'(T) curve and most samples are rubbery at this temperature. Thus, we define the T_g as the temperature at which the loss modulus peak occurs. The loss modulus peak is sharpest for VE/styrene blend, due to its low cross-link density and homogeneous resin formation.[22-24] The bio-based VE blends have a lower T_g relative to the VE/styrene blend although these blends have a higher cross-link density. The broadening in glass to rubber transitions and reduction of the loss modulus peaks further suggests a higher cross-link density in VE blends using bio-based reactive diluents. The reduced T_g relative to VE/styrene is a function of the less stiff nature of

the bio-based reactive diluents. In particular, the aliphatic Mlau produced the lowest T_g. The very broad loss modulus peak of VE/FA-GM could indicate some heterogeneity/micro-phase separation of this resin sample, although the samples had similar optical clarity relative to the other polymer samples. This behavior caused VE/FA-GM to have a lower temperature loss modulus peak while it had a higher temperature tan δ peak relative to VE/FM. Overall utilizing bio-based reactive diluents results in polymers with a noticeably reduced T_g when compared to their styrenic counterparts, due to the increased length of the side chain substituents; however the cross-link density is much higher especially when blending with FA-GM and Mlau.

7.4 Conclusion

A new bio-based polymerizable compound, FA-GM, has been successfully synthesized using a mild proton transfer reaction catalyzed by TBAB and the reaction optimized for bulk synthesis to minimize reaction time, solvents, and the formation of polymerized products, most likely due to homo-polymerization. Reaction using 2.5 wt% TBAB and a minimum of 14 wt% acetonitrile is sufficient to facilitate the reaction in 4 hours with greater than 90% conversion to the desired product.

Two furan-based reactive diluent candidates were evaluated in as both neat monomers and components of resin blends relative to two existing reactive diluents. Furfuryl methacrylate exhibited a neat viscosity that is higher than styrene, but not so much to limit its effectiveness while FA-GM proved to possess a neat viscosity that was significantly higher than that of styrene. Resin blends using these compounds showed similar viscosity trends as was found in the neat monomer. The furanic-based candidates had a significantly higher cross-linking density when compared to styrene blends due to increased cross-linker extent of cure and reduced incorporation of the bio-based diluents into the network. The bio-based polymers had storage moduli that were comparable relative to styrene in the glassy region even though the materials proved to have lower T_gs.

Although the viscosities of the model resin systems have shown an increase when styrene is replaced with the bio-based reactive diluents, it may be possible that these compounds can be used in ternary blends in conjunction with styrene or other low viscosity diluents as tool to help mitigate the HAP and VOC characteristics of styrene based resins. Using ternary blends, properties can be tailored to include viscosities and T_gs similar relative to commercial vinyl ester resins while lowering styrene contents substantially and helping to minimize the environmental impact.

References

1. Pilato, L.; Michino, M. *Advanced Composite Materials*, Springer: New York, 1994.

2. Quilter, A. Aircraft Maintenance Technology 2004, October.

3. Potter, P. *Ampitiac* **2003**, *7*, 37–40.

4. Griffiths, B. *Composites Technology* **2006**, August, 60–62.

5. EPA. In 40 CFR Part 63, 2003, p 19375–19443.

6. Cordesman, A. H.; Al-Rodhan, K. R.. Center for Strategic and International Studies Washington, D.C., 2005.

7. Greenwood, C.; Hohler, A.; Hunt, G.; Liebreich, M.; Sonntag-O'Brien, V.; Usher, E.; United Nations Environment Programme: New York, 2007.

8. Kirschenbauer, S. P. *Fats and Oils: and Outline of their Chemistry and Technology*; Reinhold Publishing Group Corporation: New York, 1960.

9. Bunker, S. P.; Wool, R. P. *J. of Polymer Science Part A-Polymer Chemistry* **2002**, *40*, 451–458.

10. Khot, S. N.; Lascala, J. J.; Can, E.; Morye, S. S.; Williams, G. I.; Palmese, G. R.; Kusefoglu, S. H.; Wool, R. P. *J. of Applied Polymer Science* **2001**, *82*, 703–723.

11. La Scala, J. J.; Sands, J. M.; Orlicki, J. A.; Robinette, E. J.; Palmese, G. R. *Polymer* **2004**, 45, 7729–7737.

12. La Scala, J. J.; Orlicki, J. A.; Winston, C.; Robinette, E. J.; Sands, J. M.; Palmese, G. R. *Polymer* **2005**, *46*, 2908–2921.

13. Biorefineries - Industrial Processes and Products; Wiley-VCH: Wienheim, Germany, 2010.

14. Khalafi-Nezhad, A.; Rad, M. N. S.; Khoshnood, A. Synthesis-Stuttgart 2003, 2552–2558.

15. Stevens, M. P. *Polymer Chemistry, an Introduction*; Oxford University Press: New York, 1990.

16. Nielsen, L. E.; Landel, R. F. *Mechanical Properties of Polymers and Composites*; Marcel Dekker Inc.: New York, NY, 1994.

17. Rey, L.; Galy, J.; Sautereau, H.; Lachenal, G.; Henry, D.; Vial, J. *Applied Spectroscopy* **2000**, *54*, 39–43.

18. Poisson, N.; Lachenal, G.; Sautereau, H. *Vibrational Spectroscopy* **1996**, *12*, 237–247.

19. Dean, K.; Cook, W. D.; Rey, L.; Galy, J.; Sautereau, H. *Macromolecules* **2001**, 34, 6623–6630.

20. Boyd, S. E.; La Scala, J. J.; Palmese, G. R. *J. of Applied Polymer Science* **2008**, *108*, 3495–3506.

21. Geng, X.; La Scala, J. J.; Sands, J. M.; Palmese, G. R. *SAMPE Symposium and Exhibition*, Baltimore, MD, 3-1 June 2007.

22. Flory, P. J. *J. of Applied Polymer Science* **1992**, *46*, 432–493.

23. Palmese, G. R.; McCullough, R. L. *J. of Applied Polymer Science* **1992**, *46*, 1863–1873.

24. La Scala, J. J.; Logan, M. S.; Sands, J. M.; Palmese, G. R. *Composites Science and Technology* **2008**, *68*, 1869–1876.

25. Ziaee, S.; Palmese, G. R. *J. of Polymer Science Part B-Polymer Physics* **1999**, 37, 725–744.

8.   Furan-Based Epoxy Cross-Linkers

8.1   Introduction

Furan groups are aromatic and represent a potential biobased replacement for phenyl rings that are components of high-performance epoxy resins. This section examines methods to prepare furan-based epoxides and begins to develop structure-property relationships.

8.2   Experimental

8.2.1 Synthesis: Furan-Based Epoxy Was Synthesized Via Various Synthetic Routes

bHMF, epichlorohydrin, water (5 mL), and benzyl trimethyl ammonium chloride were put in a flask under nitrogen gas. The reaction was carried out at 100 °C for 5 h. Next, 40 wt% NaOH solution was added dropwise to the mixture while it was stirred at 100 °C for 2 h. The organic phase was extracted with ethyl acetate and washed with deionized water several times. Ethyl acetate was evaporated by a rotary evaporator.

8.2.1.1 New Approaches to Synthesize Furan-Based Epoxy

8.2.1.1.1 *Dimethyl Formamide (DMF) Instead of Water*. Based on the previous synthetic condition, only one reagent was changed. DMF replaced water to investigate the effects of water on the synthesis. bHMF (20.5 g), epichlorohydrin (59.2 g), DMF (30 mL) and benzyl trimethyl ammonium chloride (1.18 g) were mixed and heated up to 100 °C. The reaction was conducted for 5 h. Next, 40 wt% NaOH solution (14 g) was added dropwise for 2 h.

8.2.1.1.2 *Water Control*. The control of water is an important factor because water can act as a promoter for this reaction and produce the by-product at the same time. Therefore, the least amount of water to obtain a high yield and minimize the by-product should be found out. The optimal amount of water was 0.5 mL, bHMF (20.16 g), epichlorohydrin (70 g), water (0.5 mL) and benzyl trimethyl ammonium chloride (2.9 g) were mixed and heated up to 100 °C. The reaction was performed for 5 h. Then, 40 wt% NaOH (19 g) was added dropwise for 2 h.

8.2.1.1.3 *Scale-Up of Furan-Based Epoxy*. bHMF (100 g), epichlorohydrin (216.5 g), water (2.5 mL), and benzyl trimethyl ammonium chloride (14.48 g) were mixed by a mechanical stirrer in a 3-L flask under nitrogen gas. A homemade heating controller and mantle were used for reaction temperature control. The reaction was performed at 130 °C for 6 h. After the reaction temperature changed from 130 to 90 °C, 40 wt% NaOH solution (93.6 g) was added dropwise for 2 h.

8.2.1.1.4 *Small-Scale Synthesis of Furan-Based Epoxy Without Water (Two Step Reaction).*
bHMF (12.8 g), epichlorohydrin (55.5 g), and benzyl trimethyl ammonium chloride (1.85 g)
were mixed under nitrogen gas. The solution was heated at 100 $^{\circ}$C for 18 h. Then, 40 wt% NaOH
(4.8 g) was added dropwise for 2 h.

8.2.1.1.5 *Conventional Synthesis of Furan-Based Epoxy (One Pot Reaction).* bHMF (10 g) and
epichlorohydrin (72 g) were mixed in a flask to which a Dean-Stark trap was connected. The
solution was heated to 120 $^{\circ}$C, and epichlorohydrin was refluxed under nitrogen gas for 1.5 h.
Next, 40 wt% NaOH solution (6.24 g, 9.36 mL of water) was added dropwise for 2 h. Water
(~10 ml) was trapped in a Dean-Stark tube.

8.2.1.1.6 *Quantitative Determination of the Epoxy Content of Epoxy Resins (EEW).* The test
method was followed by ASTM D 1652-90.

8.2.2 Resin Cure

Furan-based epoxy was mixed with PACM (Bis(p-aminocyclohexyl) methane, Air Products)
based on mole ratio and/or the epoxy equivalent weight (EEW). The mixture was cured at 95 °C
for 3 h and postcured at 150 °C for 3 h.

Furan-based epoxy monomer was cured with 1 wt% of DPI (diaryliodonium
hexafluoroantimonate, E-beam-induced cationic cure of epoxide) in a DSC hermetic cell.

8.2.3 Furan-Based Epoxy Characterization

A 500-MHz Varian Unity Inova NMR in the Department of Chemistry at Drexel University was
performed to characterize the chemical structure of the furan-based epoxy monomers. A sample
with a concentration of 30 mg/1 mL was prepared with chloroform-d or DMSO-d6 as a solvent.
NIR spectroscopy (NEXUS 670, Thermo Nicolet) was used to collect NIR spectra of samples
operated by OMNIC version 5.2a. The number of scans and resolution were 32 and 8,
respectively. A kinetic study was also carried out by using NIR spectroscopy. An NIR spectrum
was collected every 15 min at 95 °C. A DSC measurement was performed using a DSC Q2000
(TA instrument) to obtain the T_g and curing temperature. A temperature ramping function from
−60 to 200 °C at a rate of 10 °C/min was selected. The T_g was determined by the middle of the
transition. The thermomechanical properties of furan-based epoxy thermosetting resins were
measured by using DMA. Rectangular samples with approximate dimensions of 17.5 × 12.0 × 2
mm^3 were tested by using a TA Instruments Q800 in the single cantilever method. The samples
were tested at 1 Hz with a deflection of 7.5 μm, and the temperature was ramped from −20 to
150 °C at a rate of 2 °C/min. At the T_g, the storage modulus decreases intensely, and the loss
modulus reaches the highest point. In this report, the temperature at which the peak in the loss
modulus occurred was selected as the T_g of the cured resin.

8.3 Results and Discussion

8.3.1 Furan-Based Epoxy Synthesis and Characterization

Furan-based epoxy was synthesized by the reaction between furan derivative and epichlorohydrin. The catalyst, benzyl trimethyl ammonium chloride, was used to prevent potential side reactions. The catalyst was insoluble in the solution of furan derivative and epichlorohydrin. Water was added to improve the miscibility. The yield of the furan-based epoxy was about 85%. In order to reduce the by-product, DMF was used as a solvent instead of water. However, the yield was very low (below 20 wt%), meaning that the replacement did not work well. The amount of water was decreased to obtain a suitable yield and low by-product. The solution of epichlorohydrin and catalyst was prepared in advance. Water was added slowly in the solution, and the whole solution was checked to find out the point that it turned clear. The method made it possible to minimize the amount of water. After separation and purification processes, the yield was about 65%.

Large-scale synthesis (~180 g) was tested with the water-controlled method. However, the method failed to synthesize furan-based epoxy because of the leak between the lid and the reactor. Epichlorohydrin was evaporated through the leak during the reaction. The large-scale synthesis will be tested after the leak is fixed by a gasket.

Another synthetic method was tested without water. In this case, furan derivative, epichlorohydrin, and benzyl methyl ammonium chloride were used to prepare a solution. Over 12 h was required to reach about 50% of yield. The last test was a conventional synthetic method. The advantages are a short reaction time (3.5 h) and high yield (70%). This method can be directly compared to the method without water at which a catalyst was used.

8.3.2 Furan-Based Epoxy Cured With DPI

The furan-based epoxy monomer obtained from the water-controlled method was used for this cure process. In order to find out a reasonable cure temperature, 1 wt% of DPI was mixed with furan-based epoxy, and a DSC experiment was conducted to confirm the exothermic peak at which the cure process occurs. Figure 129 shows that a shoulder and a peak appeared at 140 and 168 $^\circ$C, respectively. It was found that the cure temperature for this sample could be near 160 $^\circ$C. The second scan was carried out with the sample as shown in figure 130. There was no exothermic peak, meaning that the sample was cured completely. However, T_g was not clear on this DSC thermogram.
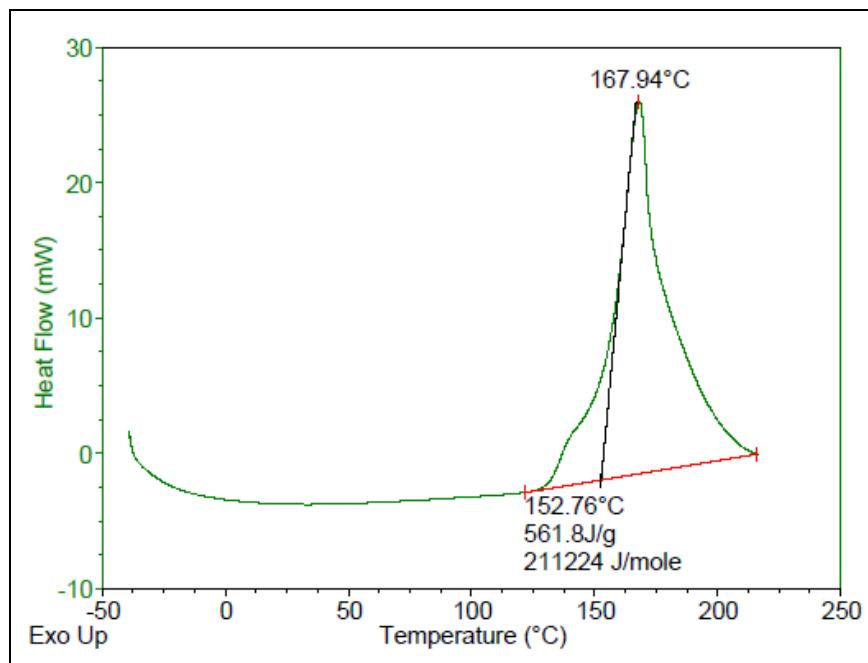
Figure 129. Furan-based epoxy cured with 1 wt% DPI in DSC hermetic cell.
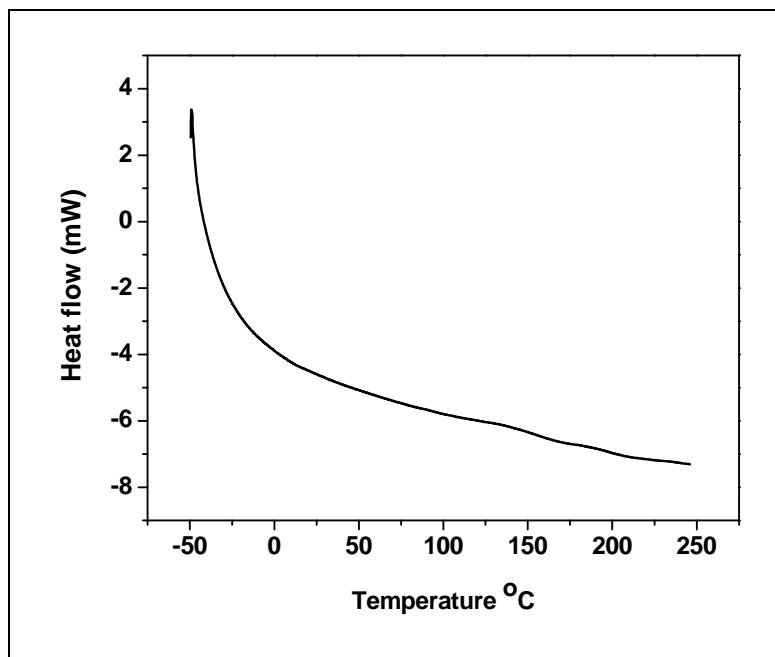
Figure 130. The second DSC scan of furan-based epoxy cured with 1
            wt% DPI.

8.3.3 Furan-Based Epoxy Cured With PACM

The furan-based epoxy obtained from the water-controlled method was used for the DSC experiment (figure 131) to find out the cure temperature. Furan-based epoxy and PACM were mixed by the stoichiometric method. The cure process started at 38 °C, and the peak cure temperature for this system was found at about 100 °C. Figure 132 shows the NIR spectra of the mixture of furan-based epoxy and PACM. The cure process was monitored every 15 min at 95 °C. Initial NIR spectrum (red) exhibits an epoxy peak at 4500 cm^{-1} and an amine peak at 4900 cm^{-1}. The next spectrum did not show the peaks, meaning that most of the epoxy and primary amine group reacted in 15 min at 95 °C. DMA was used to obtain the storage modulus (E' at 25 °C) and T$_g$ from the peak of the loss modulus. The mixture of furan-based epoxy was prepared based on the mole ratio. The E' at room temperature was 3.6 GPa and the T$_g$ was 43 °C, as shown in figure 133.
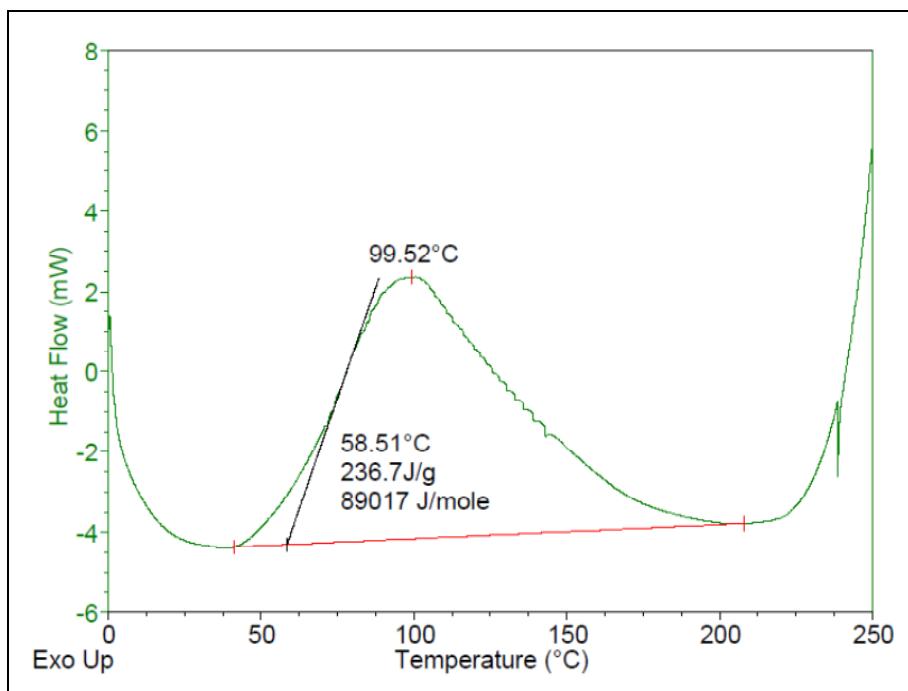
Figure 131. Furan-based epoxy resin cured with PACM based on EEW.

179
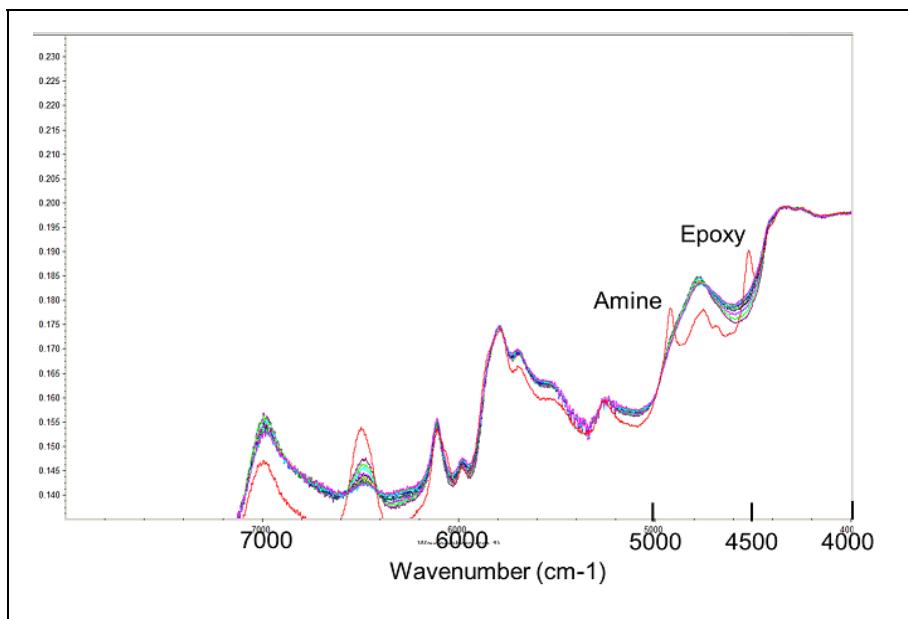
Figure 132. The cure kinetics of furan-based epoxy and PACM by using NIR at 90 °C for 3 h. All spectra were obtained every 15 min. The red spectrum is an initial one before heating up.
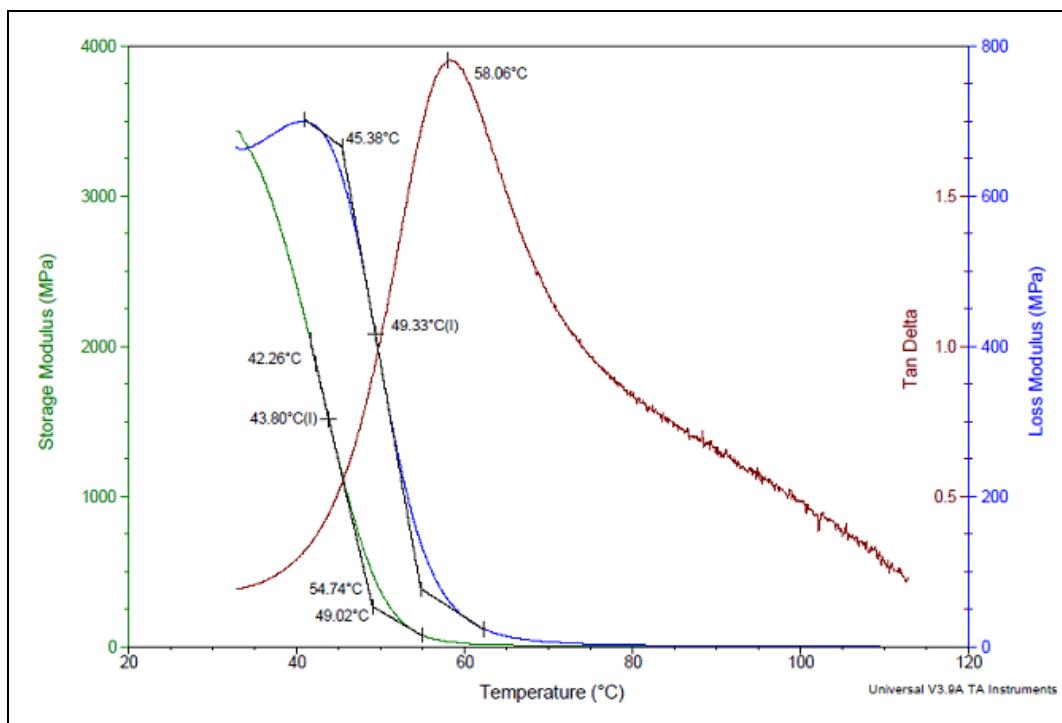
Figure 133. The DMA data of furan-based epoxy and PACM system based on a mole ratio of 2 and 1. The T_g from loss modulus was 43 °C.

Furan-based epoxy monomers synthesized from the conventional method and the method without water were cured with PACM. A DSC experiment was performed to obtain the T_g. It was expected that the furan-based epoxy from the method without water could show higher T_g than that from the conventional method because of the low EEW value. From figures 134 and 135, it was confirmed that the hypothesis was correct: the T_g's from the conventional method and the method without water were 7 and 22 °C, respectively. The T_g might increase if a furan-based epoxy having an EEW close to the theoretical EEW value could be prepared.
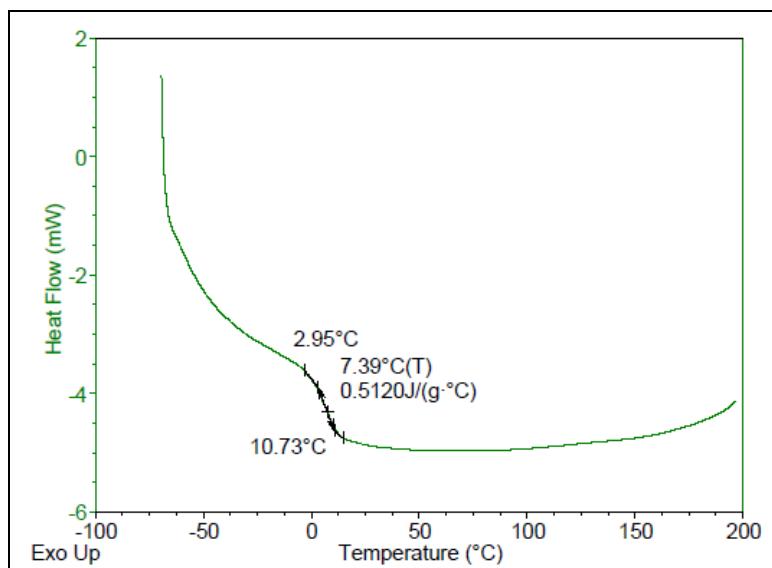
Figure 134. DSC thermogram of PACM and furan-based epoxy from the conventional method.
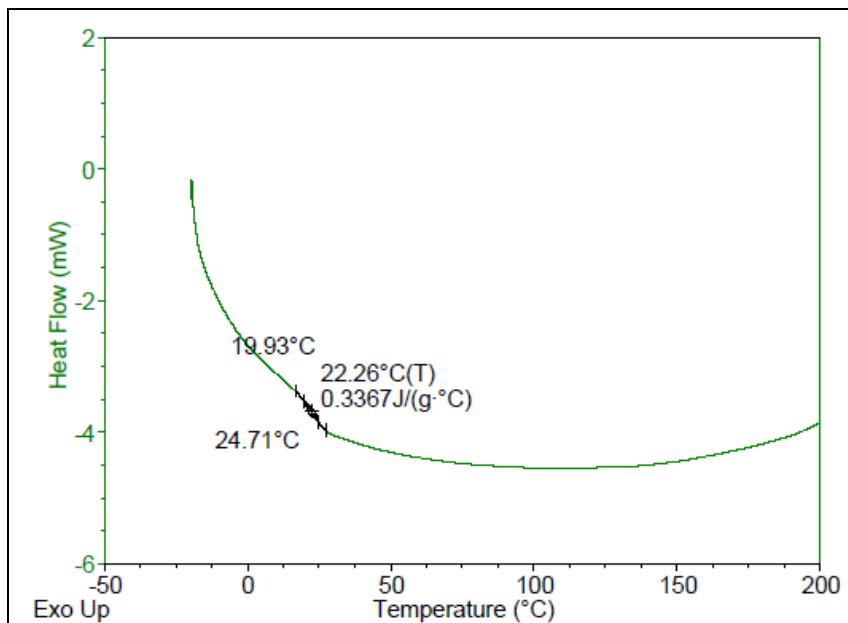
Figure 135. DSC thermogram of PACM and furan-based epoxy from the method without water.

181

8.4   Conclusion

To obtain a high yield and reduce by-product, furan-based epoxy was synthesized via various synthetic approaches, such as using DMF instead of water and applying the water-controlled method, the method without water, and the conventional method. Furan-based epoxy from the method without water showed the lowest EEW value. However, optimization is needed to obtain furan-based epoxy with a high yield, short reaction time, and reduced side reaction. In order to increase the T_g of furan-based epoxy resin, the chemical structure is being analyzed by using GPC and mass spectroscopy. In addition, the synthetic strategy will be updated based on the characterization of chemical structures and the properties of thermosetting resins. Besides the furan-based epoxy and PACM system, furan-based epoxy itself was cured with the catalyst, DPI of 1 wt%. The characterization is still being investigated by using modulated differential scanning calorimetry (MDSC) and DMA. Table 18 highlights the work that needs to be accomplished in this section and time lines.

Table 18. Future work and time lines for 2012 and 2013.

Task No.	Calendar Year / Task	2012				2013			
		Quarter							
		1	2	3	4	1	2	3	4
1.	Preparation of biobased monomers	🟨	🟨	🟨	🟨				
1.1.	Scale-up of furan-based epoxy monomer	🟩	🟩						
1.2.	Scale-up of sugar-based monomers and modifications	🟩	🟩		🟩				
1.3.	Synthesis of sugar-based epoxy monomer	🟩							
1.4.	Synthesis of sugar-based vinyl ester monomer		🟩						
1.5.	Synthesis of sugar-based unsaturated polyester monomer			🟩					
1.6.	Scale-up of sugar-based monomers		🟩	🟩	🟩				
2.	Resin preparation		🟨	🟨	🟨	🟨	🟨		
2.1.	Cure analysis		🟩	🟩	🟩				
2.2.	Resin properties			🟩	🟩	🟩	🟩		
3.	Biobased composite preparation				🟨	🟨	🟨	🟨	🟨
3.1.	Properties of carbon fiber/biobased resin composites				🟩	🟩	🟩	🟩	🟩
3.2.	Investigation of interface between carbon fiber and biobased resin					🟩	🟩	🟩	🟩

9.   Isosorbide-Based Unsaturated Polyester Cross-Linkers

9.1   Introduction

Most of the thermosetting resins are produced from petroleum feedstocks. Because of the high prices of fossil fuels and the demand to protect health and the environment, there is a heightened interest in manufacturing polymeric materials from renewable materials with similar or better mechanical and thermal properties compared to those currently produced from petroleum resources. For a long-term goal, using renewable resources as a feedstock will help to stabilize the cost and supply of polymeric materials. Many different renewable resources such as starch (*1*), cellulose (*2*, *3*), and lignin (*4*) can be used as a feedstock for biobased thermosetting resins.

There are several types of thermosetting resins, such as epoxy, VE, and UPE. Unsaturated polyester resins are widely used as the matrix materials for polymer composites because of the relatively low cost, good balance of properties, and adaptability to many fabrication processes. There are many publications regarding the synthesis, analysis, curing process, and properties of UPE resins. UPE resins are products formed by a condensation reaction between unsaturated and saturated acids/anhydrides and diols. The UPE is mixed with a reactive diluent (typically vinyl monomers such as styrene and methyl methacrylate) to obtain a liquid mixture with a low viscosity that can be easily cast or molded without high pressures and polymerized at rates faster than the homopolymerization rate of the UPEs by themselves (*5*). Unsaturated sites (i.e., carbon-carbon double bonds) react with reactive diluents by radical initiators to form 3-D polymer chain networks. Epoxy thermosetting resins are the class of polymeric materials that contain more than one epoxy group situated terminally, cyclically, or internally on the molecule and will create a cross-linked solid product based on thermosetting reaction.

In UPE, 1,4;3,6-dianhydro-D-glucitol (isosorbide) (*6*, *7*) is an attractive material. The polymers derived from isosorbide, which have been investigated, include polyesters (*8*), polycarbonates (*9*), polyurethanes (*10–12*), and polyamides (*13–15*). Isosorbide is a renewable material derived from sorbitol that is obtained from glucose (*16*). It consists of two combined tetrahydrofuran rings with cis-arrangement, showing a V-typed molecule and two hydroxyl groups. Technically, the precursor containing ring structures is a high-potential candidate for the production of high mechanical and thermal performance resins. Jasinska and Koning (*17*) reported that the biobased UPEs from isosorbide, MA, and succinic acid were polymerized and analyzed. However, the polymers with broad PDI were obtained via a complex synthetic process at a high reaction temperature (~230 °C) where a toxic catalyst (titanium [IV] n-butoxide) was used for the polymerization. MA is manufactured from n-butane as a feedstock. It is also possible to produce MA in biological processes (*18*).

The first epoxy resin was introduced in the late 1930s with the reaction of bisphenol A and epichlorohydrin, creating DGEBA resin. Most epoxy resins are chemical and corrosion resistant, have good mechanical and electrical behavior, and can adhere to many types of materials. Besides isosorbide, one major molecule from hexoses is 5-hydroxymethylfurfural (HMF), consisting of aldehyde, hydroxy, and furan. Furan-based epoxy resin was prepared from the furan derivative.

A biobased unsaturated monomer (UPE1), a chain-extended molecule (UPE2), and sequence-inversed monomer (UPE3) derived from isosorbide and MA were synthesized under a moderate condition. The cross-linker itself is not polyester. However, once the cross-linker is cured with a reactive diluent, the polymer chain network will become cured polyester. The end group on the cross-linkers was modified with the hydrophobic group to improve the solubility with reactive diluents, such as styrene and methyl methacrylate (MMA). In addition, many thermosetting resins use VOCs and HAPs in the manufacturing process (*19, 20*). Most of the reactive diluents are VOCs and HAPs. These chemicals risk the health and safety of plant employees and the general public. It is important that scientists find an environmentally friendly natural replacement for these materials to reduce or remove this risk. A biobased reactive diluent is also introduced as a replacement for styrene. From a furan derivative, furan-based epoxy resin was synthesized and cured with PACM to obtain thermosetting epoxy resins.

9.2 Experimental

9.2.1 Synthesis of Isosorbide-Based Cross-Linkers (UPE1, UPE2, and UPE3)

Isosorbide (0.183 mol, 26.85 g) and MA (0.42 mol, 38.67 g) were put in a 250 mL round flask. A nitrogen gas environment was prepared with a schlenk line. After toluene (10 mL) was injected, the flask was put in an oil bath at 100 °C, and the reagents were mixed for 30 min. N,N-dimethyl benzyl amine (0.55 mL, 3.66 mmol) was injected into the flask, and the reaction was carried out for 18 h. The cross-linker (UPE1) was put in a vacuum oven to evaporate toluene for 24 h. The obtained cross-linker (UPE1) is a monomer-type shown in figure 136. The yield was about 90 wt%.

To synthesize the chain-extended molecule (UPE2) shown in figure 136, the mole ratio of isosorbide and MA was 2 to 3. MA (15 g, 0.154 mol) and isosorbide (15 g, 0.1026 mol) were dissolved in toluene (10 mL) at 100 °C under a nitrogen gas environment. A catalyst, N,N-dimethyl benzyl amine (0.31 mL, 2.05 mmol), was added in the mixture, and the reaction was conducted for 18 h. The yield was about 90 wt%.

The sequence-inversed monomer (UPE3) was also prepared, and the sequence order was isosorbide-maleate-isosorbide (figure 136). The mole ratio of isosorbide and MA was 2 to 1. Synthesis condition and termination processes are the same as the processes for UPE1.
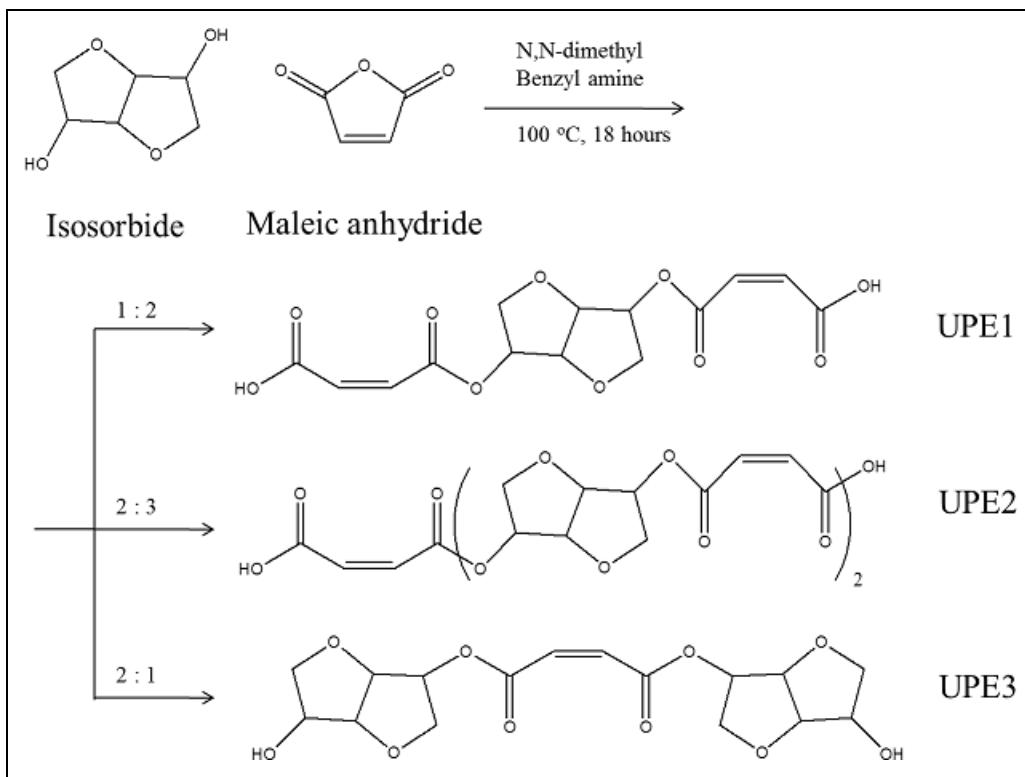
Figure 136. Synthesis of biobased monomer (UPE1), chain-extended molecule (UPE2), and sequence-inversed monomer (UPE3).

9.2.2 End Group Modification

The hydroxy end on UPE1 and UPE2 was converted to hydrophobic end, such as hexyl (H) or benzyl (B) groups. One end and two ends were modified to investigate the effect of the modification on solubility with reactive diluents. The benzyl-one end modified UPE2 and hexyl-two ends modified UPE1 are symbolized as B-UPE2 and H-UPE1-H, respectively.

H-UPE1: The synthetic route of H-UPE1 is shown in figure 137. UPE1 (16.1 g) was put in a 250-mL round flask, and toluene (10 mL) was injected in the flask under nitrogen gas. The flask was immersed in an oil bath at 100 °C. 1-hexanol (5.33 g) and p-toluenesulfonic acid (0.18 g) were mixed in a beaker, and the solution was injected in the flask. The reaction was carried out for 18 h at 100 °C. The final solution was diluted with ethyl acetate and washed with DI water three times. The ethyl acetate and unreacted 1-hexanol were evaporated by using a rotary evaporator. The yield was about 70%.
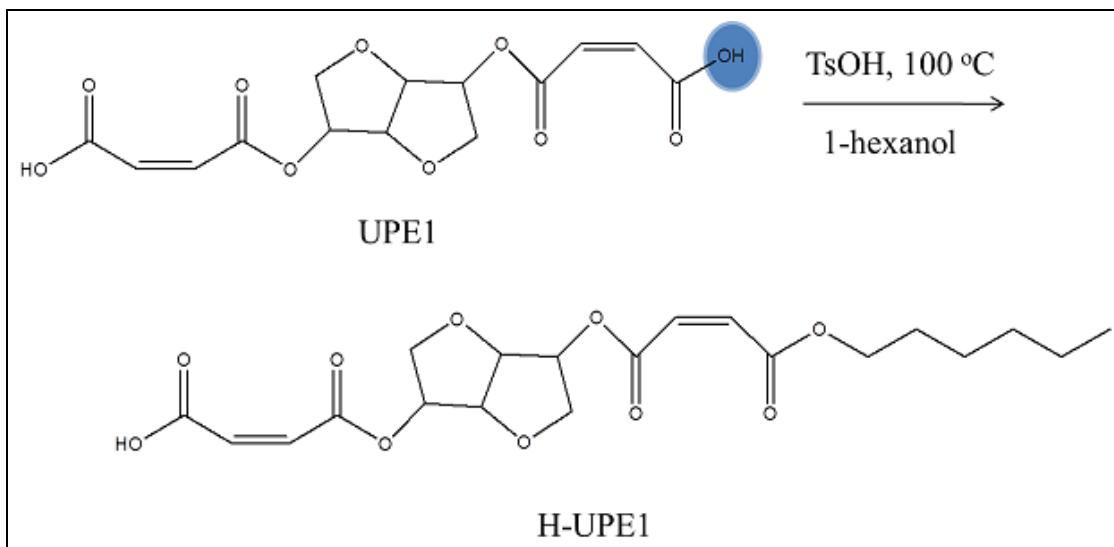
Figure 137. End group modification of UPE1 from hydroxy to hexyl group.

H-UPE1-H: UPE1 (20.82 g) and toluene (10 mL) were mixed in a flask under a nitrogen gas environment at 100 °C. The solution of 1-hexanol (13.72 g) and p-toluenesolfonic acid (0.233 g) was injected in the flask. The yield was about 80%.

H-UPE2: UPE2 (14.4 g) was mixed with toluene (10 mL) at 100 °C under nitrogen gas. 1-hexanol (2.1 g) and p-toluenesulfonic acid (0.086 g) were injected in the flask, and the reaction was conducted for 20 h. The yield was about 70%.

H-UPE2-H: UPE2 (14.4 g) was blended with toluene (10 mL) at 100 °C under nitrogen gas. 1-hexanol (5.1 g) and p-toluenesulfonic acid (0.086 g) solution were added in the flask. The yield was about 80%.

B-UPE1: The synthetic route of B-UPE1 was shown in figure 138. UPE1 (27.2 g) was put in a 250-mL round flask, and toluene (10 mL) was injected in the flask under nitrogen gas. The flask was immersed in an oil bath at 100 °C. Benzyl alcohol (8.63 g) and p-toluenesulfonic acid (0.3 g) were mixed in a beaker, and the solution was injected in the flask. The reaction was carried out for 20 h at 100 °C. The final solution was diluted with ethyl acetate and washed with deionized water three times. The ethyl acetate and unreacted benzyl alcohol were evaporated by using a rotary evaporator. The yield was about 65 wt%.

B-UPE1-B: UPE1 (16.51 g) was added in a flask and prepared in a nitrogen gas environment. Toluene (10 mL) was injected, and the flask was placed at 100 °C. The solution of benzyl alcohol (11.51 g) and p-toluenesulfonic acid (0.184 g) was added in the flask, and the reaction was performed for 20 h. The yield was about 70%.

B-UPE2: UPE2 (20 g) was mixed with toluene (10 mL). The solution, p-toluenesulfonic acid (0.12 g) and benzyl alcohol (4.153 g), was injected in the flask. The yield was about 70%.

186
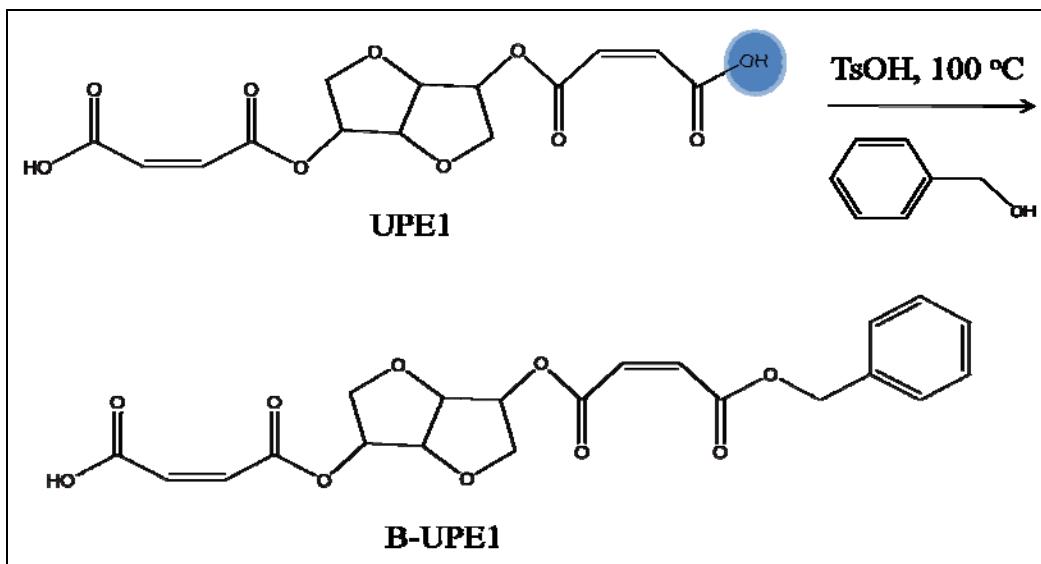
Figure 138. End group modification of UPE1 from hydroxy to benzyl group.

B-UPE2-B: UPE2 (18.1 g) was blended with toluene (10 mL), and the solution, p-toluenesulfonic acid (0.1083 g) and benzyl alcohol (6.8 g), was injected in the flask. The yield was about 75%.

9.2.3 Preparation of UPE3 Diglycidyl Ether

The reaction, shown in figure 139, was carried out with a Dean-Stark trap and condenser under a nitrogen gas environment. UPE3 (6.94 g) and epichlorohydrin (6.9 g) were put in a flask. The solution was heated to reflux at 120 °C. Sodium hydroxide (1.6 g) in water (5 g) was added dropwise to the flask for 2 h. Then, the reaction was left for 1 h to complete. After the solution was cooled to room temperature, the solution was filtered, diluted with ethyl acetate, and washed with water. Solvents were evaporated by a rotary evaporator.
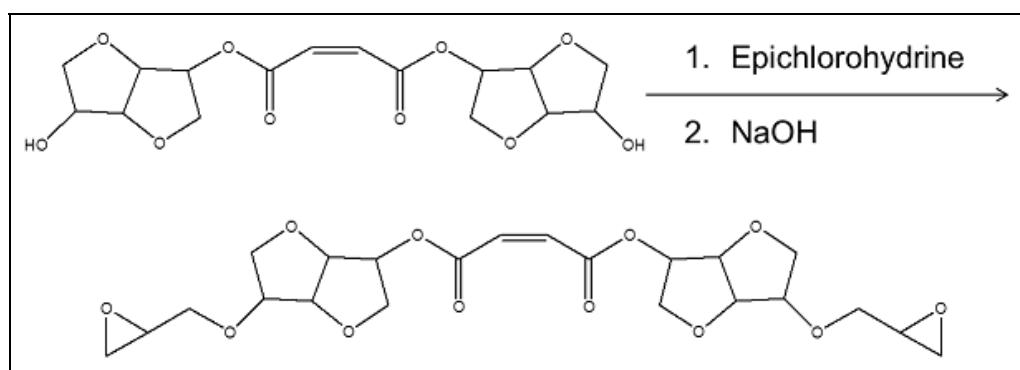
Figure 139. UPE3 glycidyl ether by the reaction of UPE3 cross-linker and epichlorohydrin.

9.2.4 Blending of Unmodified Cross-Linker and Reactive Diluent

The initial blending condition of cross-linker and reactive diluent was 70 and 30 wt%. If cross-linker mixed completely with reactive diluent, the result was 70/30. If cross-linker did not mix well with reactive diluent, a double layer should be observed (figure 140). The example is a UPE1/styrene (70/30) mixture. The mass of unmixed reactive diluent layer was measured, and the amount of the reactive diluent mixed with cross-linker was determined by the mass of the unmixed reactive diluent.

Figure 140. Photograph showing insolubility of
UPE1/styrene (70/30).

9.2.5 Blending of Modified Cross-Linker and Reactive Diluent

All modified UPE cross-linkers were mixed well with styrene and MMA of 30, 40, and 50 wt%, respectively. All blending was clear, and there was no phase separation.

9.2.6 Resin Cure

A modified cross-linker solution containing various amounts of reactive diluents such as styrene, methyl methacrylate, and MAA was prepared. The mixtures were cured overnight at 70 °C using a Norox MEKP-9, whose mass was 3 wt% of the total cross-linker solution weight, and then postcured at 150 °C for 3 h.

9.2.7 Polymer Characterization

The isosorbide-based cross-linkers and their thermosetting resins were analyzed by NMR, GPC, mass spectrometry (MS), MDSC, or DMA. The chemical structures of unmodified and modified cross-linkers and the number-average molecular weight (M_n) were determined by ^{1}H NMR. All samples were dissolved in dimethyl sulffoxide-d6 (DMSO-D6) or CDCl$_3$ solvent for NMR analysis. Spectra were acquired at 25 °C using the 500-MHz Unity Inova Varian NMR instrument operated with VNMR 6.1B software. The pulse sequence was as follows: relaxation delay (0.3 s), pulse (54.6°), acquisition time (3.744 s), width (4000.00 Hz), number of data points (32,768), and total acquisition time (1 min, 4 s).

Waters AutoSpec Ultima Q triple sector mass spectrometer was carried out with positive ion CI mode (chemical ionization) by using methane as the ionizing gas [CI+ with CH$_4$]. A solid probe was ramped from 50 to 150 °C at a rate of 25 °C/min.

M_w, M_n, and PDI (M_w/M_n) were determined by a GPC system consisting of a Waters 515 HPLC pump, a Waters RI 2410 detector, first column (Perkin-Elmer, single pore size, effective molecular weight range: up to 2000), and second column (Perkin-Elmer, mixed pore size, linear molecular weight range: 200 ~ 2,000,000). GPC was carried out at a flow rate of 1.0 mL/min at 30 ℃ and eluted with DMF. The sample concentration was 1.0 ~ 1.5 mg/mL. A calibration curve was developed with polystyrene standard data and estimated molecular weights.

The thermomechanical properties of UPE thermosetting resins were measured by using DMA. Rectangular samples with approximate dimensions of $17.5 \times 12.0 \times 2 \text{ mm}^3$ were investigated by using a TA Instruments Q800 in the single cantilever method. The samples were tested at 1 Hz with a deflection of 7.5 μm, and the temperature from –20 to 150 °C was ramped at a rate of 2 °C/min. Two temperature ramp experiments were carried out for each sample. The DMA traces for the first and second ramps were almost identical, meaning that cure and postcure processes were applied properly for this polymer system. At the T_g, the storage modulus decreases intensely, and the loss modulus reaches the highest point. In this report, the temperature at which the peak in the loss modulus occurred was selected as the T_g of the cured resin.

An MDSC measurement was performed using a DSC Q2000 (TA instrument) to obtain T_g from reversible heat flow. The modulation temperature amplitude, modulation, and ramp rate were ±1.0 °C, 60 s, and 3 °C, respectively. The T_g was determined by the middle of the transition.

9.3   Results and Discussion

9.3.1 Synthesis of Isosorbide-Based Cross-Linkers

The chemical structures of UPE1 and UPE2 were confirmed by ^{1}H NMR as shown in figure 141. The main peaks of the UPE cross-linkers were assigned based on the literature (*17*). According to Jasinska and Koning (*17*), the chemical structure was confirmed by using two-dimensional NMRs, such as Correlation Spectra (COSY), Heteronuclear Multiple-Bond Correlation Spectra, and Heteronuclear Single Quantum Correlation Spectra; this allowed them to determine the sequence of specific protons and carbons. As shown in figure 141(a), the unsaturated part (a,b) was found near 6.4 ppm, and the protons (d,g) attached between isosorbide and maleate appeared near 5.3 ppm. The peak integration ratio of (a,b) and (d,g) was 2 to 1, meaning that the monomer type of the cross-linker consisting of one isosorbide and two maleic acid half esters, UPE1, was obtained successfully. Figure 142 shows the mass spectrum of UPE1. The magnified insert contained the target molecular weight, 343 g/mol. However, the MS spectrum provides only qualitative information. Figure 143 shows GPC data of the UPE1 cross-linker, where M_w, M_n, and PDI were 344 g/mol, 324 g/mol, and 1.06, respectively. Those results confirmed that the monomer type of UPE cross-linker, UPE1, was synthesized with a narrow molecular weight distribution.
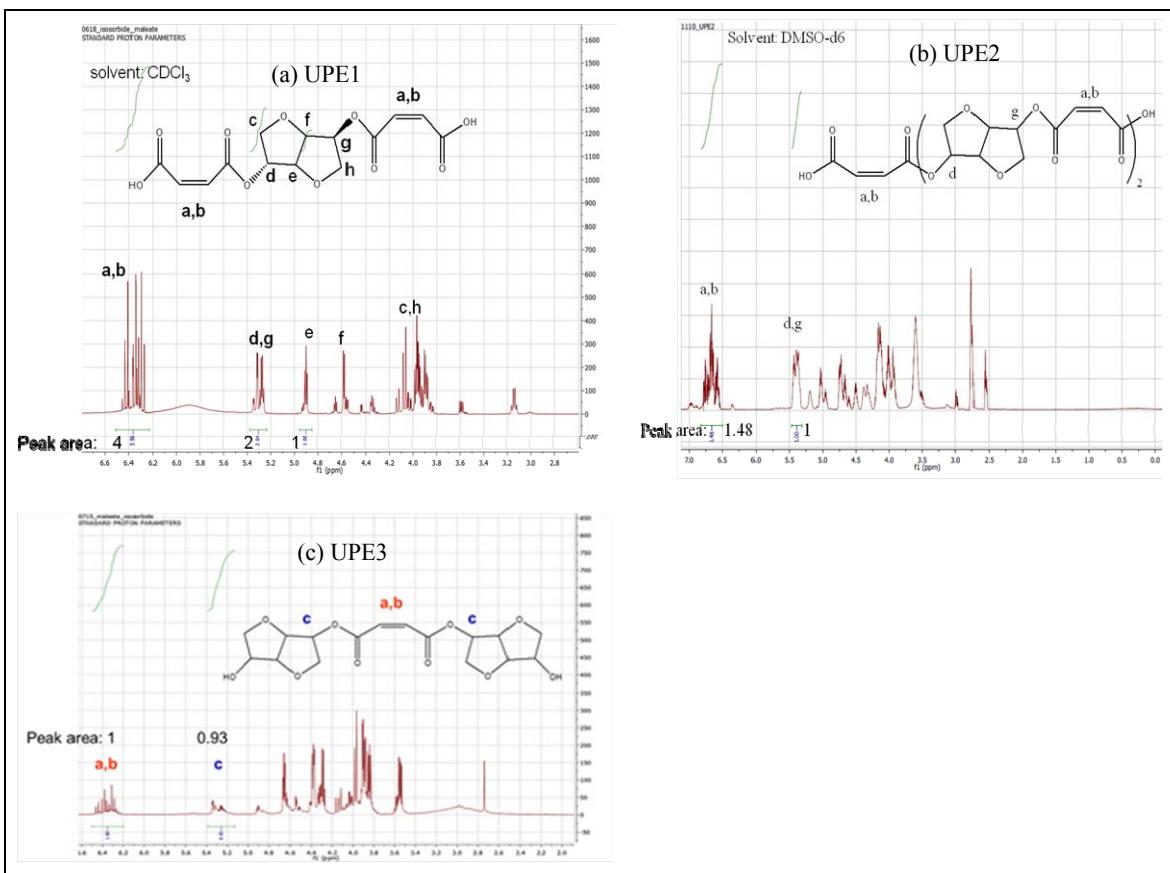
Figure 141. NMR spectra of isosorbide-based cross-linkers: (a) UPE1, (b) UPE2, and (c) UPE3.
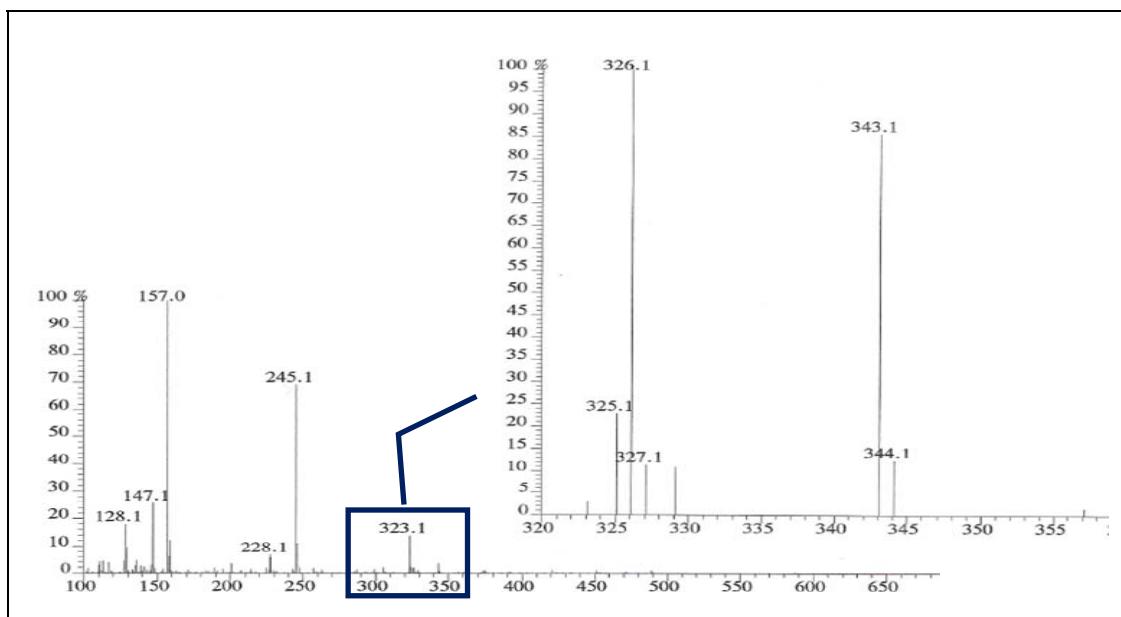
Figure 142. Mass spectrum of UPE1.

	Mw	Mn	PDI
UPE1	344	324	1.06
UPE2	614	450	1.36
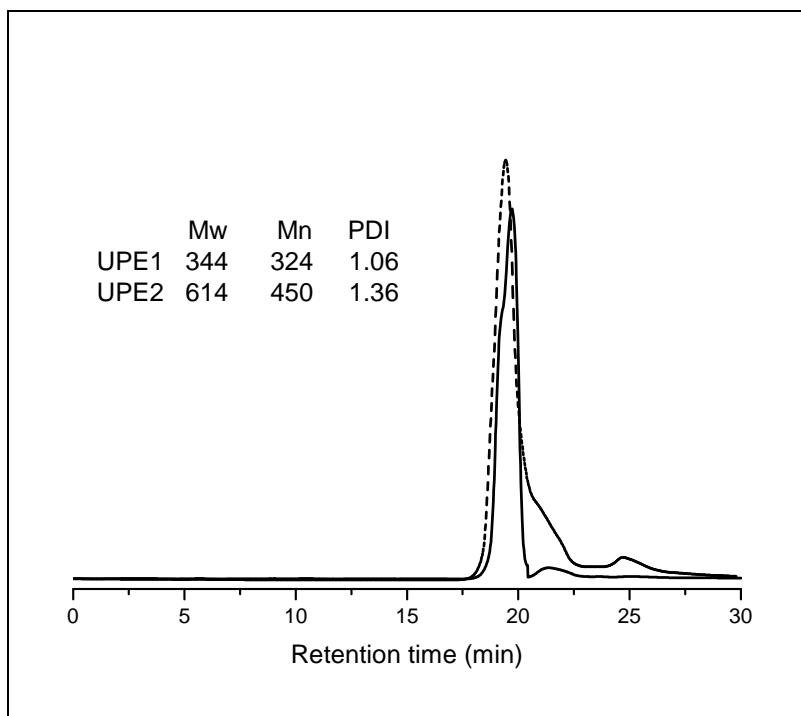
Figure 143. GPC data of UPE1 (solid line) and UPE2 (------).

The chemical structure of the chain extended type of UPE cross-linker, UPE2, was also confirmed by ^{1}H NMR and GPC. The target molecular weight was 556 g/mol (number average repeating unit (n) = 2). The peak integration of (a,b) and (d,g) was 1.48 to 1, indicating that the number average molecular weight was 574 g/mol (n = 2.08) (figure 141 (b)). GPC (figure 143) confirmed that M_w, M_n, and PDI were 614 g/mol, 450 g/mol, and 1.36, respectively. UPE3 was also confirmed by NMR. The integration ratio of (a,b) and c was 1:1, meaning that the molecule consists of two isosorbides and one maleate.

9.3.2 Blending of UPE Cross-Linkers and Reactive Diluents

The synthesized UPE cross-linkers were mixed with various reactive diluents, such as styrene, MMA, and MAA to prepare thermosetting resins. Table 19 summarized the blending results. However, the cross-linkers showed a poor solubility with reactive diluents (figure 140). UPE1 was mixed with styrene of up to 1.5 wt%, while UPE2 was blended with styrene of up to 15 wt%. For UPE thermosetting resins, 25–60 wt% of the reactive diluent is used in general. The solubility of the cross-linker and the reactive diluent became a big problem when preparing thermosetting resin. MMA demonstrated better solubility than styrene. However, UPE1 and UPE2 still showed a poor solubility of up to 10 and 30 wt% with MMA, respectively. MAA was blended completely with UPE cross-linkers.

191

Table 19. Blending of UPE cross-linkers and reactive diluents. Initial blending condition: cross-linker/reactive diluent (70/30 wt%).

Unsaturated Polyester	Styrene	Methyl Methacrylate (MMA)	Methacrylic Acid (MAA)
UPE1	98.5/1.5	90/10	70/30
UPE2	85/15	70/30	70/30
UPE3	92/8	84/16	70/30

Most of the reactive diluents have hydrophobic properties rather than hydrophilic ones. Based on the chemical structure of the UPE cross-linkers, it was expected that the end group modification of the hydroxy ends on the UPE cross-linkers would be a key point to solve the solubility problem. Two different types of hydrophobic end groups (hexyl and benzyl) were selected to improve blending properties.

9.3.3 End Group Modification of Cross-Linkers

The one hydroxy end of UPE1 cross-linker was modified to hexyl group. The modified UPE1 is symbolized as H-UPE1. As one more example, the symbol B-UPE2-B means that two hydroxy ends of UPE2 cross-linker were converted to two benzyl groups. H-UPE1, B-UPE1, B-UPE1-B, B-UPE2, and B-UPE2-B were prepared, and NMR confirmed their chemical structures as shown in figure 144. Figure 144(a) showed the chemical structure of H-UPE1. The integration ratio of (a,b) and (d,g) was 2 to 1, and the integration of the methyl group on the hexyl group, $-OCH_2(CH_2)_4CH_3$, was 1.6, indicating that H-UPE1 was prepared successfully. In the case of B-UPE1 (figure 144(b)), the number of protons at the connection between isosorbide and maleate (d,g) at the unsaturated part (a,b) and at benzene (c) are theoretically 2, 4, and 5, respectively. The NMR spectrum (figure 144(b)) proved the chemical structure of B-UPE1. Figure 144(c) shows that the integration of benzyl (c) was two times higher than that of B-UPE1, meaning that B-UPE1-B was obtained. The chemical structure of B-UPE2 was also confirmed as shown in figure 144(d). The number average repeating unit (n) was 1.8, which was consistent with the previous UPE2 result and therefore proved the reproducibility. The integration of benzyl (c) indicated that B-UPE2 was also synthesized successfully because the number of protons on (d,g) and (c) was 3.56 to 5, respectively, and the integration ratio of (d,g) and (c) was 1 to ~1.4.
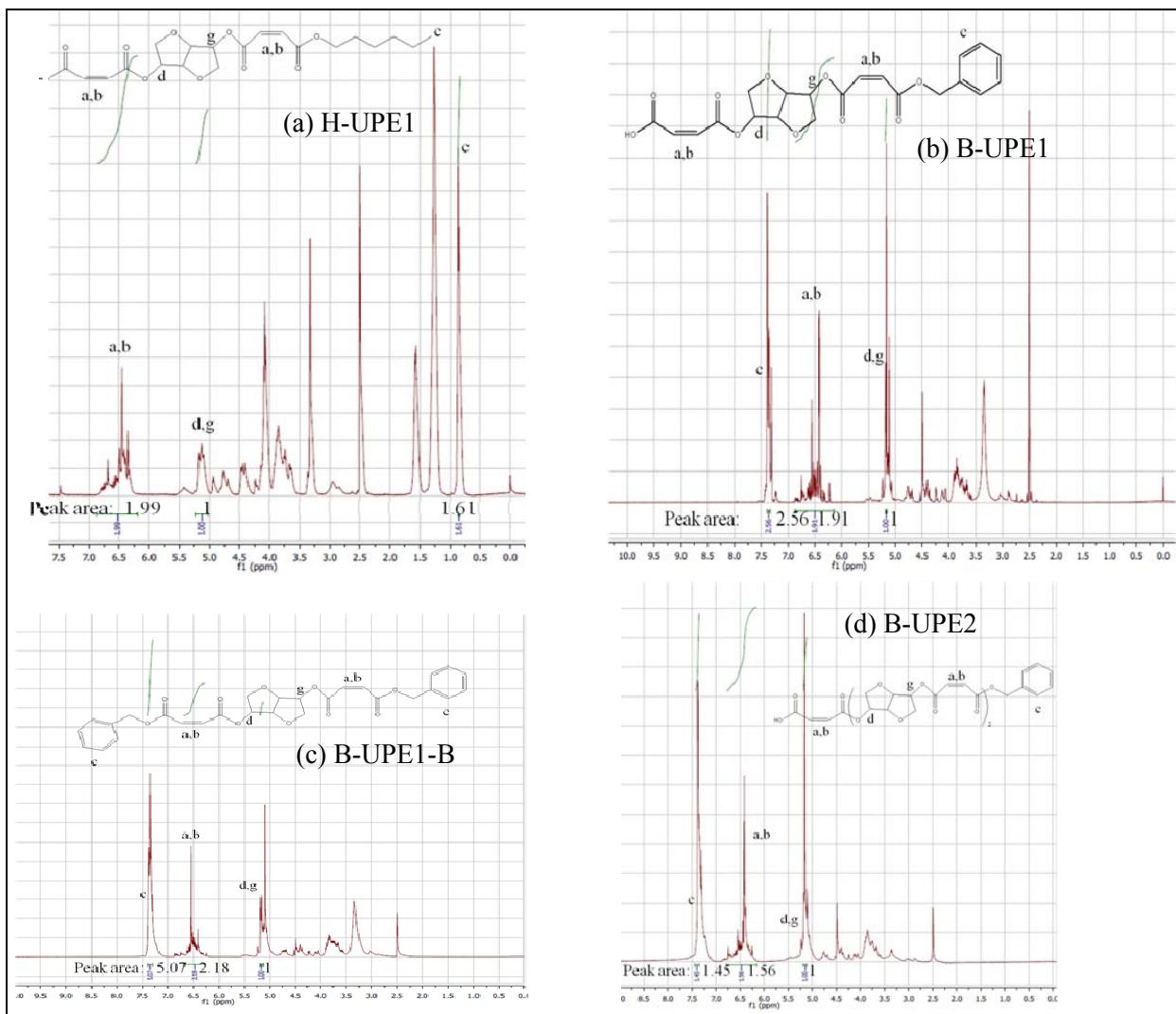
Figure 144. NMR spectra: (a) H-UPE1, (b) B-UPE1, (c) B-UPE1-B, and (d) B-UPE2.

9.3.4 UPE3 Diglycidyl Ether

Instead of end group modification, UPE3 attempted to obtain epoxy material as shown in figure 139. UPE3 diglycidyl ether should be dissolved in organic solvent. However, the final product was water-soluble, meaning that the reaction condition was not suitable for this reaction, and sodium hydroxide could attack ether linkage so that more hydroxy group might be generated. In most cases, sodium hydroxide is used to prepare epoxy resin.

9.3.5 Resin Cure

Table 19 summarized the cure results of modified cross-linkers (70 wt%) and reactive diluents (30 wt%). Most modified cross-linkers cured with styrene provided solid materials, while cured H-UPE1-H and H-UPE2-H were sticky. Cured, modified UPE resins with MMA and MAA showed low T_g below room temperature, and their status was viscous liquid, sticky, shrank, and/or bent.

193

Table 20. Cure results of modified cross-linkers (70 wt%) and reactive diluents (30 wt%).

Unsaturated Polyester	Styrene (30 wt%)	MMA (30 wt%)	Methacrylic Acid (30 wt%)
H-UPE1	Solid, flexible	Liquid	Shrank, bent, sticky surface
H-UPE1-H	Sticky solid	Liquid	shrank, bent, sticky surface
H-UPE2	Solid, flexible	Liquid	Shrank, bent, sticky surface
H-UPE2-H	Sticky solid	Liquid	Shrank, bent, sticky surface
B-UPE1	Solid	Sticky solid	Sticky solid
B-UPE1-B	Solid	Sticky solid	Sticky solid
B-UPE2	Solid	Sticky solid	Sticky solid
B-UPE2-B	Solid	Sticky solid	Sticky solid

The double bond in uncured and cured cross-linkers was monitored by FTIR (figures 145 and 146). The H-UPE1 has an unsaturated part (double bond) near 1620 cm^{-1}. After it was cured with 30 wt% styrene, the strong intensity decreased significantly, meaning that the double bond reacted with diluents (figure 145). The H-UPE1 cure with 30 wt% MMA showed the decrease of double bond (figure 146). However, a solid polymer was not formed but instead a viscous liquid was obtained. The reasons for this are unclear, but they may indicate evaporation or phase separation of the reactive components to a position outside of the FTIR beam path.
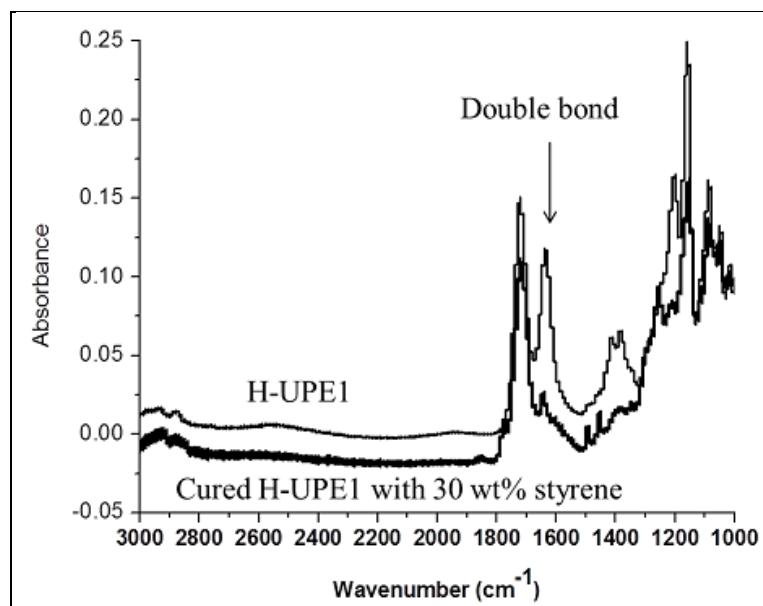
Figure 145. FTIR spectra of H-UPE1 and cured H-UPE1 with 30 wt% styrene.
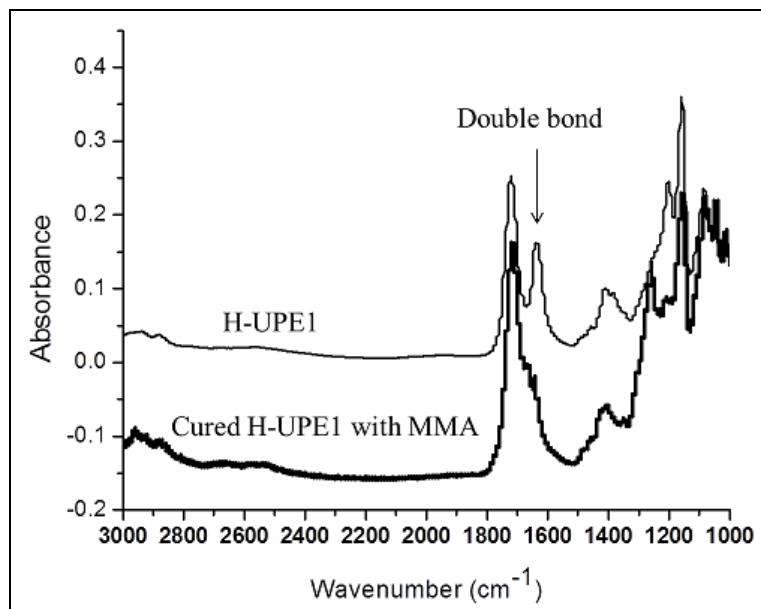
Figure 146. FTIR spectra of H-UPE1 and cured H-UPE1 with 30 wt% MMA.

9.3.6 Polymer Properties

The modified UPE cross-linkers mixed well with the 50 wt% styrene, while the unmodified UPE1 and UPE2 mixed with the styrene at a maximum concentration of 1.5 and 15 wt%, respectively. End group modification made it possible to mix the UPE cross-linkers with various amounts of styrene and prepared thermosetting resins. In order to investigate thermal and mechanical properties of the UPE thermosetting resins, DMA was employed to obtain the storage modulus (E' at 25 °C) and the T_g. The summary was displayed in table 21.

Table 21. T_g and E' at 25 °C in cured modified UPE resins with various amounts of styrene.

Unsaturated Polyester	Styrene					
	30 wt%		40 wt%		50 wt%	
	T_g (°C)	E' (GPa)	T_g	E'	T_g	E'
H-UPE1	3	0.5	—	—	—	—
H-UPE2	1, 8 (2nd)	0.25	—	—	—	—
B-UPE1	43	3.2	58, 70 (2nd)	3.6	47, 70 (2nd)	2.75
B-UPE1-B	—	—	28	2.7	35	3.4
B-UPE2	26	2.2	47, 65 (2nd)	3.1	53, 80	3.6
B-UPE2-B	21	2.1	30, 42 (2nd)	3.2	40, 55 (2nd)	3.3

The storage modulus and loss modulus of H-UPE1 and H-UPE2 cured with 30 wt% styrene were shown in figure 147. The H-UPE1 and styrene mixed well because of the end group modification by the hexyl group, and DMA displayed one peak of the loss modulus, indicating that there were no phase separation and microphase separation. The T_g and storage modulus at 25 ^{o}C were low, such as ~3 °C and 0.5 GPa, respectively. The T_g was determined by the peak of the loss modulus (21). The H-UPE2 and styrene also mixed well. However, microphase separation may occur in this resin because there were two peaks of the loss modulus. The T_g of the cured H-UPE2 resin was similar to that of the cured H-UPE1 resin, while the storage modulus of the cured H-UPE2 was lower than that of the cured H-UPE1.
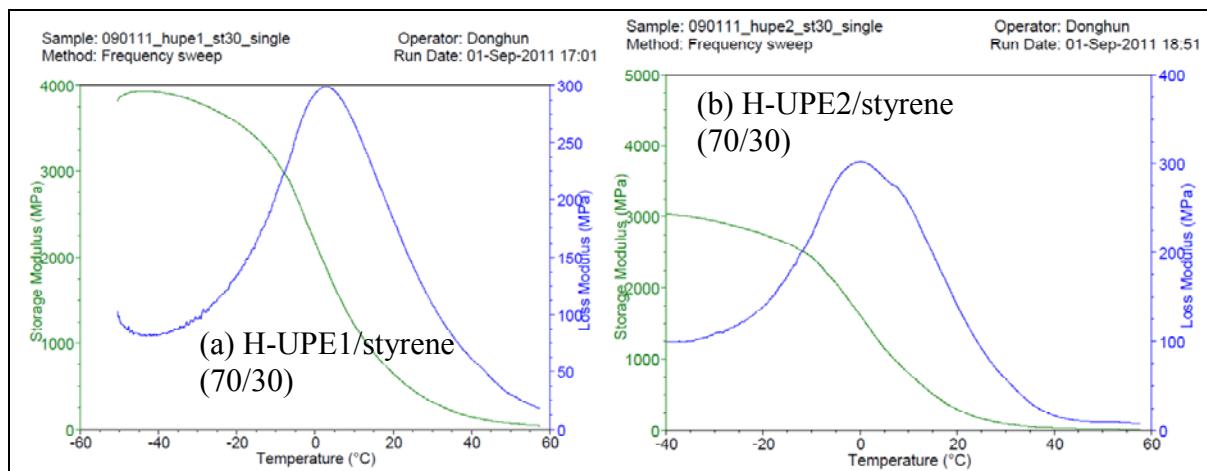
Figure 147. DMA data of cross-linkers cured with 30 wt% styrene: (a) H-UPE1 and (b) H-UPE2.

The hexyl end group could make the T_g decrease because of the plasticizer effect. Therefore, a different end group that includes a ring structure was tested to increase the thermal and mechanical properties of the thermosetting resins. In this report, the benzyl group was introduced at the end of the cross-linkers. Figure 148 shows the storage modulus and loss modulus as a function of temperature for B-UPE1 cured with various amounts of styrene, such as 30, 40 and 50 wt%. Before the cure process, the B-UPE1 and styrene mixture was clear, meaning that phase separation did not occur. Microphase separation may occur in the resins containing 40 and 50 wt% styrene because there was a peak and shoulders on the loss modulus. Overall, the benzyl end group provided higher T_g and modulus than the hexyl end group. B-UPE1 (60 wt%) with 40 wt% styrene exhibited a T_g of ~58 °C and a storage modulus at 25 °C of ~3.6 GPa while B-UPE1 (70 wt%) with 30 wt% styrene showed ~43 °C and ~3.2 GPa, respectively. The storage modulus and T_g increased when the amount of styrene was increased. These results are reasonable because the T_g of pure polystyrene is about 100 °C. However, the values decreased at the B-UPE1 (50 wt%) cured with 50 wt% styrene, and the microphase separation may occur based on the apparently broad loss modulus. In addition, there were three possible peaks near 25, 47 and 70 °C, suggesting that double end modification could provide better solubility of the cross-linkers and styrene.
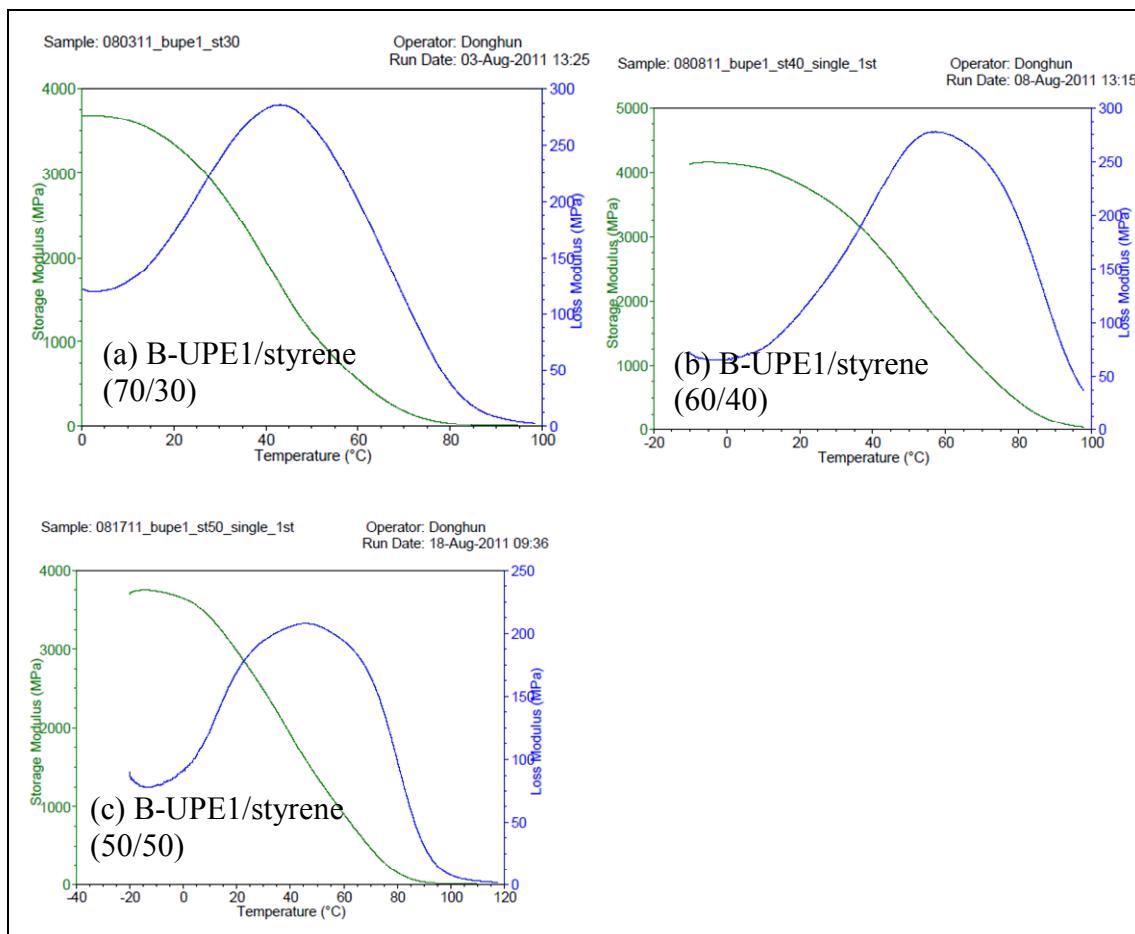
Figure 148. DMA, the B-UPE1 resins cured with styrene of 30, 40, and 50 wt%.

Figure 149 shows the DMA data of B-UPE1-B cured with 40 and 50 wt% styrene. Based on the mixture and the loss modulus of B-UPE1-B/styrene (60/40), there was no evidence of phase and microphase separation. B-UPE1-B/styrene (50/50) showed the improvement of the solubility between the cross-linker and styrene compared with B-UPE1/styrene (50/50). However, the introduction of one more benzyl group caused the reduction of T_g from ~47 to ~35 °C, while the storage modulus at 25 °C is from ~2.75 to 3.4 GPa.
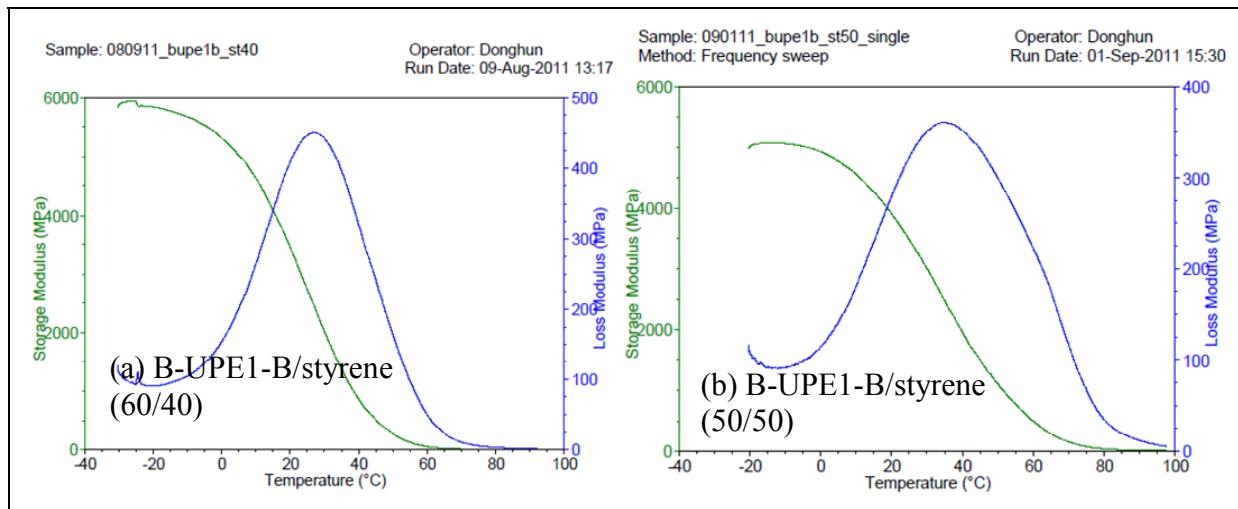
Figure 149. DMA, the B-UPE1-B resins cured with 40 and 50 wt% styrene.

One hydroxy end of the UPE2, the chain extended type of UPE1, was also modified by the benzyl group to improve the solubility of the UPE2 cross-linker and styrene. The B-UPE2 blended well with the 30, 40, and 50 wt% styrene to form apparently clear mixtures. After the curing process, DMA results were obtained, as shown in figure 150. The T_g and storage modulus at 25 °C increased when the amount of styrene was increased. The B-UPE2 resin cured with 30 wt% styrene showed a T_g of ~26 °C and a storage modulus of ~2.2 GPa at 25 °C with one peak of the loss modulus. According to the loss modulus of the B-UPE2/styrene (60/40) sample, one peak was shown at ~47 °C, and a shoulder appeared at ~65 °C. Furthermore, the shoulder turned to one peak at ~80 °C in the B-UPE2/styrene (50/50) sample. It was revealed that microphase separation might occur in the samples containing 40 and 50 wt% styrene. The B-UPE2/styrene (50/50) showed a T_g of 80 °C and a storage modulus of 3.6 GPa at 25 °C, which were the highest values among samples in this report. We expected that one end modification was insufficient to completely blend the UPE2 cross-linker with styrene. Therefore, both end group modifications of UPE2 were conducted; figure 151 exhibits storage and loss moduli of B-UPE2-B resin cured with 30, 40, and 50 wt% styrene, respectively. The modification in two end groups of UPE2 seemed to answer the problem of microphase separation. However, adding one more bulky end group caused a significant reduction of T_g, from 80 °C (B-UPE2/styrene (50/50)) to 40 °C (B-UPE2-B/styrene (50/50)).
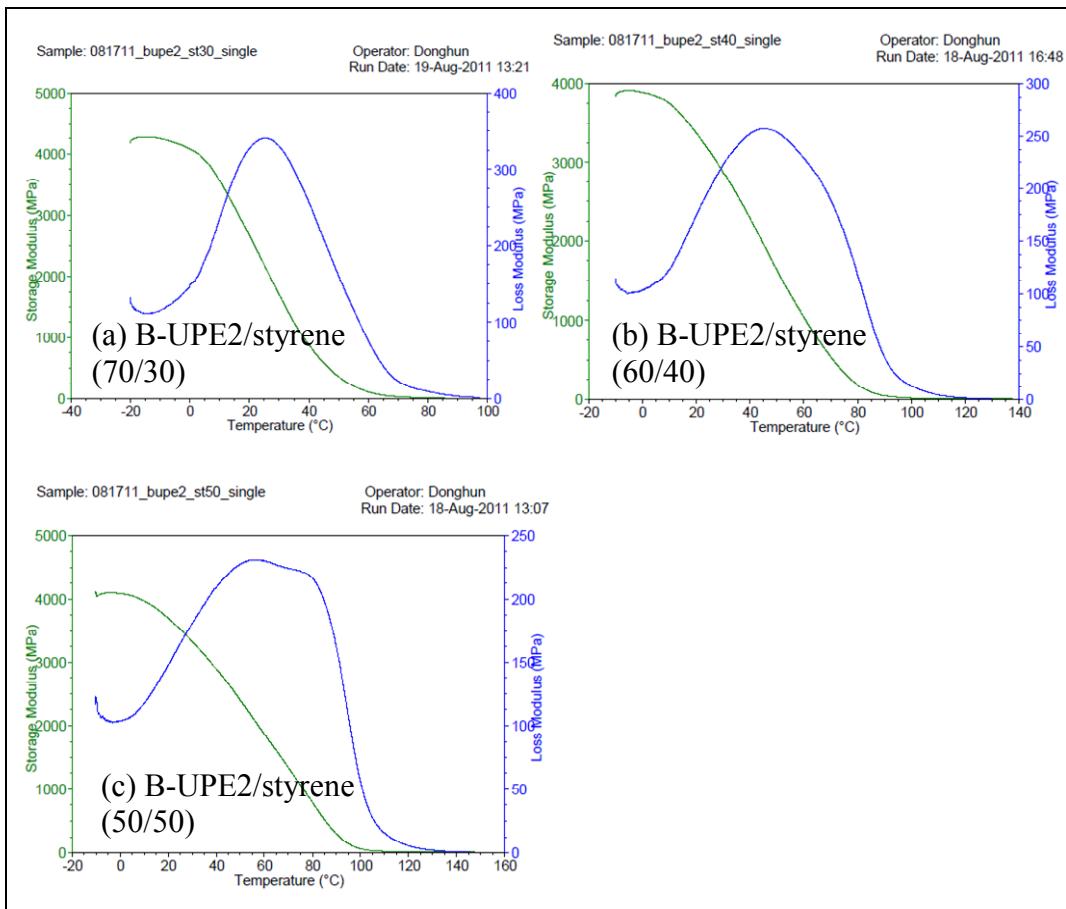
Figure 150. DMA, the B-UPE2 resins cured with 30, 40, and 50 wt% styrene.
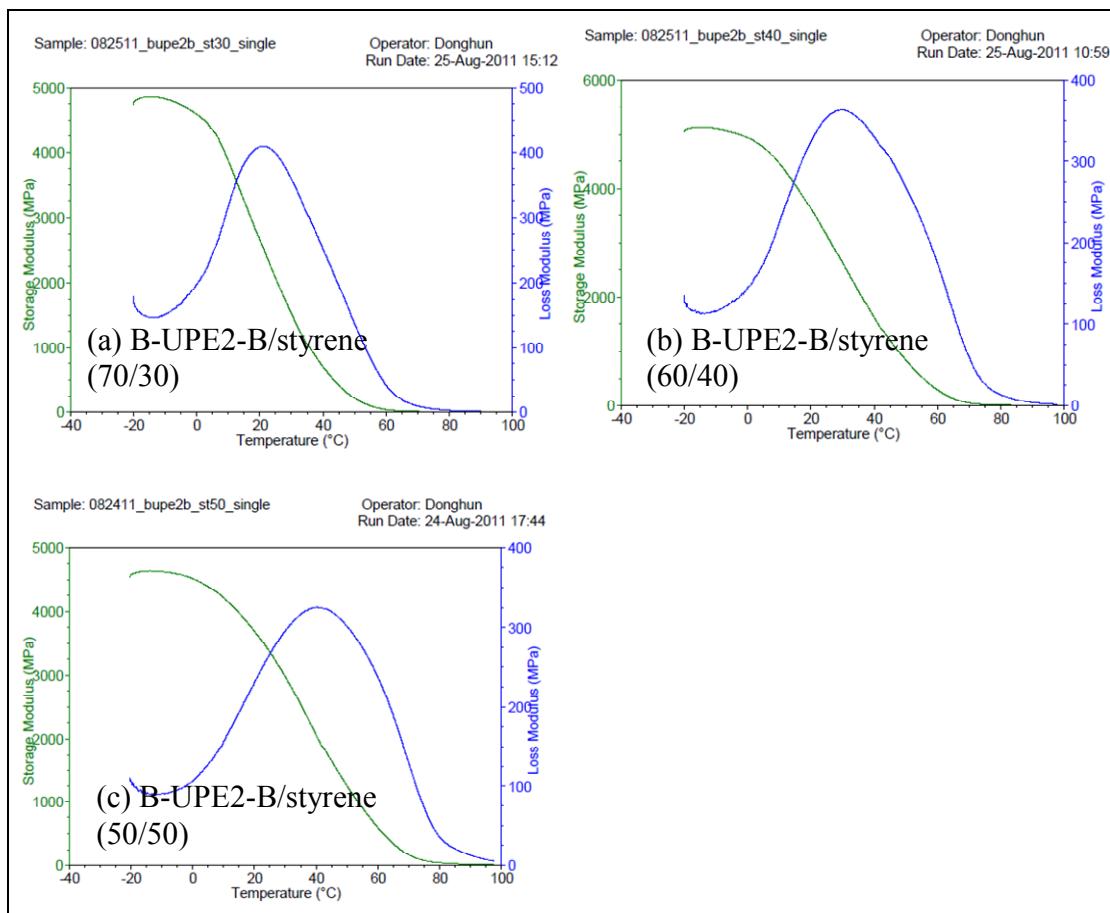
Figure 151. DMA, the B-UPE2-B resins cured with 30, 40, and 50 wt% styrene.

9.3.7 Ternary Blends

Thus far, this section has covered the properties of biobased UPE thermosetting resins cured with styrene. As a reactive diluent, styrene has been used for several decades because of its low cost and excellent properties. Recently, scientists have been researching a replacement for styrene that uses renewable sources. Because styrene is a HAP and VOC, the EPA presented legislation to limit styrene emission from composite manufacturing (*19*). La Scala et al. (*19*) reported that fatty acid–based monomers were used as a styrene replacement to reduce styrene emissions. An MFA monomer was prepared by the reaction between lauric acid (one of the fatty acids) and glycidyl methacrylate with 1 wt% of AMC-2 at 90 °C. The synthesized monomer was symbolized as MLau. The MLau efficiently replaced about 15 wt% styrene while maintaining proper thermal and mechanical properties of thermosetting resins. The MLau was received and used for this research.

The ternary blend of B-UPE1 (60 wt%), styrene (30 wt%), and MLau (10 wt%) was cured. The T_g was obtained by modulated DSC (figure 152), showing that the T_g determined from the reversible heat flow curve was ~60 °C. B-UPE1/styrene/MLau (60/30/10) should be compared to B-UPE1/styrene (60/40). Therefore, the effect of 10 wt% styrene replacement was found.
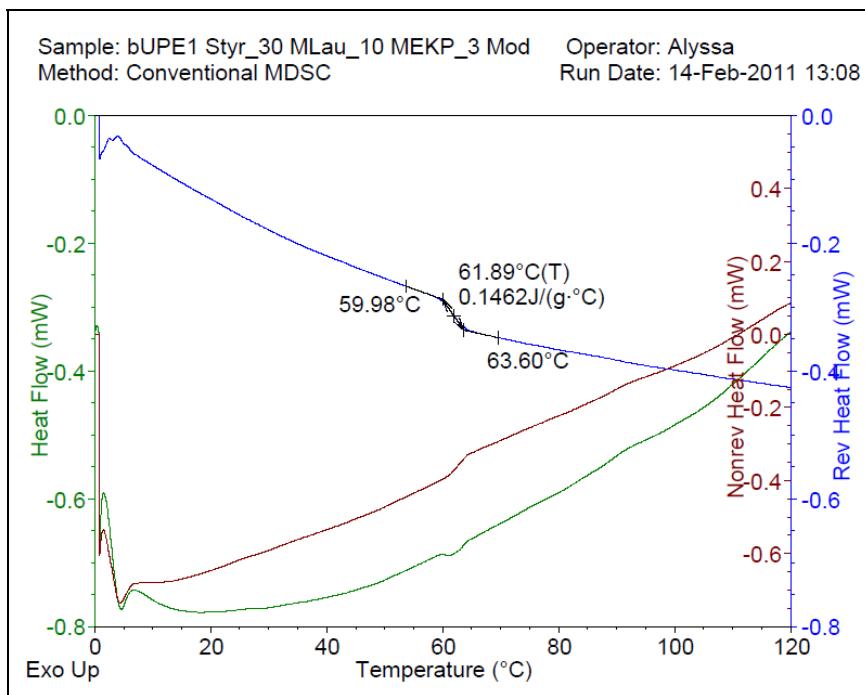
Figure 152. MDSC thermograms, B-UPE1/styrene/MLau (60/30/10).

From B-UPE1/styrene (60/40) (figure 148 (b)), there were a shoulder at ~72 °C and a peak at ~60 °C recognized as T_g. The biobased reactive diluent (MLau) did not show a significant decrease in T_g, and the result suggested that the fatty acid–based monomer would be a promising candidate as a styrene replacement.

9.4   Conclusions

Biobased UPE cross-linkers were prepared via the reaction between isosorbide and MA. The cross-linkers of a monomer type (UPE1), a chain-extended type (UPE2), and a sequence-inversed type were confirmed and characterized by NMR, MS, and GPC. However, the cross-linkers did not mix well with reactive diluents such as styrene and methyl methacrylate. To improve the blending of cross-linkers and styrene, the hydroxy end on cross-linkers were converted to hydrophobic ends such as hexyl and benzyl group. One- and two-end modifications were conducted to prepare thermosetting resins. Based on loss modulus results, one-end modification showed microphase separation, while two-end modification provided the improvement. However, two-end modification caused the reduction of T_g compared to one-end modification. A fatty-acid based monomer was used as a styrene replacement to reduce styrene emissions. The styrene replacement of 10 wt% was applied with B-UPE1/styrene (60/30), and there was no significant reduction in T_g compared to B-UPE1/styrene (60/40).

References

1. Netravali, A. Starch Based Composites and Their Manufacture. *U.S. Pat. Appl. Publ.* **2010**, Vol. US 20100291822, pp 30.

2. Pinto, G.; Maaroufi, A. K.; Benavente, R.; Pereña, J. M. Electrical Conductivity of Urea–Formaldehyde–Cellulose Composites Loaded With Copper. *Polymer Composites* **2011**, *32*, 193–198.

3. Vacková, T.; Kroisová, D.; Špatenka, P. Water Desorption Kinetics of Polymer Composites With Cellulose Fibers as Filler. *Journal of Macromolecular Science, Part B* **2008**, *48*, 68–76.

4. Guigo, N.; Mija, A.; Vincent, L.; Sbirrazzuoli, N. Eco-Friendly Composite Resins Based on Renewable Biomass Resources: Polyfurfuryl Alcohol/Lignin Thermosets. *European Polymer Journal* **2010**, *46*, 1016.

5. Zaske, O. C.; Goodman, S. H. Unsaturated Polyester and Vinyl Ester Resins. In *Handbook of Thermoset Plastics*; Goodman, S. H., Ed.; Noyes Publications: Westwood, NJ, 1998; p 97.

6. Claffey, D. J.; Casey, M. F.; Finan, P. A. Glycosylation of l,4:3,6-Dianhydro-d-glucitol (Isosorbide). *Carbohydrate Research* **2004**, *339*, 2433–2440.

7. Fenouillot, F.; Rousseau, A.; Colomines, G.; Saint-Loup, R.; Pascault, J. P. Polymers From Renewable 1,4:3,6-Dianhydrohexitols (Isosorbide, Isomannide and Isoidide): A Review. *Progress in Polymer Science* **2010**, *35*, 578–622.

8. Okada, M.; Tsunoda, K.; Tachikawa, K.; Aoi, K. Biodegradable Polymers Based on Renewable Resources IV Enzymatic Degradation of Polyesters Composed of 1,4;3,6-dianhydro-D-glucitol and Aliphatic Dicarboxylic Acid Moieties. *J. Appl. Polym. Sci* **2000**, *77*, 338.

9. Chatti, S.; Schwarz, G.; Kricheldorf, H. R. Cyclic and Noncyclic Polycarbonates of Isosorbide. *Macromolecules* **2006**, *39*, 9064.

10. Braun, D.; Bergmann, M. Polymers From 1,4;3,6-dianhydrosorbitol. *J. Prakt. Chem.* **1992**, *334*, 298.

11. Cognet-Georjon, E.; Mechin, F.; Pascault, J. P. New Polyurethanes Based on Diphenylmethane Diisocyanate and 1,4;3,6-Dianhydrosorbitol 1 Model Kinetic Studies and Characterization of the Hard Segment. *Macromol. Chem. Phys.* **1995**, *196*, 3733.

12. Beldi, M.; Medimagh, R.; Chatti, S.; Marque, S.; Prim, D.; Loupy A, Delolme F: Characterization of Cyclic and Non-cyclic poly(ether-urethane)s Bio-based Sugar Diols by a Combination of MALDI-TOF and NMR. *European Polymer Journal* **2007**, *43*, 3415.

13. Philip, B.; Sreekumar, K. Synthesis and Characterization of Chiral Main Chain Polyesters With Polar Segments Tailored for Second Harmonic Generation. *J. Mater. Sci.* **2003**, *38*, 1573.

14. Caouthar, A. A.; Loupy, A.; Bortolussi, M.; Blais, J. C.; Dubreucq, L.; Medour, A. Synthesis and Characterization of New Polyamides Based on Diphenylaminoisosorbide. *J. Polym. Sci. Part A Polym. Chem.* **2005**, *43*, 6480.

15. Caouthar, A. A.; Roger, P.; Tessier, M.; Chatti, S.; Blais, J. C.; Bortolussi, M. Synthesis and Characterization of New Polyamides Derived From Di(4-cyanophenyl)isosorbide. *European Polymer Journal* **2007**, *43*, 220.

16. Kamm, B.; Gruber, P. R.; Kamm, M. *Biorefineries–Industrial Processes and Products: Status Quo and Future Directions*; Wiley-VCH: Germany, 2006.

17. Jasinska, L.; Koning, C. E. Unsaturated, Biobased Polyesters and Their Cross-Linking via Radical Copolymerization. *Journal of Polymer Science Part A: Polymer Chemistry* **2010**, *48*, 2885–2895.

18. Van Walsem, J.; Anderson, E.; Licata, J.; Sparks, K.; Mirley, C.; Sivasubramanian, M. S. Process for Producing a Monomer Component From a Genetically Modified Polyhydroxyalkanoate Biomass, PCT Patent WO 2011/100608 A1, 2011.

19. La Scala, J. J.; Sands, J. M.; Orlicki, J. A.; Robinette, E. J.; Palmese, G. R. Fatty Acid-Based Monomers as Styrene Replacements for Liquid Molding Resins. *Polymer* **2004**, *45*, 7729–7737.

20. Khot, S. N.; Lascala, J. J.; Can, E.; Morye, S. S.; Williams, G. I.; Palmese, G. R.; Kusefoglu, S. H.; Wool, R. P. Development and Application of Triglyceride-Based Polymers and Composites. *Journal of Applied Polymer Science* **2001**, *82*, 703–723.

21. La Scala, J. J.; Orlicki, J. A.; Winston, C.; Robinette, E. J.; Sands, J. M.; Palmese, G. R. The Use of Bimodal Blends of Vinyl Ester Monomers To Improve Resin Processing and Toughen Polymer Properties. *Polymer* **2005**, *46*, 2908–2921.

10. Renewable Biobased (Meth)acrylated Monomers as Vinyl Ester (VE) Cross-Linkers*

10.1 Background and Significance

VE resins are thermosetting polymers that are commonly used in a variety of applications ranging from adhesives to the resin matrices for fiber-reinforced composites. Because VE resins possess many desirable features, such as strength, toughness, low cost, low weight, and particular viscosities for processing, they are widely used in the military and commercial industry.

Viscosity is a key factor for determining the utility of VE resins because lower-viscosity resins are easier to work with and may be prepared using a larger range of methods. Petroleum-based VE resins are typically high molecular weight species that are often extremely viscous fluids or solids. They require reactive diluents in order to reduce the resin viscosity so that the resins can be processed. Typical reactive diluents, such as styrene, are generally regarded as HAPs and/or VOCs whose use is controlled by the EPA. Large research efforts have been devoted to finding ways to eliminate or reduce the use of these highly hazardous reactive diluents.

Another factor that prevents VE resins' wider commercial use is that they are frequently derived from petroleum products. Petroleum is a commodity with well-known price volatility. The environmental costs of using petroleum are also very high.

VE resins derived from renewable sources can reduce dependency on petroleum and have quickly become an imperative for continued use and development of thermosetting polymers and composites. Biorefining of material based on converting biomass into VE products has been successfully developed. For example, biorefining of triglycerides and carbohydrates has produced a wealth of new fine chemicals that are useful for the development of biobased polymers. Fatty acids and triglycerides have also been successfully developed into materials ranging from toughening agents and plasticizers to reactive diluent replacements.

U.S. Patent no. 6,121,398 (*1*) discloses functionalized triglycerides derived from plant oil that are polymerizable and their use to produce high-modulus polymers. The functionalized triglycerides may be produced via several different chemical synthesis routes. For example, epoxidized triglycerides may be produced and converted to resilient rubbers by controlling the molecular weight and cross-link density. The resultant rubbers can be used as rubber-toughening agents in rigid composites. In the examples of this patent, acrylated base resins are prepared by reacting the epoxidized triglycerides with acrylic materials, such as acrylic acid. The thermosetting resins

---

*This section is patent pending. As a result, certain details have been omitted to prevent disclosure of intellectual property.

prepared by this method are said to have properties similar to commercial bisphenol-A VE resins. Other functionalized triglycerides are described in U.S. Patent 6,825,242 (*2*).

Besides triglycerides, chemically modified carbohydrates have also been explored for use as reactive monomers. These modified sugars are useful building blocks because they provide a rigid core structure that can be functionalized in order to develop new resins. For example, anhydrosugars, or bis-anhydrohexitols, have been fashioned into epoxy resins by forming the corresponding glycidyl ethers, as described in U.S. Patent no. 3,041,300 (*3*) and U.S. Patent no. 3,272,845 (*4*). U.S. Patent no. 7,619,056 (*5*) describes a different synthesis process whereby the glycidyl ethers of these anhydrosugars can be obtained and subsequently cured with polyamines to form thermosets.

However, anhydrosugars have not been successfully used to produce low-viscosity thermosetting VE resins. Reactive diluents, such as styrene, are still commonly used for reducing the viscosity of these biobased resins. Commercial practice involves reducing the styrene content in the resin to ~33 wt%; however, this makes the resin barely suitable for composite manufacture applications. In addition, reducing the styrene content significantly reduces the toughness of these resins.

Therefore, there is a continued need to provide biobased VE resins with excellent processabilty, acceptable toughness, and a reduced dependency on reactive diluents.

10.2 Experimental

10.2.1 Synthesis of Biobased Monomers

A number of synthesis procedures were used to prepare and optimize the preparation of the desired products. These methods are described in the following sections.

Synthesis of BIO-X-1 (Method 1). A schematic of Bio-X-1 products is shown in figure 153.

Stoichiometric amounts of modified carbohydrate derivative and triethyl amine were dissolved into dichloromethane and cooled to 0 °C before slowly adding dropwise 2–2.5 molar equivalents of acryloyl chloride or methacryoyl chloride. The reaction mixture was slowly warmed to between 21 and 30 °C and stirred for an additional 15–24 h. This reaction was quenched with a saturated solution of sodium bicarbonate and then stirred vigorously for 20–45 min before partitioning the layers. The organic solution was sequentially washed with aqueous saturated sodium bicarbonate, water, and aqueous saturated sodium chloride, and dried over $MgSO_4$. The solvent was then removed under reduced pressure. The product was a pale yellow to light brown oil. ^{1}H NMR analysis showed that the degree of (meth)acrylation was 1.8–2.0 (meth)acrylate groups per molecule.
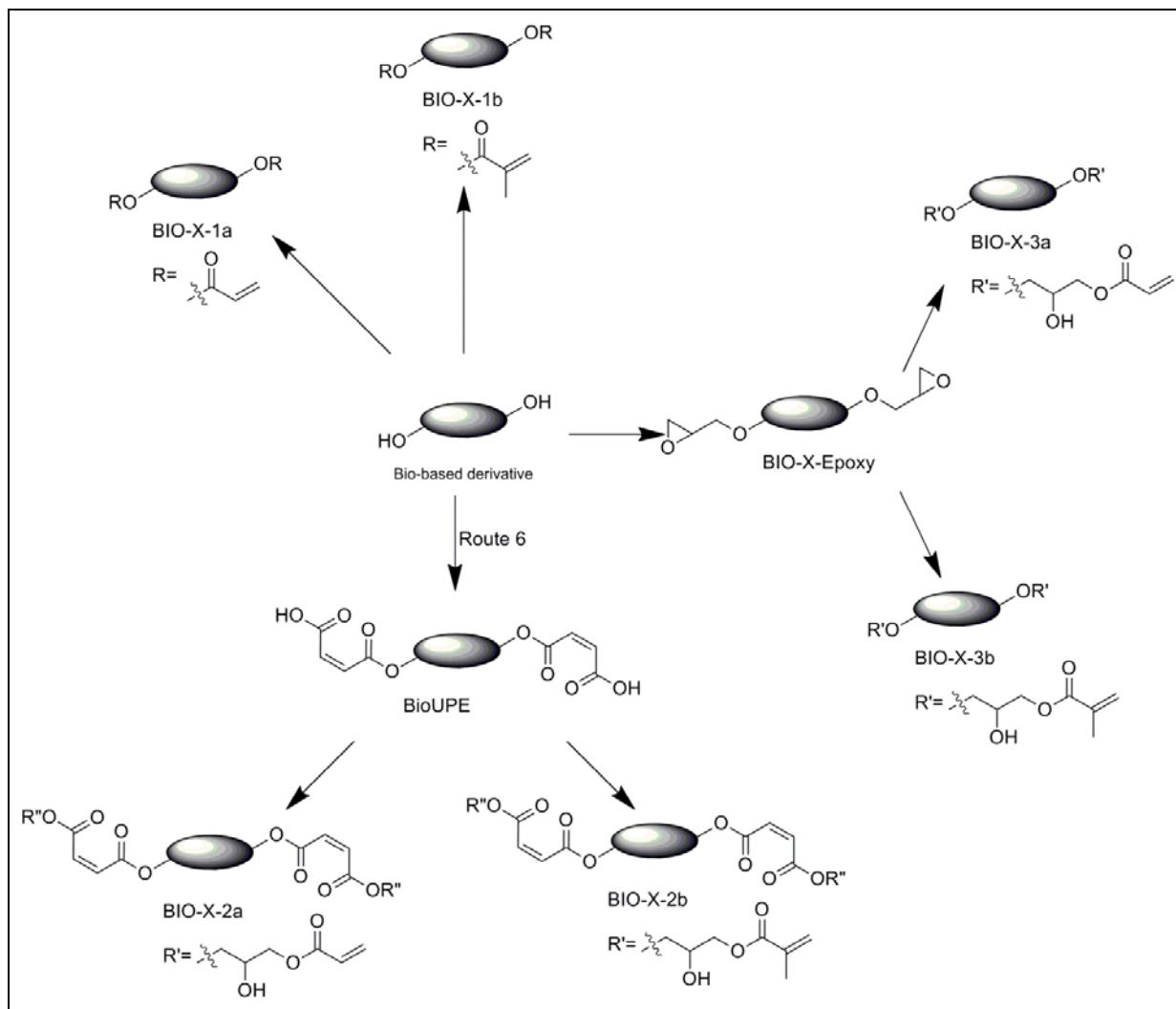
Figure 153. Schematic of bio-x cross-linkers.

Synthesis of BIO-X-1 (Method 2). Stoichiometric amounts of carbohydrate derivative and triethyl amine were dissolved into dichloromethane before adding a catalytic amount of dimethylaminopyridine (4-DMAP, 2.0-10.0 mol%) and cooling to 0 °C. Once the reaction mixture reached the desired temperature, 2–2.5 molar equivalents of acrylic anhydride or methacrylic anhydride were slowly added dropwise. The reaction mixture was slowly warmed to between 21 and 30 °C and stirred for an additional 15–24 h. This reaction was quenched with a saturated solution of sodium bicarbonate and then stirred vigorously for 20–45 min before partitioning the layers. The organic solution was sequentially washed with aqueous saturated sodium bicarbonate, 1-M hydrochloric acid, water, and aqueous saturated sodium chloride, and dried over $MgSO_4$. The solvent was then removed under reduced pressure. The product was a clear to pale yellow oil. ^{1}H NMR analysis showed that the degree of (meth)acrylation was 1.8–2.0 (meth)acrylate groups per molecule.

Synthesis of BIO-X-1 (Method 3). The carbohydrate derivative was melted at 68 °C before adding hydroquinone (0.2 mol%) and 2.0–2.5 molar equivalents of acrylic acid or MAA. After the addition of a catalytic amount of *p*-toluenesulfonic acid (0.5–2.5 wt%), the reaction temperature was raised to 130–145 °C and the progress followed by acid number titrations. After 18–36 h, the reaction mixture was cooled to room temperature and dissolved in ethyl acetate. The organic solution was washed sequentially with aqueous saturated sodium bicarbonate, water, and aqueous sodium chloride, and dried over $MgSO_4$. The solvent was then removed under reduced pressure, and the product appeared as a pale yellow to light brown oil. ^{1}H NMR analysis showed that the degree of (meth)acrylation was 1.5–1.7 (meth)acrylate groups per molecule.

Synthesis of BIO-X-1 (Method 4). The carbohydrate derivative and 2–2.5 molar equivalents of either methyl acrylate or methyl methacrylate were melted together at 68 °C before adding a free radical inhibitor (0.1 mol% of hydroquinone) and a catalytic amount of acid, such as *p*-toluenesulfonic acid (1.0–3.5 mol%). The temperature was raised to, and maintained at, 85 °C for 5–10 h or until the reaction was complete. The product's appearance varied from a light to dark brown oil. ^{1}H NMR analysis showed that the degree of (meth)acrylation was 1.5–1.8 (meth)acrylate groups per molecule.

Synthesis of BIO-X-Epoxy. The carbohydrate derivative was heated at 60 °C until a homogeneous melt was formed before adding epichlorohydrin (2.0–4.0 molar equivalents) and stirring at 100 °C for 4–6 h. Next, 50% aqueous sodium hydroxide (2.0–4.0 molar equivalents) was added to the pale yellow reaction mixture, and the reaction mixture was stirred for an additional 3–5 h. The sodium chloride by-product that precipitated out of solution formed a thick paste that was separated by filtration. The remaining yellow liquid was dissolved in diethyl ether, and the organic solution washed with water, dried over $MgSO_4$, and condensed under reduced pressure to yield the product as a pale yellow oil. ^{1}H NMR analysis showed signals in the expected ranges. In addition, epoxide titrations completed in accordance with ASTM 1652-04 showed that the resulting structures possessed 1.4–1.9 epoxy groups per molecule.

Synthesis of BIO-X-3 (Method 1). A stirred solution of Known 1 and either acrylic acid or MAA (2.0–2.5 molar equivalents) with a catalytic amount of AMC-2 (Aerojet chemicals, 2.5–10 mol% based on Known 1) was heated to 100 °C for 2–5 h. The reaction mixture was cooled to room temperature. The resulting blue-green product was characterized by ^{1}H NMR. Analysis showed that there were 1.8–2.0 (meth)acrylate groups per molecule.

Synthesis of BIO-X-3 (Method 2). Known 1 and either acrylic acid or MAA (2.0–2.2 mole equivalents) were dissolved in acetonitrile and refluxed with a catalytic amount of tetrabutylammonium bromide (TBAB, 5–20 mol% based on isosorbide) for 3–8 h. The reaction progress was followed by acid number titrations. The reaction mixture was then cooled and the acetonitrile removed under reduced pressure. The resulting oil was dissolved in ethyl acetate, and the organic solution was washed sequentially with water, aqueous saturated sodium

bicarbonate, and aqueous saturated sodium chloride, dried over magnesium sulfate, and concentrated under reduced pressure. The product appeared as a light yellow to light brown oil. ^{1}H NMR analysis showed that there were 1.75–1.9 (meth)acrylate groups per molecule.

Synthesis of BioUPE-1. The carbohydrate derivative and hydroquinone (0.1 wt%, based on the carbohydrate derivative) were heated to 70 °C until a homogeneous melt was formed. Freshly pulverized MA (2–2.5 molar equivalents) was slowly added portionwise to this bright yellow solution. The reaction mixture was allowed to melt and homogenize over a period of 15–35 min. The reaction temperature was raised to 87–95 °C and dimethylbenzyl amine (DMBA, 1.0 wt%, based on the carbohydrate derivative) catalyst was slowly added dropwise. The reaction mixture was stirred vigorously for 2–5 h while maintaining the reaction temperature between 87 and 95 °C. At the conclusion of the reaction, the product was cooled to room temperature and appeared as a viscous, hard yellow gel. ^{1}H NMR analysis showed that there were 1.8–2.0 maleate groups per molecule.

Synthesis of BIO-X-2 (Method 1). BioUPE-1 was softened at 70 °C before adding glycidyl acrylate or glycidyl methacrylate (2.0–2.02 molar equivalents) and a catalytic amount of AMC-2 (Aerojet chemicals, 2.5–10 mol% based on the moles of Product 6). The temperature was maintained at 70 °C for 4–6 h before allowing the reaction to cool to room temperature. The resulting emerald-colored viscous gel was characterized by ^{1}H NMR and found to have 1.9–2.0 glycidyl (meth)acrylate groups per molecule.

Synthesis of BIO-X-2 (Method 2). BioUPE-1 and either glycidyl acrylate or glycidyl methacrylate (2.0–2.2 mole equivalents) were dissolved in acetonitrile and refluxed with a catalytic amount of tetrabutylammonium bromide (TBAB, 5–20 mol% based on isosorbide) for 3–8 h. The progress of the reaction was followed by acid number titrations. The reaction mixture was then cooled, and the acetonitrile removed under reduced pressure. The resulting oil was dissolved in ethyl acetate, and the organic solution was washed sequentially with water, aqueous saturated sodium bicarbonate, and aqueous saturated sodium chloride, dried over magnesium sulfate, and concentrated under reduced pressure. The product appeared as a light yellow to light brown oil. ^{1}H NMR analysis showed 1.7–2.0 glycidyl (meth)acrylate groups per molecule.

Formulation and Curing of BIO-X-1 Resin Systems (Method 1). Resin systems were blended to obtain a desired range of compositions. All samples were blended to homogeneity using an ARE-250 Thinky planetary mixer at 2000 rpm for 5 to 10 min. Free radical polymerization of each resin was initiated by the addition of 0.375 wt% CoNap and 1.5 wt% Trigonox 239 A (Trigonox). The resin was purged with nitrogen prior to the addition of the initiator and promoter for ~15 min to prevent oxygen inhibition during curing. The purged resin mixture with added initiator and promoter was poured into a horizontal silicone mold and allowed to cure at room temperature inside an oven with a constant low flow of nitrogen to avert oxygen inhibition. It was then postcured for 3 h at temperatures between 170 and 190 °C.

208

Formulation and Curing of BIO-X-2 resin systems (Method 2). Resin systems were blended to obtain a desired range of compositions. All samples were blended to homogeneity using an ARE-250 Thinky planetary mixer at 2000 rpm for 5 to 10 min. Free radical polymerization of each resin was initiated with the addition of 0.375 wt% CoNap and 1.5 wt% methyl ethyl ketone peroxide (MEKP). Prior to the addition of initiator and promoter, the neat resin was purged with nitrogen for ~15 min to prevent oxygen inhibition during curing. The purged resin mixture with added initiator and promoter was poured into a silicone mold and allowed to cure at room temperature inside an oven with a constant low flow of nitrogen to avert oxygen inhibition. It was then postcured for 3 h at temperatures between 170 and 190 °C.

10.2.2 Rheological Characterization

A steady-state flow procedure was used to obtain viscosity in the formulated BioUPE/styrene blended resins before the initiator and accelerator were added on an AR 2000 Rheometer (TA Instruments). A 40-mm parallel plate geometry (TA Instruments) was used with a Peltier plate for optimal temperature control over the course of the experiment. The resin samples were placed between the plates and gap spacing (i.e., sample thickness) set at 1000 μm. The sample rheology was measured in steady shear flow experiments at 25 °C. The shear rate was increased from 0.001 to 100 s^{-1} and then decreased back to 0.001 s^{-1}, and 10 measurements were taken per decade. At a given shear rate, the shear stress was measured every 2 s. The shear rate and viscosity were recorded when the shear rate stabilized to within 5% tolerance for three consecutive points. For low-viscosity samples, low shear rates generally produce too little torque for accurate measurement, while high shear rates produce too much torque for viscous samples. This was ascertained by torque maps at each shear rate. Viscosity was determined as the average viscosity across the shear rate range where appropriate torque maps were produced.

10.2.3 Dynamic Mechanical Analysis

The thermomechanical properties of the polymer samples were measured using TA Instruments Q800 DMA in 35-mm dual cantilever clamp geometry. Bars were cut into nominal dimensions of $60 \times 12 \times 3$ mm^3 and sanded on both sides to ensure uniform cross-sectional area. The samples were tested at 1 Hz with a deflection of 7.5 μm while subjected to a temperature sweep at a rate of 2 °C/min starting at −50 °C and ending at 250 °C. Two temperature ramp experiments were run for each sample. The temperature at the loss modulus peak was considered as the T_g of the material (*16*).

10.2.4 Flexural Properties

Flexural modulus and strength were measured in accordance with ASTM D 790 for selected samples. Samples with approximate dimensions of $3 \times 25 \times 80$ mm were tested.

10.3 Results and Discussion

10.3.1 Preparation of Bio-X Monomers

In one aspect, the present invention relates to the development of anhydrosugar-based monomers for VE resin systems. The monomers are derived from plant cellulose or carbohydrates, which are renewable sources. Eight of these monomers derived from isosorbide are shown in figure 153 as BIO-X-1, BIO-X-2, and BIO-X-3. These monomers may be used as low-viscosity cross-linkers for thermosetting VE resins, which can replace petroleum-based VE thermosetting resins for nearly all of their applications.

One important feature of these anhydrosugar-based monomers is their relatively low molecular weight due to their confined core structure resulting from the limited carbon chain length of these naturally occurring sugars. The low molecular weights of these anhydrosugar-based monomers can be used to reduce the overall viscosity of VE resins containing them, which, in turn, can reduce the dependency on reactive diluents. This has the advantage of reducing the use of reactive diluents yet still producing VE resins with acceptable toughness and processability.

A number of different synthetic routes may be employed to produce these anhydrosugar-based monomers. Figure 153 shows some of the applicable synthetic routes. The starting materials are industrially refined from naturally occurring sugars by a two-step process: (1) reducing glucose, mannitose, or idose, respectively, and (2) subjecting the reduced glucose, mannitose, or idose to an acid-catalyzed dehydration to produce the modified carbohydrate parent structure.

In synthetic route 1 of figure 153, the anhydrosugars are acrylated to produce an acrylated monomer, BIO-X-1a, which is capable of free radical polymerization. Several exemplary methods may be used to produce BIO-X-1a from anhydrosugars. One method involves acylation of the hydroxyl groups of anhydrosugars using either acryloyl chloride or acryl anhydride and a base catalyst in an aprotic solvent. A second method involves esterification of anhydrosugars using acrylic acid and catalyzation using either acidic or basic conditions. A third method involves transesterification of anhydrosugars using methyl acrylate and catalyzation by either an acid or base catalyst. The reacting ester can be any combination of a parent acid that is an acrylate and a matching alcohol used to form the ester, which is 1–8 carbon atoms long. The small molecule alcohol of 1–8 carbon atoms is selected since it has a relatively low boiling point and can easily evaporate as the reaction progresses.

Synthetic route 2 of figure 153 is similar to synthetic route 1 in that the anhydrosugars are functionalized using a variety of different methods to produce a methacrylated derivative, BIO-X-1b, which is capable of free radical polymerization.

Several exemplary methods may be used to produce BIO-X-1b from anhydrosugars. One method involves acylation of the hydroxyl groups of anhydrosugars using either methacryloyl chloride or methacryl anhydride, catalyzed by a base catalyst in an aprotic solvent. A second method involves esterification of anhydrosugars using MAA and catalyzation by either acidic or

210

basic conditions. A third method involves transesterification of anhydrosugars using methyl methacrylate and catalyzation by either an acid or base catalyst. The reacting ester can be any combination of a parent acid that is a methacrylate and a matching alcohol used to form the ester, which is 1–8 carbon atoms long. The small molecule alcohol of 1–8 carbon atoms is selected since it has a relatively low boiling point and can easily evaporate as the reaction progresses.

Synthetic route 3 of figure 153 produces an intermediate referred to as Product 3 or BIO-Epoxy.

In synthetic route 4 of figure 153, BIO-Epoxy is treated with acrylic acid in the presence of a chromium-based catalyst, such as AMC-2 (Aerojet chemicals, Rancho Cordova, CA). The reaction is carried out at 90–105 °C, with 2.0–5.0 wt% catalyst based on the total weight of the reaction mixture. Alternatively, the synthetic route 4 can be carried out using another suitable method. For example, reaction of BIO-Epoxy with acrylic acid in refluxing acetonitrile catalyzed with 12–25 mol% tetrabutylammonium bromide (TBAB), based on the number of moles of BIO-Epoxy, will also result in BIO-X-3a. This reaction can be monitored using acid number titrations until the desired acid number is reached and the reaction is complete. Product 4 has the formula.

In synthetic route 5 of figure 153, BIO-Epoxy is treated with MAA in the presence of a chromium-based catalyst, such as AMC-2 (Aerojet chemicals, Rancho Cordova, CA). The reaction is carried out at 90–105 °C, with 2.0–5.0 wt% catalyst based on the total weight of the reaction mixture. Alternatively, BIO-Epoxy may be reacted with MAA in refluxing acetonitrile catalyzed with 12–25 mol% TBAB, based on the number of moles of BIO-Epoxy. The resultant product is also BIO-X-3b. This reaction can be monitored for completion using acid number titrations.

Both synthetic routes 4 and 5 open the epoxide rings on BIO-Epoxy to produce two free hydroxyl groups. These hydroxyl groups can be further functionalized with a number of different R groups. Examples of such R groups include acrylates, methacrylates, maleates, glycidyl ethers, or an alkyl, alkenyl, or aryl substituent.

Synthetic route 6 of figure 153 is maleination of anhydrosugars, which results in BioUPE. In an exemplary reaction, anhydrosugars and MA are melted together to form a homogeneous solution before adding a base catalyst and stirring at 75–95 °C for 2–5 h. BioUPE can be used as a cross-linking agent, or it can be used as an intermediate for synthetic routes 7 and 8.

Synthetic routes 7 and 8 in figure 153 are analogous reactions, wherein the treatment of Product 6 with a glycidyl VE, such as glycidyl acrylate or glycidyl methacrylate, produces BIO-X-2a and BIO-X-2b, respectively. Use of the AMC-2 catalyst in 0.5–3.0 wt% based on the total reaction mixture at low temperatures results in the formation of the desired product in excellent yields.

Alternatively, synthetic routes 7 and 8 can be carried out by TBAB-catalyzed refluxing in acetonitrile. Reaction of BioUPE with a glycidyl VE, such as glycidyl acrylate or glycidyl methacrylate, in refluxing acetonitrile catalyzed with 2.5–20 mol% TBAB, based on the number

of moles of BioUPE, results in BIO-X-2a and BIO-X-2b, respectively. This reaction can be monitored using acid number titrations until the desired acid number is reached and the reaction is complete. Product 7 has the formula.

The reaction of BioUPE with glycidyl VEs results in the opening of an epoxide ring and the formation of two free hydroxyl groups in BIO-X-2a and BIO-X-2b. These hydroxyl groups can be further functionalized with a number of different R groups. Examples of such R groups include acrylates, methacrylates, maleates, glycidyl ethers, or an alkyl, alkenyl, or aryl substituent.

10.3.2 Bio-X Resin Formulation and Viscosity

The anhydrosugar-based monomers of the present invention have been characterized both chemically and physically. IR spectra for each individual monomer show absorbance peaks in the expected regions for key functional groups. ^{1}H NMR experiments have also been used for structure confirmation. Chemical shifts for ^{1}H NMR peaks are in agreement for each monomer and appear as expected. Physical properties of these monomers have also been tested and exhibited viscosities from as low as 120 cP to being unmeasurable without the aid of reactive diluent. Overall, these anhydrosugar-based monomers are low cost, have a low viscosity and low volatility, and possess multiple polymerizable sites. These monomers are also reactive with other VE monomers.

The anhydrosugar-based monomers of the present invention are ideally suited for use as VE cross-linkers. The anhydrosugar-based monomers exhibit suitable viscosities for producing new low-viscosity resins that require a minimal amount of reactive diluent. These anhydrosugar-based monomers can partially or completely replace petroleum-based cross-linkers used in the manufacture of VE resins. Preferably, the anhydrosugar-based monomeric cross-linkers of the present invention are used as the only VE cross-linkers in the VE resin systems.

In another aspect of the present invention, the anhydrosugar-based monomers may be used as viscosity modulators. The anhydrosugar-based monomers have a confined core structure resulting from the limited carbon chain length of the naturally occurring sugars from which they are derived. The small core of these anhydrosugar monomers results in relatively low molecular weight anhydrosugar-based monomers that can be employed to reduce the overall viscosity of VE resins because of their low molecular weight in comparison with petroleum-based, relatively high molecular weight cross-linkers. Thus, the monomers of the present invention are well-suited for modulating the viscosity of VE resins by varying the amount of anhydrosugar-based monomer used in blends with petroleum-based, high-viscosity cross-linkers.

10.3.3 Bio-X Resin Properties

In yet another aspect of the present invention, the anhydrosugar-based monomers may be used as T_g enhancers in VE resins. T_g decreased as resin viscosity increased. On the other hand, the T_g of VE resins increased as the anhydrosugar-based monomer concentration increased. Thus, the

212

anhydrosugar-based monomers may be used as T_g enhancers for VE resin systems. The ideal T_g for VE resins can be varied over a wide range, for example, 40–250 °C, depending on the intended end use and the temperatures at which the resins will be used. The amount of anhydrosugar-based monomer in a particular VE resin system may be varied in order to achieve the desired T_g for the VE resin.

In yet another aspect of the present invention, the anhydrosugar-based monomers may be polymerized with themselves to form novel VE polymers. In one embodiment, a VE resin system may be made from a single, pure anhydrosugar-based monomer of present invention. In another embodiment, two or more different anhydrosugar-based monomers may be polymerized with one another to form VE co-polymers. The anhydrosugar-based monomers can be polymerized to form linear, branched, hyperbranched, and cross-linked polymers. The neat monomer can be treated with a free-radical initiator, with or without a promoter, in order to induce curing to form the polymers. These polymers have properties comparable to petroleum-based VE-derived polymers, exhibit similar stiffness and toughness, and can have T_g's ranging from 0 to 270 °C.

Bio-X-1 has exhibited a T_g of 250 °C or higher (figure 154). This T_g is a major breakthrough in that this high T_g has never been achieved by a VE or UPE. Only epoxies and other higher-performing resins have been able to achieve these types of properties while costing easily ten times the amount of a VE. Furthermore, there is essentially no loss factor for this material. Thus, this appears to be a nearly elastic polymer (as opposed to a viscoelastic polymer). This may be detrimental to properties, as it could indicate low toughness. However, it could also be beneficial in regard to low amounts of creep and stress relaxation.
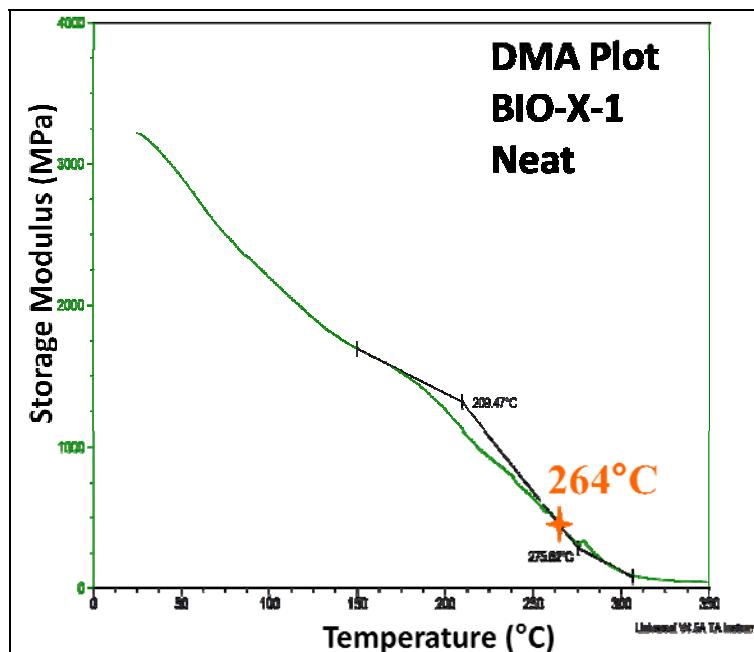
Figure 154. DMA storage modulus of Bio-X-1 as a function of
temperature.

213

A binary resin system may also be formed from one or more anhydrosugar-based monomers blended with a reactive diluent to produce VE resins. In such binary resin systems, the compositions will typically contain 50–80% by weight of anhydrosugar-based monomers and 20–50% by weight of reactive diluents, with all weights being based on the weight of the product resin mixture. The reactive diluents may be petroleum or biobased. These resins have been found to have very low viscosities ranging from 5.0 to 110,000 cP, which would make them ideal for liquid molding, composite layups, and VARTM processing, as well as a wide range of other applications.

In general, compositions may include 1–100% by weight of anhydrosugar-based VE monomers, 0–99% by weight of reactive diluent, such as the reactive diluents described herein, with all weights being based on the total weight of the resin product.

The binary resin systems may be cured using a free-radical initiator, in the presence or absence of a promoter, to produce bioderived copolymers that have similar properties to polymeric materials produced from petroleum products. These polymers possess stiffness and toughness equivalent to petroleum-derived VE resins, with T_g's ranging from 45 to 235 °C.

Exemplary reactive diluents suitable for use in the present invention are petroleum-based and biobased compounds with a single polymerizable site. Suitable petroleum-based reactive diluents include, but are not limited to, styrene, 2-hydroxymethacrylate, methyl methacrylate, methyl acrylate, aryl-methacrylates, aryl-acylates, aliphatic methacrylates, and aliphatic acrylates. Suitable biobased reactive diluents include, but are not limited to, furfuryl methacrylate, tetrahydrofurfuryl methacrylate, furfuryl acrylate, tetrahydrofurfuryl acrylate, furoic acid glycidyl methacrylate (FA-GM), furoic acid glycidyl acrylate and methacyrlated lauric acid, methacrylated octanoic acid, MFAs, and acrylated fatty acids.

A ternary resin system may also be formed by blending one or more anhydrosugar-based monomers with commercial VE and reactive diluents. Ternary compositions will typically include 5–15% by weight of reactive diluent(s) and 85–95% by weight of VE cross-linker monomers, wherein the composition of the cross-linker monomers is 15–70% by weight of anhydrosugar-based monomers and 30–70% by weight of commercial VE resin, with the all weights being based on the weight of the product resin mixture. The commercial VE is preferably a petroleum-based VE.

Commercial VEs may be derived from any source. A broad range of commercial VEs is suitable for use in the ternary resin systems of the present invention. Some examples of suitable VEs are methacrylated and acrylated glycidyl ethers of bisphenols. Suitable bisphenols include bisphenol A, hexafluorobisphenol A, bisphenol E, bisphenol F, tetramethyl bisphenol E, tetramethyl bisphenol F, bisphenol M, bisphenol C, bisphenol P, and bisphenol Z. Methacrylates and acrylates of ethoxylated bisphenols may also be employed, as well as methacrylates of acrylates of commercial epoxy products.

Commercial VEs with vinyl functionality greater than two may also be employed. Examples include acrylic and alkyl-acrylic VEs of epoxy novolacs and acrylates of tris-hydroxyphenylmethane glycidyl ether (THPM-GE), ethoxy phenol novolacs, and ethoxylated tris-hydroxyphenylmethane. In addition, brominated versions of these systems, such as brominated bisphenol A–based VEs, may be employed. Bisphenol VEs are the preferred VEs used in the ternary systems of the present invention because of the desirability of making structural composites from the resultant polymers.

In a ternary resin system, the anhydrosugar-based monomers of the present invention can be added to enhance the T_g of certain resins and/or to adjust the resin viscosity to improve the flow characteristics. The addition of the anhydrosugar-based monomers also increases the sustainability of the resins and reduces the reliance on reactive diluents, such as styrene, while maintaining or improving the properties of petroleum-based commercial resins. Use of the anhydrosugar-based monomers in varying concentrations in relation to the petroleum-based VE and reactive diluent components can allow for the tailoring of the resin properties for specific applications and the tailoring of the properties of polymeric materials that result from these resins.

The resins containing the anhydrosugar-based monomers can be cured using any method that makes use of free radically initiated reactive curing systems, including, but not limited to, thermal cure, room temperature cure, electron beam cure, and ultraviolet cure.

The anhydrosugar-based monomers can be polymerized to form linear, branched, hyperbranched, and cross-linked polymers for a wide array of applications, including biosensors, rheology modifiers, biomaterials, and polymerizable surfactants for media encapsulation. The anhydrosugar-based monomers can also be used for the production of polymer matrix composites, which are used in military, automotive, recreational, and marine applications. Exemplary products that may be made from these polymer matrix composites include body panels and armor for vehicles, composite hoods, and boat hull structures. In addition, these polymer matrix composites can be used with traditional thermosetting vinyl and polyester resins as a gel coating material to provide a protective coating for composites and other surfaces.

The use of anhydrosugar-based monomers as VE cross-linkers, T_g enhancers, and viscosity modulators has been tested experimentally and found to be successful. Thermosetting liquid molding resins using anhydrosugar-based monomers to replace some or all of the petroleum-based VE or UPE resin cross-linkers, blended with common reactive diluents, also have acceptable resin viscosities and polymer mechanical properties similar to those of commercial petroleum-based VE/styrene polymers.

215

The thermomechanical and rheological properties for a number of example resin blends can be seen in table 22. The neat resins and resin blends can easily be tailored to meet a desired range of T_g or viscosity depending on the application. Ternary blends show that the addition of the novel resins to commercial resin blends can aid in either reducing the viscosity or increasing the T_g in order to improve performance (table 23).

Table 22. Thermomechanical and rheological properties of biobased cross-linker neat and cured with an additional comonomer (binary blends).

Biobased Resin	Reactive Diluent	Additional Cross-Linker	Viscosity (cP at 25 °C)	T_g (°C)	Storage Modulus (MPa at 25 °C)
BIO-X-1	Neat	NA	120	250	2900
BIO-X-1	35% styrene	NA	5	212	3234
BIO-X-1	35% FM	NA	16	122	3421
BIO-X-1	35% Mlau	NA	73	107	2220
BIO-X-2	Neat	NA	620125	90	3073
BIO-X-2	35% styrene	NA	172	130	3293
BIO-X-2	35% FM	NA	2234	101	3361
BIO-X-2	35% Mlau	NA	102351	50	1648
BIO-X-1	NA	20% Viapal 450	1098	58	3623
BIO-X-2	NA	50% RDX	Untestable	130	3200
BIO-X-3	NA	20% RDX	Untestable	212	3100

Table 23. Thermomechanical and rheological properties of Bio-X-1 and Bio-X-2 ternary resins as a function of reactive diluents and additional cross-linker content.

Biobased Resin	Additional Cross-Linker	Reactive Diluent	Viscosity (cP @ 25 °C)	T_g (°C)	Storage Modulus (MPa @ 25 °C)
10% BIO-X-1	80% RDX	10% styrene	8981	145	2893
50% BIO-X-1	40% RDX	10% styrene	480	169	2893
80% BIO-X-1	10% RDX	10% styrene	68	244	3352
10% BIO-X-1	80% RDX	10% FM	22830	128	3404
50% BIO-X-1	40% RDX	10% FM	701	157	3525
80% BIO-X-1	10% RDX	10% FM	92	263	3455
10% BIO-X-1	80% RDX	10% Mlau	58995	169	3322
50% BIO-X-1	40% RDX	10% Mlau	1445	165	3206
80% BIO-X-1	10% RDX	10% Mlau	153	193	2927
80% BIO-X-2	10% RDX	10% styrene	16115	118	3758
80% BIO-X-2	10% RDX	10% FM	45709	126	3044
80% BIO-X-2	10% RDX	10% Mlau	12376	87	2916
50% BIO-X-2	40% Viapal 450	10% styrene	2710	56	2816
50% BIO-X-2	40% Viapal 450	10% FM	700	140	157
50% BIO-X-1	40% RDX	10% styrene	480	169	2893

10.3.4 Flexural Properties

Good polymer samples will have strength, modulus, and toughness of >100 MPa, >2 GPa, and >100 J/m^2, respectively. The flexural properties of Bio-X-1 were measured. The resulting polymer had a modulus of 4.4 ± 0.2 GPa and strength of 90 ± 4 MPa. The results indicate that the polymer is a bit brittle but extremely stiff. In fact, this polymer has properties in many ways superior to that of high-temperature epoxies. High T$_g$ epoxies typically have T$_g$ >200 °C, similar strength, and generally ~2.5 GPa room temperature modulus.

10.4 Summary and Conclusions

The content of this section is currently being patented because of the excellent properties of these anhydrosugar-based monomers, resins, and polymers. The results indicate many of the novel cross-linkers produce resin with low viscosities (<2000 cP), which enable composite liquid molding. The polymer properties are excellent, with T$_g$'s of some resins as high as 250 °C with 100% biobased content and with many other resins with T$_g$'s well above 150 °C and even above 200 °C.

References

1. Wool, R. P.; Kusefoglu, S. H.; Palmese, G. R.; Zhao, R.; Khot, S. N. High Modulus Polymers and Composites From Plant Oils. U.S. Patent 6,121,398, 2001.

2. Sulzbach, H.; Bemmann, R.; Hoefer, R., Skwiercz, M. Method for Production of Radically Post-Cured Polymers by Addition of Diallyl Phthalates. U.S. Patent 6,825,242, 2004.

3. Morrison, J. G. Polyglycidyl Ethers of Ether Anhybro Hexitols, Method of Production, and Aqueous Solutions Thereof. U.S. Patent 3,041,300, 1962.

4. Zech, J. D.; Le Maistre, J. W. Bisglycidyl Etheks of Isohexides. U.S. Patent 3,272,845, 1966.

5. East, A.; Jaffe, M.; Zhang, Y.; Catalani, L. H. Thermoset Epoxy Polymers From Renewable Resources. U.S. Patent no. 7,619,056, 2009.

11. Sugar-Based Vinyl Ester (VE) Epoxy-Linkers[*]

11.1 Introduction

As previously discussed, biobased VE and epoxy resins are desired to make more sustainable composites. The previous chapter shows that anhydrosugars can be used to produce excellent resins. While these anhydrosugars can be used to produce high-performing resin and are based on renewable resources, the drawback to these derivatives is that they still require extensive chemical modification in order to produce the parent scaffold, which drives up the base cost of the novel resin. The natural carbohydrate derivatives for these anhydrosugars have a wealth of functionality that can be modified by similar chemical means to generate a new class of resins. Oligosaccharides, when viewed as potential candidates, as a core scaffold have a great deal of structural features that would promote the development of high-performance, low-cost, and renewable cross-linking thermosetting resins.

In 2002, global sugar production was estimated to be ~143 million tonnes annually with the United States responsible for 3% of the total production. Historically, the price of sugar per pound fluctuates, but in recent years the price has been around $0.25–$0.30/lb, which equates to roughly $600/tonne. Unrefined carbohydrates potentially could offer a low-cost highly cross-linking resin that could be utilized in a number of applications. Thus, this chapter investigates the use of sugar-derived VE and epoxy resins.

11.2 Chemistry and Formulation

Synthesis of BIO-Y-1: A methacrylated carbohydrate derivative was prepared as detailed in figure 155. Triethylamine was added to a stirred suspension carbohydrate derivative in dichloromethane and cooled to 0 °C before methacryloyl chloride was slowly added and warmed to room temperature. After 18 h, the solid had been completely dissolved, and the reaction was quenched with water (100 mL) and allowed to stir for an additional 30 min. The layers were partitioned, and the aqueous layer washed with an aliquot of DCM. The combined organic layers were washed sequentially with water (2 × 75 mL), sodium bicarbonate (50 mL), and brine (50 mL), dried over magnesium sulfate, and condensed under reduced pressure. The product appeared as a dark brown tacky gel. FTIR analysis indicated the presence of –OH functionality, meaning that the reaction had not proceeded to completeness. ^{1}H NMR spectroscopy showed that there were 5.75 methacrylates per molecule.

---

[*]This section is patent pending. As a result, certain details have been omitted to prevent disclosure of intellectual property.
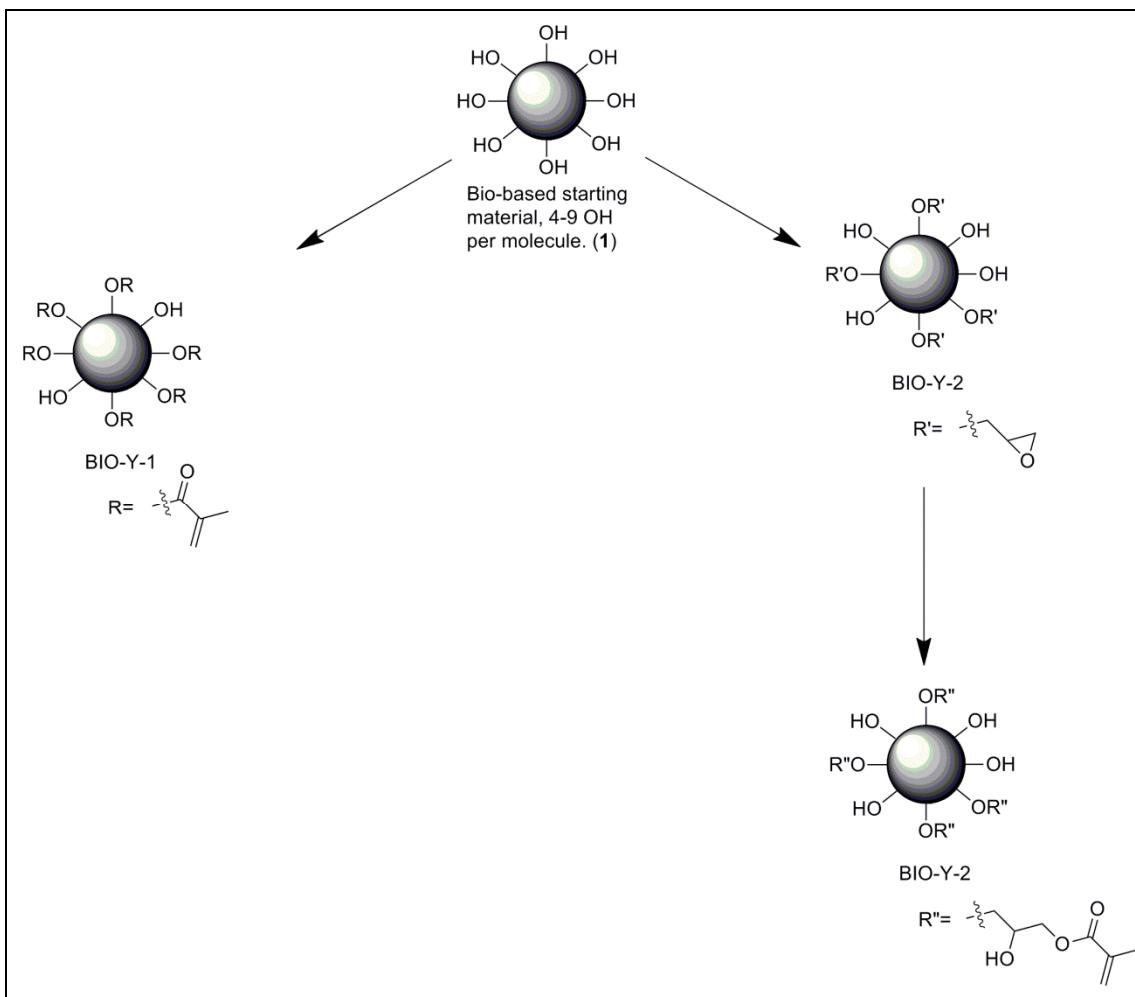
Figure 155. Schematic of sugar-based cross-linkers.

Synthesis of BIO-Y-2: Carbohydrate derivative (5.0 g, 14.61 mmol) and tin (II) fluoride (958.6 mg, 6.118 mmol, 3.0 mol% based on OH content) were suspended in excess epichlorohydrin (20.0 mL, 255.34 mmol) and refluxed for 24 h before removing the excess epichlorohydrin under reduced pressure. The dark reddish-orange oil was diluted with toluene (10 mL) before sodium hydroxide was added dropwise in water (5.245 g, 131.125 mmol in 10.0 mL) and stirred at room temperature for 12 h. The reaction mixture was poured into water (300 mL) and extracted with ethyl acetate (3 × 200 mL). The combined organic layers were washed sequentially with water (3 × 100 mL) and then brine (3 × 100 mL), dried over magnesium sulfate, and then condensed under reduced pressure.

Synthesis of BIO-Y-3: BIO-Y-2 (3.0249 g, 3.8274 mmol) and MAA (2.6351 g, 30.619 mmol) were mixed together and heated to 75 °C before AMC-2 catalyst was added and allowed to react for 24 h. The reaction mixture was dissolved in ethyl acetate (100 mL) and washed with sodium bicarbonate (4 × 50 mL), water (50 mL), and brine (100 mL), and then dried over magnesium sulfate and concentrated under reduced pressure.

219

Formulation and Curing of BIO-Y-1: Resin systems were blended so that their composition consisted of 65 wt% BIO-Y-1 (2) and 35 wt% styrene. The resin mixture was blended using an ARE-250 Thinky planetary mixer at 2000 rpm for 5 to 10 min until the sample was homogenous. Free radical polymerization of each resin was initiated with 1.5 wt% Trigonox with 0.375 wt% CoNap added as a promoter. Resins were cured overnight in a horizontal rubber mold at room temperature and then postcured at 120 °C for 2 h before any analysis was carried out.

Curing of BIO-Y-2: Epoxidized carbohydrate derivatives were produced as shown in figure 155. Epoxy products were characterized using NMR spectroscopy and by titration in accordance with ASTM 1652-04 in order to determine the number of epoxy groups per molecule. For this investigation, 0.2 g of epoxy was dissolved with a 1.2-M solution of tetraethylammonium bromide solution in acetic acid (9 mL) in dichloromethane (9 mL) with a crystal violet indicator. Samples were titrated with a solution of 0.1 N perchloric acid in acetic acid until the end point was reached. The epoxy number was calculated using equations 6 and 7. Equation 6 allows for calculation of the weight percent epoxide for the sample; this value depends on the volume of perchloric acid in acetic acid titrated. Equation 7 allows for calculation of the epoxy equivalent weight, which accounts for the molar mass of an epoxy group as shown in table 24 for three samples. This equation also allows for calculation of the epoxy number, with respect to the molecular weight of the epoxidized product.

$$E = 4.3 \times V \times \frac{N}{m_{epoxy}} \, , \tag{6}$$

$$W = 43 \times \frac{100}{E} = \frac{Molecular\,Weight}{Epoxy\,Number} \, , \tag{7}$$

where

E = weight percent epoxide (%),

V = volume of perchloric acid reagent required to titrate the standard (mL),

N = normality of perchloric acid reagent (N),

m_{epoxy} = mass of epoxy specimen used (g),

W = epoxy equivalent weight (%), and

Molecular Weight= molecular mass of epoxidized product.

Table 24. Epoxy number calculation for Bio-Y-2.

Sample No.	Mass	$V_{titrant}$	E	W	EN
1	0.3443	13.38	16.71	257.3	2.31
2	0.3212	12.40	16.60	259.03	2.29
3	0.3063	11.86	16.65	258.26	2.30

Results of the titration experiments showed that very limited substitution occurred. The desired epoxy number of 4–6 epoxies per molecule was not reached. Instead, ~1.7–2.2 epoxy groups were added per molecule (3a). Once the product epoxy values were calculated using equations 6 and 7, the appropriate amount of PACM amine curing agent can be calculated using equation 8.

$$\frac{52.5}{W} = \frac{m_{PACM}}{1g\ epoxy} . \tag{8}$$

BIO-Y-2 (4.0226 g) was mixed with PACM amine curing agent (0.8125 g) in an orbital mixer for 5 min before the resin was poured into a horizontal DMA mold and cured at 120 °C for 3 h. The sample was then cooled at room temperature. DMA analysis was performed, and the sample had a T_g of 42.35 °C (loss modulus).

Formulation and Curing of BIO-Y-3: BIO-Y-3 (0.3116 g) was dissolved in styrene (0.1591 g) and free radically polymerized using Trigonox, with CoNap used as an accelerant at room temperature for 18 h and then postcured at 120 °C for 24 h. The resin cured into a hard dark brown material.

11.3 Results and Discussion

Syntheses of the primary resins were accomplished starting from a single starting material and then modified in a single reaction step that can add polymerizable functionality to the numerous sites arranged around the core molecule. For the synthesis of the first novel resin, BIO-Y-1, the core scaffold was directly methacrylated using either methacryoyl chloride or methacrylic anhydride in dichloromethane. These highly reactive reagents were ideal for modifying this structure and easily esterified a number of the free hydroxyl groups. Initially, the starting material was not soluble in organic solvent; however, as the reaction progressed, the product slowly increased in solubility and dissolved in the reaction solvent. By the conclusion of the reaction, no solid starting material remained. This qualitatively indicated that the highly hydrophilic character of the starting material had been modulated and that the desired methacrylate "caps" had been installed. NMR analysis of the product showed that of the eight potential sites for modification, we were successful in adding methacrylate groups to an average of 4.5–5.5 hydroxyls around the structure. Because of the highly functionalized nature of the starting material and the lack of specificity of the reaction, we cannot determine which hydroxyl groups were substituted and if the same groups are modified from molecule to molecule. For the

purposes of our investigation, this is not important; as long as there is a mixture of compounds with similar reactivity, we can formulate a biobased resin system.

Initial formulations dissolved the tacky BIO-Y-1 resin in 35% styrene and cured using a standard CoNap and Trigonox package with a room temperature methodology. The cured resins hardened into dark opaque materials and were subjected to DMA. The preliminary results indicated that the novel resin system had a T_g of 64 °C (figure 156) with reactive diluent. As seen in figure 156, the material showed interesting characteristics, but the testing was incomplete because the sample failed at moderate temperatures. We must continue to investigate this avenue to determine the complete scope of the new material's characteristic and define potential application.
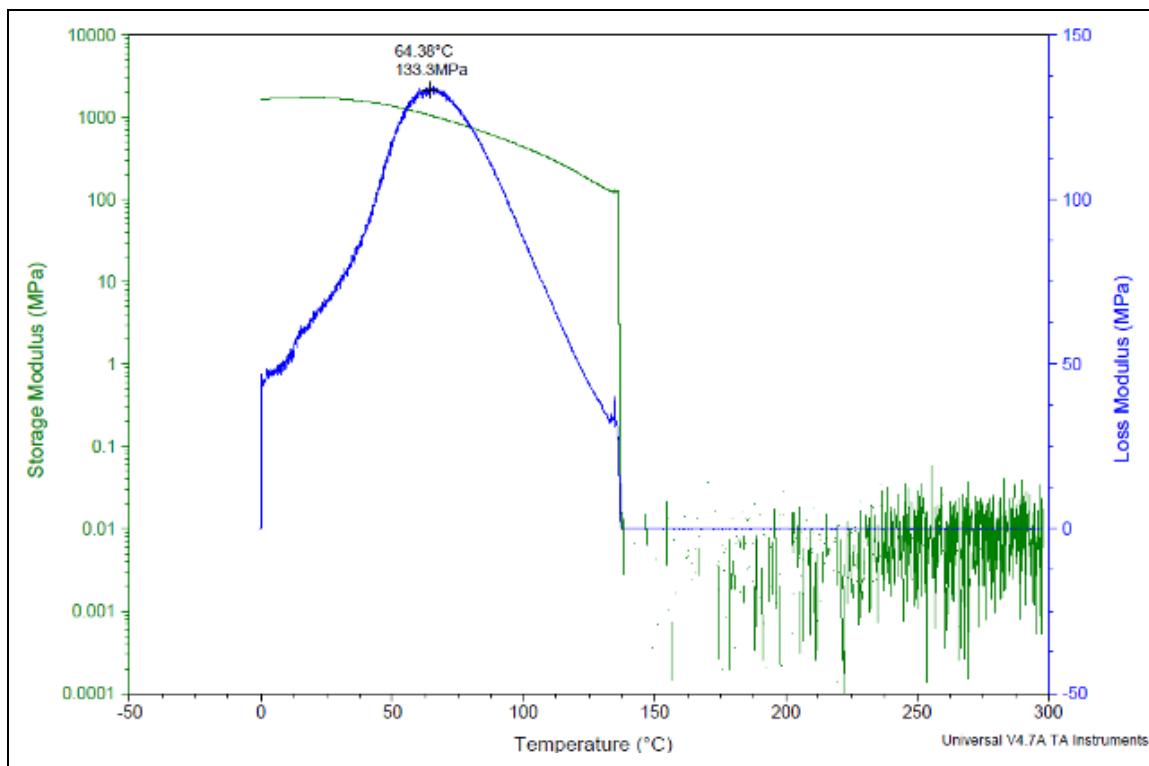
Figure 156. DMA BIO-Y-1. (Samples are poor; they should be remade and retested.)

The synthesis of resin BIO-Y-2 proved to be more challenging than originally envisioned. Common epoxy synthesis is carried out on a substrate using excess epichlorohydrin in aqueous sodium hydroxide; however, when this methodology was applied to the starting material, no reaction was observed and the starting material was unrecoverable because of alkaline degradation. Using alternate methods, the synthesis of BIO-Y-2 was realized when the starting material was treated with the Lewis acid tin fluoride in refluxing epichlorohydrin. Subsequent base treatment reformed the oxirane ring, completing the synthesis of BIO-Y-2. We were not able to accurately determine the degree of epoxidation using NMR; thus, we turned to epoxy titrations as described in ASTM 1652-04. The results of those experiments indicated that we had

on the order of 1.2–1.5 epoxide groups per molecule—a significant difference from the goal of 4–6 per molecule or the maximum of 8. The development of this synthesis is only in the beginning stages, and our investigations will continue in an effort to optimize the conditions. Ideally, the resulting optimization studies will allow us to tailor the reaction to produce a range of resins with varying degrees of substitution that will result in different materials.

With the limited success that was experienced with the initial synthesis of BIO-Y-2, materials characterization of the cured resins began in earnest. The results of the epoxy titration allowed us to calculate the appropriate equivalent weight of the PACM amine curing agent. The cured BIO-Y-2 resin hardened into clear reddish-brown material and was subjected to DMA analysis. The resulting material had a modest T_g of 42 °C (figure 157) with a storage modulus of 2.7 GPa at 25 °C, indicating a potential for higher-performing materials as more epoxy substituents are added. Materials characterization will continue as the synthesis is refined and new resin systems result.
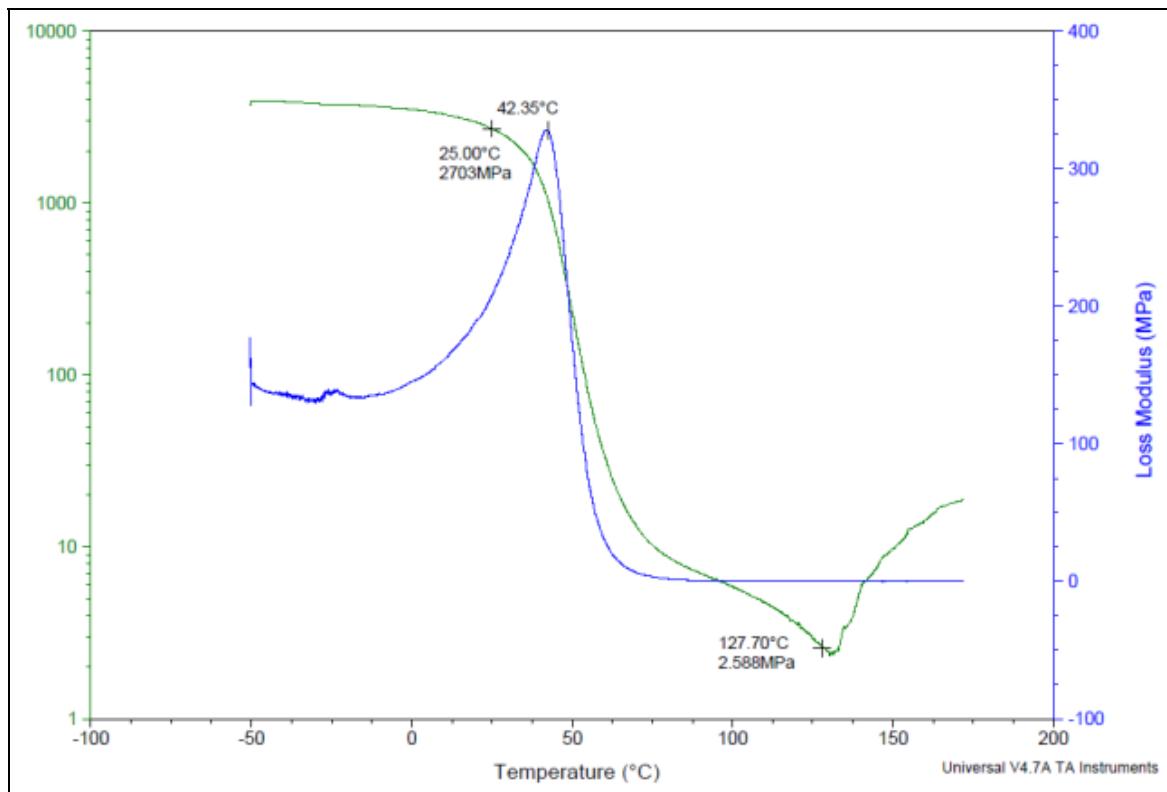
Figure 157. DMA BIO-Y-2.

11.4 Conclusions

Thus far, we have successfully synthesized a new class of carbohydrate-based resins. Future synthetic efforts will focus on optimizing the reactions in order to control the degree of functionalization that can be attained. By synthesizing these resins with controlled degrees of functionality, we should be able to produce cured material that exhibits different properties.

223

Initial DMA analysis of the resins shows materials with low T_g's, but they were promising for future development. These resins need to continue to be developed and formulated in order to produce materials that can be utilized in commercial applications.

In this avenue of novel resins, we have only begun to discover the possibilities. Methodologies developed to modify these base structures can be use to modify simpler or more complex carbohydrates. Modification of monosaccharides, polysaccharides, or even cellulose can open a new avenue for resin systems that can offer renewable solutions for the needs of future polymers.

12. Life-Cycle Cost Analysis

12.1 Lignin-Based Carbon Fiber

It is expected that lignin-based carbon fibers will cost significantly less than current carbon fibers. The DOE's initiative to develop lignin-based carbon fibers to make lighter-weight, affordable automobiles is centered on the reduced costs of lignin-based carbon fibers. Their goal, although not yet realized, is lignin-based carbon fiber costing $5–7/lb. Current aerospace carbon fiber costs approximately $25/lb, and commercial-grade carbon fiber costs about $15/lb. The DOE has yet to obtain lignin-based carbon fibers with the appropriate performance, so truly assessing the feasibility of the cost is not possible at this time.

There are significant costs associated with manufacturing carbon fibers from rayon, PAN, or pitch. Figure 158 breaks down the costs of carbon fiber production. Some of the cost is the raw material, especially for Rayon and PAN, but much of the cost results from the manufacturing method. The high-energy process used to melt pitch fibers and oxidize and carbonize all types of carbon fibers is a large element. However, this cost is likely to be very similar for lignin-based fibers. On the other hand, PAN in particular generates toxic chemicals during manufacture that impose significant costs to prevent worker fatality and minimize environmental pollution. Lignin-based carbon fibers would have no need for much of these emissions control facilities and should obtain reduced costs.
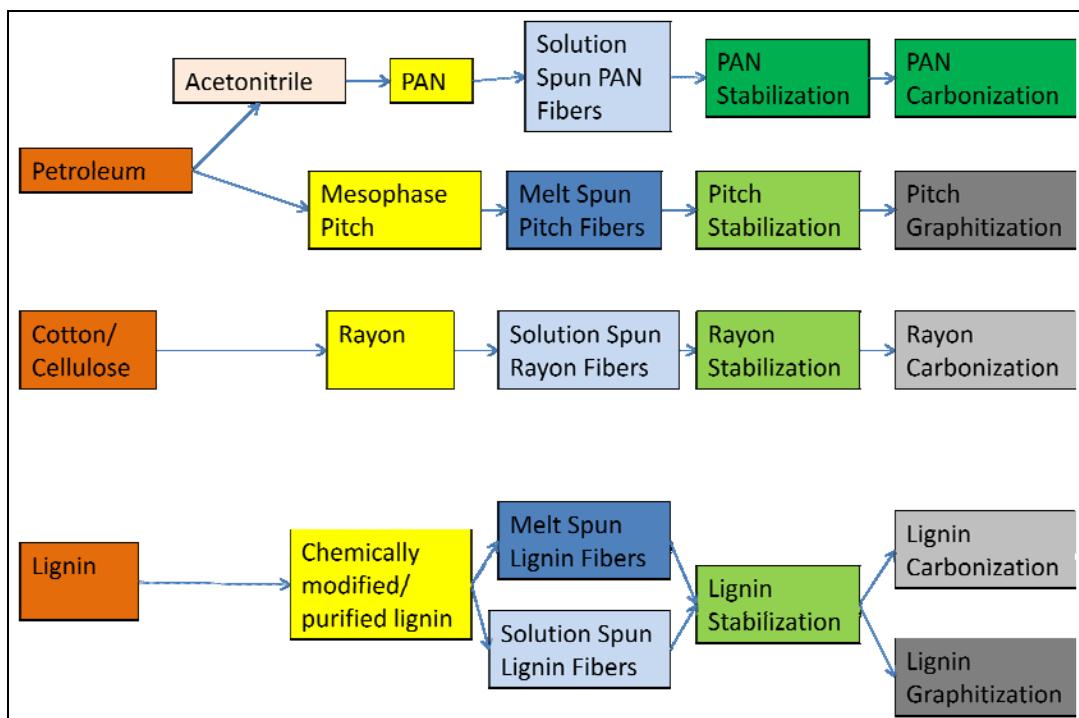
Figure 158. Cost breakdown of carbon fiber manufacture.

An analysis done by Oak Ridge National Laboratory shows the cost breakdown for low-grade PAN-based carbon fibers in figure 159 (*1*). These carbon fibers cost approximately $10/lb. The PAN precursors are by far the largest cost component and represent an even higher share of the cost for aerospace-grade carbon fiber. In fact, much of the other costs in figure 159 remain relatively unchanged for aerospace-grade fibers. The cost of acrylontrile is only $1.0/lb, and the cost of low-performance acrylic fiber is only ~$1/lb (*2*, *3*). Thus, much of the precursor cost is the solution fiber-spinning method necessary to orient the fibers and reduce the size of the fibers to less than 30 μm in diameter. The hazardous solvents play a significant role in raising this cost. Table 25 lists the potential cost savings associated with lignin-based carbon fibers. Overall, lignin-based fibers are expected to result in cost reduction of approximately $1.5/lb (*1*). A cost reduction for aerospace-grade fibers could be as high as $5/lb but will highly depend on the ability to prepare high-performance lignin-based carbon fibers shown by this work. Oxidative stabilization represents 75%–80% of fiber residence time and 18%–20% of cost (*1*). Low-cost methods like UV stabilization of methacrylate functional lignin should help decrease the cost (~$0.9–$1.6/lb cost savings) potentially as much as half and reduce residence time to less than 20%–50% of the total process. Carbonization and graphitization cost nearly one-quarter of the carbon fiber cost. Lignin-based fibers should reduce or eliminate the need for emissions capture equipment to capture HCN and other hazardous emissions. This should decrease the cost of carbonization/graphitization again by $0.4–0.8/lb. Surface treatment, spooling, and packaging are likely to have similar costs for lignin-based and current carbon fibers. The overall cost savings for lignin-based carbon fibers relative to PAN-based fibers is thus $2.50–$8.70/lb.
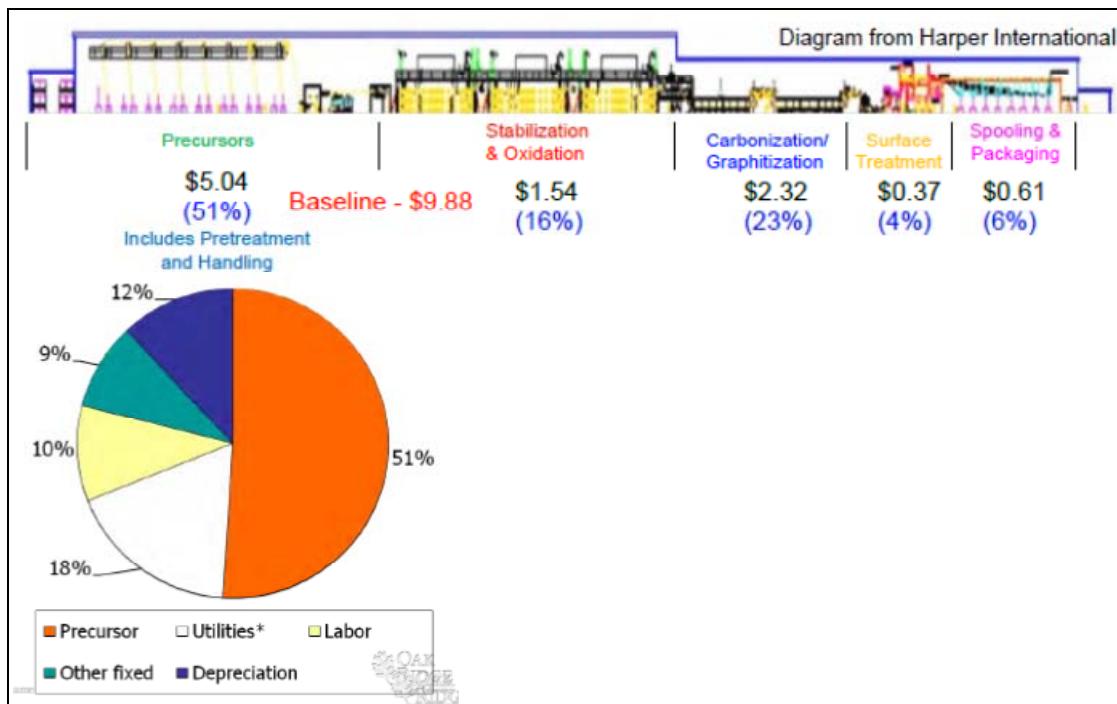
Figure 159. Cost breakdown for low-grade PAN-based carbon fiber (*1*).

Table 25. Cost savings associated with lignin-based carbon fibers relative to current PAN-based carbon fibers.

Processing Step	Raw Materials	Utilities	Labor	Capital Depreciation	Totals Minimum	Maximum
Precursors	$1-5	$0-0.25	$0.1-0.5	$0-0.25	$1.10	$6.00
Stabilization	$0	$0.5-0.8	$0.1-0.3	$0.3-0.5	$0.90	$1.60
Carbonization/graphitization	$0	$0	$0.1-0.3	$0.4-0.8	$0.50	$1.10
Surface Treatment	$0	$0	$0	$0	$0.00	$0.00
Packaging	$0	$0	$0	$0	$0.00	$0.00
Total =	$1-5	$0.5-1.05	$0.3-1.1	$0.7-1.55	**$2.50**	**$8.70**

As of now, it is too soon to estimate the costs of the manufacture and purification of bacteria decomposed lignin. These will be estimated before the end of the project. These could represent reduced or increased costs relative to chemically modified lignin-based carbon fibers. However, all the costs for lignin-based manufacture of carbon fiber should apply.

12.2 Biobased Resins

The baseline costs of commercial thermosetting epoxy, VE, UPEs, and their components are shown in table 26. UPEs are among the cheapest resins, with prices ranging from $1 to $2/lb. UPE monomers themselves are a bit more expensive, but the price of styrene is quite low at $0.7–$1.2/lb. VE monomers cost more than $4/lb, and their resulting styrenated resins cost anywhere from $2 to $4/lb. Epoxy resins are far more expensive at $5–$50/lb depending on the performance level. Epoxies that perform lower than VEs cover the lower scale, while epoxies that perform similar to VEs cost $10–$15/lb. Epoxies with high-temperature performance (>200 °C) cost more than $20/lb and up to $50/lb. Polyurethanes cost $2–$6/lb.

Table 26. Cost of commercial monomers and resins.

Resin/Monomer	Price (min)	Price (max)
VE resins	$2.00	$4.00
VE monomers	$4.00	$5.00
Styrene	$0.70	$1.20
Methyl methacrylate	$0.90	$1.20
UPE resins	$1.00	$2.00
UPE monomers	$1.50	$2.50
Epoxy resins	$5.00	$50.00
Epoxies	$5.00	$100.00
Amines	$4.00	$20.00
Polyurethanes	$2.00	$6.00
Polyols	$1.00	$5.00
Isocyanates	$3.00	$7.00

The estimated price of biobased resins should be calculated using the weighted costs of the reactants and the costs of the reaction, and establishing a price markup for profit. Because of the proprietary nature of some of these monomers (patent application), the details of the chemicals used to prepare these monomers cannot be fully disclosed. The reaction and separation costs, if applicable, were not calculated for the purposes of this report, but will be calculated for the final report. The price markup used was 50%. The estimated resin prices are shown in table 27. The resins tabulated have an estimated price of roughly $1/lb to a little over $4/lb. This is right in line with some of the lower-cost resins, as shown in table 26.

Table 27. Estimated monomer costs.

Monomer	Component 1	Comp 1 Cost	Component 2	Comp 2 Cost	Monomer Cost	Monomer Price (50% markup)	Cost relative to Baseline Min	Cost relative to Baseline Max
Bio-X-1 Crosslinker	Proprietary	$3.97	MAA	$2.00	$2.90	$4.36	-$0.4	$0.6
Bio-R-1 Diluent	Proprietary	$3.00	GM	$2.65	$2.80	$4.21	-$3.5	-$1.6
Bio-X-2	Saccharide	$0.44	MAA	$1.00	$0.75	$1.13	$2.9	$3.9
Bio-UPE	Isosorbide	$4.00	MA/TPA/EG	$0.50	$1.58	$2.37	-$1.4	-$0.4
Bio-Y-1	Proprietary	$3.97	Epichlorohydrin	$2.00	$2.87	$4.30	$0.7	$45.7
Bio-Y-2	Saccharide	$0.44	Epichlorohydrin	$1.00	$0.76	$1.14	$3.9	$48.9
Bio-PU-1	Proprietary	$4.00	Proprietary	$0.20	$2.53	$3.80	-$1.8	$2.2
							>$1 savings	
							>$0 savings	
							<$1/lb Added Cost	
							<$2/lb Added Cost	
							>$2/lb Added Cost	

Table 27 shows the differential in cost relative to a similar performing baseline resin. The table shows the difference in price relative to the minimum and maximum cost of this resin. Some monomers have higher costs than the baseline (yellow, orange, or red shading); this includes Bio-R-1 (FA-GM) and Bio-UPE (isosorbide UPE resins)—an indication that these monomers are very likely to be uneconomically feasible. Bio-X-2, Bio-Y-1, and Bio-Y-2 had lower costs (green or light green shading) than both the minimum and maximum resin cost. This indicates that as long as the reaction costs are low, these resins will be economically feasible and could likely displace existing monomers. The other resins that are more expensive than the minimum baseline monomer but cheaper than the maximum are less certain. These may prove to be economically feasible or not, depending on reaction costs and performance. Yet, cost reduction may be low, thus there may be a small driving force toward displacing existing monomers with these unless there are performance advantages or other life-cycle cost advantages.

References

1. Warren, C. D. *Low Cost Carbon Fiber Overview*; Oak Ridge National Laboratory: Oak Ridge, TN, May 2011.

2. Alibaba.com. http://price.alibaba.com/price/priceLeafCategory.htm?categoryId=100001628 (accessed 26 April 2012).

3. Warren, C. D. *Future Low Cost Carbon Fiber for Autos: International Scale-Up and What Is Needed*; Oak Ridge National Laboratory: Oak Ridge, TN, September 2008.

13. Summary, Conclusions, and Future Work

13.1 Accomplishments

We have accomplished numerous things in this project. Bacteria can successfully decompose lignin into useable structures for carbon fiber formation. Approximately 300 strains of bacteria that decompose lignin were identified, including *Pseudomonas*. We have chemically fractionated lignin to alter its molecular weight distribution and usefulness for separating chemically modifying lignin. Various chemical modifications of lignin have been successful for use in carbon fiber development. These methods, which include acetylation and methacrylation, have developed separation strategies to produce good carbon fiber precursors. Both melt-spinnable and solution-spinnable lignin-based fibers were produced. Thermo-oxidation and UV curing were successful stabilization methods for these fibers. Carbon fibers were produced from a few types of lignin and chemically modified lignin. The resulting mechanical properties were relatively poor, but there are obvious steps that need to be undertaken to improve these properties. Electrical conductivity of these fibers ranged from moderately conductive, similar to that of PAN-based fibers, to highly conductive, indicating significant graphitic content.

Numerous biobased resins were developed, many of which had excellent properties. Lignin-based model compounds have shown to be an excellent reactive diluent to replace styrene in VE resins. The resulting VE polymers have T_g's, mechanical properties, and other properties similar or better than that of styrenated VEs while producing much less emissions. Sugar/cellulose-based UPEs have been prepared. To solubilize these polyesters in common reactive diluents, the molecules must be end-capped or copolymerized during polyester synthesis with aliphatic components. These components reduce the T_g to no higher than 50 °C, and the mechanical properties are modest. Sugar-based epoxies have demonstrated good properties, but much more work is needed in this area. Sugar-based VEs have been prepared with T_g and modulus higher than that of any known commercial VE. In addition, we have begun developing structure-property relationships for these biobased resins. Life-cycle analysis shows that lignin-based carbon fibers have at least a $2/lb benefit relative to current carbon fiber technology. Furthermore, various biobased resins appear to be cheaper than commercial resins by as much as a few dollars per pound.

13.2 Project Status

The Gantt chart (table 28) shows the originally proposed schedule as well as the current modified schedule. In general, the project is on schedule, if not ahead of schedule. We have encountered a number of "go/no-go" decisions and have proceeded forward as a "go" for all:

- Feasibility of microbial degradation of lignin.

- Preparation of lignin-based oligomers for fiber production.

- Demonstration that lignin-based materials have proper rheological characteristics for fiber production.

- Demonstration that UV cross-linking and thermo-oxidative stabilization can successfully stabilize lignin-based carbon fibers.

- Lignin-based polymers can be successfully carbonized into fibers.

- Carbohydrate derivatives have potential for producing high-performance resins.

The following "no-go" decisions were made as subsets of the tasks that are not explicitly listed:

- Singlet oxidation decomposition of lignin.

- Water washing of lignin to reduce ash content.

- Isosorbide-based unsaturated polyesters.

Deliverables will identify optimum biobased formulations or conditions to produce resins or fibers. We expect to complete journal papers and technical reports for each of the milestones with deliverables.

Table 28. Gantt chart showing originally proposed and current schedule.

Task #	Quarter / Task	2010 Q1	Q2	Q3	Q4	2011 Q1	Q2	Q3	Q4	2012 Q1	Q2	Q3	Q4	2013 Q1	Q2	Q3	Q4
1.1	Preparation of Lignin-Based Oligomers for Fiber Production				?												
1.1	Preparation of Lignin-Based Oligomers for Fiber Production				Y												
1.2	Chemical Analysis of Lignin Decomposition Products																
1.2	Chemical Analysis of Lignin Decomposition Products																
1.3	Rheostructural Investigation to Determine Melt-Processability							?									
1.3	Rheostructural Investigation to Determine Melt-Processability							Y									
1.4	UV-Thermal Dual Mechanism Crosslinking/Stabilization and Carbonization							?									
1.4	UV-Thermal Dual Mechanism Crosslinking/Stabilization and Carbonization							Y									
1.5	Carbonization and Graphitization of Lignin-Based Fibers								?								
1.5	Carbonization and Graphitization of Lignin-Based Fibers								Y								
1.6	Testing and Analysis of Bio-Based Fibers																
1.6	Testing and Analysis of Bio-Based Fibers																
2.1	Preparation of Bio-Based Monomers				?												
2.1	Preparation of Bio-Based Monomers																
2.2	Chemical Analysis of Bio-Based Chemicals																
2.2	Chemical Analysis of Bio-Based Chemicals																
2.3	Resin Preparation and Cure Analysis						?										
2.3	Resin Preparation and Cure Analysis						Y										
2.4	Resin and Polymer Properties																
2.4	Resin and Polymer Properties								Y								
3	Testing and Analysis of Bio-Based Composites																
3	Testing and Analysis of Bio-Based Composites																
4	Environmental and Life Cycle Analysis																
4	Environmental and Life Cycle Analysis																
5	Reporting																
5	Reporting																
	Transition Final Composites systems																

Legend:
- Scheduled Task (yellow)
- Completed Task (black)
- Task with Report (blue)
- Report Completed (dark blue gradient)
- Go Decision (yellow with ?)
- Go Decision (green with Y)

231

In section 1, we listed the overall goals of the project. The following outline shows what has been completed (green), what is ongoing (blue), and what has yet to be accomplished in the remaining 2 years of the project (orange).

A) Microbial degradation of lignin: work has shown good potential and will continue through project end.
   a. Demonstrate that microbial degradation of lignin is feasible for producing carbon fiber precursors: successfully accomplished.
   b. Identify optimum bacteria for decomposition of lignin. We have identified a number of potential bacteria but have not identified the optimum.
   c. Produce microbially degraded lignin at small to moderate scale. We have produced two batches at small scale to demonstrate feasibility but need to scale up optimum lignolytic bacteria processes for carbon fiber preparation.
   d. Perform life-cycle cost analysis for production of microbially degraded lignin as carbon fiber precursors relative to PAN.
B) Chemical modification/degradation/fractionation of lignin. We have identified modification methods but have not optimized reactions or combined methods of chemical modification.
   a. Identify optimum chemical methods to obtain lignin-based carbon fiber precursors. We have identified acetylation and methacrylation.
   b. Produce chemically modified lignin at small to moderate scale. We have produced modified lignin at high enough levels for carbon fiber batch production, but work will be ongoing with new chemically modified lignin samples.
C) Lignin-based carbon fiber development
   a. Identify modified lignin samples with optimum rheological properties for fiber spinning. We have identified chemically modified lignin with proper rheological properties, but work is ongoing as new chemically modified lignin samples are produced.
   b. Identify modified lignin samples that can be stabilized to prevent fusion of fibers during carbonization. We have identified stabilization methods, but work is ongoing as new chemically modified lignin samples are produced.
   c. Identify modified lignin samples that can be used to produce carbon fibers with high modulus and high strength. We have prepared carbon fibers from lignin, but properties are low.
   d. Produce high-performance carbon fiber at small to moderate scale.
   e. Perform life-cycle cost analysis for production of chemically modified lignin as carbon fiber precursors relative to PAN. We have completed the cost analysis for many variants but will keep doing this work for new lignin samples through project end.
D) High-performance biobased resins: much has been completed, but work is still ongoing
   a. Identify biobased epoxy, polyamine, UPE, and VE cross-linkers that produce $T_g>150$ °C when used in conjunction with standard resin components or other biobased components: successfully accomplished.
   b. Identify biobased reactive diluents for UPE and VE resins that produce T_g no less than 10 °C lower than that of styrene-based resins: successfully accomplished.
   c. Produce optimum biobased resins at 250-g scale for composite production:

successfully accomplished.
d. Perform life-cycle cost analysis for biobased resins relative to comparable epoxies, UPEs, and VE resins. We have completed the cost analysis for many resins but will keep doing this work for new resins and old resins through project end.

E) High-performance biobased composites: future work
a. Demonstrate composite production using biobased carbon fiber and biobased resins.
b. Develop biobased composites with properties similar to that of comparable non-biobased composites.

13.3 Future Work

Future work was generally discussed throughout this report for the particular research areas. Thus, in this section, we generalize the future work discussion.

Microbial decomposition of lignin has been successful. Approximately 300 different bacterial strains have been identified but have not yet quantified the characteristics of the more successful lignolytic bacteria, including gram staining, to what extent they degrade lignin, and how fast they degrade lignin. In order to produce carbon fibers, larger-scale production of the bacteria decomposed lignin must be prepared. In addition, a feasibility study must be performed to assess whether such a process is commercially and economically feasible. A chemical engineering design problem will be proposed at Clemson and Drexel to obtain this information.

Chemical modification of lignin will continue. In particular, combinations of hydroxyl, acetate, and methacrylate functionality will be used to enable easy stabilization of the polymeric fibers. Work must be done to assess ash content in these modified lignin samples to determine whether this is playing a role. In addition, we must orient the fibers during spinning and improve the processing during carbonization to produce higher-performing carbon fibers.

Isosorbide-based unsaturated polyesters have shown to be unsuccessful in developing high-performance polyesters. Measurements to assess structure-property relationships will be completed in the near future to wrap up this work. In addition, publications will be completed, but no other work will be performed.

Epoxy-based furans and carbohydrates are in development. So far, we have not achieved optimum functionalization, thus we will try additional chemical methodologies and variants. No diamines have been produced as of yet. However, some will be produced in 2012 from furans as well as depolymerization of chitosan.

Measurements to assess structure-property relationships of lignin-model compounds will be accomplished during 2012. One journal article has already been submitted, and another one will be submitted soon. One to two additional publications will be completed during 2012 and 2013 on this topic.

Furan-based reactive diluents have had inferior properties relative to baseline diluents. Structure-property relationships have been developed. An article outlining the assessment of the use of these diluents has been submitted to one journal and an additional one to two articles will be completed in 2012.

Carbohydrate-based VEs have demonstrated excellent success. These resins are being patented and will soon be published in a number of journal articles to show their properties and structure-property relationships.

Although not presented in this report, we have begun to show the potential for making polyurethane resins with higher T_g's than commercial high T_g polyurethanes. Thus, we will begin to explore and potentially expand on this research area.

Life-cycle analysis of processes, carbon fibers, and resins will be continually assessed during the course of this project.

List of Symbols, Abbreviations, and Acronyms

3-D	three-dimensional
ABP	acryloyl benzophenone
Ace_SKL	acetylated softwood Kraft lignin
Ace_Soda	acetylated Soda (protobind 1000) lignin
ACRES	Affordable Composites from REnewable Sources
ARL	U.S. Army Research Laboratory
B-UPE	benzyl end group modified UPE
bAMF	2,5-bis(aldehydyemethyl)furan
bHMF	2,5-bis(hydroxymethyl)furan
bNMF	2,5-bis(aminomethyl)furan
Bio-R	proprietary reactive diluent
Bio-X	proprietary anhydrocellulose cross-linker
Bio-Y	proprietary carbohydrate cross-linker
CAEFF	Center for Advanced Engineering Fibers and Films
CCM	Center for Composite Materials at the University of Delaware
$CDCl_3$	deuterated chloroform
CoNap	Cobalt Naphthenate
COSY	correlation spectra (NMR)
DGEBA	diglycidyl ether of bisphenol A
DMA	dynamic mechanical analysis
DMAP	4-dimethylaminopyridine
DMBA	dimethylbenzyl amine
DMF	dimethyl formamide
DMSO	dimethyl sulfoxide

DMSO-d$_6$	dimethyl sulfoxide with six (all) deuterated protons
DOD	Department of Defense
DOE	Department of Energy
DPI	diaryliodonium hexafluoroantimonate
DSC	differential scanning calorimetry
E	modulus of material
E'	storage modulus
E''	loss modulus
ECN	brand of organosolv lignin
EEW	epoxy equivalent weight
EPA	Environmental Protection Agency
ESTCP	Environmental Security Technology Certification Program
FA-GM	furoic acid-glycidyl methacrylate
FM	furfuryl methacrylate
FTIR	Fourier transform infrared spectroscopy
GDM	glycerol dimethacrylate
GPC	gel permeation chromatography
H-UPE	hexyl end group modified UPE
HAP	hazardous air pollutant
HCl	hydrochloric acid
HCN	hydrogen cyanide
HMF	hydroxymethylfurfural
IDT	initial decomposition temperature
Indulin AT	brand of softwood Kraft lignin
KPL	Kraft pine lignin
LMC	lignin model compound
MA	maleic anhydride

MA_Ace_SKL	methacrylated and acetylated softwood Kraft lignin
MAA	methacrylic acid
MDSC	modulated differential scanning calorimetry
ME	methacrylated eugenol
MEKP	methyl ethyl ketone peroxide
Meth_KPL_UD	methacrylated Kraft pine lignin from the University of Delaware
Meth_SKL	methacrylated softwood Kraft lignin
MFA	methacrylated fatty acid
MG	methacrylated guaiacol
MHex	methacrylated hexanoic acid
MLau	methacrylated lauric acid
MLMC	methacrylated lignin model compound
MMA	methyl methacrylate
M_n	number average molecular weight
MOct	methacrylated octanoic acid
MP	mesophase pitch
MS	mass spectrometry
MV	methacrylated vanillin
MVGDM	methacrylated vanillin glycerol dimethacrylate
M_w	weight average molecular weight
NIR	near infrared
NMR	nuclear magnetic resonance
NSWCCD	Naval Surface Warfare Center Carderock Division
ORNL	Oak Ridge National Laboratory
PACM	Bis(p-aminocyclohexyl) methane, air Products
PAN	polyacrylonitrile
PCR	polymerase chain reaction

PDI	polydispersity index
PI	photoinitiator
Protobind 1000	soda lignin
PME	poly(methacryl eugenol)
PMG	poly(methacryl guaiacol)
PMMA	poly(methyl methacrylate)
PS	polystyrene
RPM	revolutions per minute
SEC	size exclusion chromatography
SEM	scanning electron microscopy/microscope
SERDP	Strategic Environmental Research Development Program
SKL	softwood Kraft lignin
SP	softening point
$Tan(\delta)$	ratio of loss modulus to storage modulus
TBAB	tetrabutyl ammonium bromide
TFT	twinkling fractal theory
T_g	glass transition temperature
T_m	melting temperature
TGA	thermogravimetric analysis
THF	tetrahydrofuran
THPM-GE	tris-hydroxyphenylmethane glycidyl ether
TLC	thin layer chromatography
UPE	unsaturated polyester
UV	ultraviolet
VARTM	vacuum-assisted resin transfer molding
VE	vinyl ester

VE828   vinyl ester 828

VOC   volatile organic compound

wt%   weight-percent

NO. OF
COPIES ORGANIZATION

  1   CLEMSON UNIV
       DEPT OF CHEM & BIOMOLECULAR
       ENGRG
       A OGALE
       CLEMSON SC 29634-0909

  1   CLEMSON UNIV
       ANIMAL & VETRNRY SCI
       A GREENE
       CLEMSON SC 29634-0909

  1   DREXEL UNIV
       G R PALMESE
       3141 CHESTNUT ST
       PHILADELPHIA PA 19104

  1   UNIV OF DELAWARE
       R P WOOL
       ACADEMY ST
       NEWARK DE 19716

  2   SERDP
 (1 HC WEAPONS SYS & PLATFORMS
 1 CD) SERDP & ESTCP PROG OFC
       B SARTWELL
       901 N STUART ST STE 303
       ARLINGTON VA 22203-1853

       ABERDEEN PROVING GROUND

  5   DIR USARL
 (3 HC RDRL WMM
 2 CD)   J ZABINSKI
       RDRL WMM A
         J SANDS (1 CD)
         E WETZEL (1 CD)
       RDRL WMM B
         M VANLANDINGHAM
       RDRL WMM C
       J LA SCALA

241

INTENTIONALLY LEFT BLANK.